Design of a structural device for vibroacoustic measurements in a wind tunnel

Giulia Mazzeo

▶ To cite this version:

Giulia Mazzeo. Design of a structural device for vibroacoustic measurements in a wind tunnel. Other. Université de Lyon; Università degli studi di Napoli Federico II, 2021. English. NNT : 2021LYSEC035 . tel-03553374

HAL Id: tel-03553374
https://theses.hal.science/tel-03553374
Submitted on 2 Feb 2022

N°d'ordre NNT : 2021LYSEC35

THÈSE de DOCTORAT DE L'UNIVERSITÉ DE LYON

Opérée au sein de :

l'Ecole Centrale de Lyon

En cotutelle internationale avec :

Università degli studi di Napoli "Federico II"

Ecole Doctorale ED 162

Mécanique, Energétique, Génie civil et Acoustique

Spécialité de doctorat: Mécanique des solides, des matériaux des structures et des surfaces

Soutenue publiquement à huis clos le 20/09/2021, par:

Giulia MAZZEO

Design of a structural device for vibroacoustic measurements in a wind tunnel

---

Devant le jury composé de :

CINEFRA Maria	PhD Professeur associée	**Rapporteure**
CIAPPI Elena	PhD Senior Chercheuse	**Rapporteure**
JUVÉ Daniel	Professeur émérite	**Examinateur**
CARRERA Erasmo	PhD Professeur	**Examinateur**
HAMBRIC Stephen	PhD Professeur	**Examinateur**
ICHCHOU Mohamed	Professeur des Universités	**Directeur de thèse (FR)**
BAREILLE Olivier	Maître de conférences HDR	**Co-Directeur de thèse (FR)**
DE ROSA Sergio	PhD Professeur	**Directeur de thèse (IT)**
FRANCO Francesco	PhD Professeur	**Co-Directeur de thèse (IT)**

Abstract

In the industrial field of transportation, which includes aeronautics, automotive, railways an naval, the vibrational response of a structure to a pressure fluctuation due to a turbulent flow is the main subject of research. The reason lays on the consequences that the turbulent flow-induced vibrations can cause, such as fatigue problems and structural damage.

Test panels are often analysed in wind tunnels in order to obtain the vibroacoustic characteristics, hence it is necessary to ensure the purity of the measurements performed in the facilities. With the present work, it is wanted to develop a structural design for a device which would play as support for flat panels inside a large-scale wind tunnel. The design based on material and geometry choice has been performed through a system of design guidelines developed with Statistical Energy Analysis which would ensure an energy transmission decoupling between the support and the test model. The designed device is then analysed in the high and low frequency domains, in order to evaluate the performances of the structure.

Together with the design guidelines, an "off-line" validation method is proposed in order to test the structure even before its allocation in a wind tunnel. The proposed method is an experimental adaptation of the Pseudo-Equivalent Deterministic Excitation method (PEDE_M) which is based on the approximation of a Turbulent Boundary Layer (TBL) excitation in two different asymptotic behaviours: at low frequencies (LF) as an Incident Diffuse Field, and at high frequencies (HF) as a totally-uncorrelated pressure field as a Rain-On-the-Roof excitation.

Both the design guidelines and the "off-line" validation method are meant to be the tools for for a fast but efficient structural design process and for the verification of the model.

TABLE OF CONTENTS

LIST OF TABLES

LIST OF FIGURES

Introduction

Industrial and scientific context

The vibrational response of structures to a flow excitation is still an issue of many works in literature and remains an important path of research. Considering several industrial fields as aeronautics, automotive, railways and naval, the presented topic preserves its versatility because cars, trains, submarines and aircraft are all subjected to pressure fluctuations due to a turbulent flow. The consequences of turbulent flow-induced vibrations might be several; interior induced vibrations can exceed the design prefixed requirements and cause damages to the payload or to any good transported by a generic vehicle; exterior vibrations of the vehicle external surfaces could cause fatigue problems and structural damages. Moreover, wall-pressure fluctuations (WPFs) are one of the main sources of airborne noise, together with the structure-borne sound generated by the vehicle due the flow excitation, which can result in discomfort for passengers and in noise pollution of the environment that can undermine the public health. As a consequence of the aforementioned problems, the structural vibrational response to a flow excitation needs to be predicted at the design stage of structures.

The objective of predicting a structural response to a flow excitation is still a challenge in the research field, since the Turbulent Boundary Layer (TBL) excitation presents intrinsic characteristics. It is a random excitation represented as stochastic pressure distribution, with correlation properties depending on the convective flow effect and with a broadband frequency range in which it strongly changes its behavior. Because there are not analytical formulation regarding the excitation exploited by WPFs, conventional methods for the description of structural response due to a TBL-induced surface pressure fluctuations rely on the development of semi-empirical models based on both theory and experimental results. These models basically describe the WPFs as Cross Spectral Density (CSD) of wall-pressure generated by the TBL, depending on flow and boundary-layer parameters. The disadvantage of these models stands on the variety of experiments with which they were developed, in fact each model presents a different prediction of the TBL behavior varying the frequency region of interest. Moreover, the flow and boundary-layer parameters show some inconsistency. As a consequence, experimental measurements are often required as reference data to not only asses the TBL parameter inconsistencies, but also to compare and validate which semi-empirical model is better for a reliable structural response formulation.

For these reasons and others more, wind tunnel facilities are still very used for vibroacoustic experiments, for the analysis of new materials performances, for the improvement of existing models or elaboration of new semi-empirical models for TBL excitation, for mandatory final test of any vehicle design. Wind tunnels architectures were improved over the years, trying to assess easier experiment setups and to overcome measurements difficulties as background noise or vibrations transmission. However, although there are generic procedures for the design of a wind tunnel facility, according to the required performances, the versatility of test models does not allow to establish a generic procedure which would ensure a structural energy transmission decoupling between the test model and the support located in the test section of the wind tunnel. Furthermore, most of wind tunnels might result expensive, especially if for a long time of use and, nevertheless, the experiments would not be efficiently performed due to the setup or other technical complications.

Research target

Industrial and scientific contexts showed two main problems:

- a lack of generic procedure for what concerning experimental setup of a test model inside a wind tunnel facility, which would take into consideration the energy transmission that a generic support would pass to the test model, invalidating the experimental measurements executed.

- the necessity of alternative methods which would recreate the effect of a TBL excitation over a structure without the implementation of a wind tunnel facility.

As a consequence, the presented research is composed mainly in two different studies.

The first one focuses on the establishment of an easy procedure to design a support for any test model with the main aim of ensuring an energy transmission decoupling between them. The procedure will allow to quickly obtain the best design parameters to use for the structural design and to determine in advance an approximated value of the difference of vibration velocity levels of the two coupled systems.

The second study refers to the "off-line" validation of the designed structure; a simplified experimental method has been developed for the determination of the structural response to a TBL excitation without using a wind tunnel facility for the application of the aerodynamic load.

Manuscript structure

Specifically, the manuscript is composed of five chapters.

In the first chapter, a bibliography research is developed about three main topics: (1) wind tunnels architectures, with an attention on the test section designs and setup procedures for the allocation of the test model inside the test section; (2) energy transmission decoupling and developed theories about it; (3) TBL excitation formulation and alternative methods for the determination of the structural response to a TBL excitation, which would not require an actual aerodynamic load application.

In the second chapter, the design procedure is introduced and explained in its passages, showing also the effect that different parameters as area, thickness, type of material would result in the energy transmission between two subsystems. A simple model, then, is studied in order to evaluate the design process in high frequency domain.

In the third chapter, the same design process is applied to a complex structure, designed to be a support for test panels and to be located and used in large-scale wind tunnels. The coupled system support-test panel is then studied in the high and low frequency domains as well.

With the fourth chapter, the second topic is introduced; the alternative method called Pseudo-Equivalent Deterministic Excitation method (PEDE$_M$) would be explained and applied on a simple system as a panel in order to recreate a TBL excitation and to predict its structural response. Comparison with reference semi-empirical models will be discussed to determine the frequency range of applicability of the method.

Finally, in the fifth chapter, a development of PEDE$_M$ is presented as experimental method to apply as "off-line" procedure for the prediction of the structural response to a TBL excitation. The new method is introduced ad than applied first with a numerical simulation and then in comparison with experimental data collected in two different wind tunnel facilities. It is wanted to show that the proposed "off-line" validation can be applied for the structural design verification.

CHAPTER 1

STATE OF ART

1.1 Introduction

The final aim of this research work is to design a test model support to be located in a wind tunnel facility in order to perform vibroacoustic measurements over test panels subjected to an aerodynamic load formulated as a TBL excitation. The structural design is wanted to be validated "off-line", meaning that it is not required a final test in a wind tunnel facility.

In order to do so, three different topics have been investigated with a bibliography research:

- Section 1.2: wind tunnel architectures, with a focus on test section and test model support designs;
- Section 1.3: energy transmission decoupling formulation and its development through different methods;
- Section 1.4: alternative TBL excitation methods, looking for an "off-line" experimental application that does not imply the use of a wind tunnel facility.

1.2 Wind tunnels

The wind tunnel invention was dictated by the necessity of recreate the physical conditions to study the effect of an air flow over a structure with the final aim of finding the aerodynamic laws which govern the flight.

The actual first design of a working wind tunnel is accredited to Frank H. Wenham [1], which consisted in a horizontal duct long approximately 3.7m with a fan-blower powered by a steam engine. With Reynolds studies, it has been demonstrated that scaled model experimental data can be a reference for full scale models too, if a certain flow parameter (now known as Reynolds number) was the same for both models [2]. Wright brothers performed experiments with a wind tunnel too, in order to collect new experimental data which allow them to achieve the final goal of flight.

Nowadays, wind tunnels are implemented not only for aircraft design purposes, but also for new scientific challenges regarding any fluid-structure interaction. For what concerning the industrial engineering of transportation, wind tunnels experiments are now mandatory tests for aircraft [3], trains [4], automotive [5]. Tests on scaled model buildings are also performed in wind tunnels facilities in order to study the gust effects over tall buildings [6] or bridges [7] and general wind-related environmental problems. Experimental tests can be performed in order to study new materials and detect their performances based on structural vibrations transmission end emitted noise [8]: these two characteristics are fundamental to analyse, in order to improve the comfort inside any vehicle subjected to a turbulent flow. Wind tunnel applications can even be found in sports, for which the aerodynamic of a ball or of a board are studied in order to improve their performances during a competition [9].

Because of their versatile use, the design process of a wind tunnel gets a lot of attention in the research field, in order to find better techniques which can ensure air flow conditions suitable for experimental data collection. Different architectures were developed, each with its advantages and disadvantages.

1.2.1 Wind tunnel architecture

Although Wright brothers achieved the final goal of the flight, the wind tunnel that they designed had its defects: the driver system was positioned directly in front of the test section, generating swirling air motion and turbulence; despite the presence of vanes and honeycomb screens, the flow was not uniform; there was no diffuser for a pressure recovery and this generated turbulence at the exit of the wind tunnel and it propagated upstream in the test section [10]. Ever since the Wright brothers, engineers continuously provided improvements

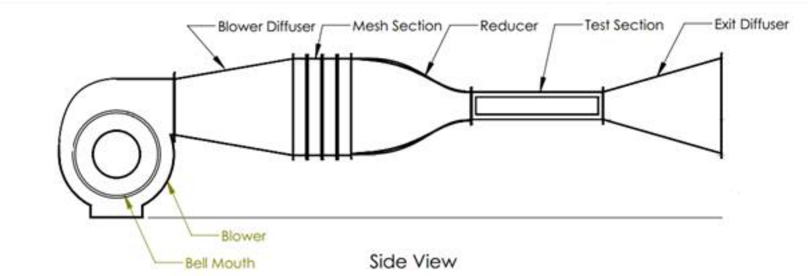

Figure 1.1: Blower wind tunnel: the drive system is located upstream the test section.

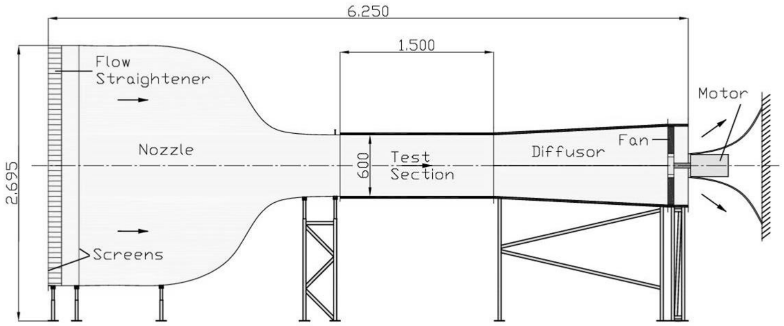

Figure 1.2: Suction wind tunnel: the drive system is located downstream the test section.

for the wind tunnel design, although the methods and the theories on which the design is based did not change for several decades.

The general objective of a wind tunnel is to recreate a parallel steady flow in a specific part of the facility called "test section", in which experiments are performed. Independently from the type of architecture and the required flow speed, a wind tunnel always consists in:

- *Drive system*: it has the objective of creating the flow motion. Wind tunnels can be categorized for the type of drive system as: blower, suction or blow-down. Blower wind tunnels present a fan upstream the test section which blows air through it (Figure 1.1). Suction wind tunnels, on the other hand, present the fan downstream the test section, in order to pull the air through it (Figure 1.2). Blow-down wind tunnels are equipped with a nozzle and a pressurized air storage tank; the difference of pressure between upstream and downstream would create the air motion inside the test section (Figure 1.3). The choice among these drive systems depends principally on the requested air speed.

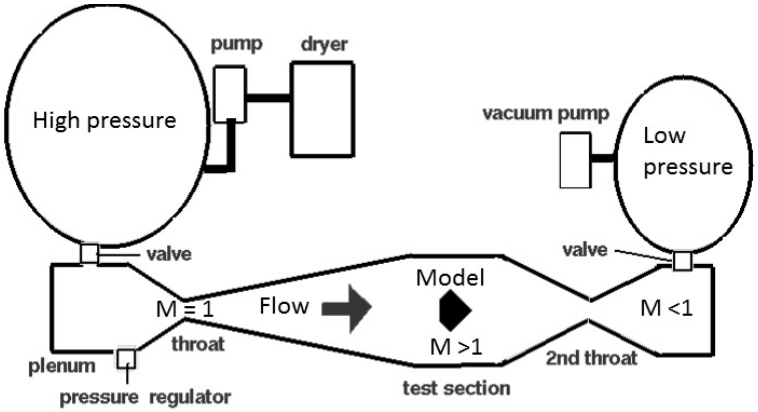

Figure 1.3: Blow-down wind tunnel: the difference of pressure created between upstream and downstream the test section generates an air flow motion.

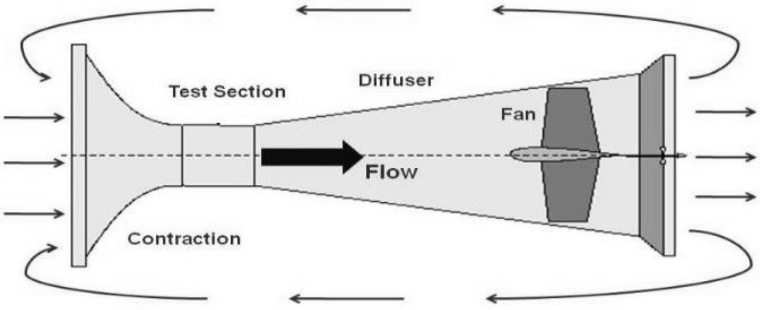

Figure 1.4: Open-circuit wind tunnel.

- *Ducts system*: tunnel geometry varies dependently with the requested flow speed (especially if subsonic or supersonic), together with the available space that can be used. Its main objective is to stabilize the air flow so that it keeps itself parallel and with constant speed for as much time as possible. Two major configurations that can be recognized based on the ducts system are: open-circuit and closed-circuit. In the open-circuit one, the air is gathered from the room where the wind tunnel is located (Figure 1.4), while in the closed-circuit one, the same air circulates inside the ducts system.

- *Contraction and diffuser*: these two specific parts of the ducts system are essential for the regulation of the flow speed inside the test section. Specifically, for subsonic

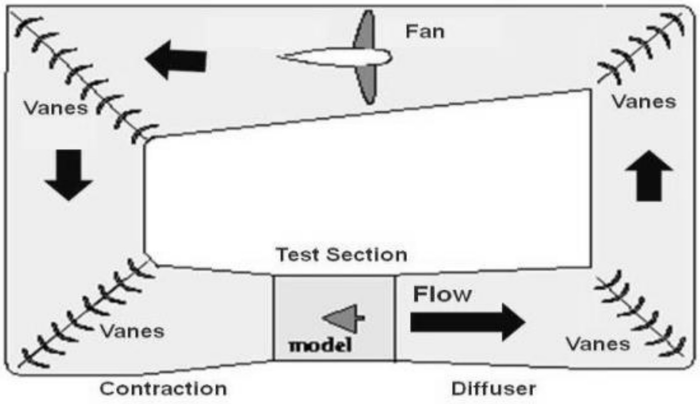

Figure 1.5: Closed-circuit wind tunnel.

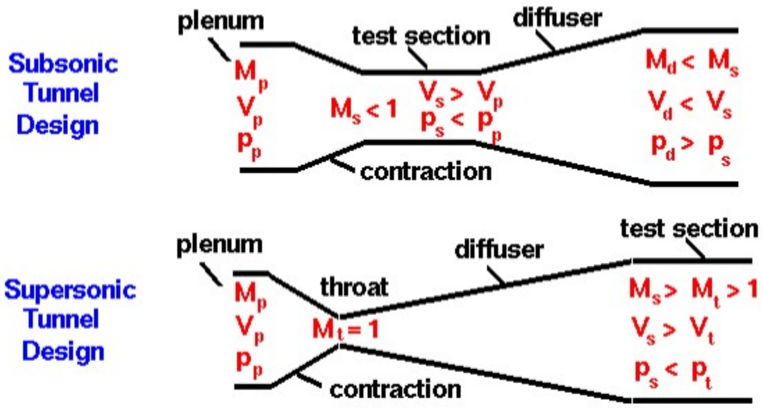

Figure 1.6: Difference of wind tunnel design between subsonic (on the top) and supersonic (on the bottom) flow speed. M: number of Mach, V: flow speed, P: pressure.

flow speeds, the contraction is a convergent nozzle placed upstream and the diffuser is placed downstream, while for supersonic flow speeds, contraction and diffuser are both upstream the test section. The junction section between contraction and diffuser is called "throat" and it is the smallest cross-sectional area in a supersonic wind tunnel where a number of Mach $M = 1$ is reached and with which the passage from subsonic to supersonic flow is possible (Figure 1.6).

- *Test section*: as already mentioned before, the test section is the wind tunnel part in which the test model is located and where measurements are taken. The choice of its size would dictate the design conditions for the rest of the facility. Last categorization that could be done for wind tunnel facilities depends on their size. They can be divided in small-scale and large-scale, depending on the test model dimensions located inside the test section. For large-scale wind tunnels, it usually means for full-scale models as automotive and trucks [11], while in small-scale wind tunnels, scaled models or simply small models are analysed [12].

The design process is always focused on a clever balance among distinct constraints as budget, available space, required maximum flow speed, required maximum test section size. Obtaining the largest test section and the highest flow speed are the tasks kept as priorities during the design process. As a consequence, every design process would start establishing first the requested flow speed (referring to the Reynolds and Mach numbers) and test section dimensions. These fixed parameters would dictate the dimensions of contraction and diffuser. Then, depending on the available budget and space, the choice between open-circuit and closed circuit can be made. Last decision to take would be the type of drive system.

For low-speed wind tunnels, first guidelines were suggested by Bradshaw and Pankhurst [13]. The designer point of view was taken into consideration, evaluating different existing wind tunnel configurations and collecting the common data for each facility section. It is mentioned a dependence between the flow speed and the test model size, accompanied by an easy logical proportion that helps to estimate the maximum test model size in function of Reynolds number. It is then affirmed the relationship that occurs between test model size and test section size, which must be such as to minimize tunnel interference. Because aerodynamic test models are considered, balances for the force and moment estimation on the model and false walls for the allocation of half-symmetrical model or for total scaled models leaning on the floors are the nearest mention to a support system for a test model.

Later with Mehta, Bradshaw would give other guidelines with a focus on the wind tunnel blower [14]. Again, it is made relevant just the sizing of the test section in order to ensure an optimal allocation of the test model inside it, considering different situations as for a complete aircraft model, for boundary layer development on the wind tunnel floor, for complexes of buildings or for one isolated tower building or smoketacks.

Pope and Goin [15] published their book about high-speed wind tunnels design; the considered tests regard mostly to aerodynamic models and several suggestions are given about the most rigorous way of mounting the test model inside the test section. A support system based on a "sting" mounted behind the aircraft model, such that it would not interfere with air flow, is presented, together with a highlight on the fatigue problem by which the sting is subjected. Nevertheless, it is affirmed: *"the model support and drive system should be very well engineered with large margins of safety on every point of design. They are the heart of wind tunnel, are subject to a more severe environment than is usually estimated, and have to work essentially all time the tunnel is running"* [15].

Also Barlow *et al.* [16] published their own book on low-speed wind tunnels design, giving a 360° prospectus about configurations, design guidelines, experimental settings and required corrections. Again, all details are expressed for what concerning the test section dimensions in order to make adequate space for the test model, keeping a constant pressure and allowing the flow to close right after the test model, before entering in the diffuser. Endplates - or contraction plates - are here explained as solution for the disposition of two-dimensional airfoil model inside the test section, focusing the attention on the outcome effect due to the reduction of cross-sectional area of the test section. The drag generated by struts, which sustain the test model, is discussed and calculated in order to foresee the interference created to the air flow. Different struts positions are showed, always with a focus on the aerodynamic point of view.

A more concise design guidelines are also presented by Cattafesta *et al.* [17]. The main notable difference from the previous manuals results in a more compact and logical prospect, which would simplify the decisions made about the design criteria of the facility; moreover, acoustic measurements are taken into account; solutions for the vibrations transmission due to the operating drive system are finally mentioned. In particular, these solutions are intended to be carried out only at the end of the construction with ducts treatments; it is then suggested to measure the transmission loss factor between the tunnel drive system and the test section through correlation and coherence analysis.

As matter of fact, as the years go by, the wind tunnel design criteria changed in order to consider new kind of experiments that could be performed in the facility, which would be no longer just about the aerodynamics of a vehicle, but they would consider the general fluid-structure interaction physics, the structure-borne sound due to an aerodynamic excitation, the wall-pressure fluctuations air-borne sound, and so on. As a consequence, design techniques to reduce the background noise coming from the drive system were introduced. Major part of facilities are hence equipped with anechoic chambers which enable the background noise reduction.

Procedures for this type of design can also be found in literature. There are projects born from scratch as the aeroacoustic wind tunnel of Beihang University [18], in which only the aeroacoustic treatment is mentioned; the anechoic wind tunnel facility at University of Florida [19], for which the drive system mechanical vibrations have been isolated using a large concrete slab laying on a sand bed, isolated from the surrounding foundation with a retainer concrete wall. Still, this adjustment was not enough for the tunnel structural vibrations reduction, so rubber sleeves were added. Or again, the Carleton University facility [20], in which a new removable anechoic chamber has been designed for the specific purpose of panel structures analyses. In fact, all the removable test section surfaces, expect the test panel, were treated with acoustic foam to minimize reverberation. The test panel was a round acrylic panel, mounted in the test section in order to host several microphones for the measurements of the wall-pressure fluctuations. There are also proceedings for the adaptation of test sections for vibroacoustic measurements; one case to mention just as example is the Virginia Tech Stability Wind Tunnel [21], where two new anechoic chambers and a removable test section were designed and an iterative acoustic treatment was performed in order to add foam layers in different wind tunnel locations.

These design improvements presented in the aforementioned literature took care essentially of the steadiness of the air flow created inside the whole facility, or of the acoustic treatment in order to ensure the right function of microphones for the wall-pressure fluctuation measurements. For what concerning structural vibrations transmission, the main encountered problem has been the drive system induced-vibrations. As a consequence, specific experiments run in wind tunnel facilities, where test panels are the tested model, have been studied, in order to find experimental setup procedures which take care of the energy transmission from support to test model.

1.2.2 Supports setups for models tested in a wind tunnel

An experimental setup has been described for the acoustic wind tunnel of the Marcus Wallenberg Laboratory (MWL) [22]. The facility consists of a 9m long duct suspended in a reverberant room, where part of the duct was the test section. A test panel can be mounted in one of the four walls of the test section, recreating a clamped boundary condition. Induced-vibrations were encountered from the duct to the test panel due to the flow excitation; for this reason, two 40×40mm steel bars have been installed in the duct walls upstream and downstream the test section. Moreover, it has been seen necessary to add a constrained damping layer too.

At CIRA (Italian Aerospace Research Center) [23], there is the transonic tunnel PT-1, which is able to operate in the Mach number range $0.1 \leq M \leq 1.4$. The panels under experiment were constrained to test section wall through a rigid frame, by two parallel bolted lines along the edges perpendicular to the flow, and one single bolted line along the edges parallel to the flow. In order to verify the measurements purity, 4 accelerometers were positioned on the rigid frame.

Another panel setup in a wind tunnel facility is found at the Sherbrooke anechoic wind tunnel [24], where this time the panel has been just flush-mounted in a plywood frame of dimensions 20×10cm^2 and almost 2cm thick.

As final example to mention, at the Institute of Sound and Vibration Research (ISVR), there is an open jet anechoic wind tunnel, in which the vibrational response of a car window subjected to a TBL excitation has been simulated [25]. The support installed in the test section consisted of an acoustic baffle made of MDF board (15mm of thickness), covered by a dense acoustic foam and supported by stands which were clamped to the floor for a stable set-up. The test panel was mounted in the acoustic baffle without any direct connection, with the purpose of avoiding any energy transmission between them.

It is wanted to include in the literature review also the research work of Park, Siegmund and Mongeau, which focused on the flow-induced vibrations of a viscoelastic support for a test panel subjected to a TBL excitation [26]. The model under analysis was a side-glass window panel supported by a rubber seal. The study was based on the Rayleigh-Ritz method which, according to the authors, requires less computational effort if compared with other methods as Finite Element Method (FEM) or Boundary Element Method (BEM). However, it is limited to simple structural geometries and it is based on modal analysis, meaning that natural frequencies and mode shapes calculation is required and this limits the operational frequency range to the low frequencies. The methodology mainly consists in describing the coupling between panel and supports by considering translational and rotational springs at the panel edges. The springs stiffness has been considered complex. An approximation of the wall-pressure spectrum has been considered in order to get the solution. With their work, the authors demonstrated that the modal response of a plate is highly effected by the wave reflections along the edges, hence also the velocity response and the sound radiation are influenced by the energy dissipated at the boundaries [27]. Comparisons with experimental data confirmed what has been said [28], for two different types of seals. It must be said, though, that this method focuses on the panel vibrations reduction due to an optimal seals design. There are no applications of this method that have as final aim the energy transmission decoupling between a panel and its support, in order to be sure that the measured structural vibrations are a consequence of the only TBL excitation.

1.2.3 Conclusions

Wind tunnel experiments were and still are mandatory tests to carry out, both in an industrial context and in scientific researches regarding fluid-structure interaction. The main advantage worthy of note is that there is a widespread literature dedicated to wind tunnel design and required corrections for an increase of the quality of the experiments. On the other hand, each designer or experimenter applies his own methodology for the experiment setting, especially for the support system which sustains the test model inside the test section. The test model allocation inside the test section is always dependent on the type of experiment and, consequently, on the experimenter himself. With a particular attention to the structural vibration measurements, the corrections applied to ensure the purity of the collected experimental data are different from each other. This is the reason for which a methodology for the design of a generic support for test models to be located in wind tunnel facilities is seen necessary to develop.

1.3 Energy transmission analysis: methods proposed in literature

In the previous section, it has been raised the problem of the wind tunnel measurements quality, due to the support system which sustains the test model under analysis. In particular, it has been questioned the support design methodologies to ensure an isolation or reduction of energy transmission between support and test model. In this section, the concept of energy transmission coupling will be analysed, from the origin of the study until today, where different methods can be used for this type of analysis.

It can be said quite surely that first researches about the energy transmission between systems were conducted by Lyon and Maidanik [29], who were interested in disciplines as room acoustics, noise control, kinetic energy and turbulence. They started from the simplest system imagined: two coupled oscillators. By just solving their equations of motion and with the lonely assumption of statistically independent applied forces, the Coupling Power

Proportionality (CPP) was obtained, for which the power transmitted between two coupled oscillators is directly dependent on the difference of their energies. Moreover, the concept of energy transmission as heat distribution among modes, or the interpretation of modal energies as "temperatures" of systems, was already hinted. The definition of Coupling Loss Factor (CLF) as term that describes the transmission from one system to another is presented shortly after by Lyon and Eichler [30]; just one year later, with Scharton [31], the energy transmission among three systems was already under analysis. Separately, also Newland [32] participated on the study of power transmission between oscillators, giving an additional hypothesis for which the coupling should be "weak". Since then, the study of power flow and energy sharing among structures have been developed and deepened until one of the most famous energetic method was born: Statistical Energy Analysis, or SEA [33].

1.3.1 Statistical Energy Analysis

SEA was originally established for the study of fluid-structure interactions due to the large number of modes within an acoustic domain. This method was very early extended to structure-structure interactions, a field which is today one of the most treated subjects for SEA studies. Nowadays, there are several references about SEA in literature which can give a comprehensive explanation about this method [34, 35, 36]. Even though it was developed starting from the modal approach, the same expression of the CLF was found starting from the wave propagation approach [37]. Later on, Fahy would have presented the duality that occurred between modal and wave approach in the SEA [38] and more recently, clarifications about the necessary assumptions - through the modal approach and/or wave propagation approach - in the SEA framework are explained [39].

For *statistical*, it is intended that there is not a precise description of the structure under analysis, but this would be defined as ensemble of a certain number of subsystems, which are categorized by their dynamical behaviour in terms of wave propagation. *Energy* is the main variable to be studied, from which the vibrational velocity of each subsystem can be recovered. Finally, the term *analysis* refers to a qualitative approach more than to a proper theory as the Finite Element Method (FEM) can be. It is then identified the main difference that occurs between SEA and FEM: structures response is not studied in a deterministic way, concentrating the analysis on their modal characteristics, but as averaged vibrational response over a frequency domain. The method predicts the average response in three senses: the spatial average, the ensemble average and the frequency average.

(i) Spatial average is a consequence of the fact that the method predicts the overall vibration levels of the subsystem instead of the level of every single point on the subsystem.

(ii) Ensemble average refers to the average taken over a number of identical structures, which have random dynamic properties due to manufacturing tolerances.

(iii) Frequency average arises from the fact that SEA analysis is performed in frequency bands, which may be constant bandwidth or 1/3 octave bands.

As a consequence, the SEA is evaluated in a high frequency range, where the number of modes is great enough to consider the mean value response as an acceptable description of the structure dynamic behaviour (Figure 1.7).

As matter of fact, high-frequency studies based on a modal approach present limitations due to uncertainties on modal parameters and prohibitive computation times generated by the required mesh sizes. SEA, on the other hand, presents the advantage of having a small model size for the complete analysis of a complex structure. When the model required for a Finite Element Analysis is compared with the one required for SEA, it is obvious that the model for SEA makes the analyst more comfortable in analysing complex structures in a short period of time. Also, it allows the analyst to describe the system in a simpler way. This makes it possible to analyse the system even with simple hand calculations.

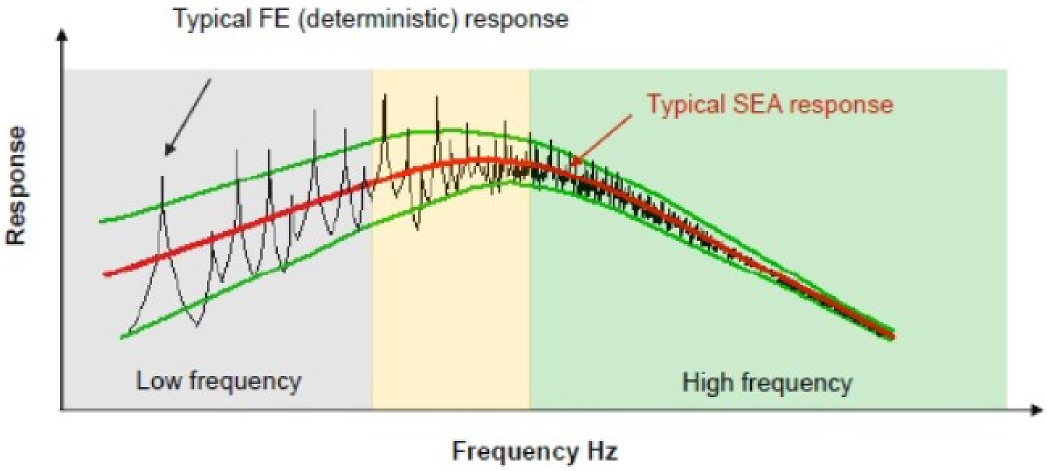

Figure 1.7: Comparison between a general deterministic response and SEA response in a frequency domain

Each subsystem is considered as an ensemble of oscillators whose natural frequencies present a uniform probability to be inside the considered frequency range. In other words, it is equal to say that each subsystem mode has same energy, same amplitude and same damping. For the extension of the method to multi-modal systems, Lyon made several hypotheses which are listed but not discussed in this work:

(i) The excitation spectrum is broadband, and the excitation forces are statistically independent. There are no pure tones in the input spectra.

(ii) There is no energy generation or dissipation in the couplings between the subsystems; in other words, the coupling is assumed to be conservative.

(iii) The damping loss factor is the same for each mode within a subsystem and frequency band.

(iv) Modes within a subsystem do not interact except to share equally partitioned energy.

After Lyon, other researchers dedicated their studies to SEA, finding new ways to express SEA equations, or understanding the assumptions and trying to overcome them.

In the following subsections, alternative methods to SEA are presented and explained, in order to find which is the best for design purposes.

1.3.2 Energy Flow Analysis

As said before, in the 1960s there was a high focus on the power flow analysis and on finding a representation of the coupling between two or more systems. One of the limitations that has been encountered with SEA is the description of a structure as group of resonant models considered all equally excited. As a consequence, each subsystem is described by a unique value and detailed information about the spatial variation of energy in the single subsystem is lost. An alternative method which had as aim to overcome this limitation was presented by Nefske and Sung [40]. At the beginning, the proposed name for this method was Power Flow Analysis and it was developed together with a FEM approach. In fact, a differential governing equation of the power balance within a system has been deduced; it has an analogous representation of the heat conduction governing equation. Then, the differential equation is solved numerically by implementation of a finite element formulation.

Later, the concept of energy flow described with a heat conduction equation was discussed by Wohlever and Bernhard [41], who developed the complete methodology for rod and beams systems. With Bouthier, the extension of the method to vibrating membranes [42], vibrating plates [43] and acoustic enclosures [44] was obtained.

Another limitation of SEA encountered was the application of any sort of excitation over the subsystems of a structure. In particular, with SEA, only a totally uncorrelated pressure field can be applied over each subsystem, as an equipartition of energy is assumed in all the spatial structural domain. With Han and Mongeau [45], Bernhard was able to express the power injected over a system through two different methods: the impedance method and the transfer function method. An analysis on the degree of correlation, from totally uncorrelated to totally correlated, between two punctual forces is also shown. The Energy Flow Analysis (EFA) has been studied by Park *et al.* [46], for the study of in-plane wave transmission between two thin coupled plates and also by Park [47] for what concerning the application of the Mindlin plate theory with the EFA.

As last reference worthy of mention is the work of Han *et al.* [48], in which the energy flow model of a plate in contact with a mean flow is considered.

EFA is based on the analogy with the heat conduction equation, which has been questioned by Langley [49], and continued to be studied by Jezequel group [50, 51, 52, 53, 54] because the derivation of EFA method has been judged "incomplete", meaning that the solution obtained has not the assumed form of response, hence he proposed a different derivation of the method. With the Vibrational Conductivity Approach, in fact, the variable is still individuated in the energy density, but the energy flow vector is expressed as structural intensity, predicting a far field energy density proportional to $1/r$, with r defined as the radius of wave propagation, and not to $1/\sqrt{r}$ as was done before with EFA.

Energy Flow Analysis is a powerful tool that allows to know the variation of energy density in the spatial domain of a structure; it allows also the analysis of power flow at the junction between two connected systems. Because it is based on the resolution of the differential energy equation, EFA is valid at any frequency and different type of loading can be considered. It can be used for a full design procedure that wants to take into account the particular characteristics of a material, or to check the dynamic behaviour of a structure at a specific frequency that might generate structural problems. The main disadvantages encountered with EFA are related to the simplicity of geometry required for the formulation development, the extensive computational time due to an analysis limited at one frequency at the time and to a lack of literature references regarding the application of EFA for more complex materials as composite or sandwich panels.

1.3.3 Energy Distribution Approach or SEA-like

Another method developed after the exploit of SEA was the Energy Distribution Approach (EDA), also known as SEA-like, because it was born starting from the SEA assumptions and from the intention of overcoming them. Mace approached to the SEA in the early 1990s, individuating at the beginning the possibility to express SEA not only with the modal approach, but also with the wave approach [55, 56]. He got interested specifically to the Coupling Power Proportionality, one of the main properties characteristic of SEA, and on the limitation for which it is not possible to describe the energy exchange between two subsystems that are not physically connected one to each other [57]. Therefore, he investigated with Wester [58] on the nature of coupling, using a wave approach between two rectangular plates; with Rosenberg [59], on the other hand, he deepened the same problem from a modal point of view, highlighting the effect that irregular geometrical shapes can have on the calculation of the system response and on the power flow among its subsystems. To do so, analytical wave solution application and numerical modal analysis have been used as comparison. The development of EDA was born from the research of a connecting link between modal analysis and SEA, in order to understand if the results of a finite element analysis can be post-processed as energy flow models [60]. In fact, he presented two modal methods for the calculation of the averaged vibrational response of a specific subsystem inside a structure, one based on the global modes of the whole structure (which will take the name of Energy Distribution Approach, EDA) and the second one based on the singular uncoupled mode shapes of each subsystem (component-mode synthesis, or CMS). They both are analysed from a computational point of view, and the one based on global mode shapes resulted more convenient because it requires less computational time. The approach had been developed more, until it has been presented as new method which would have covered the SEA limits, hence it took also the name of SEA-like [61]. Specifically, SEA is defined as "proper-SEA" if all the following assumptions are valid:

- Coupling Power Proportionality (CPP): the transmitted power between two subsystems is linearly dependent on the difference of the subsystems energies.
- Conservation of energy: the coupling is assumed to be conservative, hence at the junction the energy can be only transmitted or reflected.
- Rain-on-the-roof (ROR) excitation: the applied excitation must be statistically independent and totally uncorrelated.

- Indirect Coupling Loss Factors are null: the coupling can happen only between subsystems that are physically connected.
- CLFs are positive: referring to the heat transfer analogy, thermal energy can travel only from the warmest to the coldest system; equally, the vibrational energy can travel only from the system with more energetic content to the one with less energy.

EDA is called SEA-like because it requires just the CPP and the ROR excitation assumptions to work. Moreover, the governing matrix equation describing EDA has strong similarities with the SEA one [62]; while SEA uses CLFs for the description of the energy transmission, EDA is based on the calculation of the Energetic Influence Coefficients (EIC), where each coefficient A_{rs} represents the amount of energy that subsystem r receives if subsystem s is the power source.

Energy Distribution Approach gave an enormous contribution for the improvement of SEA. The coupling is considered in the whole structure, hence all pairs of modes are considered, not only the resonant ones. Thanks to the EICs, it is possible to understand the coupling nature, which depends on how the modes are distributed on both frequency and spatial domain.

Two disadvantages are prominent with this approach; the first one is the necessity of global mode shapes of the entire structure, which are required in order to evaluate the coupling among the modes. This would be possible only after a finite element analysis, if the structure is too complex. The second disadvantage is the assumption of Rain-on-the-roof excitation. This assumption does not make EDA available for energetic analyses of structure subjected to other type of excitation, as the TBL one, unless approximations on the excitation expression are made.

1.3.4 MODal ENergy Analysis

The use of global modes for the determination of energy distribution inside a complex structure and the consequent difficulty encountered with the formulation of CLFs were two obstacles that Maxit and Guyader [63, 64] wanted to overcome. They proposed a method called at the beginning Statistical modal Energy distribution Analysis (SmEdA); it was based on the oscillators relation developed in SEA and the further application of the dual modal formulation, for which the coupling between two systems can be expressed both through modal approach and wave propagation approach. The formulation of CLFs thus requires just the knowledge of the modes for the uncoupled subsystems and modal damping; for more complex structures, a finite element analysis might be useful for the determination of modes. The energy transmission is here analysed as energy exchange between a mode of one subsystem and a mode of another subsystem. Later on [65], the cross-modal terms were included, meaning that the hypothesis of broadband statistically independent and totally uncorrelated excitation has been overcome, together with the approximation of taking only resonant modes. The spatial variation of the energy distribution inside one subsystem has been taken into account too [66]. Finally, the indirect couplings are provided with another extension of the model, that would be named simply MODal ENergy Analysis (MODENA) [67]. As its previous versions, MODENA is based on the direct calculation of the coupling between two modes of two subsystems, individuating the coupling as gyroscopic, so keeping the assumption that the coupling is conservative. Then, a matrix of transfer functions referred to each pair of coupled modes is obtained and consequently, coupling coefficients are defined, so that the direct relation between total energies of each mode and transmitted power in between can be formulated. The coupling coefficients present an exact formulation if the applied forces are totally uncorrelated; otherwise, their formulation would be just an approximation. Thanks to this formulation, the coupling strength is also evaluated, in order to understand the coupling coefficients behaviour in function of their strength. It has been seen that for high values of coupling, the verse of energy transfer becomes inverted, as the two modes involved in the coupling present an "anti-thermodynamic" behaviour.

1.3.5 Conclusions

Different methods, all developed from Statistical Energy Analysis or Finite Element Method, were presented and discussed. All of them have as final aim the study of energy transmission between two subsystems of a structure; all of them tried to overcome the assumptions made for SEA, in order to expand its scope.

The present work wants to develop a design procedure which is able to estimate the energy transmission between two subsystems, both excited by a Turbulent Boundary Layer excitation. It has been seen that all the proposed methods were not able to overcome to the assumption of broadband totally uncorrelated excitation required by SEA. MODENA is the only one reaching a good approximation. It has also been seen that the coupling strength is still a topic under discussion that creates confusion about the rightful application of SEA or any other energetic method. Smith [68] proposed a definition of "weak coupling" based on a comparison between CLF and Damping Loss Factors (DLF): if CLF presented a higher value compared to DLF, then the coupling is considered strong. Mace and Wester [58] took advantage of the wave approach for the formulation of two parameters that would determine for which condition the energy got transmitted or reflected at the junction. Then, Finnveden [69] found a unique parameter γ, dependent on subsystems modal overlap factors and asymptotic mobilities, that represents the modal interaction or, for an ensemble of modes, the coupling power. Having a value of $\gamma < 1$ means that the conductivity of two elements is approximately equal to the travelling wave estimate, hence the two elements are not so influenced by each other and they can be retained uncoupled. The extension to multi-modal coupled subsystems has been covered with an iterative solution by Bessac, Gagliardini and Guyader [70]. Lafont *et al.* [71] analysed all the proposed parameters for the evaluation of coupling and they are all valid. What can be inferred from these methods is the common necessity for the subsystems to have a high value of modal overlap factor, in order to ensure that the condition of weak coupling is guaranteed by a huge number of modes in a frequency band and/or a high value of DLF.

With a focus on the design purposes, in particular on the simplicity and velocity of the design procedure, Statistical Energy Analysis has been chosen among all the proposed methods. Even though it is not the most accurate, and the assumptions made it seems very limited, SEA is the only one that can ensure a fast analysis in the high frequency (HF) regime, without the requirement of a modal analysis to get mode shapes and natural frequencies, with easy formulation for different subsystems (1D, 2D or 3D), but that can still ensure the possibility of design optimization through the change of parameters as area, thickness, stiffness and DLF. To overcome on the assumption of Rain-on-the-roof excitation required by SEA, TBL excitation is analysed in the next section, focusing on the research of alternative methods for its representation.

1.4 Equivalent expressions of structural response to an aerodynamic excitation

In the previous sections, different design techniques for wind tunnels facilities have been presented, stressing on the necessity of a generic and fast methodology to design a support for test models which can ensure an energy transmission decoupling between two systems. In order to assess the problem, Statistical Energy Analysis has been proposed for its simplicity as methodology to approach to the design rules. Consequently, it has been raised the problematic of the description of a spatially correlated excitation inside a SEA framework.

In this part of bibliography research, it is wanted to focus the attention on alternative methods for the TBL representation. Firstly, because it is wanted to apply a TBL excitation in a SEA framework, hence it is necessary to convert a correlated pressure field in a totally uncorrelated one, as the Rain-On-the-Roof excitation is. Secondly, for the final purpose of the structural design, it is wanted to test the developed structure without the use of a wind tunnel facility. As a consequence, investigations about how to obtain a structural response due to a TBL with alternative instrumentation are carried out too.

For what concerning the representation of vibrational response of a structure subjected to a generic load, the first problem encountered is the coupling between the structure and the type of excitation. Guyader *et al.* [72] recognized that the energy transmission between two simple systems, as for example plates, is governed by three different mechanisms: spectral, spatial and excitation coupling. To reach the SEA formulation, three assumptions were made: (i) loads applied on two different systems are uncorrelated, (ii) each load applied on each system has a spatial delta-correlation, and (iii) loads must be described as mechanical point excitation. Dimitriadis and Pierce [73] reached the same conclusions when they tried to reach SEA formulation as Guyader did, with the only difference that Guyader used global mode shapes of coupled systems, while Dimitriadis and Pierce used local mode shapes of uncoupled systems.

Narrowing the study on the excitation exploited by a fluid-structure interaction, Pan and Bies [74] concentrated their attention on the modal interaction between a sound field and the structure on its boundary. Taking as numerical model a plate coupled with an acoustic cavity, they individuated the term which describes the modal interaction. This parameter can be calculated as spatial integral of the product between the structure mode shapes and the acoustic cavity mode shapes. It is then found a coupling coefficient that would estimate the level of fluid-structure coupling strength. The coupling term found by Pan and Bies is nothing else than the cross-acceptance function that can be derived from the Cross-Spectral Density (CSD) of the structural response subjected to a generic distributed random pressure field formulation [75].

Hence, the main problem to solve is to find a suitable TBL formulation which would enable analytical simplifications, and at the same time would conserve the spectral and spatial content of a turbulent boundary layer.

1.4.1 Turbulent Boundary Layer and its representations

When a structure is in a flow of velocity U_∞, there is an interaction between the fluid and the wall of the structure. At the wall, the viscosity of the fluid imposes adhesion so the relative velocity of the flow is zero at this level, then beyond a certain distance, called the

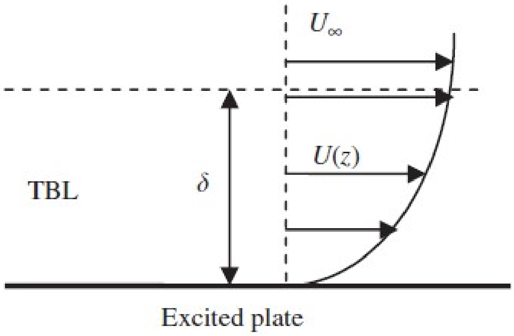

Figure 1.8: Turbulent Boundary Layer development over a plate for an asymptotic flow speed U_∞.

thickness of the boundary layer [76], the interaction between the flow and the structure is zero; the further away from the wall, the more the velocity increases to the velocity of free flow (Figure 1.8).

Until today, there is a lack of theoretical and numerical validated models which can describe the wall-pressure fluctuations (WPFs) [77]. To describe the aerodynamic excitation exploited by a turbulent flow over a structure, in fact, semi-empirical models have been developed, which always need to be compared with a reference.

As 1-point spectra, for example, one can take into consideration the Goody model [78]. It is considered one of the best empirical model, obtained from a previous theoretical formulation developed by Howe [79], because it is the model that fits at the best the empirical collected data in a very large Reynolds number range. Nevertheless, it is preferable to express WPFs as Cross Spectral Density (CSD) because, thanks to the wavenumber-frequency representation, the dispersion relations due to propagation of acoustic waves or the convection of turbulent flow are immediately visible. As 2-point spectra model (Figure 1.9), there are different correlation function expressions that can be used.

Corcos model [80, 81] and Mellen model [82] are provided of two free parameters for the description of the flow condition. Both models describe a convective pattern with exponential correlation decay; the main difference between these two representations lies in how this correlation decays in longitudinal and transverse directions. While Mellen

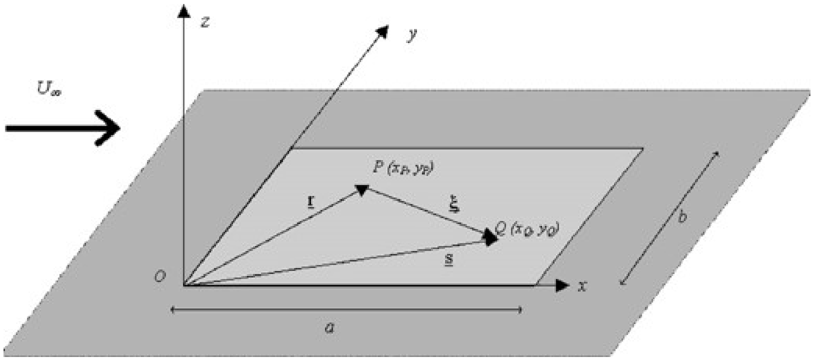

Figure 1.9: Representation of a plate subjected to an air flow of asymptotic speed U_∞; two points are represented to stress the dependence that 2-points spectra excitation models have on the distance between them.

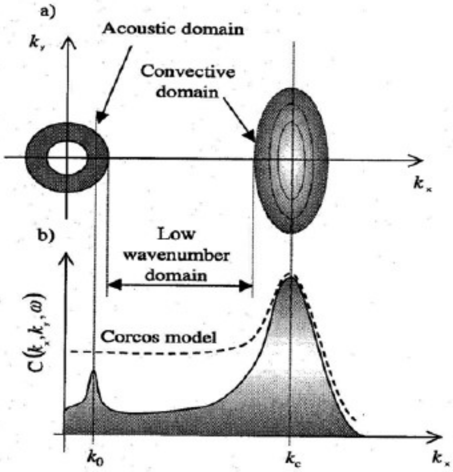

Figure 1.10: Chase model in the wavenumber domain.

chose an elliptic shape for the frequency/wavenumber domain, Corcos presented an easier representation for which longitudinal and transverse correlation can be considered separated. Corcos model is precise for the description of WPFs in the convective region, especially around the convective coincidence frequency, where structural wavenumber and convective wavenumber are coincident. In the subconvective region, on the other hand, this model tends to overestimate the actual WPFs value.

Chase [83] wanted to overpass the limits that other older models presented; the aim was to represent at the best the so called "subconvective" domain, integrating the acoustic contribution in the convective region (Figure 1.10).

Without going too deep with the explanation of the terms presented in Chase model, it is important to mention that seven independent coefficients have been determined for the description of both the convective region and the acoustic domain. Although it is recognized the precision that this model has in the subconvective region, the use of so many free parameters can result inconvenient.

Corcos model is still one of the first choices for what concerning the prediction of the structural response to a TBL excitation for the following reasons:

- space variables are separated;
- the correlation function does not depend on the points location, but just on their relative distance;
- the correlation decay is expressed in exponential form along both directions in the same way;
- the phase-variation is encountered just along the stream-wise direction;
- it presents an optimal TBL representation around the convective region;
- it allows the calculation of closed-form expressions for a panel response.

As matter of fact, in the following subsections, alternative methods for the TBL excitation representation are discussed, and most of them based, indeed, their methods on the Corcos model.

1.4.2 TBL excitation as a Rain-in-the-Roof

One of the first methods recur to the spatial extent equivalence [84], with which Ichchou *et al.* were able to obtain an equivalent correlation function $C^{eq}(\omega)$ by solving the cross acceptance function considering a spatial δ-correlation as the ROR excitation presents [85]. In this way, the TBL excitation (based on Corcos model) would be described as a spatially uncorrelated excitation, keeping the spectral information about TBL inside the $C^{eq}(\omega)$ expression.

The application of the Equivalent-TBL (ETBL) excitation finds an optimal agreement with the exact solution of a plate response to a TBL Corcos-like excitation in the HF domain, where the correlation lengths present much smaller values if compared to the length of the excited structure.

The ETBL excitation formulation finds its application also in numerical simulations as Finite Element Method (FEM) [86]. In particular, it is stressed the huge limit that a FE numerical simulation encounters once it is wanted to represent the structural response to a TBL excitation until a certain excitation frequency. As matter of fact, the translation of a convective stochastic load in a discrete coordinate field has its own complexity due to the minimum FE dimensions choice for the mesh realization. There is, indeed, an aliasing frequency, after which the aerodynamic load is not well represented through the FE mesh and consequently, the structural response diverges. More the convective speed is low, more the FE mesh needs to be fine in order to move the aliasing frequency as much as possible in the HF domain. Always in [86], together with another spatially uncorrelated expression of a TBL excitation based on the work of Hong and Shin [87], the ETBL excitation is compared with the formal TBL Corcos model; it can be appreciated that with a delta-correlation spatial distribution, the dependence on the FE mesh resolution is avoided and there are no more problems of structural response divergence.

1.4.3 TBL excitation as an Uncorrelated Wall Plane Waves

The attempt of recreating a structural response to a TBL excitation with an "off-line" methodology started in the sixties with Fahy [88], who suggested the use of shakers or loudspeakers to simulate the TBL wall-pressure fluctuations, but because of practical difficulties encountered at the time, he never tested these alternative solutions. For what concerning the use of shakers, it has been noticed that the shakers location does not depend on the convective flow speed, but a preliminary modal analysis of the structure is essential in order to know the number and the location of the shakers [89]. The real first study about the implementation of loudspeakers for the off-line prediction of a structural response to a TBL excitation was carried out by Elliott *et al.* [89], followed by Maury and Bravo [90, 91]. The result of the application of their developed method was the inconvenient use of a large number of loudspeakers.

Aucejo *et al.* proposed the same method, introducing this time a synthetic array of acoustic sources, in order to solve the problem of the required huge number of loudspeakers [92]. The method is based on the assumption that the effect of a TBL excitation over a structure can be approximated by a state of diffuse field inside the same structure. The diffuse field can be created with the summation of the effect of an infinite number of uncorrelated wall plane waves (UWPWs), with same amplitude, and with origin from all spatial directions. The concept of synthetic array is reproduced thanks to sequential measurements. Maxit [93] continued his study about UWPWs focusing on the criterion for finding the cutoff wavenumbers in the parallel and normal directions of the flow, so that the wavenumbers truncation would not effect the structural response with a divergence. Marchetto *et al.* investigated firstly the actual reproduction of a Diffuse Acoustic Field (DAF) over a simple structure, i.e. a panel, developing a method based on the sensitivity functions calculation [94], then the same method has been applied for the case of a TBL excitation application [95] and, finally, experimental tests were performed in order to prove the validity of the UWPWs excitation method [96]. Karimi *et al.* have further developed this approach by investigating if the radiated sound power of a panel subjected to a TBL excitation can be estimated using UWPWs [97] from an analytical and numerical point of view; immediately after, a hybrid approach which links UWPWs and FEM has been presented [98] and finally it has been applied for synthesizing realizations of an airfoil surface pressure induced by incoming turbulence [99].

What it can be said about the UWPWs method is that it is based on the same assumption with which the Equivalent TBL excitation has been derived: when frequency increases, especially after passing the convective coincidence frequency, the TBL excitation presents the same characteristics of a Rain-on-the-Roof excitation, which corresponds formally to an infinite number of uncorrelated excitations points. In [39], it has been demonstrated that the assumption of ROR excitation application implies the state of diffuse field inside a system. As a consequence, the application of a Rain-on-the-roof or of an Uncorrelated Wall Plane Waves will lead to the same solution.

1.4.4 TBL excitation as spatial-correlated pressure field

The original intention of Elliot *et al.* work [89] was to understand how to recreate the spatial-correlation function characteristic of the TBL excitation. With Maury *et al.* [100], an actual simulation of a TBL pressure field with the use of an array of loudspeakers has been developed, focusing the attention on the required number of loudspeakers necessary to obtain the spatial correlation function similar to the TBL one. Later on, Bravo and Maury would describe the methodology applied behind the actual experiment [90, 91]; they had to use a near-field array of acoustic sources, i.e. loudspeakers, driven by a set of mutually correlated signals in order to rebuild the pressure field correlation function over a grid of microphones located next to the panel surface. As it has been said before, the number of required loudspeakers is prohibitive for this type of experiment. Moreover, in [101], the use of actuators as shakers or piezoelectric elements has been re-evaluated, even though it must be specified that the good agreement was found in a frequency range over the convective coincidence frequency. As it can be deduced, the work of Maury and Bravo paved the way to the study of off-line methodology for the reconstruction of a structural response to a TBL excitation, approximating the aerodynamic excitation as a spatially uncorrelated pressure field; the attempt to describe the actual TBL spatial correlation seems not to have been pursued.

Berry, Dia and Robin [102] proposed a new strategy, called Wave Field Synthesis

(WFS). Originally proposed by Berkhout *et al.* [103], the WFS is based on the Huygens' construction principle, for which a wave field generated by a source in a give time can be reconstructed if the wave-front is substituted by a set of secondary sources in a later time. With the application of this principle, researchers were able to calculate the CSD of the required monopole source for the reconstruction of the sound pressure over the test panel. The method got applied for three different excitation cases: acoustic plane wave, diffuse acoustic field and turbulent boundary layer. What it has been noticed with this approach is that WFS is able to reconstruct the first two types of excitation, but it encounters some limitations for what concerning the TBL excitation reconstruction. The problem is related to the TBL correlation scales, which are significantly smaller than the correlation scales of the reproduced acoustic field.

Robin, Berry and Moreau [104], proposed the Planar-Nearfield Acoustic Holography (P-NAH), originally created for the prediction of acoustical quantities on a surface, and then applied for the reproduction of a sound field. Considered two parallel surfaces, one representing the test panel and the other representing the sound pressure source, and given the CSD of the pressure field on the test panel, it is possible to know the corresponding particle velocity CSD on the parallel surface; this means that the monopole array for the sound pressure field reproduction is now described by the particle velocity over its surface. For the principle of reciprocity, it is hence possible to obtain the sound pressure field that the monopole array should generate.

The two methods have been applied for experimental procedures [105, 106], keeping a focus on the realization of subsonic and supersonic TBL excitation. The main difference between these two conditions lies in the number of reproduction sources considered in the array, in order to respect the pressure field correlation lengths. For supersonic TBL, the convective wavelength results greater than the acoustic wavelength, so the source array sound pressure field is able to reproduce the TBL excitation. For subsonic TBL, the convective wavelength is smaller than the acoustic one, thus the number of sources cannot be related to the acoustic wavelength anymore. To obtain a faithful reproduction of a TBL excitation, there should be at least 4.2 monopoles per correlation wavelength.

1.4.5 TBL excitation as Pseudo-Equivalent Deterministic Excitation

As last method dedicated to the prediction of a structural response to the WPFs generated by a TBL, the Pseudo-Equivalent Deterministic Excitation method (PEDE$_M$) is here presented [107]. PEDE$_M$ has been developed starting from the Pseudo-Excitation Method (PEM); this finds its roots in the seismic structural analysis. Going back to the 1980, Der Kiureghian [108] proposed at the time a new CQC method for random vibration analysis of structures subjected to stationary excitations. This has been officially introduced as Pseudo-Excitation Method in [109] and then used by Lin [110] as algorithm for random seismic responses, non-stationary random seismic responses [111], vibration analysis of wind-excited structures [112]. An analysis of the real excitation also can be developed using the Inverse Pseudo-Excitation Method (IPEM) [113].

PEM is based on the simple concept that a generic zero-mean stationary random excitation can be substituted by a pseudo-equivalent harmonic excitation whose amplitude is equal to the square root of the PSD of the original excitation. Consequently, with the Frequency Response transfer function, one can get the response and the PSD of the response to this excitation. In other words, it is possible to get the pseudo-harmonic response, which is the response to an equivalent harmonic excitation. PEM is formally an exact numerical representation of the excitation since it is based on the modal decomposition of the load CSD matrix. Depending on the characteristics of the CSD matrix, different types of methodologies can be applied in order to get the modal decomposition. The most efficient one perhaps is the Cholesky scheme [114], or also called LDL decomposition. PEM was originally introduced with the final aim of solving the high computational time required for the application of a standard random vibration method. Even though it gave a great contribution, PEM still presents a computational time unacceptable, since the extrapolation of the eigensolutions at each frequency through modal decomposition, can be time consuming.

PEDE$_M$ comes to help by introducing some approximations based on the study of the load matrix eigensolutions behaviour in function of frequency. With this eigensolutions analysis performed over a TBL excitation, it has been noticed two asymptotic behaviours. In the HF region, the TBL excitation can be approximated as a totally uncorrelated pressure field, as a Rain-on-the-Roof; the eigenvectors related to this type of load are identified as the columns of an identity matrix. In the low frequency (LF) region — or more precisely, in the limit condition of $\kappa \implies 0$, where $\kappa = \omega\Delta/U_c$ is an adimensional frequency dependent on frequency ω, convective flow speed U_c and on the mesh size Δ used the sample the excitation spatial distribution — the TBL excitation is reduced to a normal incident wave, hence the pressure field is totally correlated [107]; the eigenvectors related to this type of load are identified as the columns of an all-1 matrix. With these approximations, the eigensolutions calculation is significantly reduced and a good reproduction of the structural response to a TBL excitation is obtained.

1.4.6 Conclusions

With PEDE$_M$, one can see reunited the two main approximations considered for a TBL realization that many others used in their own researches. Although the use of a spatially uncorrelated pressure field (ROR excitation) has been tested many times and different applications now exist, the realization of a totally correlated pressure field may still provide some complications, from numerical and experimental point of view.

PEDE$_M$ has been chosen as starting point for the development of an "off-line" validation method of structural design. In Chapter 4, the basic theory concerning PEDE$_M$ and its development is introduced, in order to provide all the necessary tools at the beginning of Chapter 5, where explanation and application of the "off-line" methodology is shown.

1.5 Main Conclusions

As conclusion of this first chapter, a brief recapitulation is herein given:

- from the wind tunnel facilities literature survey, it has been discovered that there is a solid knowledge about the general guidelines for the structural design of this kind of facilities. On the other hand, when it is wanted to focus the attention on the methodologies of allocation of a test model inside the test section, there is a huge variety of techniques, most of them are not tested before while others are improved during the test in the wind tunnel. With the final aim of guarantee the purity of the measurements taken inside a wind tunnel, guidelines for the structural design of a support for test models are here proposed.

- For the development of these design guidelines, it is wanted to use a method that would be easy, fast to use, and that would ensure its application for any type of support it is wanted to design. In the second literature survey, different methods have been analysed in order to choose the most adequate for the exposed intentions of this work. Statistical Energy Analysis has been picked for its simplicity and the incredible low computational time. Moreover, it permits the design analysis for any kind of material and any kind of structure.

- By choosing the SEA as method of the development of the support design guidelines, it is required by the SEA that the described excitation must have a totally uncorrelated spatial distribution, as a Rain-On-the-Roof excitation. Thus, as last literature survey, it has been wanted firstly to understand the TBL excitation, and secondly to study alternative methods for its representation. Because it is wanted to validate the structural support, this research work wants to offer not only the guidelines for its design, but also an "off-line' methodology for the experimental test of the support before bring it inside the wind tunnel.

~~In Chapter 2, a theory introduction to SEA is given, in order to provide the necessary tools for the comprehension of the design guidelines development. Then, a design development of a simple, but characteristic of a real setting of a support-test panel system is shown and described step by step. In Chapter 3, the design guidelines are then applied for a complex structure created to be located in a large-scale wind tunnel facility.~~

CHAPTER 2

AN ENERGY TRANSMISSION DECOUPLING TECHNIQUE FOR A SIMPLE STRUCTURE

2.1 Introduction

The aim of the present research work is to develop a design of a structure which would support a test panel in order to perform vibroacoustic measurements in a wind tunnel facility and collect information about the effects of a TBL excitation over the aforementioned panel. The target of this design procedure is to ensure a purity of measurements; in the specific, it is wanted that the TBL-induced vibrations of the support will not effect the test panel vibrations, so that the measured structural acceleration and emitted noise will not be contaminated.

In the previous chapter, it has been noticed that there is not a unique procedure for what concerning the support design. Depending on the choices of the wind tunnel designer or on the experimenter who would use the facility, the procedure to ensure the measurements purity would change. Moreover, different methods for the calculation of energy transmission from one subsystem to another have been presented, highlighting their advantages and disadvantages.

For the development of the formulation to use for the design process, Statistical Energy Analysis has been chosen as method to start with. The reasons of this choice are several:

- the support-test model system is a structure that, most of the time, is created on the spot before a wind tunnel test; hence, the experimenter cannot spend too much time on the elaboration of the support, but he needs a quick process in order to set-up the experiment. With SEA, the calculation does not spend a high computational time, whether they are for a simple or a complex structure.

- specific material properties are not required for the design process; SEA subsystems are treated as they have an equivalent-isotropic behaviour, because of the assumption of equipartition of energy inside all subsystems, for which the wave propagation is homogeneous in all directions. Therefore, if one considers as example a laminate composite material, this would not be described in function of material properties in the main directions (i.e. E_x, E_y, ν_{xy}, etc.), but in function of their averaged value. This choice may be interpreted as lack of information from a local point of view, but since the target is to evaluate the energy transmission between two different systems, their average behaviour is enough to take in consideration.

- SEA has been one of the first methods that concentrates its analysis on the energy transmission among subsystems of a structure. Although other methods have been developed after SEA, they all required more specific details in order to run simulations. EDA needs the mode shapes of the entire coupled structure. EFA essentially concentrates the analysis on the locally distribution of energy inside a single subsystem, which it may be considered for a more focused analysis, but not for a first approach to a structural design. SmEdA and MODENA methods recover the analysis of indirect couplings which SEA is not able to study, but they require a modal analysis for the uncoupled subsystems and, for that, it might result time consuming for the type of analysis that it is wanted to do, especially if complex structures are considered.

In this chapter, a generic process for the design of a support, which would be located in a wind tunnel facility, is presented. In Section 2.2, A brief recapitulation of SEA main formulations is given, followed by the extrapolation process for the design guidelines; in Section 2.3, the generic design rules are recovered and explained in details, considering the effect of main design parameters as geometry (area and thickness) and type of material. The design rules are then applied for a simple support-test panel system in the high frequency (HF) domain (Section 2.4). Finally, in the final section, some conclusions are drawn in order to summarize the strengths and the weaknesses of the design method.

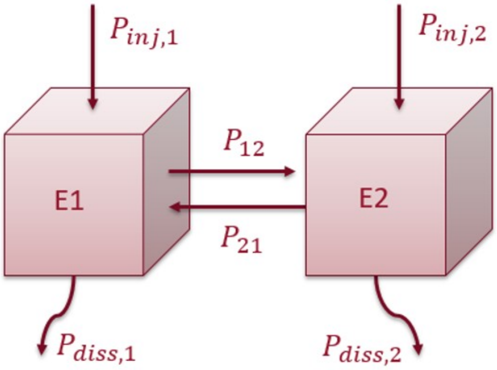

Figure 2.1: Representation of power equilibrium between two subsystems of a structure.

2.2 Development of methodology from Statistical Energy Analysis

The SEA energy method is based on the analogy with the heat transfer between systems. It consists in decomposing a complex structure into coupled substructures, or subsystems, and performing a power balance between them. The power balance expression involves the estimation of the injected power into the subsystems, the exchanged power between the subsystems and the dissipated power by the subsystems. Injected, transmitted and dissipated powers are all in equilibrium in each subsystem, as it is represented in Figure 2.1.

2.2.1 Brief introduction to SEA parameters

Without deepening in the derivation of SEA expressions, the formulas which will be useful in the developing the design process are here introduced.

Dissipated Power

The dissipated power $P_{diss,i}$ referred to the i-th subsystem is defined as

$$P_{diss,i} = \omega \eta_i n_i E_{m,i} \tag{2.1}$$

where ω is the central frequency of the considered frequency band, η_i is the Damping Loss Factor (DLF), n_i is the modal density and $E_{m,i}$ is the vibrational modal energy, defined as $E_{m,i} = E_i/n_i$, where E_i is the total energy considered inside the subsystem.

Transmitted Power

The transmitted power from a subsystem i to a subsystem j presents the linear dependence on the energies difference between two connected subsystems and here is expressed in a SEA context as

$$P_{ij} = \omega\eta_{ij}\left(E_i - \frac{n_i}{n_j}E_j\right) \tag{2.2}$$

in which the Coupling Loss Factor (CLF) η_{ij} between subsystems i and j is identified.

SEA matrix system

With Equation 2.2, the reciprocity relationship [29, 30, 31] can be introduced

$$n_i\eta_{ij} = n_j\eta_{ji}. \tag{2.3}$$

This reciprocity relationship is of practical interest since it allows, for a complex system, to determine only part of the coupling loss factors. The introduced parameters allow to express the SEA power balance. In the simple case of two subsystems, the power equilibrium on each subsystem is set:

$$\begin{cases} P_{inj,i} + P_{ji} = P_{diss,i} + P_{ij} \\ P_{inj,j} + P_{ij} = P_{diss,j} + P_{ji} \end{cases} \tag{2.4}$$

From the previous relations, one can write the following matrix system:

$$\begin{bmatrix} \eta_i + \eta_{ij} & -\eta_{ji} \\ -\eta_{ij} & \eta_j + \eta_{ji} \end{bmatrix} \begin{Bmatrix} E_i \\ E_j \end{Bmatrix} = \frac{1}{\omega} \begin{Bmatrix} P_{inj,i} \\ P_{inj,j} \end{Bmatrix} \tag{2.5}$$

The total energies are obtained by simple matrix inversion. The approach presented can be generalized to the case of n subsystems:

$$\begin{bmatrix} \eta_1+\sum_{j=2}^{N}\eta_{j1} & -\eta_{21} & \dots & -\eta_{N1} \\ -\eta_{12} & \eta_2+\sum_{j=1,j\neq 2}^{N}\eta_{j2} & & -\eta_{N2} \\ \vdots & & \ddots & \\ -\eta_{1N} & \dots & & \eta_N+\sum_{j=1}^{N-1}\eta_{jN} \end{bmatrix} \begin{Bmatrix} E_1 \\ E_2 \\ \vdots \\ E_N \end{Bmatrix} = \frac{1}{\omega} \begin{Bmatrix} P_{inj,1} \\ P_{inj,2} \\ \vdots \\ P_{inj,N} \end{Bmatrix} \tag{2.6}$$

The CLF matrix is symmetrical when considering the verified reciprocity relationship (Equation 2.3). The resolution of a SEA system thus requires the knowledge of CLFs, DLFs and the properties of the subsystems, all represented by the modal density term.

Modal density

The modal density is defined as the number of modes per unit frequency (Equation 2.7).

$$n(\omega) = \frac{\Delta N}{\Delta \omega} \tag{2.7}$$

As matter of fact, it is a statistical property which can be calculated just knowing the natural frequencies of a structure, but moving the analysis in a HF region can make this calculation time consuming. On the other hand, asymptotic formulations of modal density depend on very few parameters, and all characteristic of the structure. It is possible to obtain an analytic formulation if the exact sequence of natural frequencies is known, or refer to derived general formulas for 1D, 2D and 3D systems [115].

For a 2D system, the modal density expression is derived with the wave propagation approach [36]

$$n(\omega) = \frac{S\omega}{2\pi}\frac{\kappa(\omega)}{c_g(\omega)} \tag{2.8}$$

where S is the surface, c_g is the group velocity and κ is the wavenumber. The group velocity c_g, is the speed referred to a wave packet, which is a spatially limited perturbation. From a mathematical point of view, c_g is defined as

$$c_g = Re\left(\frac{d\omega}{d\kappa}\right) \tag{2.9}$$

Considering this definition of c_g, it is just necessary to know the formulation of the wavenumber and the calculation of the modal density for any 2D system is ensured. Wavenumber formulations are nowadays known for any kind of system and for any kind of wave propagation [36]; in literature, the research has moved towards the expression of SEA parameters for complex configurations of 2D systems as composite materials [116], and for sandwich panels [117, 118].

Coupling Loss Factors CLF

The exchanged power relation previously presented (Equation 2.2) is written in such a way to introduce the Coupling Loss Factor term η_{ij}. For the determination of this term, Lyon [33] used the modal approach, using the ensemble of two oscillators as an analogy of structure modes representation. However, the author introduced in his book [34] a notion of duality between a modal description and a wave description of the model studied. This notion of duality is very important when studying SEA models and the choice of a type of description is linked to the problem encountered. In the case of obtaining CLF using an analytical method, the simplest and most widely used approach is the wave one. Coupling loss factors are generally derived, in the case of coupling between simple subsystems such as beams, plates or shells, from the calculation of the average transmission coefficient between the subsystems. The vibrational behaviour of the structures is then represented by a superposition of plane waves solutions of the free motion equations [119]. The excitation is modeled by an incident wave on the junction at an angle θ generating reflected and transmitted waves in the coupled media (Figure 2.2).

Writing the coupling conditions at the junction then allows to obtain the amplitudes of

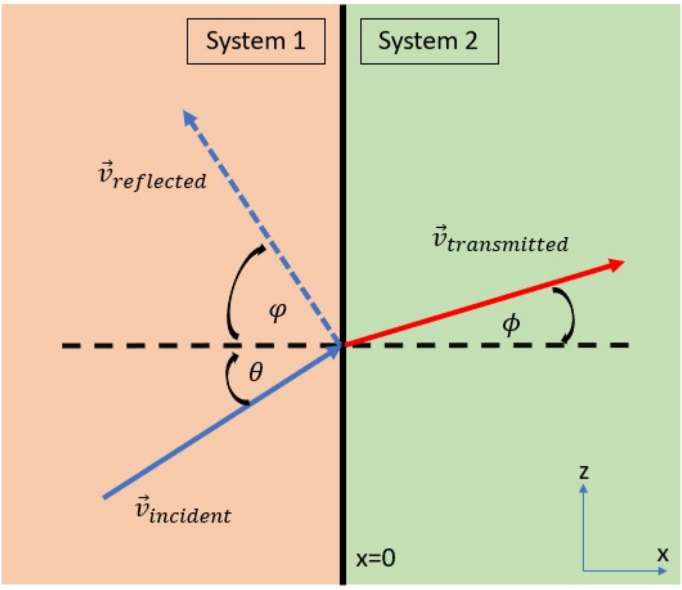

Figure 2.2: Wave transmission at the junction of two coupled systems. The wave propagation angle θ is the angle formed by the wave with the normal to the junction.

the different types of waves, and to calculate the transmission coefficient $\tau(\theta)$ defined as the ratio between transmitted power and incident power at the junction, for a type of waves considered. Lyon and Eichler [30] developed the transmission coefficient expression between two semi-infinite plates, taking into consideration the bending waves for the vibrational field representation in the coupled systems. Later on, Cremer, Heckl and Ungar [119] would able to determine the transmission coefficient for oblique incident waves. Wöhle *et al.* [120] would summarize the calculation of transmission coefficients among 2D systems for longitudinal, shear and bending wave propagation. The expression of CLF is hence defined as

$$\eta_{ij} = \frac{c_{g,i} l_{ij}}{\pi \omega S_i} \int_0^{\pi/2} \tau(\theta, \omega) d\theta \tag{2.10}$$

where $c_{g,i}$ is the group velocity of the source subsystem i, l_{ij} is the length of the junction which connects the two subsystems and S_i is the surface of the source subsystem.

Bosmans, Mees and Vermeir [121] would determine the CLF expression for orthotropic plates and later on also for anisotropic plates [122].

Modal Overlap Factor (mof)

The modal overlap factor, mof, is an indicator often used in SEA analyses to justify the validity of the diffuse field hypothesis. From the definition of the modal density within a frequency band, mof can be defined as

$$mof(\omega) = n(\omega)\omega\eta \tag{2.11}$$

One can consider the vibrational field to be diffuse for mof values greater than 1. The applicability of SEA must indeed verify a number of modes per band large enough to consider averaged energies, as well as a damping to verify that the modal overlap is large enough to make the hypothesis of a diffuse vibrational field.

Injected Power

One of the main assumptions of SEA is about the type of excitation considered over the SEA systems. Because a diffuse field is assumed inside the structure for the transmission coefficient calculation, and because SEA works with terms averaged over space and frequency domains, a statistically independent spatially uncorrelated excitation as Rain-On-the-Roof (ROR) is the only kind of excitation that can be considered in a SEA framework. The injected power expression is hence defined as

$$P_{inj}(\omega) = \frac{1}{2}Y_\infty(\omega)S_0 \tag{2.12}$$

where S_0 is the constant PSD of a ROR excitation and $Y_\infty(\omega)$ is the asymptotic mobility, obtained by integration over space and frequency domains of the point mobility [36]

$$Y_\infty(\omega) = \frac{1}{S\Delta\omega}\int_S\int_{\Delta\omega} Re\{Y(x,y;\omega)\}dSd\omega = \frac{\pi n(\omega)}{2M} \tag{2.13}$$

which results in a lighter expression dependent only on modal density and mass M of

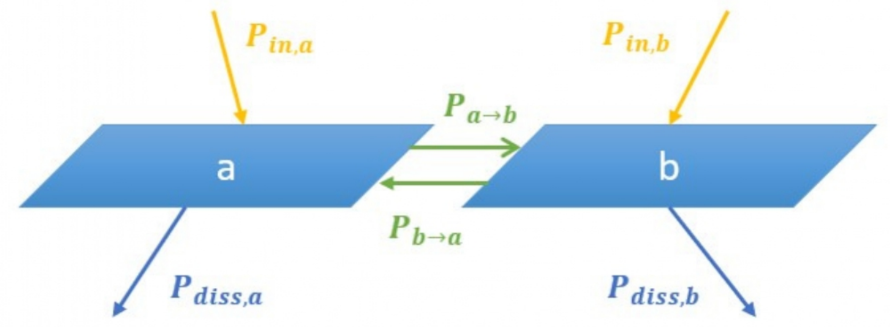

Figure 2.3: Representation of the support-test model system in a SEA framework.

the system. This expression is valid for any type of system.

2.2.2 Development of the design guidelines

As target to accomplish through the design rules, it is wanted to ensure a vibrational velocity gap between the two subsystems equal or greater than 20dB. For the application on SEA, the coupling between support and test model is already assumed to be "weak", meaning that the design rules developed with this method have a sure validity in the frequency range for which the modal overlap factors are greater than 1. For the development of design guidelines, it is first important to identify which are the systems that participate to the energy transmission and describe them in a SEA framework. With reference to Figure 2.3, one can associate to subsystem "a" the test model and to subsystem "b" the support.

Both subsystems are subjected to a TBL excitation, which is represented by the injected power P_{inj}. For the representation of a TBL excitation in a SEA framework, it is here applied the spatial extent equivalence as in [85], in order to obtain a formulation which would approximate the TBL in a totally uncorrelated Equivalent-TBL (ETBL). The injected power, hence, is defined as

$$P_{inj} = \frac{1}{2} Y_\infty S_{FF}^{ETBL}(\omega) = \frac{1}{2} Y_\infty C_{eq}(\omega) A S_{pp}^{ROR} \tag{2.14}$$

where

$$C_{eq}(\omega) = \frac{U_c^2}{\omega^2} \frac{4\alpha_x}{\alpha_y(1+\alpha_x^2)} \tag{2.15}$$

is the equivalent correlation function obtained through the spatial extent equivalence; U_c is the convective flow speed, which is usually equal to a fraction of the asymptotic flow speed ($U_c = \beta_c U_0$); α_x and α_y are the Corcos empirical coefficients, which characterize the TBL behaviour; A is the subsystem area which is subjected to the load; S_{pp}^{ROR} is the PSD of a Rain-on-the-Roof pressure field, which is usually considered unitary.

The energy transmission between the two subsystems is represented by the transmitted power P_{ij}. Hence, the energy contribution that the support (subsystem "b") gives to the test model (subsystem "a") is represented by the term P_{ba}. On each subsystem, it is possible to define the equilibrium of all powers acting on it; for the generic subsystem i, the power equilibrium is

$$P_{inj,i} + P_{ji} = P_{diss,i} + P_{ij} \tag{2.16}$$

This equilibrium stands before any SEA assumption because it is another form of the Second Law of Dynamics. The physical condition, for which both subsystems are subjected to a TBL excitation, is herein considered. The power equilibrium over the test panel, or subsystem "a", is then taken under study. The objective is to minimize the power contribution that the support (subsystem "b") transmits to the test panel; consequently, it is possible to take out from Equation 2.16 the TBL direct contribution $P_{in,a}$ and obtain the following dis-equation

$$P_{ba} \ll P_{diss,a} + P_{ab} \tag{2.17}$$

in which the relationship between the energy transmitted by the support is related to the energy outcome of the test panel. If the transmitted power P_{ba} is minimized, it means that the test panel vibrational energy is caused mostly by the direct excitation.

Once dis-equation 2.17 is considered in a SEA framework, it is possible to apply the SEA formulations and express the powers as function of the subsystems modal energies, CLFs and modal densities

$$\omega\eta_{ba}n_b E_{m,b} \ll \omega\eta_a n_a E_{m,a} + \omega\eta_{ab} n_a E_{m,a} \quad \rightarrow$$

$$\rightarrow \quad \eta_{ab}E_{m,b} \ll \eta_a E_{m,a} + \eta_{ab}E_{m,a} \tag{2.18}$$

by putting in evidence the total energies ratio E_a/E_b, one can obtain the following expression

$$\frac{E_a}{E_b} \gg \frac{n_a}{n_b}\frac{\eta_{ab}}{\eta_a + \eta_{ab}} \tag{2.19}$$

By invoking the equipartition of energy assumption, kinetic and strain energies are on average equal, hence the mean squared vibrational velocity is obtain from the total energy ($E = \frac{1}{2}M < v^2 >$)

$$\frac{< v_a^2 >}{< v_b^2 >} \gg \frac{M_b}{M_a}\frac{n_a}{n_b}\frac{\eta_{ab}}{\eta_a + \eta_{ab}} \tag{2.20}$$

Hence, it is possible to move directly in deciBel scale by defining the two subsystems vibrational velocity levels as

$$L_{v_a} = 10\log_{10}(\langle v_a \rangle^2) \tag{2.21}$$

$$L_{v_b} = 10\log_{10}(\langle v_b \rangle^2). \tag{2.22}$$

and their difference equal to $\Delta v^2 = L_{v_a} - L_{v_b}$, so that the direct vibrational velocity levels difference between two subsystems is directly connected to their properties, as mass and modal densities

$$\Delta v^2 \gg 10\log_{10}\left(\frac{n_a}{n_b}\right) + 10\log_{10}\left(\frac{M_b}{M_a}\right) + 10\log_{10}\left(\frac{\eta_{ab}}{\eta_a + \eta_{ab}}\right) \tag{2.23}$$

or, by using the asymptotic mobility definition

$$\Delta v^2 \gg 10\log_{10}\left(\frac{Y_{a,\infty}}{Y_{b,\infty}}\right) + 10\log_{10}\left(\frac{\eta_{ab}}{\eta_a + \eta_{ab}}\right) \quad \rightarrow \quad \Delta v^2 \gg \Delta Y_\infty + \Delta\eta \tag{2.24}$$

Dis-equations 2.23 and 2.24 identify the key parameters for obtaining a high vibrational gap between two subsystems. Mass and modal density are properties of the structure and they have no dependence on the type of excitation. Moreover, there has been no assumption on the description of the subsystems, meaning that the relationship is still valid for different typologies of SEA systems. The mass ratio will always return a positive value, assuming that the support mass would always be much greater than the test model. The modal density ratio might give a negative contribution, depending on the chosen size of the surface and on the wave propagation behaviour of the subsystems. For what concerning the term depending on the CLF, from a mathematical point of view the logarithmic argument returns a value always minor than 1, so it returns a value which is always negative in dB scale. There are three situations that can be analysed:

(a) $\eta_a \ll \eta_{ab}$: the logarithm gives a value $\simeq 1$, so the actual contribution of this term is approximately null. At the same time, the condition whereby the DLF is much smaller than the CLF is an indicator of strong coupling between the subsystems [68]. Because the design process is developed in a SEA framework, this particular condition can never happen;

(b) $\eta_a \simeq \eta_{ab}$: the contribution in dB of the term $\Delta\eta$ is around ≈ -3dB;

(c) $\eta_a \gg \eta_{ab}$: the fraction gives a negative value that can be approximated to $\simeq$

$10\log_{10}(\eta_{ab}/\eta_a)$. Even though this term can reach values as ≈ -30dB, this will influence very little the vibrational velocity gap prediction. That is because dis-equation 2.17 has been developed not considering the injected power $P_{in,a}$ mathematically, but keeping it present from a physical point of view. In the following sections, it will be shown that the final result of the design strategy is not affected by $\Delta\eta$.

By keeping dis-equations 2.23 and 2.24 as reference for the prediction of Δv^2, some design rules are proposed in the next section, in order to minimize the transmitted power from the support to the test panel and obtain a vibrational velocity gap between them of $\Delta v^2 \geq 20$dB.

2.3 Design technique

The pre-design process which would ensure an acceptable level of vibrational velocity gap Δv^2 between support and test model is based on the following passages:

1. individuate the SEA-subsystem types which can represent at the best the support and the test model;
2. obtain the asymptotic mobility for the two subsystems. If the subsystems are too complex for analytical formulation, use commercial softwares that can evaluate the modal density of structures;
3. use dis-equation 2.24 to obtain a first evaluation of the vibrational velocity gap by considering *only* the asymptotic mobility level ΔY;
4. iterate the calculation of ΔY trying to maximise the value by changing different support characteristics as area, thickness, material or damping;
5. check the values of Δv^2 after the application of SEA.

In order to obtain the guidelines for the support design, a simple model is considered in the following subsection, so that the effect of changing some structural parameters is explained.

2.3.1 Effect of a change of parameter in a simple application

The model under analysis is a simplified representation of a support-test panel system based on the test section setup organized at Sherbrooke wind tunnel facility (Figure 2.4). Both subsystems are described in a SEA framework as SEA-plates connected along a common edge, whose length l_{ij} is equal to the test panel perimeter. One can refer to the SEA formulation presented in the previous Section 2.2. It has been already explained that a proper SEA analysis would describe the subsystems of a structure by considering all the types of wave propagation involved in the energy transmission. Since this simple model has been described as an ensemble of plates, only the bending wave propagation is considered, because is the one that participates more to the vibrational response of the structure.

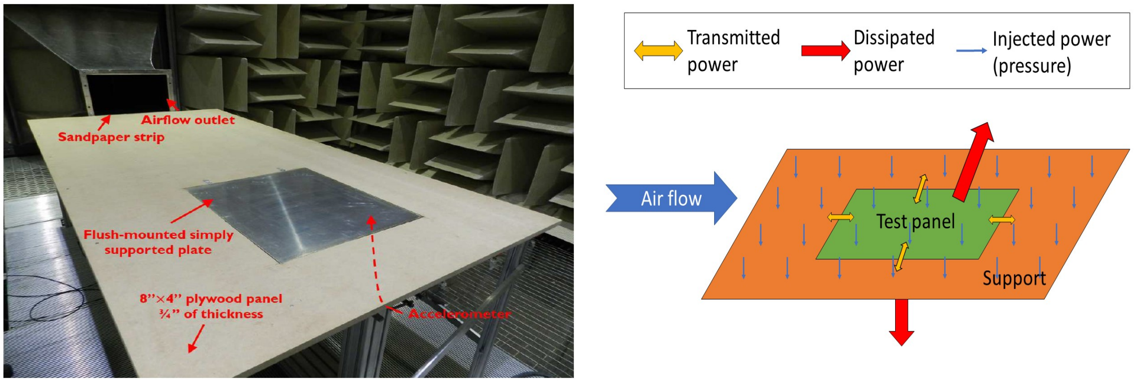

Figure 2.4: On the left: *A photo [96] of the support system setup in the open test section of Sherbrooke wind tunnel facility.* On the right: *A schematic representation of the Sherbrooke test section setup in a SEA framework; thin blue arrow represent the pressure field generated by TBL excitation, yellow arrows represent the transmitted power between the two subsystems, and red arrows represent the dissipated powers.*

In order to understand the consequences of changing several design parameters as area, thickness, material and damping, the SEA analysis starts by considering both subsystems with equal parameters (case "0"); then, these parameters will be modified to appreciate how the vibration velocity gap Δv^2 can be improved. By these analyses, the general design guidelines are derived and they can be applied for any problem of energy transmission decoupling among subsystems of one structure.

The simplified model is studied for a TBL excitation with an asymptotic flow of $U_0 = 15$ m/s and convective factor of $\beta_c = 0.8$. The aerodynamic pressure field is described in a SEA framework thanks to the Equivalent ROR excitation approximation [85] presented in the previous section (Equations 2.14-4.45), with the following Corcos coefficients values: $\alpha_x = 0.116$ along the streamwise direction and $\alpha_y = 0.700$ along the crosswise direction.

The analyses are run in a frequency range [20; 20000] Hz; for each case, the mof (Equation 2.11) is evaluated in order to know from which frequency SEA is valid. This frequency is here referred as frequency of SEA validity f_{SEA}.

For design purposes, the test panel characteristics are kept fixed and are all grouped in Table 2.1.

Test panel properties			
Young's modulus, E	Poisson's ratio, ν	Density, ρ	Thickness, h
7.1e10 Pa	0.33	2700 kg/m^3	0.001 m

Table 2.1: Test panel properties used for the development of design guidelines.

Case 0: same properties

For this reference case, test panel and support present the same main properties, in particular: mass M, bending stiffness D, thickness h, area A and DLF η (Figure 2.5). Through the mof calculation, it is possible to know the frequency of SEA validity $f_{SEA} = 800$ Hz.

As direct consequence of having the same properties values, support and test panel present same modal density and asymptotic mobility too. Hence, there is no contribution of the asymptotic mobilities ratio ΔY to the vibrational velocity gap Δv^2. On the other hand, the term $\Delta \eta$ present a maximum negative value of ≈ -1.8 dB at the highest frequency. It is

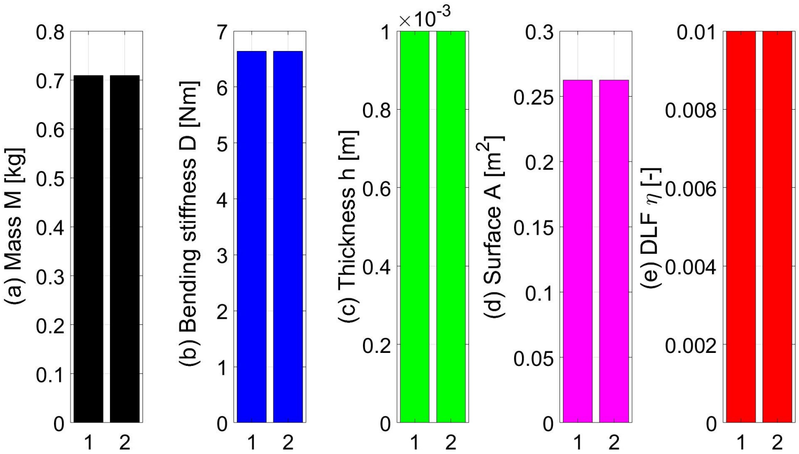

Figure 2.5: **Case 0.** *Properties values for support (2) and test panel (1); (a) Mass M [kg]. (b) Mean bending stiffness D [Nm]. (c) Thickness [m]. (d) Surface A [m^2]. (e) DLF.*

then confirmed what was previously explained in Section 2.2.2: even though $\Delta\eta$ is negative, the vibrational velocity gap does not present negative values; in fact, it is null over all the frequency range, meaning that both subsystems have the same amount of energy. This is in agreement with the heat transfer analogy [34]: if a certain number of subsystems present all the same properties and are all excited in the same way, the energy will distributes itself homogeneously in all of them. Another confirmation is given by the transmitted powers shown in Figure 2.6b: the energy flow from support (2) to test panel (1) is equal to the energy flow in the opposite direction, resulting in a null energy flow; both subsystems are in equilibrium and they do not share energy.

Case 1: change of area

Th effect of a difference of surface dimensions between two subsystems is herein analysed. The support surface dimensions are changed assuming that its area would be greater than the test panel one. This is the most realistic assumption, since the support (subsystem 2) should sustain the test panel (subsystem 1) and, at same time, it should assure enough space to let the TBL develop over the surface, in order to have a constant boundary layer over the sample under analysis. Consequently, a ratio of $A_1/A_2 = 1/4$ has been chosen. An increase of area leads to an increase of mass, as it can be seen in Figure 2.7.

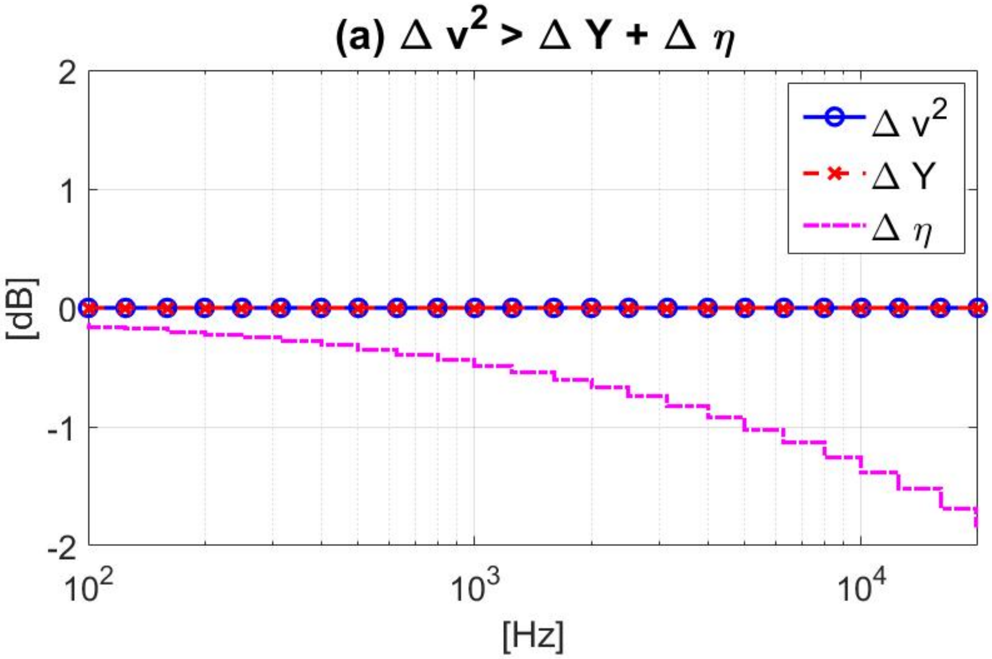
(a) $\Delta v^2 > \Delta Y + \Delta \eta$

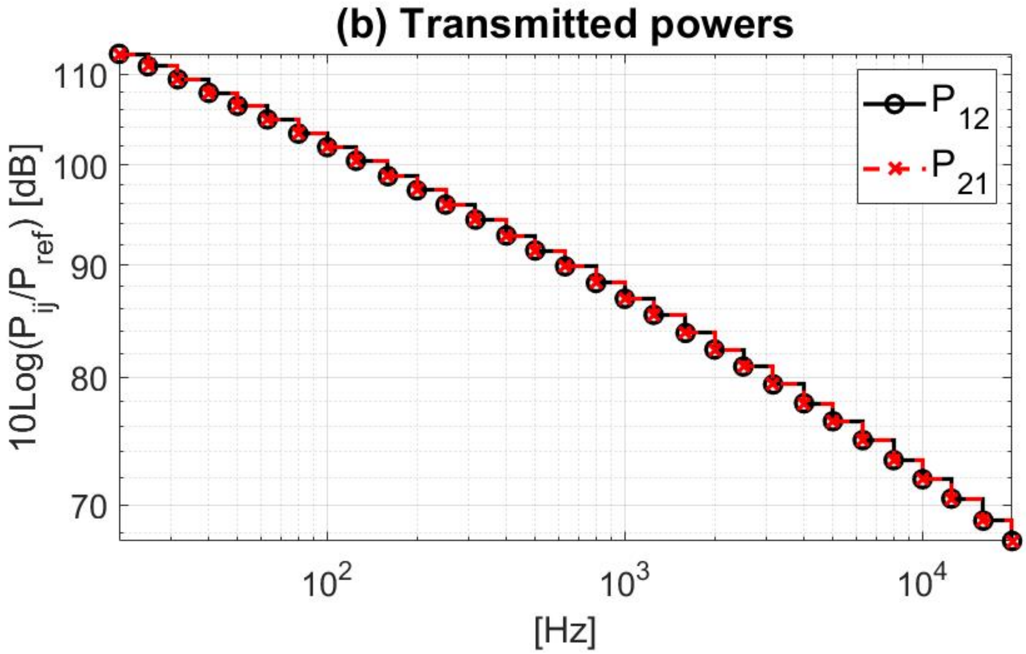
(b) Transmitted powers

Figure 2.6: **Case 0.** *(a) (−O−) Vibrational velocity level gap Δv^2, (− − × − −) asymptotic mobility ratio ΔY, (−−) contribution due to DLF and CLF $\Delta\eta$. (b) Transmitted powers between support and test panel in dB scale, with reference power $P_{ref} = 1e{-}12$ W/Hz; (−O−) P_{12} from test panel to support, (− − × − −) P_{21} from support to test panel.*

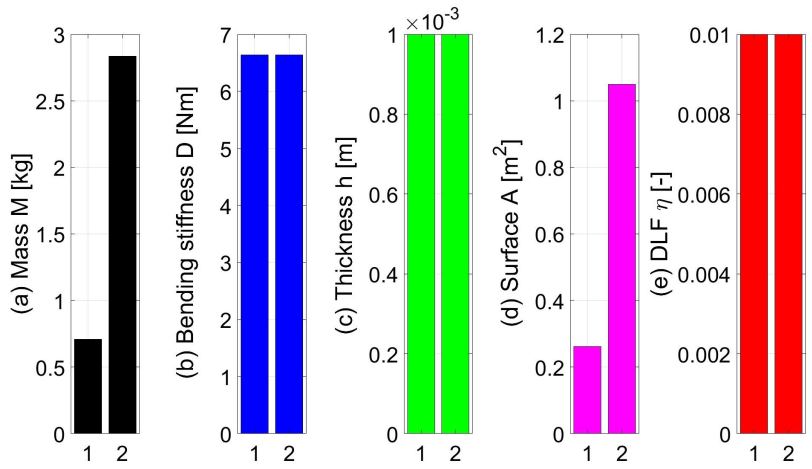

Figure 2.7: **Case 1.** *Properties values for support (2) and test panel (1); (a) Mass M [kg]. (b) Mean bending stiffness D [Nm]. (c) Thickness [m]. (d) Surface A [m^2]. (e) DLF.*

This will affect the mass ratio contribution ΔM, but also the modal density ratio Δn (Equation 2.23). Because of their linear dependence on the area, the resulting ΔY value does not give any contribution to the velocity levels gap. Again, even though $\Delta\eta$ presents a negative value (≈ -1.8 dB at the highest frequency), this does not influence the final result of the vibrational velocities. In Figure 2.8a, Δv^2 is still null over all the frequency domain, as it is as well the net transmitted power, since P_{12} and P_{21} are overlapped (Figure 2.8b).

Case 2: change of thickness

The second parameter to be changed is the thickness. It has been here assumed that the support (subsystem 2) would be thicker than the test panel (subsystem 1), so that $h_2 = 5h_1$. With the increase of thickness, there is a consequent increase of mass, but also of bending stiffness (Figure 2.9).

The bending stiffness affects the modal density value too; this has two consequences. The first one is related to the mof value, which now would ensure the SEA validity from the frequency $f_{SEA} = 1000$ Hz; the second one is related to the mobility ratio ΔY, which for this case presents a positive value of $\Delta Y = 14$ dB. This means that, for dis-equation 2.24, the vibrational velocity gap will register for sure a value higher than 14 dB. Indeed, by

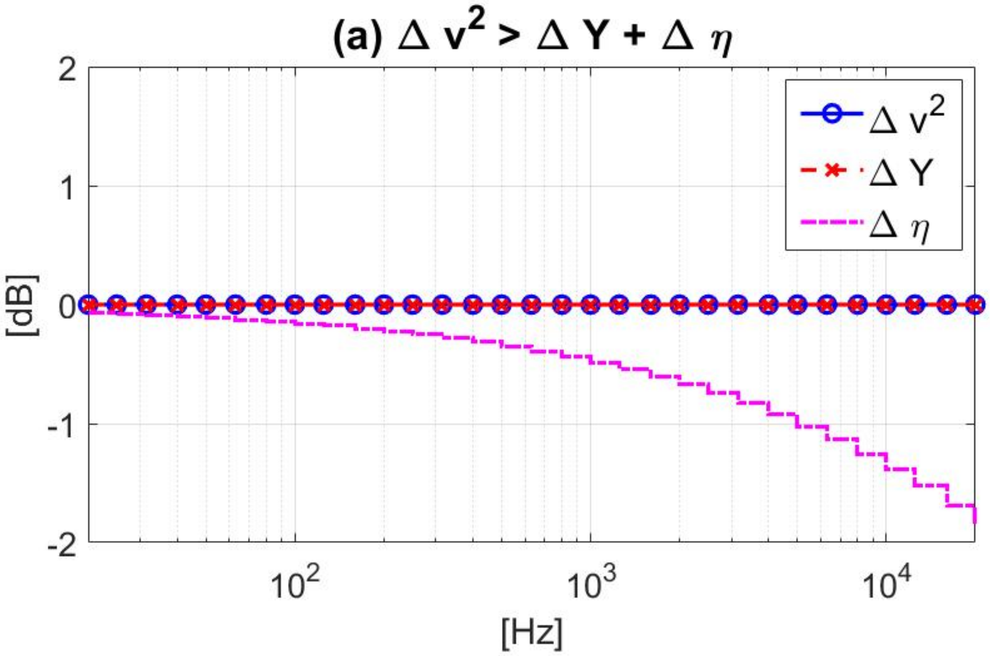

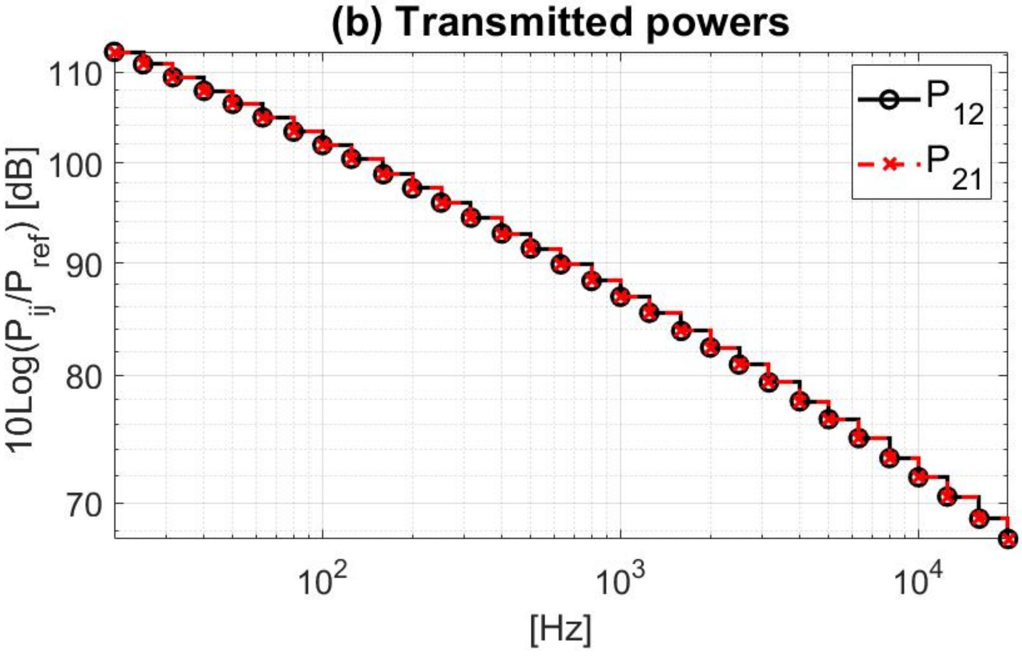

Figure 2.8: **Case 1.** *(a) (−O−) Vibrational velocity level gap* Δv^2*, (− − × − −) asymptotic mobility ratio* ΔY*, (−−) contribution due to DLF and CLF* $\Delta\eta$*. (b) Transmitted powers between support and test panel in dB scale, with reference power* $P_{ref} = 1e{-}12$ *W/Hz; (−O−)* P_{12} *from test panel to support, (− − × − −)* P_{21} *from support to test panel.*

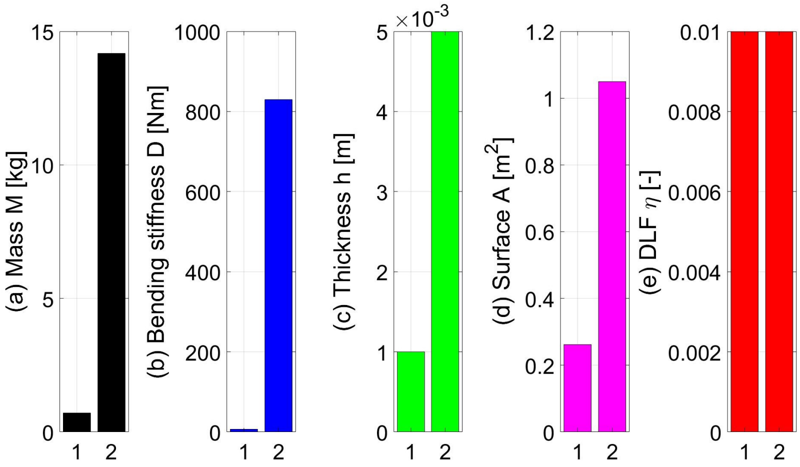

Figure 2.9: **Case 2.** *Properties values for support (2) and test panel (1); (a) Mass M [kg]. (b) Mean bending stiffness D [Nm]. (c) Thickness [m]. (d) Surface A [m^2]. (e) DLF.*

looking at Figure 2.10, it is possible to notice that $\Delta v^2 \approx 16$ dB is obtained at the highest frequency. It is then evident that a SEA-subsystem with bigger thickness would transmit less energy to another SEA-subsystem with smaller thickness; the transmitted power from test panel to support P_{12} presents higher values compared to the other one. Hence, the net transmitted power $\vec{P_{tr}} = \vec{P_{12}} - \vec{P_{21}}$ will flow from the test panel to the support and not viceversa.

Case 3: change of material

As third parameter effect, the change of material is herein considered. With the final aim of further increasing the modal density ratio, it has been chosen a sandwich panel with isotropic faces and honeycomb core: the skin is in aluminium (thickness $h_s = 0.0025$ m) while the core is made of honeycomb (48 kg/m^3, thickness $h_c = 0.02$ m), for a total thickness of $h_2 = 0.025$ m. With an increase of mass of just 1 kg, bending stiffness and thickness have increased their values significantly, with a direct effect on the reduction of the support modal density (Figure 2.11).

Since the support modal density has a lower value, the frequency of SEA validity is reduced back to $f_{SEA} = 800$ Hz. Through a rapid comparison with the previous case (Figure

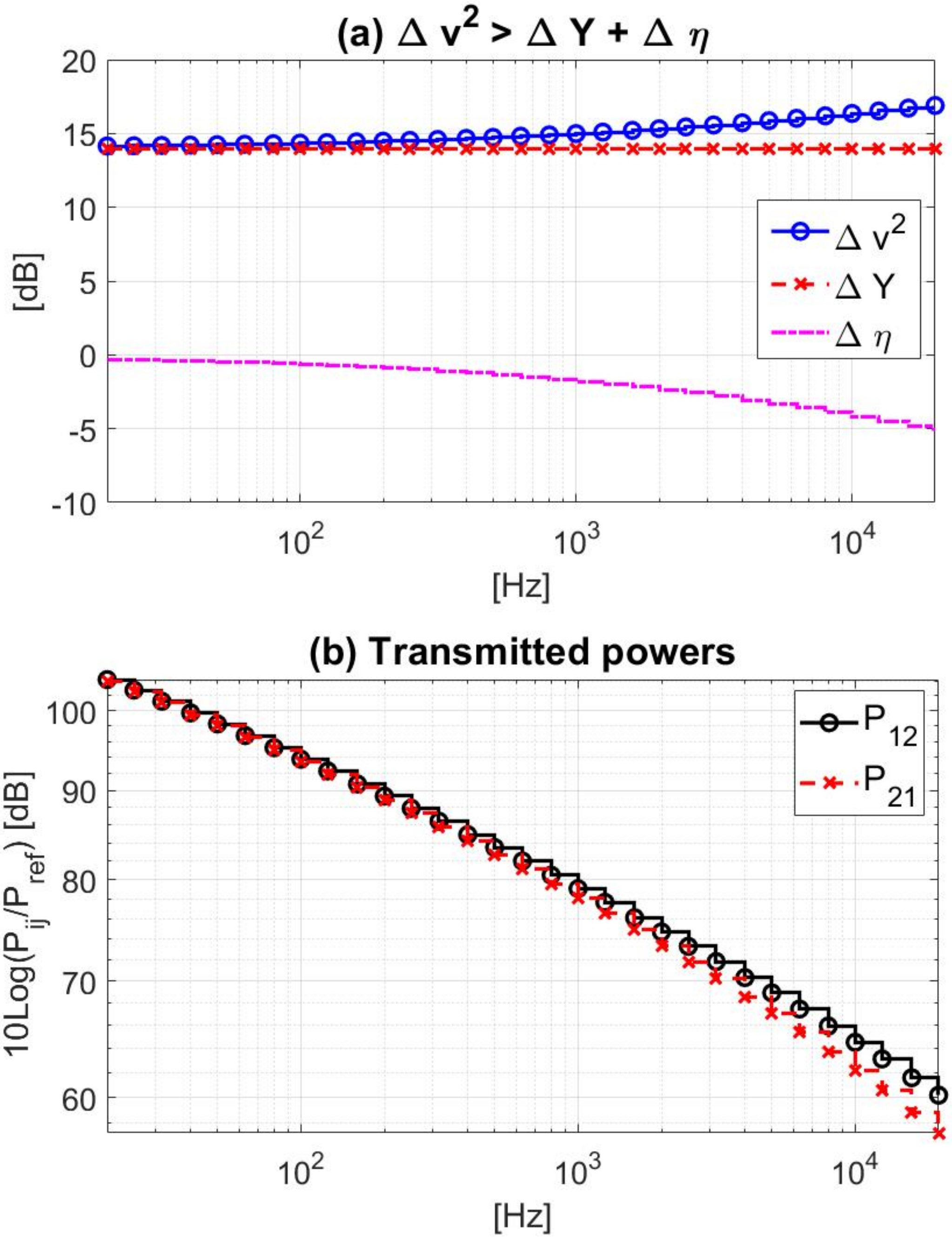

Figure 2.10: **Case 2.** *(a) (−O−) Vibrational velocity level gap Δv^2, (− − × − −) asymptotic mobility ratio ΔY, (−−) contribution due to DLF and CLF $\Delta\eta$. (b) Transmitted powers between support and test panel in dB scale, with reference power $P_{ref} = 1e{-}12$ W/Hz; (−**O**−) P_{12} from test panel to support, (− − × − −) P_{21} from support to test panel.*

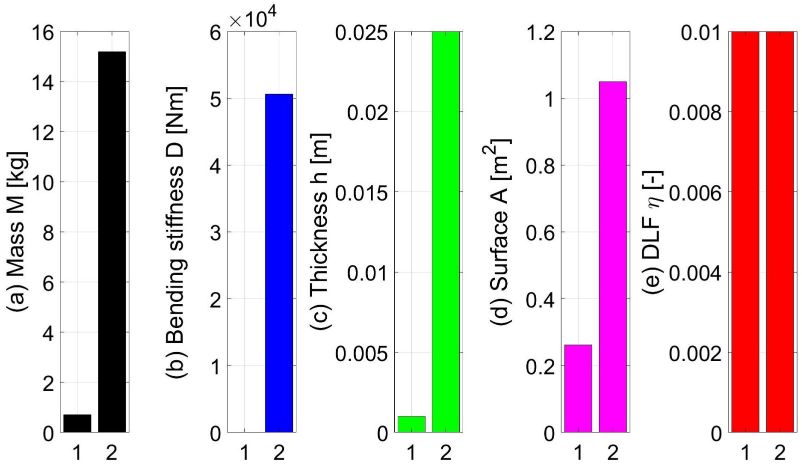

Figure 2.11: **Case 3.** *Properties values for support (2) and test panel (1); (a) Mass M [kg]. (b) Mean bending stiffness D [Nm]. (c) Thickness [m]. (d) Surface A [m^2]. (e) DLF.*

2.10a), it can be noticed that the mobility ratio level ΔY suffered a reduction to ≈ 10.5 dB. This is a fallout of the modal density expression for sandwich panels.

As matter of fact, sandwich panels present three different behaviours, depending on the frequency regime of analysis, which participate to the flexural motion: at low frequencies, classic isotropic thin panel behaviour occurs; at middle frequencies, the shear effect of the core becomes predominant; then at high frequencies, the sandwich wavenumber is characterised by the bending behaviour of its skins [123]. For the description of the sandwich modal density, these three asymptotic behaviours have been used (equations 2.25-2.26-2.27), considering two transition frequencies ω_1 and ω_2 that define the passage from one formulation to another (equations 2.28).

$$\kappa(\omega) = \left(\frac{m}{D}\omega^2\right)^{\frac{1}{4}} \qquad \omega \leq \omega_1 \tag{2.25}$$

$$\kappa(\omega) = \sqrt{\frac{m}{S}}\omega \qquad \omega_1 < \omega \leq \omega_2 \tag{2.26}$$

$$\kappa(\omega) = \left(\frac{m_s}{D_s}\omega^2\right)^{\frac{1}{4}} \qquad \omega > \omega_2 \tag{2.27}$$

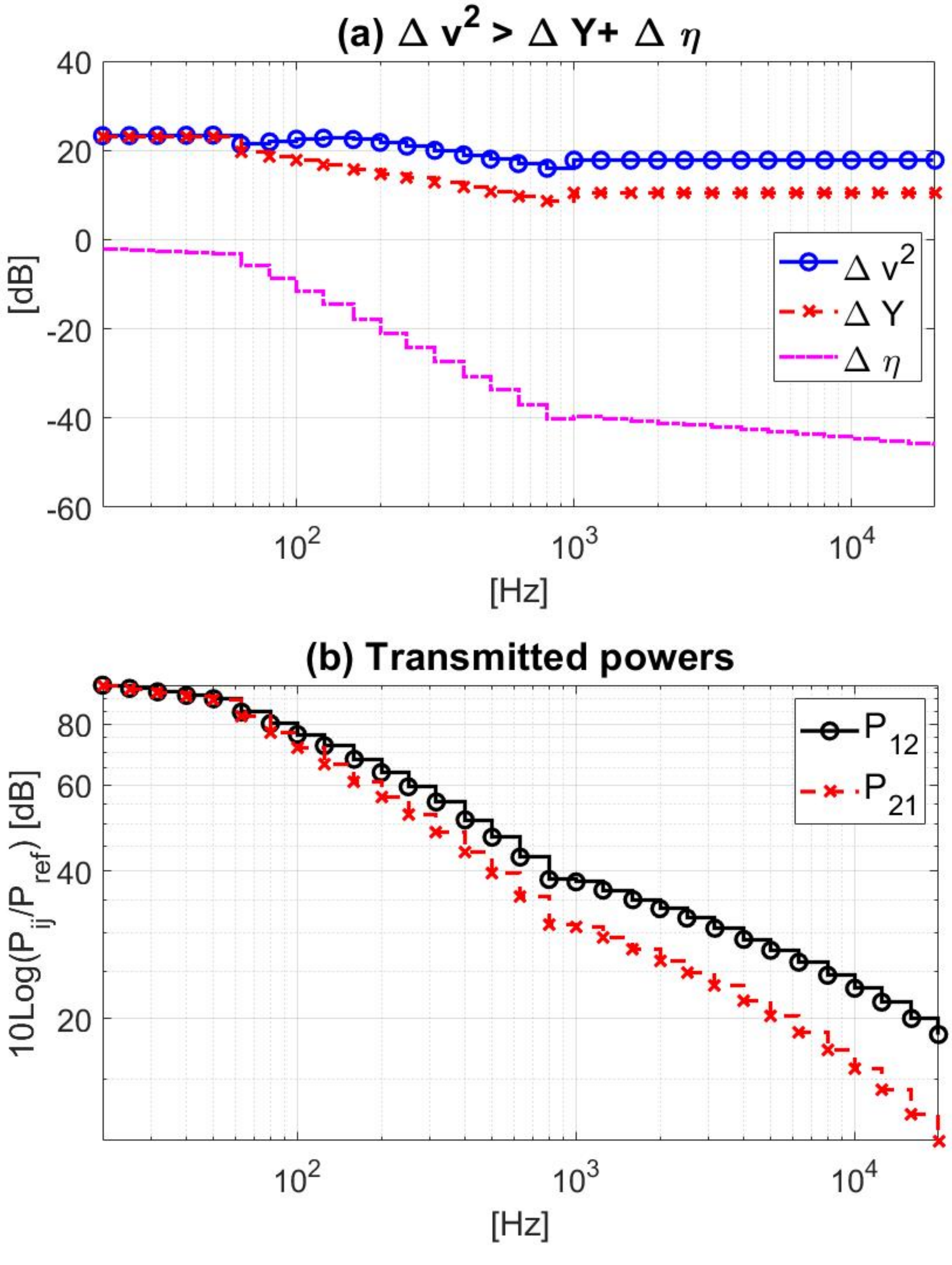

Figure 2.12: **Case 3.** *(a) (−O−) Vibrational velocity level gap* Δv^2*, (− − × − −) asymptotic mobility ratio* ΔY*, (−−) contribution due to DLF and CLF* $\Delta \eta$*. (b) Transmitted powers between support and test panel in dB scale, with reference power* $P_{ref} = 1e{-}12$ *W/Hz; (−***O***−)* P_{12} *from test panel to support, (− − × − −)* P_{21} *from support to test panel.*

$$\omega_1 = S\sqrt{\frac{1}{mD}} \quad ; \quad \omega_2 = \frac{S}{m}\sqrt{\frac{m_s}{D_s}} \tag{2.28}$$

Indeed, the sandwich behaviour is recognised in all curves plotted in Figure 2.12. Considering that at highest frequencies, the skin bending behaviour is predominant, it is here explained why the asymptotic ratio is smaller in this case if compared with the previous one of the previous case: in case 2, an aluminium plate 5mm thick is considered, while in case 3 the sandwich panel — representing the support — shows at high frequencies the behaviour of an aluminium plate 2.5mm thick. Consequently, it can be predicted, for sure, that the vibrational velocity gap Δv^2 would be at least higher than 10.5 dB. On the other hand, the term $\Delta\eta$ increased in absolute value. It appears, from the analysis of the final value of Δv^2, that the more $\Delta\eta$ increases in absolute value, the more Δv^2 will do as well. Indeed, its final value is $\Delta v^2 \approx 17.8$ dB at the highest frequency. How to justify an increase of Δv^2 if the asymptotic mobility ratio is smaller than in the previous case? The answer might be in the calculation of the CLF: as matter of fact, the term $\Delta\eta$ has increased significantly in absolute value, meaning that the CLF η_{12}, representing the factor of transmission from test panel (subsystem 1) to support (subsystem 2), became much smaller than in the previous case. With another check to the transmitted powers, it is possible to notice that the difference between them is bigger and, at the same time, both amplitudes are smaller for order of magnitude, if compared with the previous case. It is hence confirmed that both CLFs got a reduction of value choosing the sandwich as material for the support subsystem. The higher vibrational velocity gap for this case might be then justified by the increase of thickness and/or the increase of stiffness inside the support subsystem.

Case 4: change of damping DLF

As last parameter to analyse, there is the Damping Loss Factor, DLF. In the previous cases, the same value of DLF (1%) [124] was assumed for both subsystems. It is wanted to underline that, in the SEA framework, a constant DLF means considering each mode with

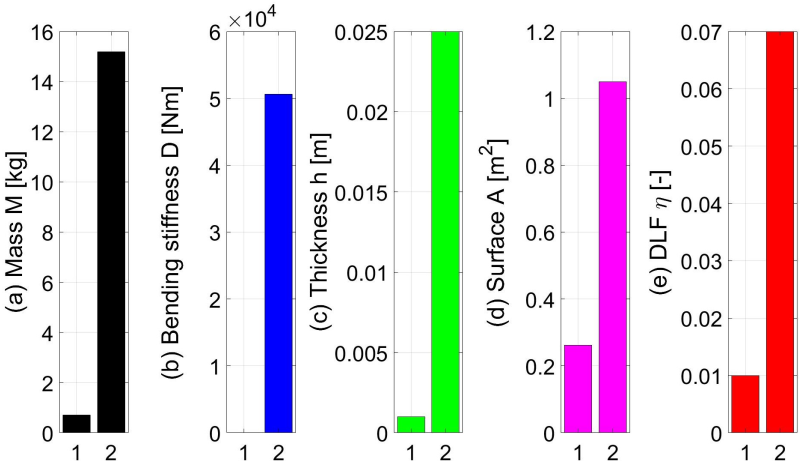

Figure 2.13: **Case 4.** *Properties values for support (2) and test panel (1); (a) Mass M [kg]. (b) Mean bending stiffness D [Nm]. (c) Thickness [m]. (d) Surface A [m^2]. (e) DLF.*

the same amount of damping. For this last case, it is assumed a DLF of 7% [125] for the support subsystem, leaving unaltered the characteristics defined in the previous case (Figure 2.13). The frequency of SEA validity is still fixed at $f_{SEA} = 800$ Hz. Unlike the other parameters, the DLF effect over the design process for an energy transmission decoupling cannot be predicted with the asymptotic mobility ratio ΔY. Nevertheless, the DLF is a parameter which characterize the amount of energy that is dissipated by a structure. It is then obvious that, by increasing the dissipated power of the support (subsystem 2), the actual energy that might be transmitted to the test panel (subsystem 1) is reduced. As it can be noticed with a comparison between Figure 2.12a and Figure 2.14a, the level of ΔY remained the same, but the actual vibrational velocity gap increased considerably, showing a value of $\Delta v^2 \approx 26$ dB at the highest frequencies.

Another consequence of a change of DLF can be seen in the transmitted powers: over all the frequency range, both terms decrease very rapidly for increasing frequency, while their difference increases. In particular, from a comparison with the previous case (Figure 2.12b), it can be noticed that the power contribution transmitted from the test panel to the support P_{12} remained always the same, while the opposite contribution P_{21} has been significantly reduced, meaning that, with an increase of DLF, the support transmits less than before.

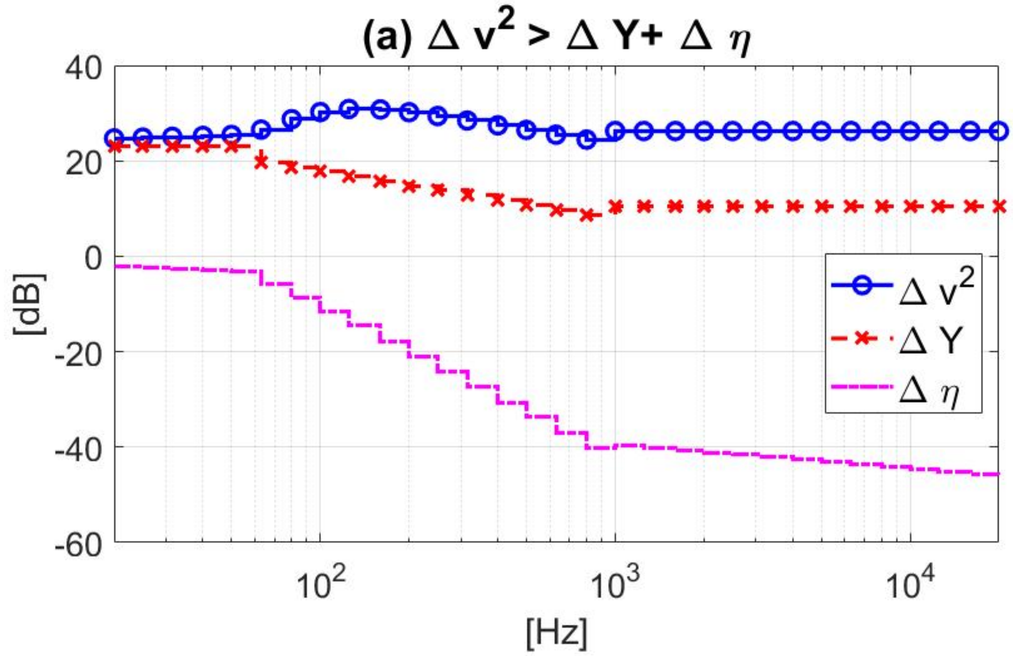
(a) $\Delta v^2 > \Delta Y + \Delta \eta$

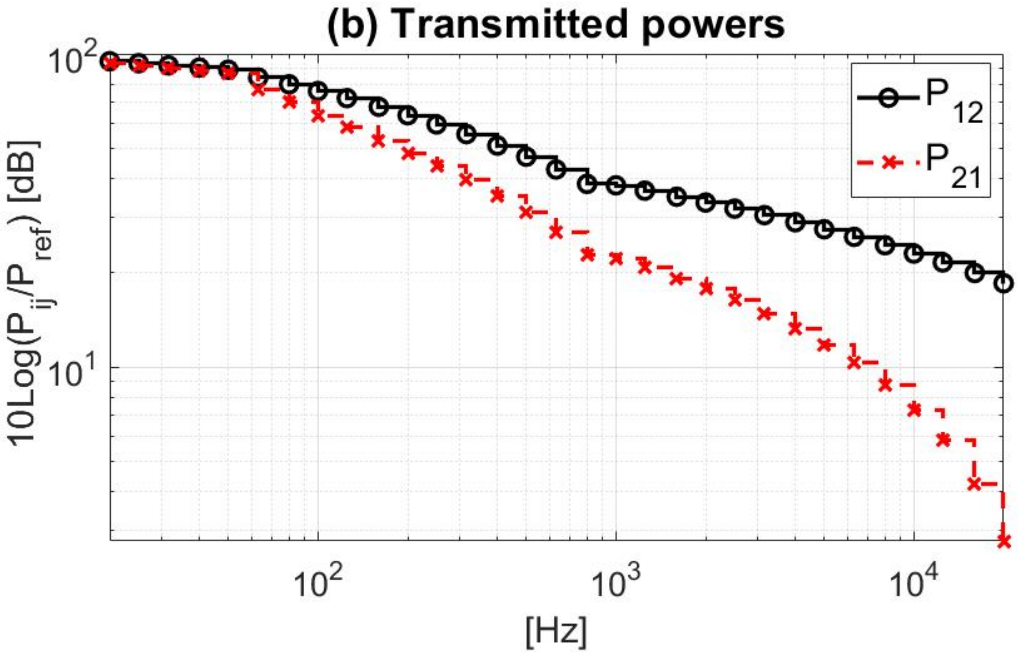
(b) Transmitted powers

Figure 2.14: **Case 4.** *(a) (−O−) Vibrational velocity level gap* Δv^2*, (− − × − −) asymptotic mobility ratio* ΔY*, (−−) contribution due to DLF and CLF* $\Delta\eta$*. (b) Transmitted powers between support and test panel in dB scale, with reference power* $P_{ref} = 1e{-}12$ *W/Hz; (−***O***−)* P_{12} *from test panel to support, (− − × − −)* P_{21} *from support to test panel.*

2.3.2 Final design guidelines for an energy transmission decoupling at HF

As result of the studied cases, it is possible to define some general guidelines which are true for 2D SEA-subsystems connected along the edges and for which it is wanted to reduce the energy transmission from one subsystem to another.

(I) A difference of area will not give any contribution to the vibrational velocity gap.

(II) A difference of thickness will result in a difference of mass between the two subsystems; this leads to a difference of asymptotic mobilities, with the thickest subsystem having the lower asymptotic mobility value. Moreover, a difference of thickness will result in a difference of transmitted powers: the power will flow just from the thinnest to the thickest subsystem and not viceversa.

(III) A change of material is recommended if it will result in higher values of mass, higher value of bending stiffness and higher value of thickness for the subsystem that it is not wanted to let transmit energy to the other.

(IV) A high DLF for a subsystem will always reduce its energy contribution transmitted to the adjacent subsystem.

By following these guidelines, the design of a simple support — as already shown in Figures 2.4-2.3 — will be analysed with the help of a commercial software VA One.

2.4 Design analysis at high frequencies

The commercial software VA One has been used for this vibroacoustic analysis, in order to evaluate a comparison between analytical expressions and numerical ones. The model under analysis is still the open test section setup of Sherbrooke wind tunnel facility (Figure 2.4). A proper introduction to the VA One environment will be given in Chapter 3, during the design analysis of the complex structural device; it is just important here to give a description of the

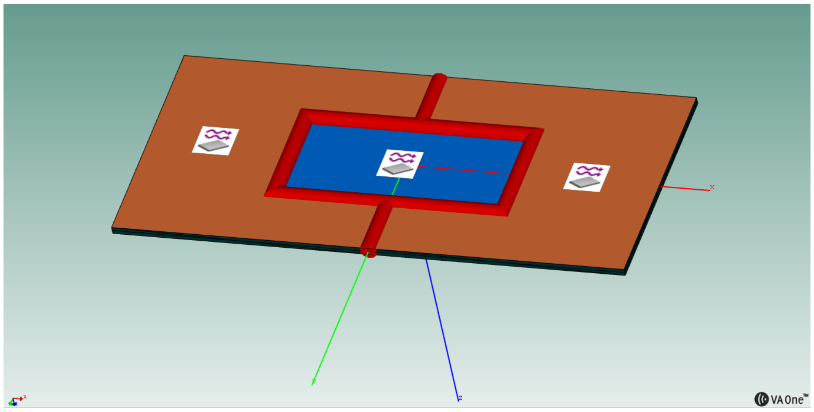

Figure 2.15: The open test section setup of the Sherbrooke wind tunnel facility, represented in a VA One environment. In blue, the test panel; in orange, the support; in red, the line junctions representative of the coupling. The three squared symbols represent the application of a TBL excitation over the structure.

model and how this has been set. In Figure 2.15, the Sherbrooke model setting is represented inside VA One.

Support (in orange) and test panel (in blue) have been described in VA One as plates. In fact, it is wanted to specify that VA One cannot create systems with particular features as holes, hence the support system has been created with two plate-subsystems called *front support* and *rear support*, indicating respectively one subsystem in the positive x-direction and the other in the negative x-direction. From a SEA point of view, by keeping the same properties for both subsystems the results will not differ. A confirm of this assumption would be given with a check on the CLFs between them: they are exactly the same (graphs not shown here); moreover, the CLFs between them and the test panel are also the same, meaning that they both shear the same amount of energy. The junctions are represented as red lines; in the VA One environment, they are responsible for the CLF calculation. Finally, the TBL excitation is represented by the three squared symbols applied over all three subsystems, it is described through the Cockburn and Robertson model [126] and it has been set for an asymptotic flow speed of $U_0 = 15$ m/s, convective factor $\beta_c = 0.8$, empirical streamwise coefficient $c_x = 0.116$ and empirical crosswise coefficient $c_y = 0.700$. The boundary layer thickness has been considered constant and equal to $\delta = 0.00185$ m.

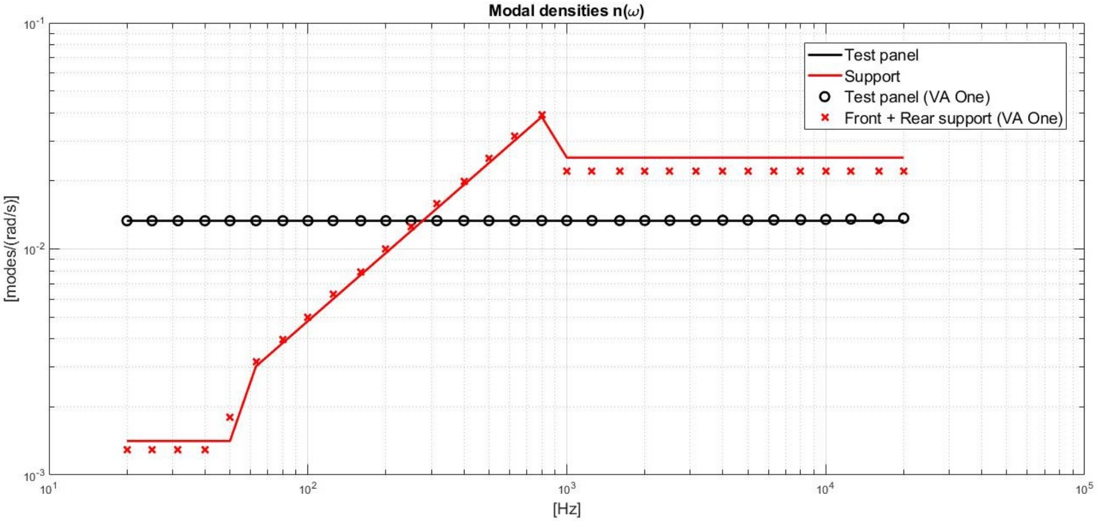

Figure 2.16: Modal density of test panel (in black) and support (in red). Solid line: analytical formulations in MATLAB; symbols O *and* $\times$*: numerical formulations in VA One.*

The materials chosen for test panel and support are the same presented in the last case for the development of the design guidelines: the test panel is in aluminium, 1 mm thick, and the support is made with a sandwich configuration, having skins in aluminium (2.5 mm thick) and core in honeycomb (48 kg/m^3 and 2 cm thick).

As it can be noticed in Figure 2.16, the description of the modal densities are well formulated and good agreement is found between analytical formulations expressed in MATLAB and numerical formulations implemented in VA One. For the test panel, the match is perfect, while for the support, little discrepancy is found at low and high frequencies. It is interesting to see that the modal density behaviour for a sandwich panel is determined by the three asymptotic behaviours (Equations 2.25-2.26-2.27) in VA One too.

The asymptotic mobilities present the same behaviour as the modal densities (Figure 2.17); indeed, Equation 2.13 depends only on modal density and total mass. This means that VA One uses the same formulation. Comparing modal density and asymptotic mobilities results, one can notice that the modal density match is obtained with the sum of front and rear support values, while the asymptotic mobility match is obtained with front and rear support considered separately. This can be explained by looking at Equation 2.8 and Equation 2.13;

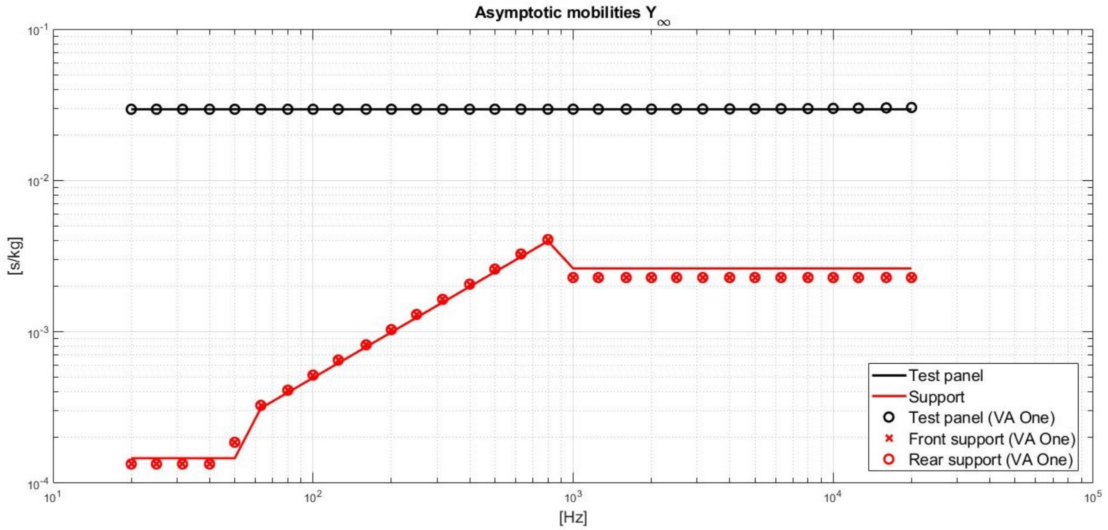

Figure 2.17: Asymptotic mobilities of test panel (in black) and support (in red). Solid line: analytical formulations in MATLAB; symbols O *and* $\times$*: numerical formulations in VA One.*

the term $n(\omega)$ has a direct dependence on the area of the subsystems, hence front and rear support values must be summed in order to consider the total area of the support. The term Y_∞ depends on the ratio $n(\omega)/M$, thus the dependence on the area disappears. This can be also interpreted as confirm of the design guideline, for which the change of area does not influence the vibrational velocity gap between two connected subsystems.

Finally, the PSD vibrational velocities of both subsystems are compared (Figure 2.18). It has been found a good agreement between analytical (MATLAB) and VA One results, even though it has been noticed that the software might use different formulations for the CLFs; this is the main explanation for which it is not obtained a perfect match between MATLAB and VA One results.

2.5 Conclusions

In this second chapter, the first main topic of the presented research has been faced. In order to develop some guidelines which would be suitable for any structural design of a support for test models to be located in a wind tunnel, the Statistical Energy Analysis, or SEA, has been chosen as methodology.

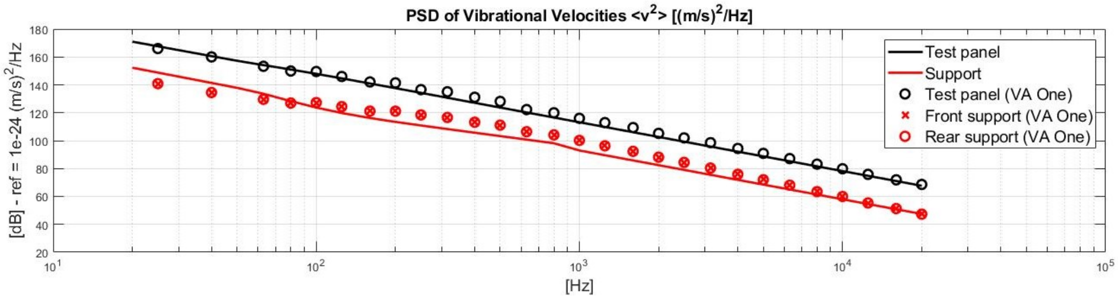

Figure 2.18: Power Spectral Densities of vibrational velocities of test panel (in black) and support (in red). Solid line: analytical formulations in MATLAB; symbols O *and* $\times$*: numerical formulations in VA One.*

After a brief introduction of the method, explaining the main parameters involved, the mathematical process that leads to the development of the design guidelines has been presented. Starting from the power equilibrium exercised over the test model, the design guidelines have been developed with the intention of reducing as much as possible the transmitted power from the support subsystem to the test model one. It has been hence recovered a dis-equation which relates the vibrational velocity gap between the two connected subsystems and the asymptotic mobilities ratio, meaning that it is possible to control and manage the final vibrational velocity gap starting from the characteristics of the systems.

A simple system composed by a test panel and a flat support has been analysed in order to extract the design guidelines in terms of choice of geometry and material. The different effects over the energy transmission between the subsystems are compared, by changing the area, the thickness, the type of material and the damping.

The final configuration — found with the iterations of aforementioned parameters — has been tested with the commercial software VA One, so that also a comparison between analytical and numerical simulations is fulfilled too.

In the next chapter, the same design guidelines are applied for the development of a complex structure which would sustain a test panel inside a large-scale wind tunnel facility.

CHAPTER 3

ENERGY TRANSMISSION DECOUPLING ON A COMPLEX STRUCTURE

3.1 Introduction

As other design rules application, the development of a complex structure in terms of structural design is herein presented and explained.

The design project was born in conjunction with the IJES project, which involved the installation of a new jet propulsion inside the high-speed wind tunnel facility of ONERA, in Modane (FR). Few indications were provided about the wind tunnel:

- the test section total diameter is $d = 10$m;
- the highest Mach number reached inside the wind tunnel is $M = 0.6$.

With the final aim of conduct vibroacoustic experiments over sample flat panels, it was required a structural support which could be located inside the wind tunnel and, at the same time, which could guarantee the purity of the measurements. Because of the considerable dimensions of the test section, all tools and instruments needed for the measurements acquisition must be included inside the structural support. Moreover, an image of a possible configuration — in terms of dimensions and location of the structure — has been provided, to underline the request of a 3-dimensional aerodynamically-shaped structural device which could be hung up in the test section (Figure 3.1).

No other information were given, hence the process of idealization, draft and actual design was organized as in the following steps:

1. First structural project: the idealization and draft of the structural device are based on the little information already illustrated before. The design will consider just the exchange of vibrations between the structural device and the sample panel and the

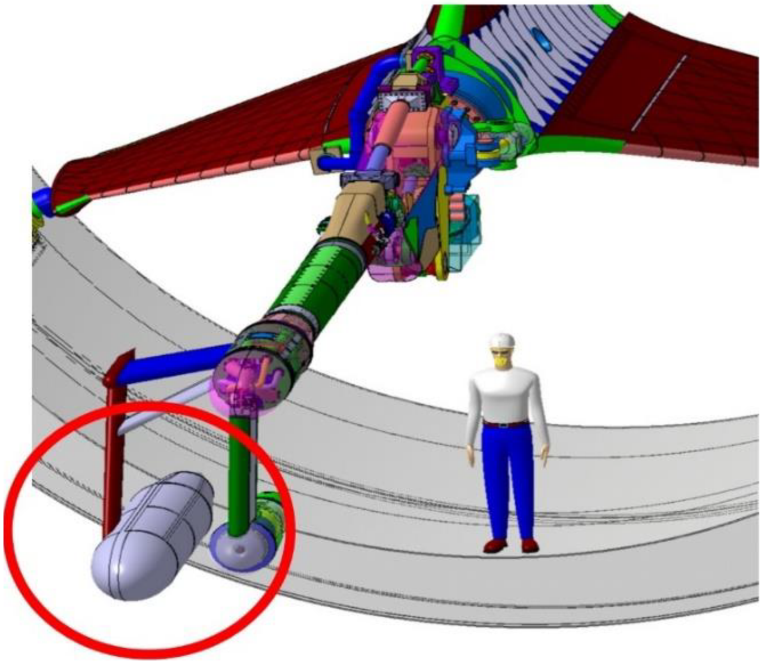

Figure 3.1: Guideline image provided by IJES project. The item circled in red is the suggested typology of structure, in terms of dimensions and location inside the test section.

type of material to be used, in comparison with the total mass of the structure, in order to keep it as much light as possible.

2. Aerodynamic project: the shape of the device needs to be re-thought, in order to take into account the development of the wall-pressure fluctuations over the structure surface and ensure a constant turbulent boundary layer over the sample panel. The change of shape will be performed considering the structural information obtained from the previous step: thickness, area, type of material.

3. Second structural project: an optimization of the structure can be applied, considering that, from the previous steps, the wall-pressure fluctuations are given and the shape is fixed.

In this chapter, the first presented step will be achieved through the application of the design rules expressed previously. In section 3.2, details about the idealization and the draft of the structural device are presented; then, the development of the design is guided through the application of the design guidelines (section 3.3). A statistical energy analysis is run for the testing of the design at high frequencies and results are presented and discussed. Finally, a modal analysis is performed over the coupled system test panel-support, together with the modal analyses performed over the two uncoupled systems, in order to evaluate if there are any differences in terms of eigensolutions.

3.2 Presentation of the structural device: the ogive

To meet the few characteristics required for the structural support, the following criteria are herein considered:

- The test section total diameter is $d = 10$m, hence the support device must have dimensions much smaller than that. Maximum dimensions of length $L_{max} = 3$m, width $W_{max} = 1.5$m and height $H_{max} = 1$m have been fixed, as if the entire structure is enclosed in a rectangular box with the aforementioned dimensions. In this way, it is ensured a total development of the TBL without incurring in boundary effects due to too less space left between test section walls and device. In particular, it has been fixed a height of at least 1m in order to ensure enough space for acoustic measurements inside the structural device. Indeed, the inner space can be used as anechoic chamber and/or measurements tools location.
- The design is tested for different asymptotic speeds, starting from very low Mach numbers ($M < 0.1$) until a maximum Mach number equal to $M_{max} = 0.6$.
- it has been taken inspiration for the first geometrical shape from the provided image, together with other images of submarines (Figure 3.2) as example; the intention is to ensure as much space as possible in the inside, together with one flat area in which it is possible to mount the sample panel.

Because of the smooth-curved shape, the structural device has been called "ogive". A picture of the ogive model developed with the commercial software CATIA v5r21 is shown

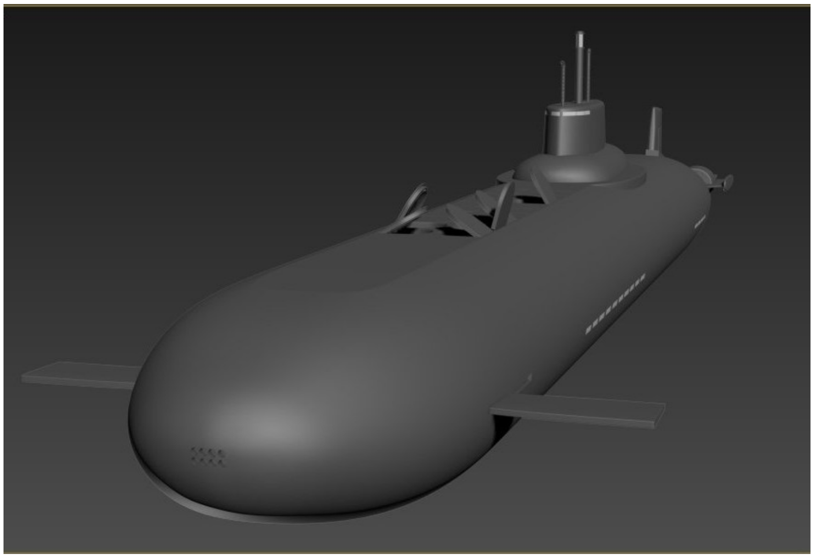

Figure 3.2: An example of submarine configuration taken into account for the development of the geometrical shape of the support device.

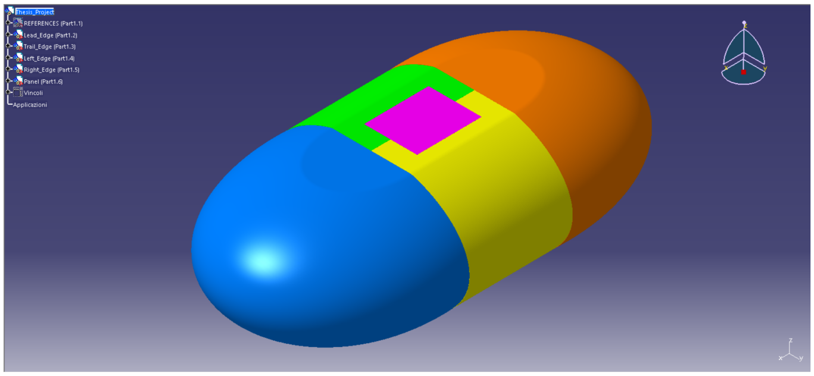

Figure 3.3: CAD model of the ogive developed with the commercial software CATIA v5r21.

in Figure 3.3. The structure presents a symmetry along both longitudinal and transversal directions, to ensure a simple reproduction and an easy analysis. Four main parts are recognized: the two bulk-heads, one at the leading edge in blue and one at the trailing edge in orange, and the two lateral parts, one on the left in green and one on the right in yellow. The firsts are double-curved shells, while the seconds are single-curved shells. An inner space with a total volume of $V = 2.673$ m^3 for measurement tools allocation has been obtained.

In Figure 3.4, the top and lateral views of the ogive are presented, together with the main measures (in mm) considered. It has been assumed for the test panel dimensions

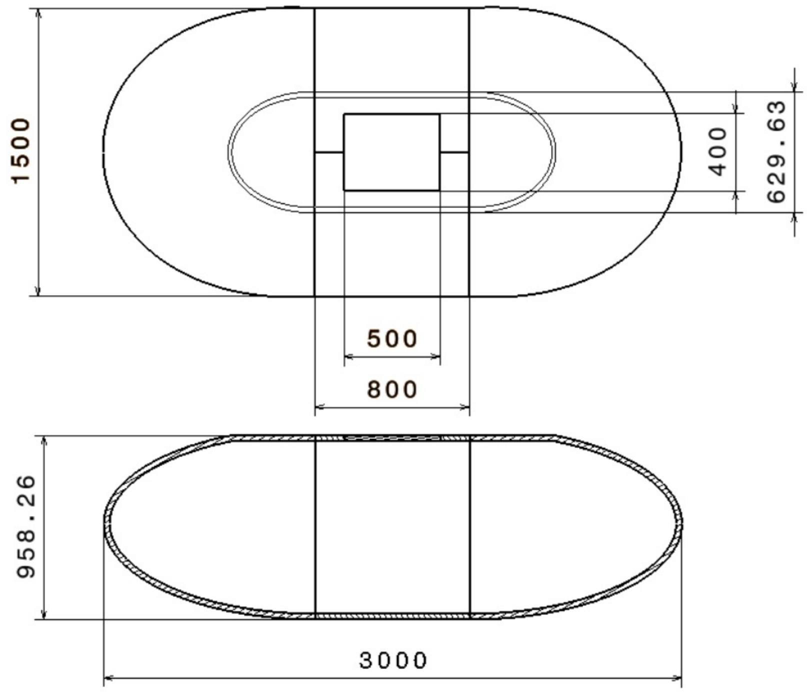

Figure 3.4: Top view (top) and lateral section view (bottom) of the ogive structure created with the commercial software CATIA v5r21.

$0.5 \times 0.4\text{m}^2$, with a thickness of 0.001m; more information about test panel will be given in the following section.

All the ogive parts have been realized inside a unique CATIA file with a "top-down" technique, in order to fix just the maximum dimensions that should not be exceeded and obtain a geometrical design dependent only on them. The file is then exported as file ".stp" (file STEP), so that it can be imported by other softwares for the structural analyses in high (HF) and low frequency (LF) domains.

As first software to be used, VA One has been selected not only for the analysis at HF, but also as ground base for the determination of the design process, calculation of modal densities and application of the design guidelines.

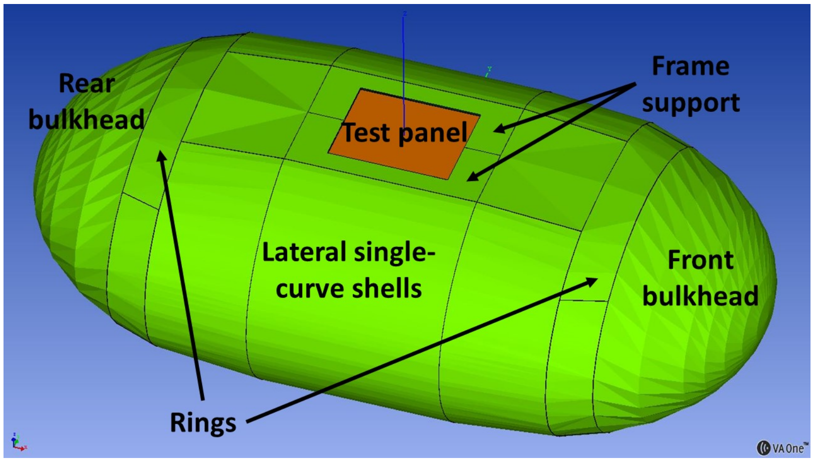

Figure 3.5: Ogive model in a VA One framework for SEA analyses.

3.3 Design rules application

By exploiting the design technique presented in Section 2.3 and keeping as reference the design guidelines obtained in the Subsection 2.3.2, it is wanted to proceed with the design process of the ogive. In Figure 3.5, the ogive is shown in a VA One framework. Before proceeding, a brief introduction to the VA One features used for the design process is given.

3.3.1 VA One settings for the ogive design process

To recreate a SEA system inside the VA One environment, three main objects are taken into account:

- *subsystems*, which are used to model the different structural and acoustic components that are able to transmit energy;
- *junctions*, which are used to model the connections between the different subsystems. As already mentioned in Section 2.4, they are responsible for the calculation of the CLFs, hence they describe how the energy is transmitted among subsystems;
- *sources*, which can describe different condition of excitation over a system in terms of injected power.

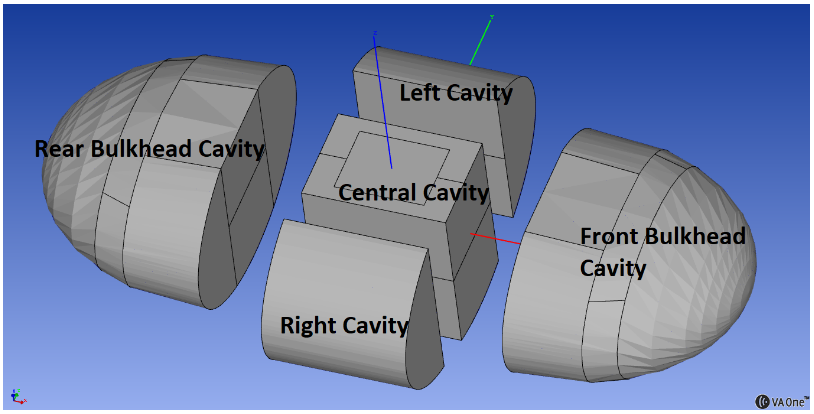

Figure 3.6: Acoustic cavities of the ogive in a VA One framework.

For the ogive description, the SEA subsystems targeted as plates, single-curved shells and double-curved shells are chosen. By looking at Figure 3.5, indeed, it is possible to recognize different elements, among which the most representative are here mentioned: the two bulkheads (front and rear), which are described as double-curved shells, the lateral single-curved shells, and the frame supports described as plates. Both SEA-plates and SEA-shells are conceived in VA One as two-dimensional SEA structural modelling subsystems. They are formulated in order to predict the energy level and vibrational velocity level for three distinct groups of resonant modes, depending on the wave-field: longitudinal, shear and bending wave propagation. Since only shells and plates are considered, only bending wave propagation is taken into account for the vibroacoustic analyses and the design process, since it is the one that participates more in the vibrational response of the structure [34]. It has been described also the inner ogive volume with acoustic cavities (Figure 3.6), to measure the Sound Pressure Level (SPL) emitted by each element of the structure and, in particular, by the test panel. The aim is to validate the design process also from an acoustic point of view, so that it would be possible to run experiments concerning not only the structural vibrations, but also the sound radiated by the sample.

Last subsystem considered is the Semi-Infinite Fluid (SIF). It represents an unbounded exterior acoustic space: the acoustic waves radiated by the subsystems connected to the SIF are not reflected back. In other words, it is wanted to describe the physical condition

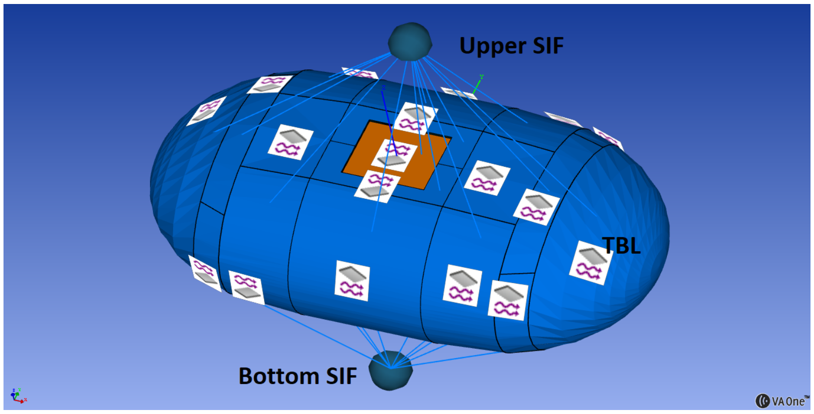

Figure 3.7: Loads and external space condition over the ogive in a VA One framework. All little squares attached on each element are representative of the TBL excitation. The two semi-spheres are the Semi-Infinite Fluid, representative of an open space and/or anechoic chamber.

of an open space around the ogive, or equivalently of an anechoic chamber. While in the previous chapter, only the line junctions were considered for the description of the energy transmission, for the design process of the ogive, all types of junctions are considered: point junctions, line junctions and area junctions.

Finally, as source responsible for the description of the injected power, the TBL excitation is chosen (asymptotic flow velocity $U_0 = 15$ m/s), described by the Cockburn and Robertson model [126], as done previously. The only change made in the TBL setting is the boundary layer thickness: for the ogive analysis, it is wanted to reproduce the development of the TBL over the ogive surface, to recreate faithfully the condition of a structure surrounded by an airflow. Hence, the boundary layer thickness is set variable with the position of each element along the x-direction. The complete setting is represented in Figure 3.7.

To develop the structural design for the ogive, the test panel properties have been fixed as done in the previous chapter; it is considered again an aluminium plate, with thickness $h = 1$ mm. The frequency range considered is $[100; 20000]$ Hz. In order to ensure a versatility of the structural device, it is suggested, for future purposes, to fix the sample model properties as *worst case scenario* is considered: by choosing as sample panel the most stiffened one in terms of material properties, it is ensured that the structural device design will guarantee the measurements purity for all other types of sample.

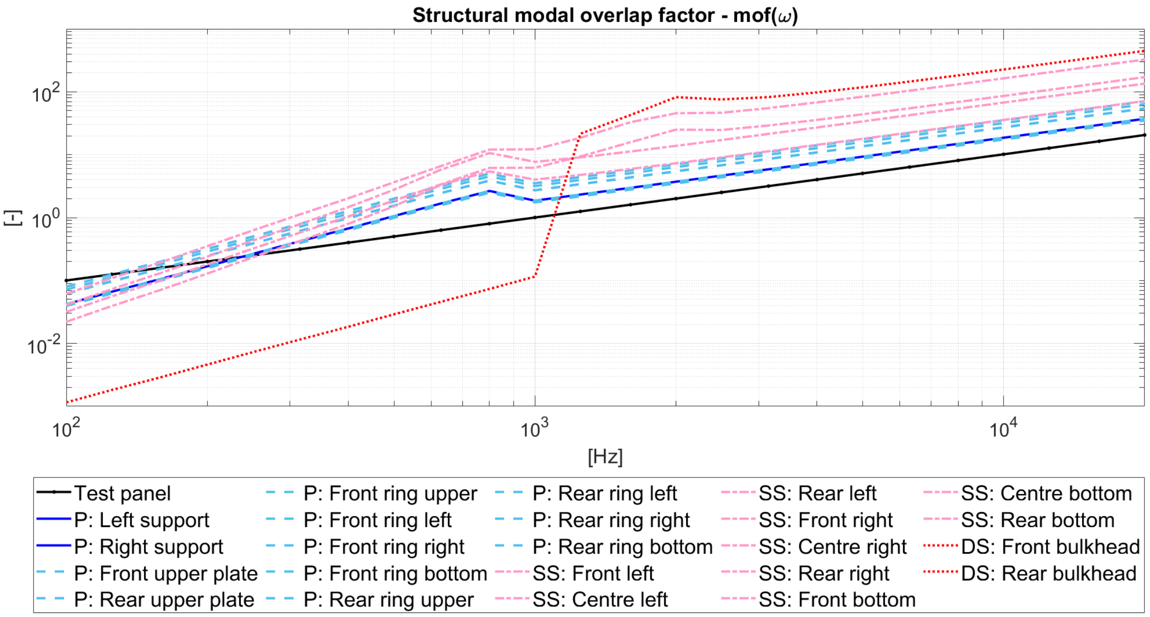

Figure 3.8: Modal overlap factors of all ogive elements. P: Plate elements. SS: Single-curved Shell elements. DS: Double-curved Shell elements.

3.3.2 First configuration

As first proposed configuration for the structural design of the ogive, material and geometry are chosen identical to the simple case presented in Chapter 2: all the SEA-elements in which the ogive has been discretized are made in sandwich, with skin in aluminium ($h_s = 2.5$ mm of thickness) and core in honeycomb (density $\rho = 48$ kg/m^3, thickness $h_c = 2$ cm).

In Figure 3.8, the modal overlap factors of all ogive elements are plotted. They are all identified by one or two letters at the beginning of their names, in order to identify how the element has been described in the VA One framework: "P" stands for Plate, "SS" for Single-curved Shell and "DS" for Double-curved Shell. It can be noticed that the frequency range of SEA validity starts from 1250 Hz.

In Figure 3.9, the modal densities are represented. Again, all elements are identified in the caption by one or two letters, so that the behaviour element is pointed out.

By looking at the modal densities of ogive elements and test panel, it is easy to distinguish the different materials involved: an aluminium plate is characterised by a constant modal

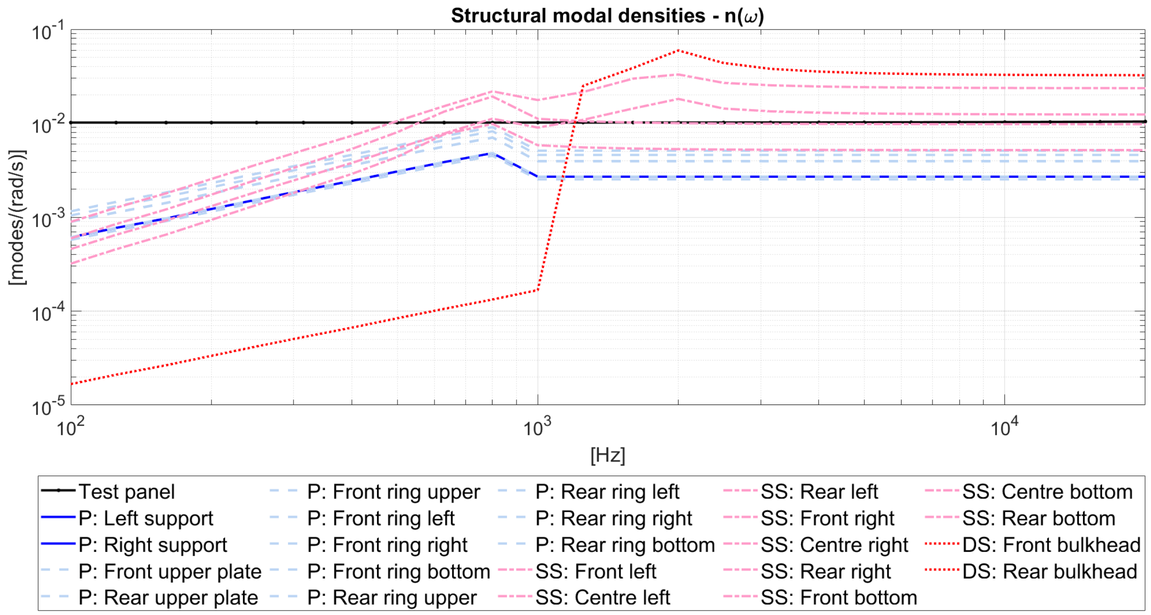

Figure 3.9: Modal densities of all ogive elements. P: Plate elements. SS: Single-curved Shell elements. DS: Double-curved Shell elements.

density, while the ogive elements present a typical sandwich behaviour already discussed in Section 2.3, for the Case 3 (Subsection 2.3.1). Moreover, it is also registered a different behaviour between the ogive plate-elements and the ogive shell-elements. As demonstrated in [127, 128], at high frequencies the modal density of the a shell approaches the one of a flat plate; it might be not evident by looking at the modal density plot *per se*, but it is obvious by looking at the asymptotic mobilities in Figure 3.10a.

As matter of fact, the asymptotic mobility is a characteristic of the material and of the thickness of the systems, hence all elements present the same mobility value, starting from ≈ 1250 Hz, which is the frequency of SEA validity. This is an additional confirm of the design rule for which the area is not a relevant design property that can influence the vibrational velocity gap between two subsystems. As last property that can be noticed from Figures 3.9 and 3.10a, the Double-curved Shells (DS) present very low values of modal density and asymptotic mobility in the LF range, then a rapid grow of the curve is registered. This is typical of the bulkheads, as they are affected by the first ring frequency, after which the DS behaviour tends to converge to the plate one. In Figure 3.10b, the asymptotic mobility

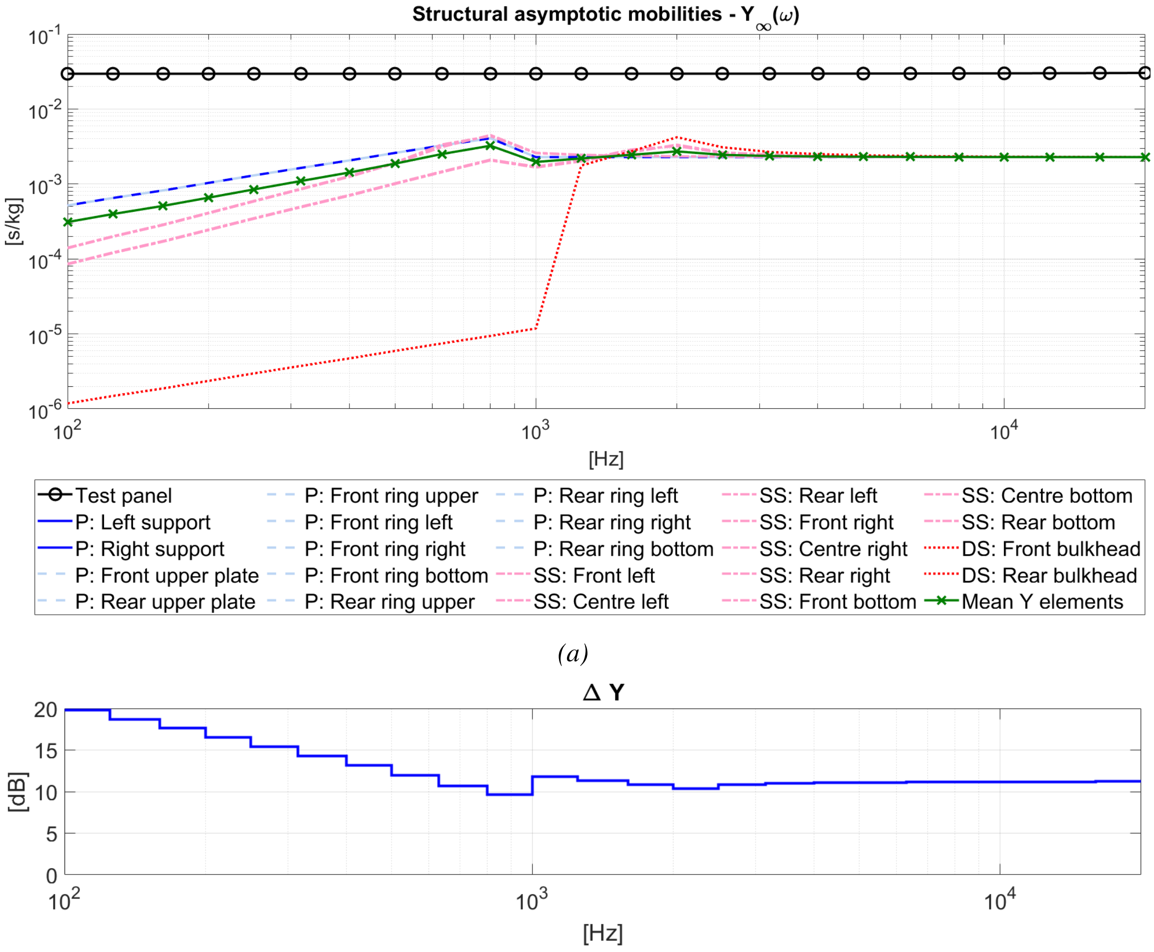

(a)

(b)

Figure 3.10: (a) Asymptotic mobilities of all ogive elements. P: Plate elements. SS: Single-curved Shell elements. DS: Double-curved Shell elements. (b) Asymptotic mobility ratio in dB between test panel mobility and the mean asymptotic mobility value of all ogive elements.

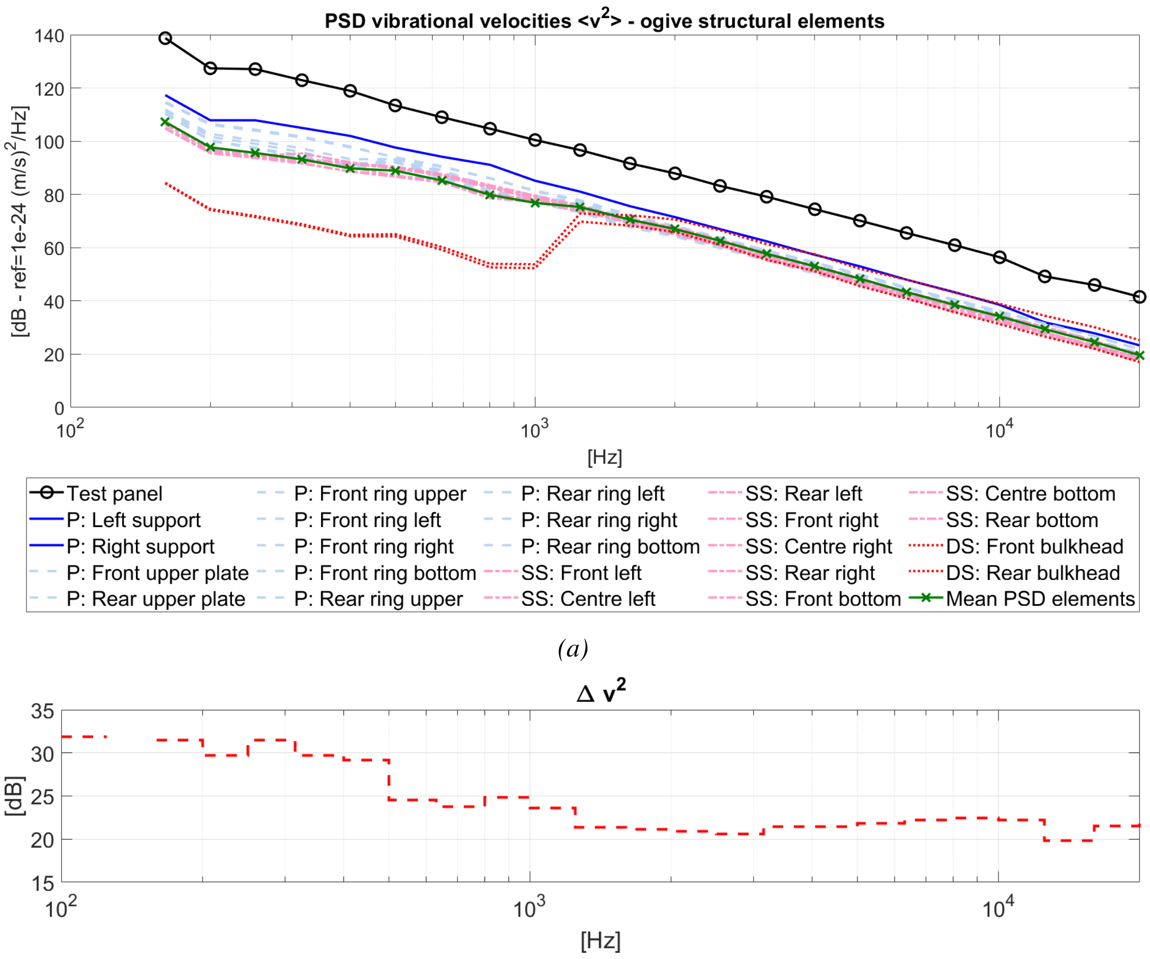

(a)

(b)

Figure 3.11: (a) PSD vibrational velocities of all ogive elements. P: Plate elements. SS: Single-curved Shell elements. DS: Double-curved Shell elements. (b) Vibrational velocity level gap in dB between test panel PSD mean value of all PSD ogive elements.

ratio between ogive elements and test panel is represented; in the HF domain, a gap of $\Delta Y \approx 11$ dB is ensured. Hence, it is expected that the vibrational velocity gap Δv^2 between sample panel and ogive would be at least higher than 11 dB. Figure 3.11a shows the PSD of vibrational velocity of each element of the support system, compared with the PSD related to the test panel.

The mean value of all ogive elements PSD is represented too. Figure 3.11b confirms that the vibrational velocity gap value, in the HF range, lies between 20 and 22 dB.

With this first configuration, it seems that the final aim is already reached. The total

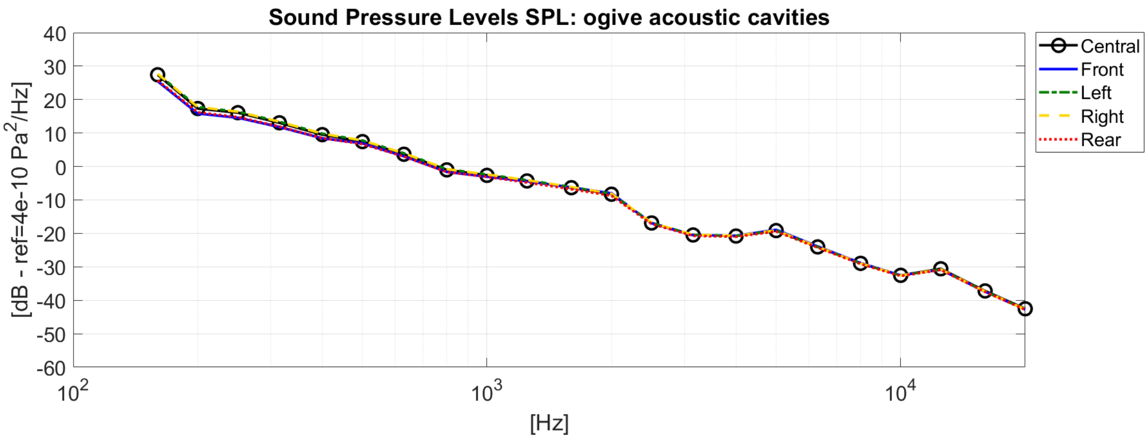

Figure 3.12: Sound Pressure Levels (dB) of the acoustic cavities inside the ogive.

mass obtained by choosing the sandwich configuration with skins in aluminium ($h_s = 2.5$ mm) and core in honeycomb (48 kg/m^3, $h_c = 2$ cm) is $W = 154.49$ kg.

As another check for the validity of the design configuration, the Sound Pressure Level (SPL) of the inner acoustic space has been calculated. As it has been already mentioned in Subsection 3.3.1, the inner acoustic space has been divided in five different acoustic cavities subsystems: front, rear, left, right and central cavity. It has been arranged this specific subdivision because it was wanted to consider the possibility of a noise control treatment of the DS and SS elements, in case their radiated power was too high and consequently it would compromise the acoustic measurements over the sample panel.

In Figure 3.12, the SPL of all the cavities are plotted. For this first configuration, no noise control treatment has been performed on any element of the structural device. As expected, the SPL is equal in all acoustic cavities, meaning that the sound radiated by the structure is equally distributed inside the ogive.

To better understand if the test panel is the element that radiates more than the other ogive elements, the injected powers in each acoustic cavity are analyzed. It is wanted to specify that it is herein used the VA One terminology: for "injected powers" is intended all the input powers into a considered SEA-subsystem. Hence, for what concerning the acoustic cavities, since they are not directly excited by the TBL pressure load, the injected powers

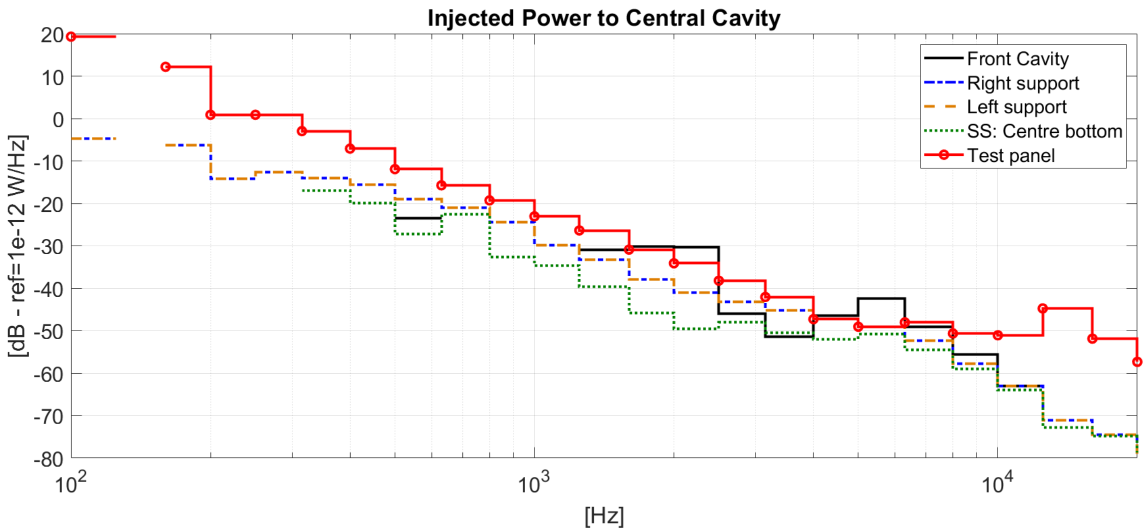

Figure 3.13: Transmitted powers to the Central cavity from the adjacent SEA subsystems.

are the transmitted powers from the adjacent subsystems.

In Figure 3.13, the transmitted powers to the Central cavity are represented. Mostly in all the frequency range, the test panel is the SEA subsystem that transmits more, but its transmitted power value is still comparable with the others. In particular, around 5000 Hz, the Front cavity transmitted power is higher than the test panel one.

In Figure 3.14, the injected powers into the other four acoustic cavities are shown. The Front cavity (Figure 3.14a) is mainly subjected to the front bulkhead transmitted power; the Left cavity (Figure 3.14b) captures the equal effects of the Left Single Shell and of the Front cavity; the Right cavity (Figure 3.14c) presents the same situation, with Right Single Shell and Front cavity transmitted powers as highest values; then, Figure 3.14d shows that Central, Left and Right cavity all contributes to transmit power to the Rear Cavity, with an additional contribution of the rear bulkhead in the HF regime.

The following interpretation has been given for these results. The TBL excitation has been described in the VA One framework with a boundary layer thickness in development along the air flow direction; hence, the front bulkhead is the most excited element of the structural device. Despite of the huge difference of performance between the test panel and the ogive, the front bulkhead vibrational velocity is such that the the subsystem would

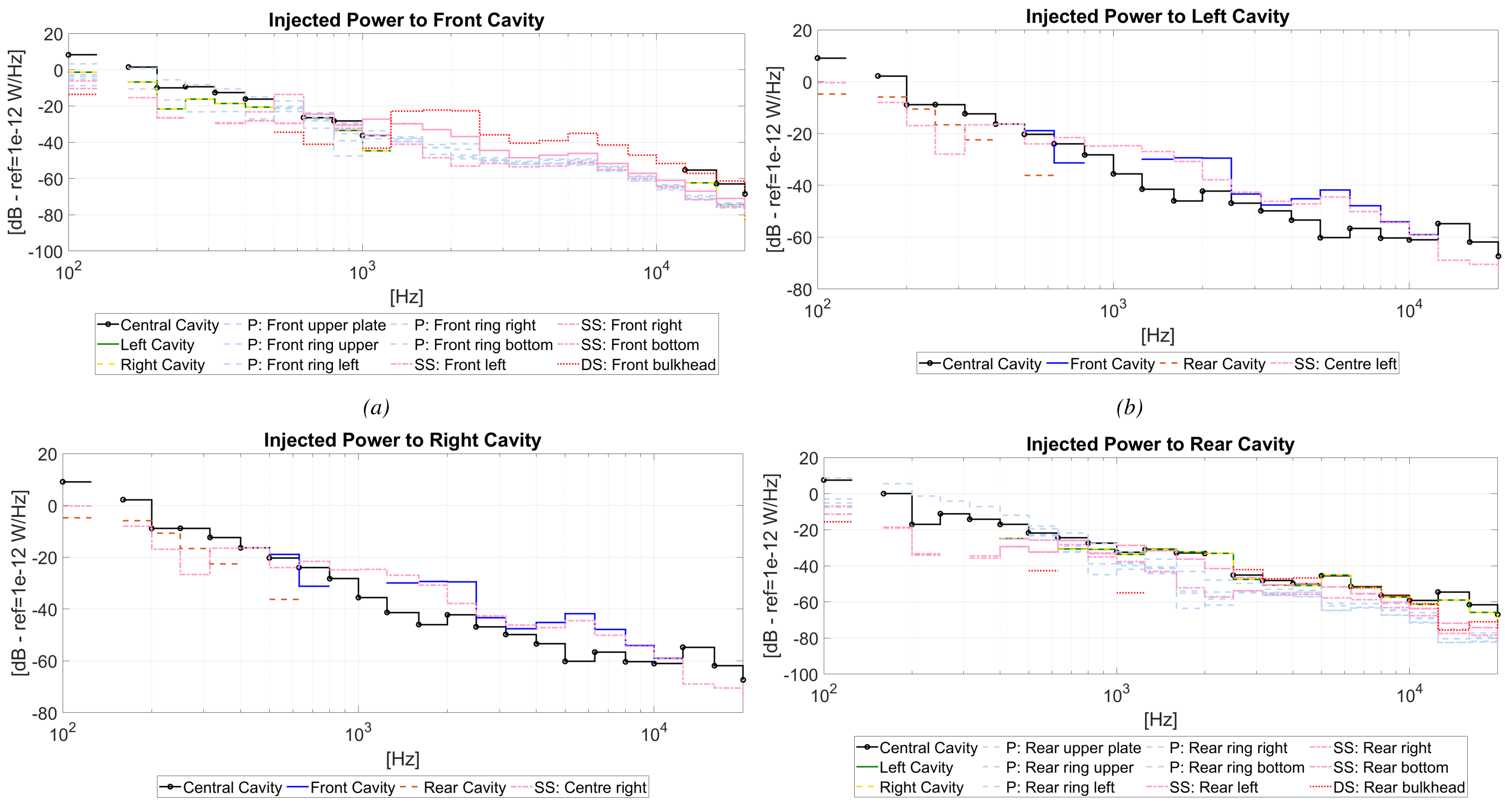

(a) *(b)*

(c) *(d)*

Figure 3.14: Injected powers to the other acoustic cavities. (a) P_{inj} to Front cavity; (b) P_{inj} to Left cavity; (c) P_{inj} to Right cavity; (d) P_{inj} to Rear cavity.

	Density [kg/m^3]	Thickness [m]	DLF
Felt	50	0.003	
Plastic foam	31	0.03	0.055

Table 3.1: NCT layers properties.

transmit its energy to the front acoustic cavity and consequently, the energy would be transmitted to the adjacent cavities, reaching the back of the ogive.

To avoid this problem, a second configuration is presented, in order to control the injected powers to the acoustic cavities and ensure that the test panel is the main transmitter of energy.

3.3.3 Optimization of design parameters

A Noise Control Treatment (NCT) is herein proposed in order to handle the SPLs and the powers transmitted by the structural elements to the acoustic cavities. It has been applied, over the internal surface of all ogive elements, a double layer of NCT composed by a first layer in felt fiber and a second layer in plastic foam. The material properties of both layers are expressed in Table 3.1. The intention is to reduce the transmitted powers from the structure to the acoustic cavities, in such a way the Central cavity would register only the power radiated by the test panel.

The first results that can be appreciated are the SPLs of the five cavities (Figure 3.15). It is evident that there is a difference in the SPLs between the previous case and the optimized one. If before, in all acoustic cavities, the energy is well distributed, now with the application of the NCT, the central cavity SPL is higher than all the other SPLs. This means that the highest radiated power is transmitted from one of the structural elements directly in contact with the central cavity, possibly the test panel.

Once the attention is passed on the injected powers to the central cavity, it is clear which element is the main responsible of the SPL (Figure 3.16). The power transmitted from the test panel to the central cavity is much higher compared to the others. Since the SEA validity

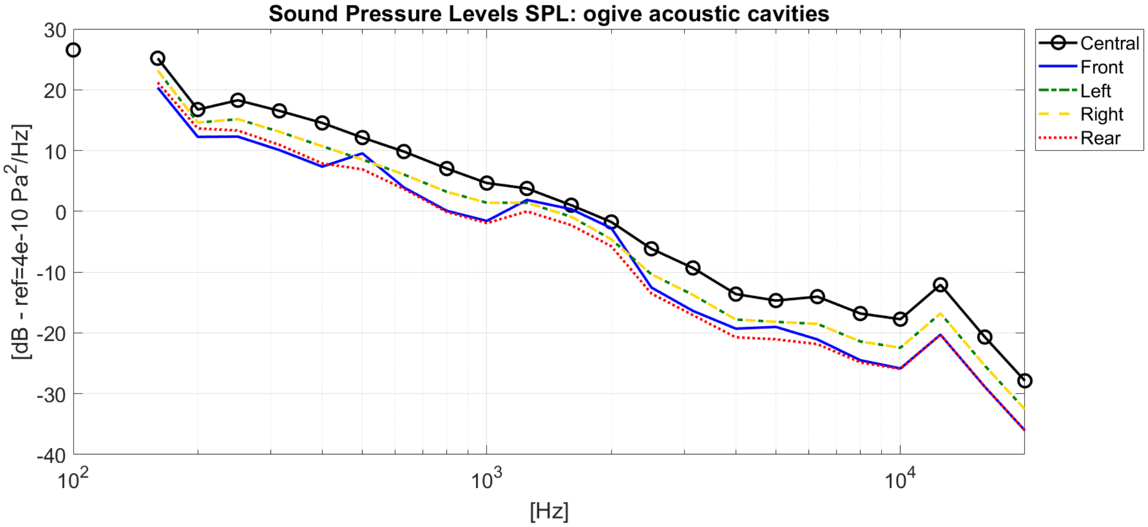

Figure 3.15: **Optimized configuration.** *Sound Pressure Levels (dB) of the acoustic cavities inside the ogive.*

frequency $f_{SEA} = 1250$ Hz, more than 20 dB of difference is registered along all the HF domain.

As last check, the transmitted powers to the other acoustic cavities have been analysed (Figure 3.17). Starting from the two lateral ones plotted in Figures 3.17b-3.17c, it can be seen that the power transmitted by the central cavity presents now higher values along all the frequency domain, while in the previous case it was smaller than the power level transmitted by the structural single shells directly in contact with the right and left acoustic cavities. In the frequency range [1000;2000] Hz, there is though an increase of the transmitted power by the aforementioned structural elements. This particular event will be commented later.

In Figure 3.17a, the injected powers in the front cavity are plotted. While in the previous case, the front bulkhead was the structural element that contributed more transmitting energy, now it is the central cavity that appears to dispense more energy in the front cavity. It can be noticed again that, in the frequency range [1000;2000] Hz, the double-shell contribution has an increase of transmitted energy, as it happened in the left and right acoustic cavities due to, respectively, the left and right single-shells.

Finally, the injected powers in the rear cavity are shown in Figure 3.17d. Again, the

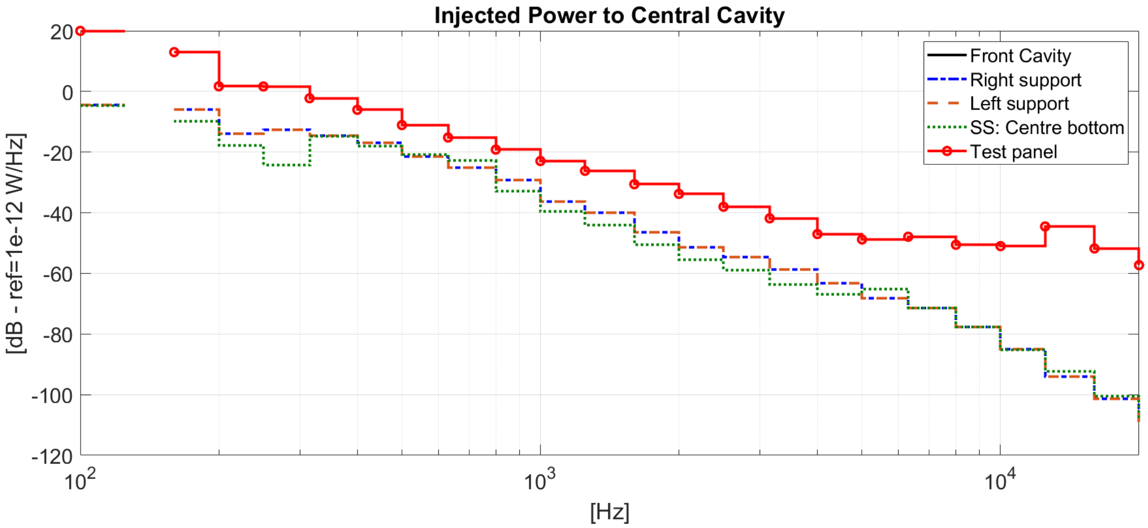

Figure 3.16: **Optimized configuration.** *Transmitted powers to the Central cavity from the adjacent SEA subsystems.*

contribution of the central cavity is the one of the highest along all the frequency range, except for that particular range [1000;2000] Hz, in which the power transmitted by the double shell results higher.

From the analysis of all these collected results, it can be said that the application of a NCT provided an improvement of the configuration, ensuring that the radiated sound power of the test article is the structural element that radiates more compared to the other ogive components. The condition for which the central cavity has the highest values of transmitted powers in all the other acoustic cavities means that the radiated sound power of the test panel is so elevated that can be propagated in the other cavities. Moreover, even though the contribution of the double and single shells in the frequency range [1000;2000] Hz is higher than the central cavity one, it is also true that this event in not evident among the injected powers in the central cavity; this can be interpreted as the radiated sound powers of single and double shells are not able to reach the central cavity.

An interpretation about the increase of transmitted powers in the frequency range [1000;2000] Hz is now given. Firstly, in this particular interval, the SEA simulation can be considered valid, since the $f_{SEA} = 1250$ Hz. Secondly, the double shells present a

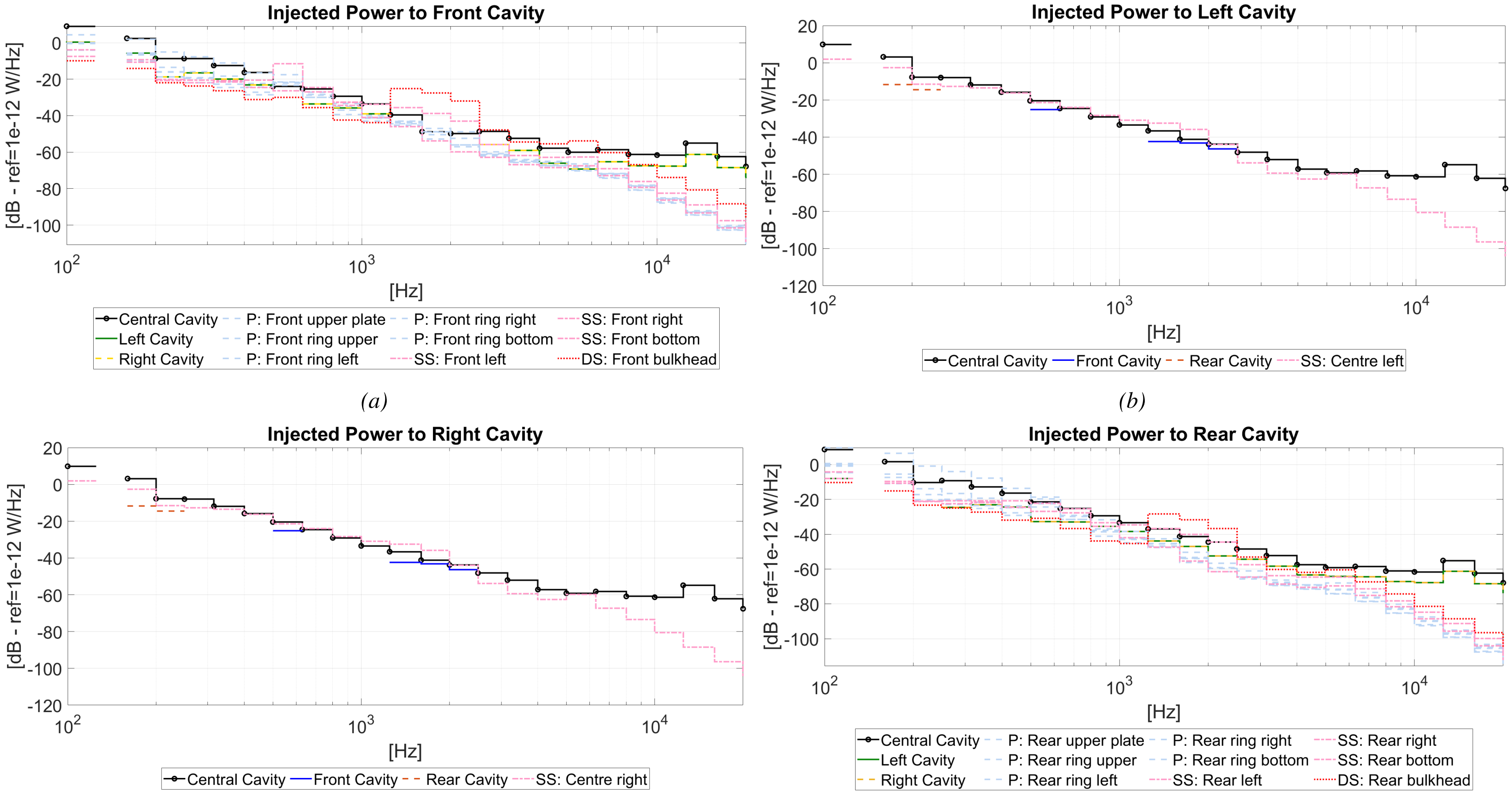

(a) *(b)* *(c)* *(d)*

Figure 3.17: **Optimized configuration.** *Injected powers to the other acoustic cavities. (a) P_{inj} to Front cavity; (b) P_{inj} to Left cavity; (c) P_{inj} to Right cavity; (d) P_{inj} to Rear cavity.*

change of behaviour, as it can be noticed in the modal density graph (Figure 3.9); indeed, in the LF region, the elements do not present high vibrational velocity values (Figure 3.11a), then their behaviours conform to the one of the other components. It might mean that the frequency ring, characteristic of the two SEA-elements, is in this peculiar frequency range. The resonance is evident also in the SPL graph in Figure 3.15.

Another important behaviour has been noticed, and it regards the test panel: from Figure 3.15 to Figure 3.17, there is a peak of amplitude recorded around ≈ 12500 Hz. By considering the equation

$$\lambda_B(\omega) = \lambda_0(\omega) \quad \Longrightarrow \quad 2\pi \left(\frac{D}{\rho h \omega^2} \right)^{1/4} = \frac{2\pi\omega}{c_0} \tag{3.1}$$

which imposes an equality between the structural flexural wavelength λ_B and the acoustic one λ_0, it is possible to recover the acoustical coincidence frequency $f_{0,c}$, defined as

$$f_{0,c} = \frac{c_0^2}{2\pi} \sqrt{\frac{\rho h}{D}} \tag{3.2}$$

Since the test panel is an aluminium plate with thickness $h = 0.001$ m, it has been calculated that the acoustical coincidence frequency is, as expected, $f_{0,c} = 11732$ Hz. The resonance with the acoustic cavities can be noticed also in the previous case, where there is no NCT. However, the effect of the resonance is more evident in the second case.

3.4 Ogive modal analysis at low frequencies

As last test performed over the coupled system ogive - test panel, a modal analysis has been conducted in order to inspect the ogive structural design and see if the decoupling is ensured also in the LF regime. The commercial software COMSOL Multiphysics has been used for this study.

The material properties considered for the complex structure are always the same, only the NCT has been excluded. Hence, the ogive has been modeled as a shell made in sandwich with aluminium skins and a honeycomb core, while the test panel is always is aluminium, with dimensions $0.5 \times 0.4 \times 0.001$ m^3.

The boundary conditions applied on both ogive and test panel have been expressed as follows: the ogive is free from any constrain, as it is suspended, so the only edges that are free are the ones on which the test panel is located; consequently, it has been applied, on the test panel, a condition of simply-supported restricted to the local system of the ogive edges. In COMSOL, this particular condition has been respected by entering a continuity condition over only the edges displacements as

$$u_{\text{ogive}} = u_{\text{test panel}} \tag{3.3}$$

$$v_{\text{ogive}} = v_{\text{test panel}} \tag{3.4}$$

$$w_{\text{ogive}} = w_{\text{test panel}} \tag{3.5}$$

while no condition has been fixed over the test panel edges rotations.

For the mesh elements dimensions, it has been chosen an extremely fine element size, with a minimum element dimension equal to $\Delta_{min} =$ 6e-4 m and a maximum one equal to $\Delta_{max} = 0.06$ m. Considering that the modal analysis has been run in a frequency range [0; 3000] Hz, the minimum element dimension calculated through the equation $\Delta_{min} = \lambda_B(\omega)/4$ is 0.02 m, so it is sure that the chosen mesh would give a faithful description of the mode shapes.

In Table 3.2, the first twenty modes of the coupled system ogive - test panel are reported, in comparison with the first eleven modes of the uncoupled test panel and the first nine modes of the uncoupled ogive. With a rapid reading of the natural frequencies, it seems that the coupled system kept the test panel natural frequencies well separated from the ogive ones. As matter of fact, the first three f_n of the uncoupled test panel differ of less than 1 Hz from the coupled system ones, then the difference starts to increase, reaching a value of

Test panel		Ogive		Coupled systems	
Mode	f_n [Hz]	Mode	f_n [Hz]	Mode	f_n [Hz]
1st (1,1)	25.2			1st	25.1
2nd (2,1)	54.8			2nd	54.4
3rd (1,2)	71.4			3rd	70.7
4th (2,2)	100.9			4th	99.7
5th (3,1)	104.1			5th	102.5
		1st	122.5	6th	124.7
		2nd	133.1	7th	131.8
6th (1,3)	148.4			8th	146.4
7th (3,2)	150.2			9th	147.7
		3rd	170.9	10th	168.0
		4th	171.4	11th	171.2
8th (4,1)	173.0			12th	171.8
9th (2,3)	177.9			13th	174.3
		5th	186.1	14th	184.4
		6th	197.2	15th	192.7
		7th	200.4	16th	203.2
		8th	207.1	17th	212.9
10th (4,2)	219.1			18th	214.5
		9th	218.6	19th	216.9
11th (3,3)	227.1			20th	221.9

Table 3.2: Modes and natural frequencies of the coupled system, in comparison with the modes and natural frequencies of the two decoupled systems, ogive and test panel.

$\approx 5 \div 6$ Hz. The same can be said about the comparison between the natural frequencies of the coupled system and the uncoupled ogive ones, which they keep a difference of $\approx 2 \div 3$ Hz.

In Figures from 3.18 to 3.21, the mode shapes of four different modes referred to the coupled system are compared with the relative mode shape of the uncoupled system (test panel or ogive, depending which mode is considered). In particular, in Figure 3.18 it is shown the comparison between the 1st mode of the complex structure and the 1st mode of the uncoupled test panel; it can be appreciated that the mode shape of the test panel is respected in the coupled system configuration. This faithful description of the test panel mode shape is maintained for all its modes; in Figure 3.20, the ninth flexural mode of the panel is perfectly represented by the coupled system, which does not present any deformation over the entire

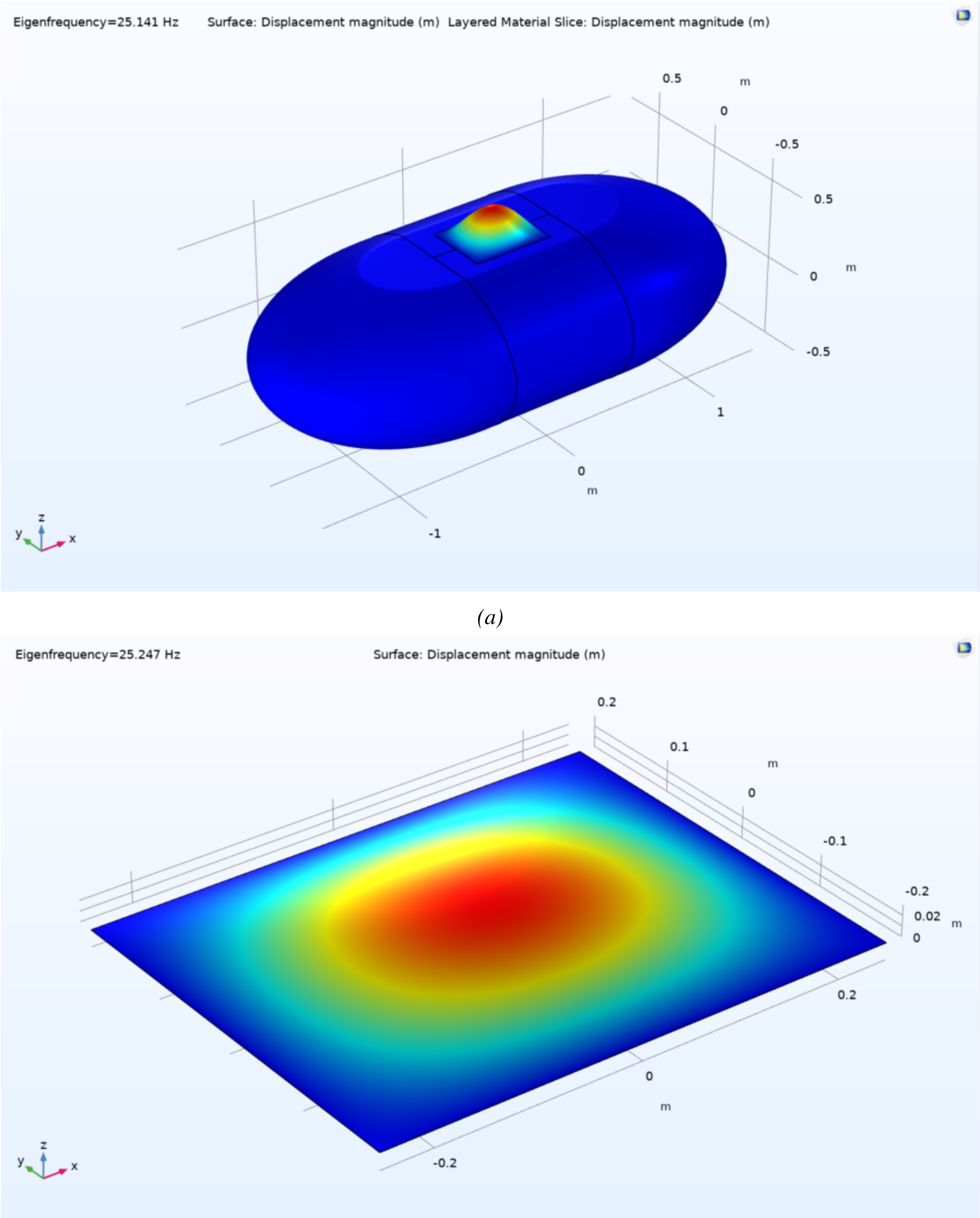

(a)

(b)

Figure 3.18: First flexural mode of the system ogive-test panel, in comparison with the first flexural mode (1,1) of just the test panel.

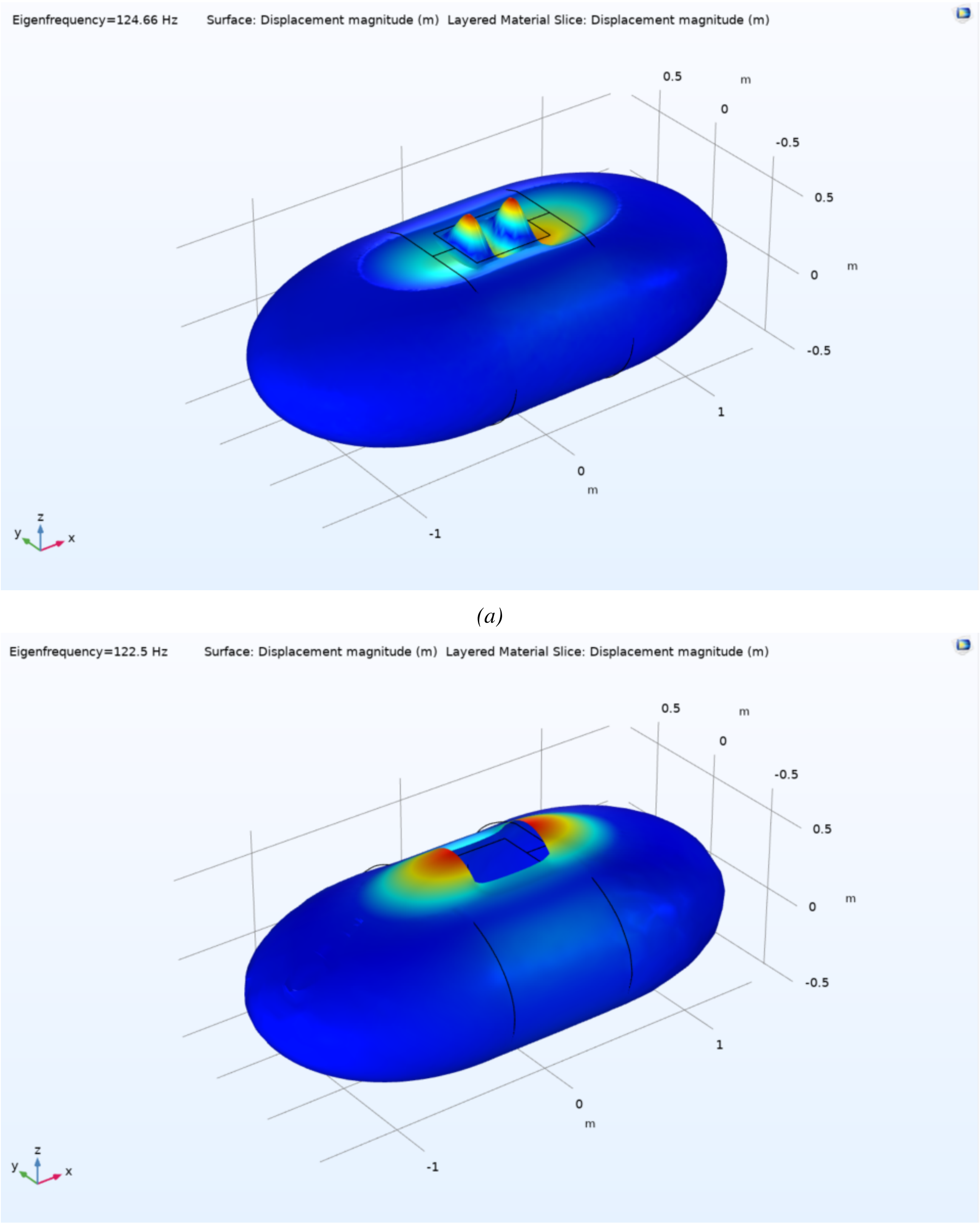

(a)

(b)

Figure 3.19: Sixth flexural mode of the system ogive-test panel, in comparison with the first flexural mode of just the ogive.

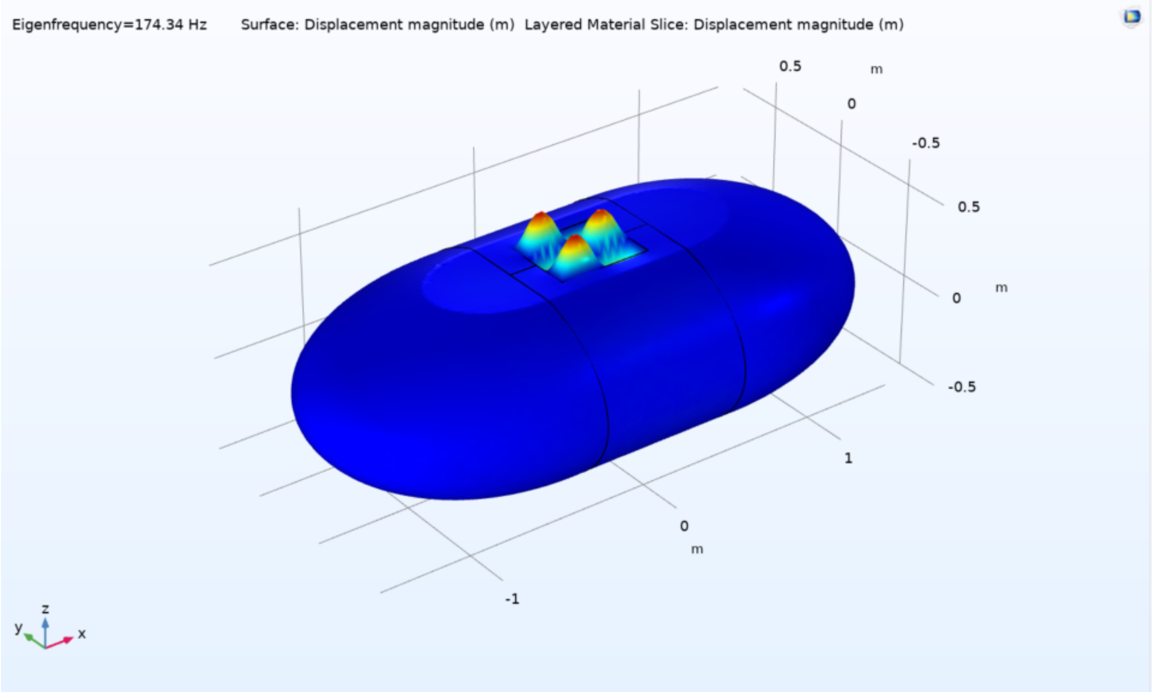

(a)

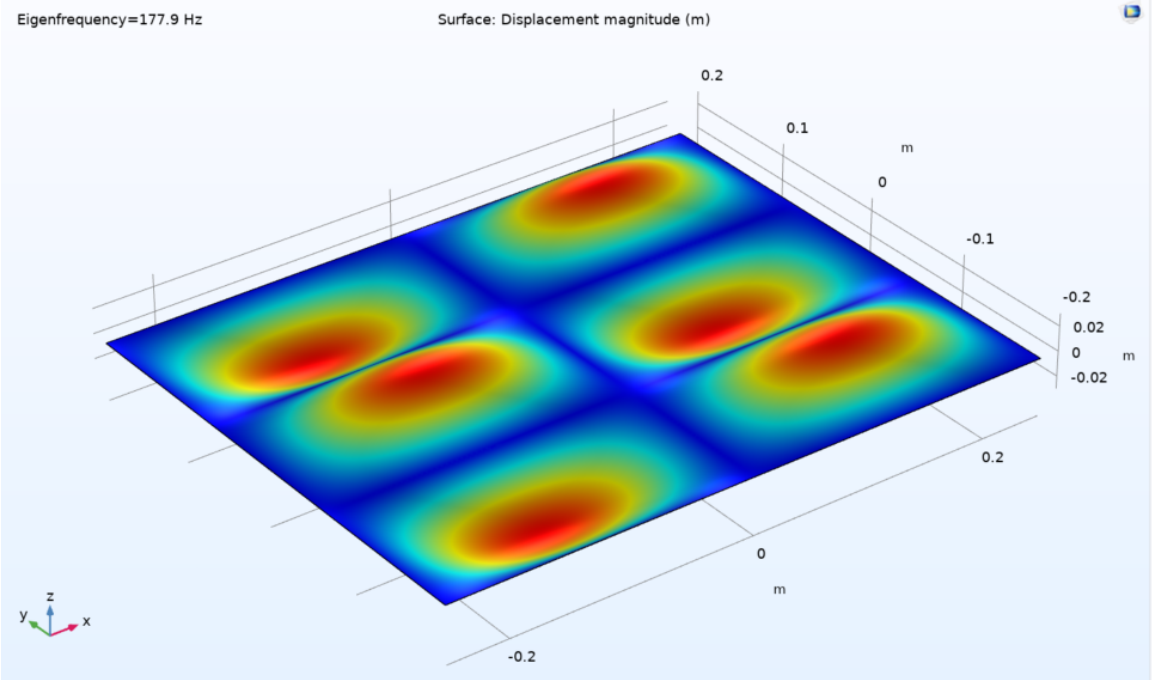

(b)

Figure 3.20: Thirteenth flexural mode of the system ogive-test panel, in comparison with the ninth flexural mode of just the test panel.

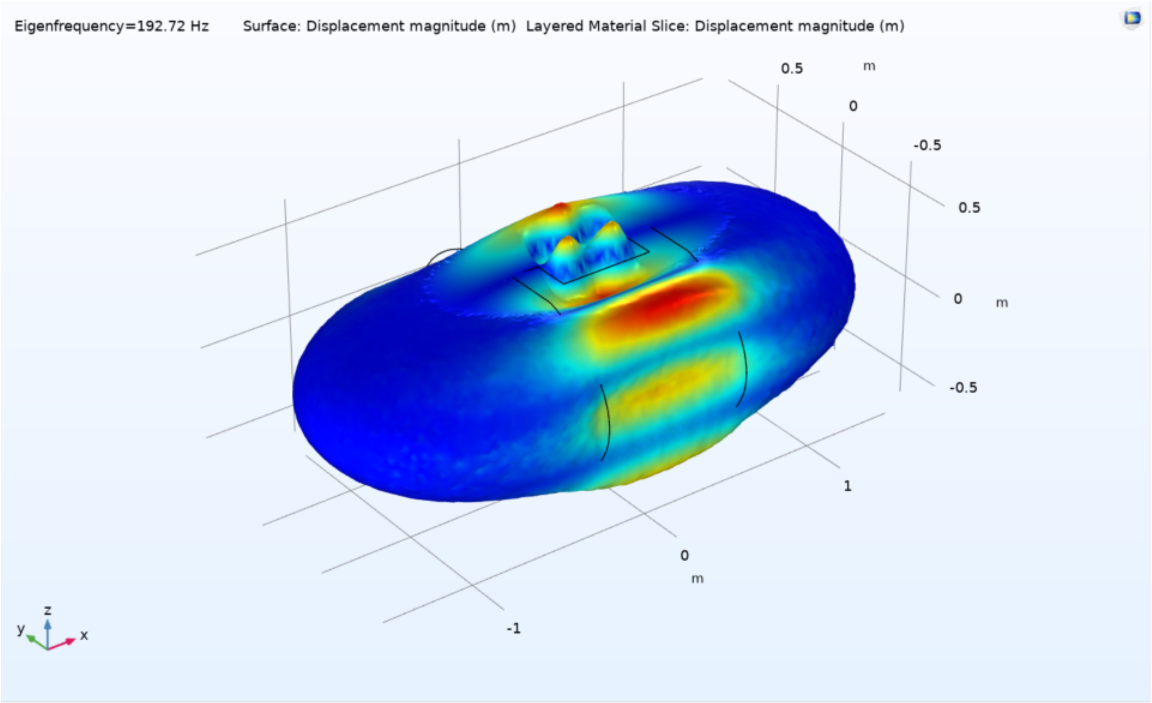

(a)

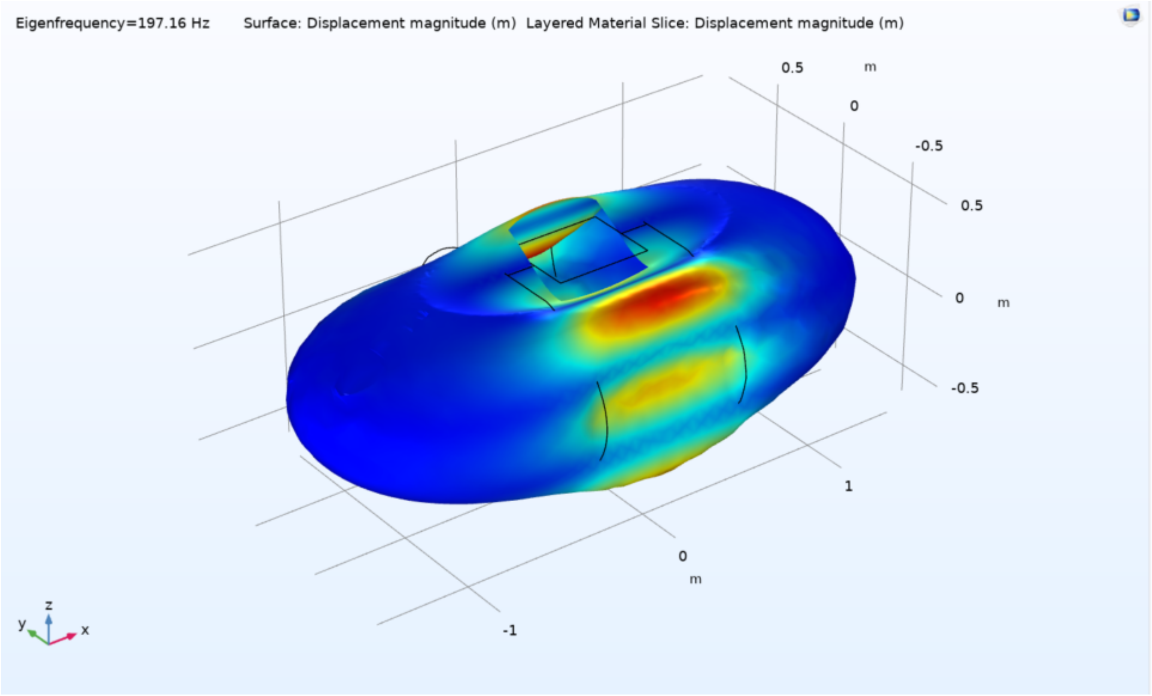

(b)

Figure 3.21: Fifteenth flexural mode of the system ogive-test panel, in comparison with the sixth flexural mode of just the ogive.

structure, except for the surface region referred to the test panel.

On the other hand, by looking at Figures 3.19 and 3.21, it is possible to see what happens to the test panel when the coupled system shows the mode shapes related to the ogive dynamic behaviour. It can be said that the mode shapes of the uncoupled ogive are well represented by the complex structure, but of course the test panel will present some deformation due to the continuity condition applied at the edges.

It might be deduced that test panel and ogive are not decoupled in the LF range, but with the structural design chosen with the design guidelines developed with SEA, it has been ensured that there is no overlap between the test panel modes and the ogive ones. This means that, once the mode shapes and natural frequencies of the ogive are found and stored, it is then easy to individuate the test panel information from its Frequency Response Function (FRF) by just not considering the already known eigensolutions referred to the support.

A simple comparison among eigensolutions of the coupled and uncoupled systems is not enough for a validation of the structure; other simulations which involve the FRF calculation of the test panel and of the ogive, for the coupled and uncoupled conditions, need to be done, in order to understand better the dynamic behaviour of this complex structure.

3.5 Conclusions

In this third chapter, it was wanted to reach the first aim of this research. It has been already introduced, in the previous pages, the process for the structural design of a support for vibroacoustic measurements in a wind tunnel facility. The suggested design guidelines can be applied for any type of structure, since they are developed from the SEA, which uses formulations averaged over space and frequency domains for the description of even complex structures. They have been applied for a simple system composed by two plates; one was the test model and the second was the frame which supported it. The guidelines worked perfectly and an ideal configuration has been found for the frame support in order to guarantee a vibrational velocity gap of ≈ 20 dB.

The same guidelines have been applied for a complex structure, herein introduced as "ogive", which can be installed in a large-scale wind tunnel facility. The shape is inspired by the submarine configurations, since the ogive would be hanged inside the test section of the wind tunnel and the air flow would embrace all the ogive surface. It has been taken in consideration the diameter of the test section, so that there would not be any effect of the flow at the boundaries. Unfortunately, no information about the pressure field generated by the facility has been given, so the geometry design of the ogive has not been conceived with an aerodynamic study.

The SEA simulation has been run with the commercial software VA One, about which a brief introduction has been provided. A first configuration is proposed, based on the use of the same configuration applied for the last case of the simple system studied in Chapter 2. Although it has been already achieved a vibrational velocity gap of ≈ 20 dB with this configuration, a study over the Sound Pressure Levels of the inner acoustic cavities has been performed. In order to ensure a radiated sound power of the test panel much higher than the one of the ogive components, a Noise Control Treatment has been applied over the inner surface of the support.

In conclusion, with a fast procedure which includes: (i) a smart structural design based on a proper material and geometry choices, and (ii) an SEA simulation, a structural device for vibroacoustic measurements has been developed. A modal analysis, developed by applying a Finite Element Method (FEM) with the commercial software COMSOL Multiphysics, has been then performed in order to compare the eigensolutions of the coupled system test panel-ogive with the eigensolutions of the two uncoupled systems. Thanks to the structural design obtained from the guidelines herein proposed, the mode shapes of ogive and test panel result to be not overlapped since the first flexural mode. Indeed the test panel preserves its natural frequencies and mode shapes in the coupled system and presents other kind of deformations concurrently with the eigensolutions of the ogive. Ideally, once the eigensolutions related to the only support are known, it would be easy to identify them in the test panel FRF by avoiding the peaks that are referred to the ogive eigenfrequencies. It is also true that a more thorough study is necessary in order to better understand the dynamic behaviour of this structural device.

It is wanted to remark that performing experimental tests inside wind tunnel facilities is a particular task with its own difficulties. Although the efforts in designing a structural device to ensure the purity of the measurements, an experimenter should remember that the acoustic background noise of the facility can be even worse than the structure-borne background noise. AT LF, indeed, the acoustic modes can dominate the WPFs easily, while at HF the turbulent flow can radiate sound directly and, at the same time, excite the wind tunnel walls which would consequently radiate sound too. Hence, not only a support structure, but also the whole test section and the facility acoustics should be designed carefully. In merit to this topic, the work of Donavan and Blake is here suggested [129], since they studied the effect on the tunnel noise of the application of different coatings over the facility walls. In merit to this problem, it is here stressed again the main advantage of SEA, with which is possible to extend the design process by including the acoustic regions.

Together with the structural design guidelines proposed in Chapter 2, a validation method of the design is proposed in the forthcoming Chapter 4, so that the structure can be tested before to be located inside a wind tunnel facility. Consequently in Chapter 5, different numerical applications are discussed in order to evaluate the proposed validation method and two comparisons with experimental data collected in two different wind tunnel facilities are then shown to demonstrate the efficiency of the method.

CHAPTER 4

ALTERNATIVE METHODS FOR THE CALCULATION OF THE STRUCTURAL RESPONSE TO A TBL EXCITATION

4.1 Introduction

In the previous chapters, it has been specified the necessity of an "off-line" validation for the designed complex structure, in order to test the functionality of the device before allocating it in a wind tunnel facility. On the other hand, it has been also highlighted the difficulties encountered in attempting to represent an aerodynamic load using different experimental tools that are not a wind tunnel.

In this chapter, the structural response of a system subjected to an aerodynamic load is discussed, the difficulties of representing this type of excitation are outlined and possible alternative solutions for its representation are enunciated. The PEDE$_M$ method, in particular, will be explained in detail and an experimental method will be extrapolated from it, in order to allow the application of an aerodynamic load through a deterministic and punctual excitation.

4.2 Theoretical background about structural response to a TBL excitation

For the study of the structural response of a generic structure subjected to an aerodynamic load, the representation of the excitation in this framework presents intrinsic difficulties, and consequently some simplifications of the problem are needed.

The aerodynamic load is generally expressed as wall-pressure fluctuations (WPFs) applied over the structure surface that is "wet" by the air flow. These pressure fluctuations are confined inside the boundary layer, which is a particular area over the structure surface in which the air flow presents null velocity at the surface and a flow velocity equal to the asymptotic air flow at the edge of the boundary layer. From a strictly theoretical point of view, it is important to say that the development of the flow starts laminar and then it becomes turbulent.

For structural dynamic analyses, two approximations are generally considered in order to express an aerodynamic load:

- because the passage from laminar to turbulent is usually very fast, the boundary layer is always considered turbulent; hence the thickness of the TBL is sometimes fixed to a constant value, or there are semi-empirical formulas which regulates the boundary layer thickness, depending on the air flow velocity;
- because the TBL is considered, indeed, turbulent, the wall-pressure fluctuations are described as a random broadband excitation.

Moreover, an additional approximation of the problem under analysis regards the fluid-structure interaction between the system and the aerodynamic load. In fact, the structure subjected to the WPFs is generally considered rigid, meaning that are no aeroelastic effects on the air flow.

Taking into account all the aforementioned approximations, statistical methods are hence employed for the description of the TBL excitation. Although much of the information to understand the turbulent mechanisms may be lost, these will not be relevant for the representation of the structural response.

4.2.1 Statistical Analysis

The statistical analysis of a random process $\{x(t)\}$ involves the study of the random variable X_i at a time t_i. In this paragraph, the different statistical quantities necessary to characterise a random process are recalled. The mean value of the random process $\{x(t)\}$ from the probability density function p is defined as

$$E[x] = \int_{-\infty}^{+\infty} xp(x)dx \tag{4.1}$$

Equally, the mean square value is defined as

$$E[x^2] = \int_{-\infty}^{+\infty} x^2p(x)dx \tag{4.2}$$

In order to introduce these statistical notions in the formulations corresponding to the response of a linear system to a random excitation, it is appropriate to recall the notions of auto-correlation. The auto-correlation function corresponds to the mean value associated with the product of the random variables x_1 and x_2

$$E[x_1x_2] = \int_{-\infty}^{+\infty}\int_{-\infty}^{+\infty} x_1x_2p(x_1,x_2)dx_1dx_2 \tag{4.3}$$

Most applications involve this auto-correlation function expressed in function of a time delay $\tau = t_1 - t_2$, in the specific case where two different time instants t_1 and t_2 are considered.

$$R(\tau) = E[x_1(t_1)x_2(t_1+\tau)] \tag{4.4}$$

A random process is said to be *stationary* if all these statistical properties are time invariant. The auto-correlation function then depends only on the time delay $\tau = t_1 - t_2$. A stationary random process is said to be *ergodic* if the time average and the time correlation function correspond exactly to the statistical average and the statistical correlation function. With the application of these two definitions, it is possible to study a random process $\{x(t)\}$ starting from a single time-dependent record $x^{(i)}(t)$ presenting the aforementioned characteristics. The time average value of this sample is hence defined as

$$\langle f(t)\rangle = \lim_{T\to\infty}\frac{1}{T}\int_0^T f(t)dt \tag{4.5}$$

the mean square value is

$$\langle f^2(t)\rangle = \lim_{T\to\infty}\frac{1}{T}\int_0^T f^2(t)dt \tag{4.6}$$

And the auto-correlation function, from a time dependence point of view, is defined as

$$\phi(\tau) = \lim_{T\to\infty}\frac{1}{T}\int_0^T f(t)f(t+\tau)dt \tag{4.7}$$

The property of ergodicity allows to express this relation

$$E[f(x)] = \langle f(t)\rangle \tag{4.8}$$

$$R(\tau) = \phi(\tau) \tag{4.9}$$

Practically speaking, all the quantities that allow the description of a random process, are basically defined in the frequency domain. Indeed, the vibrational response of a structure and the random broadband excitation applied on it are generally studied as Power Spectral Densities (PSD).

Power Spectral Density $S_x(\omega)$ is the Fourier transform of the auto-correlation function $R_x(\tau)$ [130]

$$S_x(\omega) = \int_{-\infty}^{\infty} R_x(\tau)e^{-\imath\omega\tau}d\tau \tag{4.10}$$

$$R_x(\tau) = \frac{1}{2\pi}\int_{-\infty}^{\infty} S_x(\omega)e^{\imath\omega\tau}d\omega \tag{4.11}$$

Similarly, the PSD can be defined starting from the Fourier transform $X(\omega, T)$ of the squared module of the random function $x(t)$

$$S_{xx}(\omega) = \lim_{T \to \infty} \frac{1}{T} E[|X(\omega, T)^2] \tag{4.12}$$

For this particular case, $S_{xx}(\omega)$ is called Auto-Spectral Density (ASD); from a physical point of view, it represents the function $x(t)$ energy distribution in the frequency domain.

On the other hand, by considering two different functions $x(t)$ and $y(t)$ and their corresponding Fourier transforms $X(\omega, T)$ and $Y(\omega, T)$, it is possible to define the Cross-Spectral Density (CSD) as

$$S_{xy}(\omega) = \lim_{T \to \infty} \frac{1}{T} E[X^*(\omega, T)Y(\omega, T)] \tag{4.13}$$

where X^* is the complex conjugate of X. The CSD is related to the cross-correlation function as

$$S_{xy}(\omega) = \int_{-\infty}^{\infty} R_{xy}(\tau) e^{-\imath\omega\tau} d\tau \tag{4.14}$$

$$R_{xy}(\tau) = \frac{1}{2\pi} \int_{-\infty}^{\infty} S_{xy}(\omega) e^{\imath\omega\tau} d\omega \tag{4.15}$$

4.2.2 Structural response to a random excitation

The response of a structure subjected to an ergodic stationary random excitation is considered by studying the response of a linear system subjected to a set of excitations. By considering, for example, n excitations, it is possible to define their ASD and CSD by building a matrix $[S_{xx}]$ of size $n \times n$. Because of the way the CSD matrix is built, this is hermitian ($[S_{xx}]^T = [S_{xx}]^*$).

The response of a linear system to n ergodic stationary random excitations is expressed

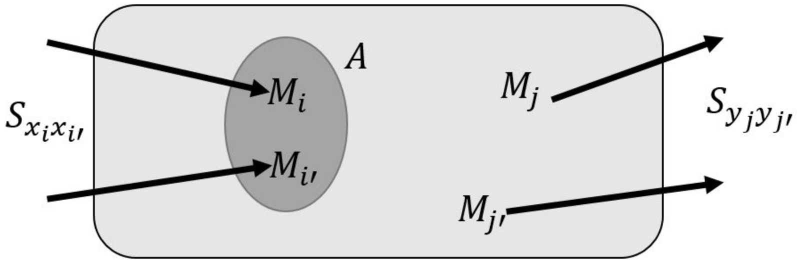

Figure 4.1: Example of continuous system response to a random pressure excitation.

through the transfer function $H(\omega)$, which links an input x_i to an output y_j as

$$Y_j(\omega) = H_{ij}(\omega)X_i(\omega) \tag{4.16}$$

which in matrix form is expressed as

$$\{Y(\omega)\} = [H(\omega)]\{X(\omega)\} \tag{4.17}$$

In the case of a continuous system excited by distributed forces, such as a wall-pressure, the output spectra can be put into the form of integration over the total excited surface A (Figure 4.1)

$$S_{y_j y_{j'}}(\omega) = \int_A \int_{A'} H^*_{ji}(\omega) H_{j'i'}(\omega) S_{x_i x_{i'}}(\omega) dM_i dM_{i'} \tag{4.18}$$

Generally, the CSD would depend on the frequency content and on the application points M_i and $M_{i'}$, but in the specific case of an aerodynamic excitation represented as a distributed pressure excitation $S_{p_i p_{i'}}(\omega)$, the CSD can be exploited as

$$S_{p_i p_{i'}}(\omega) = S_{p_i p_i}(\omega)\Gamma_{p_i p_{i'}}(x_i - x_{i'}, y_i - y_{i'}; \omega) \tag{4.19}$$

where $S_{p_i p_i}(\omega)$ is the frequency content of the excitation, usually considered constant over the excited surface, and $\Gamma_{p_i p_{i'}}(x_i - x_{i'}, y_i - y_{i'}; \omega)$ is the correlation function that describes the spatial correlation between two points $M_i = (x_i, y_i)$ and $M_{i'} = (x_{i'}, y_{i'})$ in function of their spatial distance over a frequency domain.

As already mentioned in Chapter 1, Section 1.4.1, different semi-empirical models have been developed in order to describe a TBL excitation. The Corcos model [81], defined as

$$S_{p_i p_{i'}}(x_i - x_{i'}, y_i - y_{i'}; \omega) = |S_{p_i p_i}(\omega)| e^{-\alpha_x \frac{\omega}{U_c}|x_i - x_{i'}|} e^{-\alpha_y \frac{\omega}{U_c}|y_i - y_{i'}|} e^{\imath \frac{\omega}{U_c}(x_i - x_{i'})} \tag{4.20}$$

and the Mellen model [82], defined as

$$S_{p_i p_{i'}}(x_i - x_{i'}, y_i - y_{i'}; \omega) = |S_{p_i p_i}(\omega)| e^{\left[\left(\alpha_x \frac{\omega}{U_c}(x_i - x_{i'})\right)^2 + \left(\alpha_y \frac{\omega}{U_c}(y_i - y_{i'})\right)^2\right]^{1/2}} e^{\imath \frac{\omega}{U_c}(x_i - x_{i'})} \tag{4.21}$$

are here just recalled, since they have been already introduced in detail in Chapter 1.

Equation 4.18 represents the generic response formulation of a structure to a random distributed excitation. In the low frequency (LF) domain, it is common to use a modal approach in order to calculate the vibrational response. The structures are hence characterised by their eigenmodes and natural frequencies; the vibrational response is obtained from the generalised Green's functions. In the case of random excitation, the structural response can be expressed in terms of displacement, velocity or acceleration PSD. The expression for the displacement PSD is herein defined as

$$S_{ww}(x, y; \omega) = \sum_m \sum_n \frac{\phi_m(x, y)\phi_n(x, y)}{\Re\{h_m(\omega) h_n^*(\omega)\}} \int_A \int_{A'} \phi_m(x, y)\phi_n(x', y') S_{pp'}(x, x', y, y'; \omega) dA dA' \tag{4.22}$$

where $\phi_m(x, y)$ is the mode shape referred to the m-*th* mode, $\Re$ denotes the real part, $S_{pp'}(x, x', y, y'; \omega)$ is the CSD of the excitation, A is the excited surface of the structure and

$$h_m(\omega) = \omega_m^2(1 + \imath\eta_m) - \omega^2 \tag{4.23}$$

is the Frequency Response Function (FRF) of the structure referred to the m-*th* mode by the natural frequency ω_m and the modal damping loss factor η_m. By considering Equation 4.19, it is possible to obtain a second formulation of Equation 4.22 as

$$S_{ww}(x,y;\omega) = \sum_m \sum_n \frac{\phi_m(x,y)\phi_n(x,y)}{\Re\{h_m(\omega)h_n^*(\omega)\}} S_{pp}(\omega) A_{mn}(\omega) \tag{4.24}$$

where $A_{mn}(\omega)$ is called *cross-acceptance*, defined as the double surface integral of the product between the structural mode shapes and the correlation function of the excitation (Equation 4.25).

$$A_{mn}(\omega) = \int_A \int_{A'} \phi_m(x,y)\phi_n(x',y')\Gamma_{pp'}(x-x',y-y';\omega)dydy'dxdx' \tag{4.25}$$

As mentioned in Section 1.4, the cross-acceptance represents the coupling between the structure and the excitation [74]. In other words, it is a description of how the energy is spatially distributed over the structure because subjected to a pressure field.

The calculation of cross-acceptance function might become very time consuming when it is wanted to increase the excitation frequency, especially for those structures whose mode shapes cannot be expressed analytically. In the next paragraph will be expressed the difficulties encountered for the calculation of the double numerical integration performed on the excited surface, since it must take into account the correlation lengths relative to the distributed excitation. It will be explained how the discretization can then become very fine for increasing frequency, as it happens specifically with a TBL excitation, for which the correlation lengths are expressed through a decreasing exponential function dependent on the frequency and the distance between each pair of considered points (see Equations 4.20 and 4.21).

A simplification of the $A_{mn}(\omega)$ term consists in neglecting the cross terms, which correspond to two different modal indices in the modal summation ($m \neq n$); this is possible since the terms corresponding to the same mode ($m = n$) present much higher values compared to the cross terms. When only the resonant modes are contemplated, $A_{mm}(\omega)$ is called *joint-acceptance*. This results in a significant reduction in the number of terms to be calculated to express the displacement PSD of the structural response, which now can be expressed as

$$S_{ww}(x, y; \omega) \approx \sum_{m} \frac{\phi_m^2(x, y)}{|h_m(\omega)|^2} S_{pp}(\omega) A_{mm}(\omega) \tag{4.26}$$

This assumption is indeed justified at low frequencies, where the eigenmodes do not overlap and are well separated in frequency.

4.2.3 Numerical structural response to a TBL excitation

In this paragraph, it is wanted to expose the passage from the aforementioned analytical formulation to a numerical expression of the vibrational response of a structure. Consequently, the difficulties encountered for the representation of TBL excitation in a numerical formulation are discussed.

By looking for a predictive procedure for dynamic analyses, the Finite Element Method (FEM) is the stronghold of the numerical methods applied in a LF domain. The core principle of FEM is based on the discretization of a structure in a substantial number of finite elements for which the geometrical shape is simple (triangles or quadrilaterals for 2D systems, tetrahedrons or hexahedrons for 3D systems) and the properties are homogeneous. In this way, any configuration depending on material, shape, boundary conditions, etc. can be represented and analysed.

The subdivision of a structure in finite elements allows the schematization of the system in discrete coordinates (degrees of freedom, dof), hence it allows the passage from an analytical integral formulation to an algebraic system for which each equation is related to a degree of freedom. A matrix formulation is usually adopted to assemble the algebraic equations and it works for all methods that operate with discrete coordinates [75]. Indeed, the displacement CSD of a structure subdivided in NG dofs and that presents NM mode shapes is expressed as

$$[S_{WW}(\omega)] = [\Phi][H(\omega)][S_\phi(\omega)][H^*(\omega)][\Phi]^T \tag{4.27}$$

where

$$[S_\phi(\omega)] = [\Phi]^T[S_{FF}(\omega)][\Phi] \tag{4.28}$$

In Equations 4.27 and 4.28, it is possible to recognize the following parameters:

- $[\Phi]$ is the structural modal matrix, for which each column is the eigenvector referred to a dof, hence the matrix dimensions are $[NG \times NM]$;
- $[H(\omega)]$ is the structural FRF diagonal matrix, with dimensions $[NM \times NM]$, for which each element of the diagonal is expressed as $H_m(\omega) = [\omega_m^2(1 + \imath\eta_m) - \omega^2]^{-1}$;
- $[S_\phi(\omega)]$ is the generalized force matrix, with dimensions $[NM \times NM]$;
- $[S_{FF}(\omega)]$ is the equivalent force matrix, with dimensions $[NG \times NG]$.

Equation 4.27 is here also referred as Full-Stochastic (FS) formulation of the structural response. When a distributed excitation needs to be represented in a numerical formulation, the first problem encountered is the translation of the load over the NG grid points. The formal FEM procedure wants the use of the shape function vector $\{N_F\}$ assigned to each element, so that the the single element of the $[S_{FF}]$ matrix would be expressed as

$$S_{FF_{n,k}}(\omega) = \int_{x_n}\int_{y_n}\int_{x'_k}\int_{y'_k}\{N_F\}^T\Gamma_{pp'}(x_n, y_n, x'_k, y'_k; \omega)\{N_F\}dx_n dy_n dx'_k dy'_k \tag{4.29}$$

where n and k indicated two different elements, hence the double surface integration is connected to their specific areas. As a consequence, the matrix $[S_{FF}]$ would have dimensions

$[NE \times NE]$, where NE points out the number of finite elements considered.

At this stage, it is important to notice that the numerical formulation of the structural response to a TBL excitation, as it has been presented so far, shows two difficulties, one connected to the other. The main obstacle to overcome is the high computational cost, because of the substantial number of elements to consider for meshing the structure, and also because each element requires between 3 and 6 dof depending on the element choice. The second problem encountered, which is related to the number of elements, is the discretization of the TBL over the mesh.

4.2.4 The difficulties in representing the response to a TBL excitation

There are two stage of approximations that can be performed, in order to reduce the computational cost of this numerical approach. The first stage regards the use of grid points instead of finite elements [131]. As matter of fact, applying an aerodynamic load over NG grid points means to distribute a load over NG nodal areas (Equation 4.30). Each grid point would present a nodal area equal to $\Delta x \Delta y$.

$$S_{FF_{i,j}}(\omega) = \int_{x_i-\Delta x/2}^{x_i+\Delta x/2} \int_{y_i-\Delta y/2}^{y_i+\Delta y/2} \int_{x_j-\Delta x/2}^{x_j+\Delta x/2} \int_{y_j-\Delta y/2}^{y_j+\Delta y/2} \Gamma_{pp'}(x_i, y_i, x_j, y_j; \omega) dx_i dy_i dx_j dy_j \tag{4.30}$$

The second stage of approximation takes into account the TBL behaviour in the LF region [76]; because the wall-pressure fluctuations do not change so fast, the double integration formulation can be reduced in

$$S_{FF_{i,j}}(\omega) = \Gamma_{pp'}(x_i, y_i, x_j, y_j; \omega)(\Delta x \Delta y)^2 \tag{4.31}$$

In all three expressions of the structural response, the property of hermitian matrix ($S_{FF_{i,j}} = S^*_{FF_{j,i}}$) is maintained by the load, and consequently by the displacement CSD.

Together with the high computational cost that occurs in the numerical analysis due to the necessity of filling the $[S_{FF}]$ matrix, another difficulty is encountered because of the TBL excitation expression. The translation of the TBL excitation in discrete coordinates is highly dependent on two characteristic wavelengths. One is the flexural wavelength, characteristic of the structure, the other is the convective wavelength associated to the flow speed (Equation 4.32). Equation 4.33 is indicative for the flexural wavelength of a plate, where D is the bending stiffness, ρ is the mass per unit volume, h is the plate thickness. Both wavelengths can be obtained as the reciprocal of the referred wavenumber $\kappa(\omega)$.

$$\lambda_c(\omega) = \frac{2\pi}{\kappa_c} \implies \lambda_c(\omega) = \frac{2\pi U_c}{\omega} \tag{4.32}$$

$$\lambda_B(\omega) = \frac{2\pi}{\kappa_B(\omega)} \implies \lambda_B(\omega) = 2\pi \left(\frac{D}{\rho h \omega^2}\right)^{1/4} \tag{4.33}$$

Taking as example an aluminium plate ($E = 7.0e10$ Pa, $\rho = 2700$ kg/m^3, $\nu = 0.33$) with thickness $h = 0.0016$ m subjected to a TBL excitation characterised by a convective speed $U_c = 80$ m/s, in Figure 4.2 it is possible to see both wavelengths in comparison.

The frequency for which the wavelengths intersect each other is called aerodynamic (or convective) coincidence frequency and its value can be recovered by imposing the following equivalence $\lambda_B = \lambda_c$, which gives

$$f_c = \frac{U_c^2}{2\pi}\sqrt{\frac{\rho h}{D}} \tag{4.34}$$

When a mesh is developed for a FEM application over a structure, its scheme is based on the necessity of reproducing the flexural wavelength λ_B up to the maximum excitation frequency. To obtain an acceptable representation of λ_B, minimum four elements are required. By considering the following equivalence

$$\Delta = \frac{\lambda_{B,min}}{4} \qquad \implies \qquad \Delta = \frac{2\pi}{4}\left(\frac{D}{\rho h \omega_{max}^2}\right)^{1/4} \tag{4.35}$$

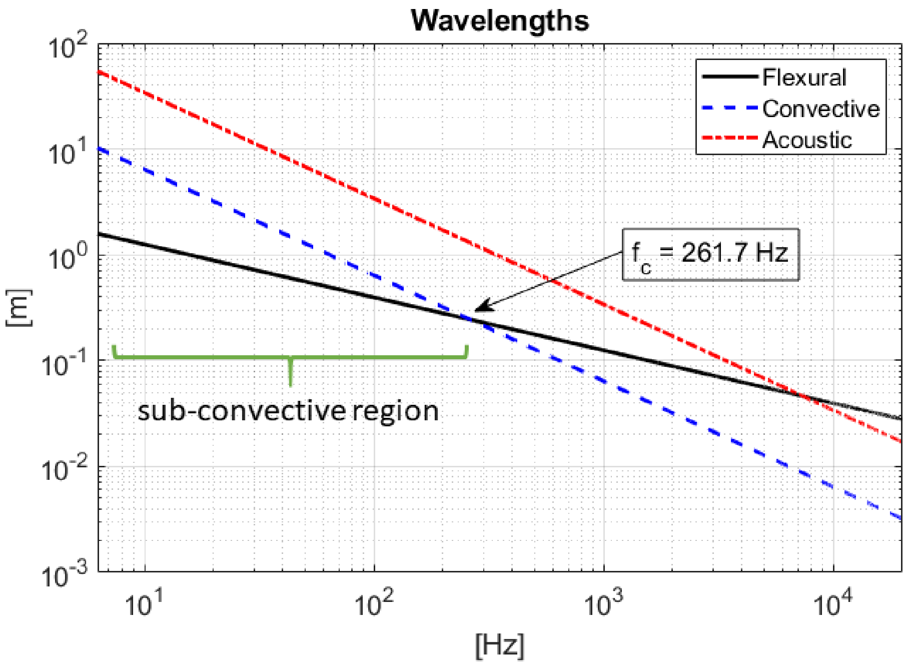

Figure 4.2: Flexural wavelength of an aluminium plate ($E = 7.0e10$ Pa, $\rho = 2700$ kg/m^3, $\nu = 0.33$) with thickness $h = 0.0016$ m, in comparison with the convective wavelength associated to a flow speed of $U_c = 80$ m/s.

and by fixing the maximum excitation frequency, it is possible to know the required dimension Δ of the single element of the mesh. This formulation is valid until the frequency region of analysis is confined in the sub-convective region, in other words for all frequencies that are on the left of the aerodynamic coincidence frequency (Figure 4.2). As matter of fact, in this particular region, the flexural wavelength presents smaller values compared to the convective wavelength. On the contrary, in the super-convective region — on the right of the aerodynamic coincidence — it is the convective wavelength that shows smaller values, thus the mesh design needs to be formulated in its function.

Indeed, a second methodology that can be applied for the determination of finite elements dimensions is to focus on the reproduction of the convective wavelength through the mesh. Equivalently to Equation 4.35, it is possible to write

$$\Delta = \frac{\lambda_{c,min}}{4} \qquad \Longrightarrow \qquad \Delta = \frac{2\pi}{4}\frac{U_c}{\omega_{max}} \tag{4.36}$$

U_0 [m/s]	Δ [m]	N_x	N_y	NG
100	0.0063	122	52	6344
75	0.0047	163	70	11410
50	0.0031	248	106	26288
25	0.0016	480	205	98400

Table 4.1: Number of elements required for an aluminium panel (0.768×0.328 *m*^{2}) *to get a convergent solution at different asymptotic speeds, with convective coefficient* $\beta_c = U_c/U_0 = 0.8$*, for a* $f_{max} = 20000$ *Hz.*

It is here evident that the convective flow speed U_c highly influences the determination of the mesh elements dimensions. In Table 4.1, it is possible to see how the number of grid points NG for an aluminium plate with dimensions 0.768×0.328 m^2 increases considerably when the asymptotic flow value decreases, for a maximum excitation frequency equal to $f_{max} = 20000$ Hz.

The necessity of a fine mesh for the discretization of TBL excitation at low convective speeds influences the computational cost of the numerical simulations, such that it is not possible to satisfy this requirement just to obtain the results until the expected maximum frequency. In fact, Equation 4.36 is used more for an opposite purpose: by fixing the single mesh element dimension Δ, it is possible to know the so-called aliasing frequency f_{al} (Equation 4.37), a frequency limit which indicates at which point of the frequency region the structural response to a TBL excitation would start to diverge.

$$f_{al} = \frac{U_c}{4\Delta} \tag{4.37}$$

As example of the aliasing effect, in Figure 4.3 it is shown the acceleration PSD of the aforementioned aluminium plate (all properties summarised in Table 4.2a) subjected to a TBL excitation with an asymptotic flow speed equal to $U_0 = 50$ m/s (Corcos model: $\alpha_x = 0.116$, $\alpha_y = 0.700$, $\beta_c = U_c/U_0 = 0.8$). In Table 4.2b, the information about the mesh dimension obtained through Equation 4.35 are reported. The maximum frequency considered for the mesh design is 20 kHz, but the numerical simulation has been run until

(a) Example panel properties		(b) Mesh design information	
Young's modulus, E	7.0e10 Pa	Maximum frequency, f_{max}	20 kHz
Poisson's ratio, ν	0.33	Element dimension, Δ	0.0076 m
Density, ρ	2700 kg/m^3	$N_x = L_x/\Delta$	101
Length, L_x	0.768 m	$N_y = L_y/\Delta$	43
Width, L_y	0.328 m		
Thickness, h	0.0016 m	$NG = (N_x + 1) \times (N_y + 1)$	4488

Table 4.2: (a) Summary of the example panel properties in terms of material and geometry. (b) Information about the mesh design.

just 5000 Hz, because it was expected to find the aliasing frequency equal to $f_{al} = 1335$ Hz.

4.3 Equivalent expressions of a TBL excitation

As already mentioned before, from a practical point of view, Corcos and Mellen models have been chosen as reference for the TBL representation (Equations 4.38 and 4.39). Their expressions are again reported, this time formulated for a numerical simulation, based on the approximation stated in Equation 4.31.

$$S^{i,j}_{FF_{Corcos}}(\omega) = (\Delta x \Delta y)^2 e^{-\alpha_x \frac{\omega}{U_c}|x_i - x_j|} e^{-\alpha_y \frac{\omega}{U_c}|y_i - y_j|} e^{i \frac{\omega}{U_c}(x_i - x_j)} \tag{4.38}$$

$$S^{i,j}_{FF_{Mellen}}(\omega) = (\Delta x \Delta y)^2 e^{\left[\left(\alpha_x \frac{\omega}{U_c}(x_i - x_j)\right)^2 + \left(\alpha_y \frac{\omega}{U_c}(y_i - y_j)\right)^2\right]^{1/2}} e^{\imath \frac{\omega}{U_c}(x_i - x_j)} \tag{4.39}$$

The exponential terms with real values in the exponent describe how the pressure field amplitude decays, depending on the distance between two points, on the empirical coefficients α_x and α_y and on the convective wavenumber $\kappa_c(\omega) = \omega/U_c$. The exponential term with imaginary values in the exponent represents the propagation term, which for both models it is related just to a single direction.

In Figure 4.4 it is possible to appreciate a comparison between the Corcos model and the Mellen one, which differ only in the shape of the load distribution. Both correlation

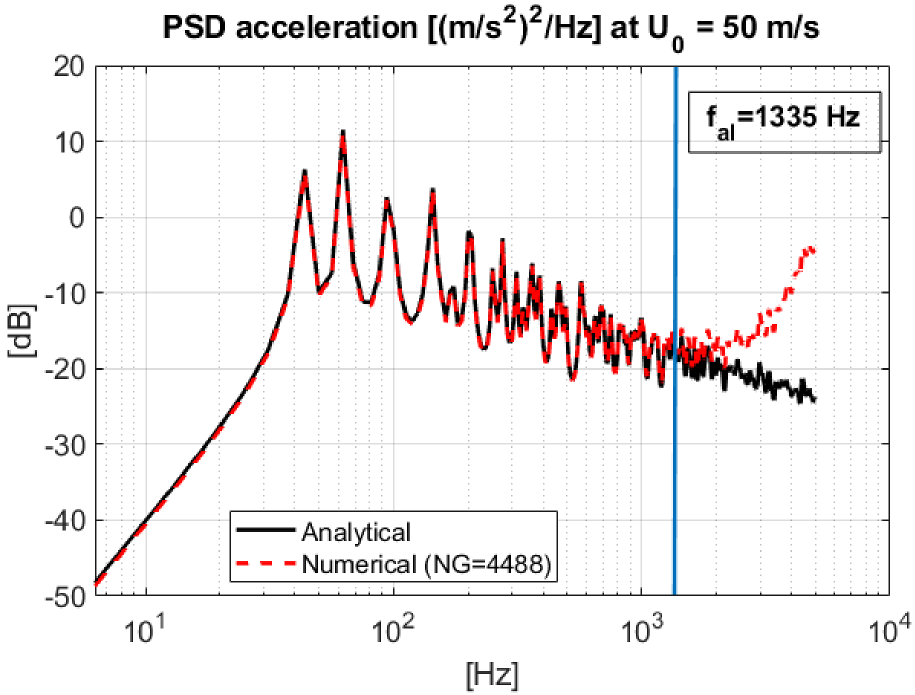

Figure 4.3: Comparison between the analytical (solid black line) and numerical (dashed red line) solution of an aluminium plate subjected to a TBL excitation with $U_0 = 50$ m/s. It is individuated the aliasing frequency f_{al}, from which the numerical solution starts to diverge.

functions have been performed for an asymptotic speed $U_0 = 75$ m/s and plotted for a determined frequency $f = 500$ Hz.

4.3.1 TBL as Rain-on-the-roof excitation

In Chapters 2 and 3, it has been presented an alternative way for the representation of a TBL excitation in a SEA framework, since one of the main assumptions on which this energetic method is based is that the applied excitation must be statistically independent and spatially uncorrelated. As matter of fact, with the explanations reported in the previous section, it is now easy to understand how it was possible to recreate a TBL excitation — which has a dependence on the spatial correlation — inside a SEA framework.

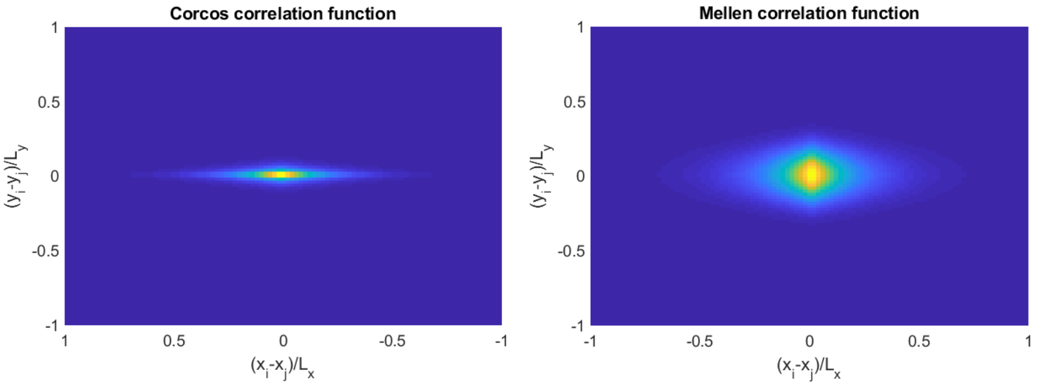

Figure 4.4: Corcos and Mellen correlation functions in comparison for an asymptotic speed $U_0 = 75$ *m/s and for a determined frequency* $f = 500$ *Hz.*

TBL as Rain-on-the-roof excitation: analytical expression

From an analytical point of view, a statistically independent and spatially uncorrelated pressure field is expressed through the following correlation function

$$\Gamma^{ROR}(x-x', y-y'; \omega) = \delta(x-x')\delta(y-y') \tag{4.40}$$

where the apex ROR stands for "Rain-On-the-Roof", a name given to this type of excitation for stressing the uncorrelation between the forces acting on different points of a surface, exactly as the rain drops are when hitting a roof. The symbol δ is indicative of the Dirac function, for which

$$\delta(x-x') = \begin{cases} 1 & \text{for} \quad x = x' \\ 0 & \text{for} \quad x \neq x' \end{cases} \tag{4.41}$$

This particular expression is very handful when it is wanted to obtain a simplification of the analytical expression of the structural response CSD, specifically for what concerning the calculation of the double integral expressed in the cross-acceptance formulation (Equation 4.25). Indeed, by considering $\Gamma^{ROR}(x-x', y-y'; \omega)$ as load correlation function, and at the same time by considering the normalization to 1 of the mode shapes orthogonal basis

$$\int_A \phi_m(x,y)\phi_n(x,y)dxdy = \delta_{mn} \tag{4.42}$$

the double surface integration of the cross-acceptance is easily solved

$$A_{mn}(\omega) = \int_A \int_{A'} \phi_m(x,y)\phi_m(x',y')\delta(x-x')\delta(y-y')dAdA' = \delta_{mn} \tag{4.43}$$

Exploiting this property of the ROR excitation, with the spatial extent equivalence [84, 26], it is possible to calculate an equivalent correlation function $C^{eq}(\omega)$ which would present the same spatial correlation as a ROR excitation, but keeping the amplitude of a TBL excitation in the frequency domain [85]. By solving the following spatial integration

$$C^{eq}(\omega) = \int_\infty \int_\infty \Re\{e^{-\alpha_x \frac{\omega}{U_c}|x-x'|}e^{-\alpha_y \frac{\omega}{U_c}|y-y'|}e^{i\frac{\omega}{U_c}(x-x')}\}dAdA' \tag{4.44}$$

the equivalent correlation function related to the Corcos model is herein derived.

$$C^{eq}(\omega) = \frac{4U_c^2}{\omega^2}\frac{\alpha_x}{\alpha_y(1+\alpha_x^2)} \tag{4.45}$$

The TBL excitation with a ROR-type spatial correlation is expressed as follows

$$S_{FF'}^{ETBL}(x-x', y-y';\omega) = S_{pp}^{ROR}C^{eq}(\omega)\delta(x-x')\delta(y-y') \tag{4.46}$$

$$= \begin{cases} S_{pp}^{ROR}C^{eq}(\omega)A \quad \text{for} \quad x=x' \quad \text{and} \quad y=y' \\ 0 \quad \text{otherwise} \end{cases} \tag{4.47}$$

where the PSD of the pressure field generated by a ROR-type excitation is always constant and hence considered unitary.

With the spatial integration extended to infinity, it is implied that $C^{eq}(\omega)$ will be accurate when the decay rates of the correlation function are sufficiently high. Always referring to the Corcos model, a high decay rate can happen when

$$\alpha_x \frac{\omega}{U_c}|x - x'| << 1 \quad \text{and} \quad \alpha_y \frac{\omega}{U_c}|y - y'| << 1 \tag{4.48}$$

in other words, when the excitation correlation lengths $l_x = \frac{U_c}{\alpha_x \omega}$ and $l_y = \frac{U_c}{\alpha_y \omega}$ result much smaller than the lengths characteristic of the structure. By looking at Figure 4.2, it is then evident that the Corcos model representation as Equivalent-TBL (ETBL) excitation would be much more accurate in the high frequency (HF) region, moving away from the convective coincidence frequency. A confirm of this statement can be seen in Figure 4.5, where the analytical velocity PSD of the example aluminium plate has been calculated for a Corcos-like TBL excitation and for the ETBL one, considering four different asymptotic flow speeds, in order to show how the convective coincidence frequency moves towards the HF region, and similarly the match between the two solutions.

TBL as Rain-on-the-roof excitation: numerical expression

From a numerical point of view, a spatially uncorrelated pressure field as the ROR excitation is expressed as CSD diagonal matrix. Indeed, for a matrix with dimensions [$NG \times NG$], on the diagonal there are the PSDs of the excitation calculated in each grid point of the system, while outside of the diagonal there are all the CSDs of the excitation between two different grid points which, because of the assumption of spatial uncorrelated field, are all null.

The ETBL excitation has been thus expressed as diagonal matrix [86], where the i-*th* element is represented as

$$S^{i,i}_{FF_{ETBL}}(\omega) = \frac{4U_c^2}{\omega^2} \frac{\alpha_x}{\alpha_y(1 + \alpha_x^2)} \Delta x \Delta y \tag{4.49}$$

While Equation 4.49 has been derived from an analytical expression [85] and then

(a) TBL vs E-TBL U_0=25 m/s

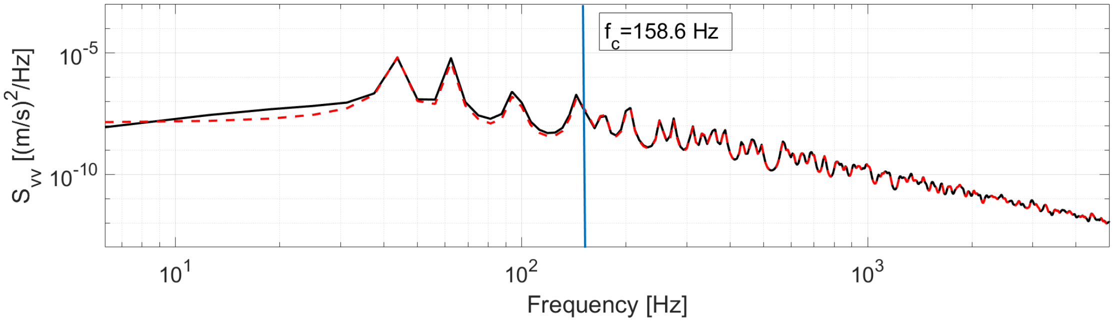

(b) TBL vs E-TBL U_0=50 m/s

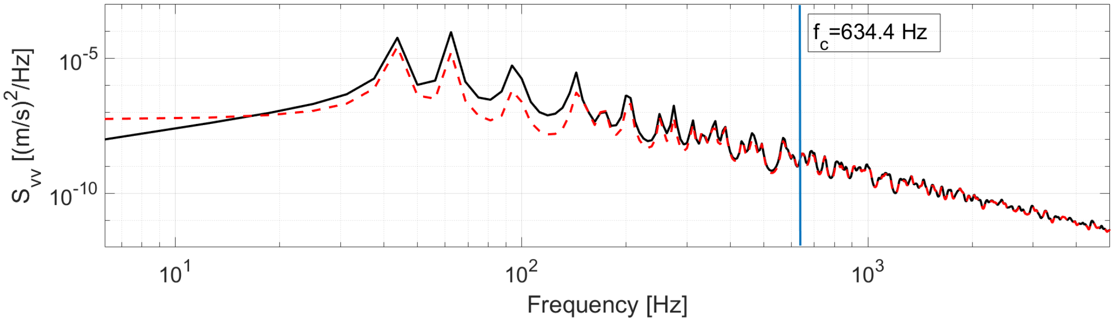

(c) TBL vs E-TBL U_0=75 m/s

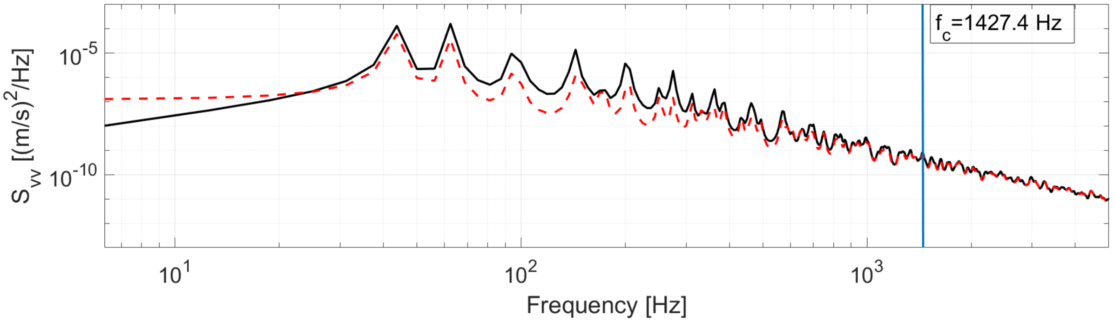

(d) TBL vs E-TBL U_0=100 m/s

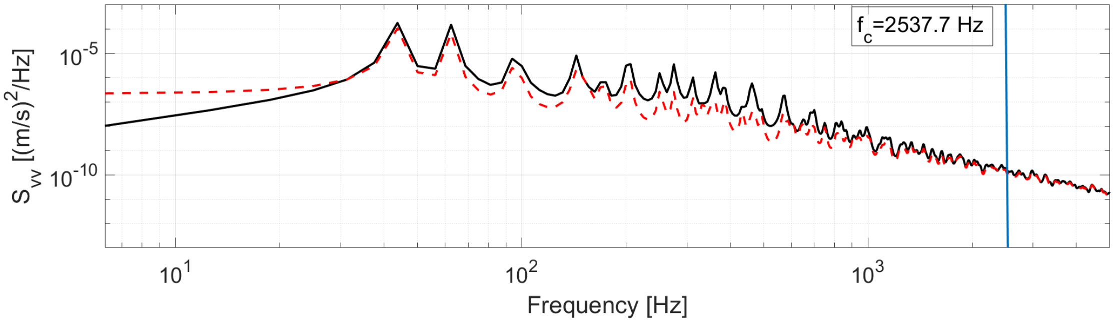

Figure 4.5: Analytical velocity PSD of an aluminium panel subjected to a Corcos-like TBL excitation (solid black line) and to an ETBL excitation (dashed red line) for different asymptotic speeds: (a) $U_0 = 25$ *m/s; (b)* $U_0 = 50$ *m/s; (c)* $U_0 = 75$ *m/s; (d)* $U_0 = 100$ *m/s.*

formalised for numerical applications, there is also a second formulation for a numerical TBL-like spatially uncorrelated excitation

$$S^{i,i}_{FF_{ETBL2}}(\omega) = \frac{\alpha_x(1+\alpha_x^2)\pi\Delta x}{\omega/U_c}\frac{\alpha_y(1+\alpha_y^2)\pi\Delta y}{\omega/U_c} \tag{4.50}$$

which has been obtained without any meticulous mathematical analysis [86] as extension of the study of the structural response of a flexural beam [87].

It is then clear that the realization of a TBL through a ROR representation is possible and from both analytical and numerical point of view it is easy to achieve. On the other hand, the description of TBL in the sub-convective region, where it is not possible to approximate the spatial correlation, but on the contrary it is essential to accurately reproduce it, the difficulties increase.

In Chapter 1, different methodologies that were able to recreate the TBL spatial correlation have been presented; most of them are based on the use of loudspeakers and microphones "synthetic" arrays [102, 104], in order to overcome to obstacle of the prohibitive number of sensors to use for an actual reproduction of the required array. The limits of these methods have been already mentioned: as long as it is intended to reproduce a TBL excitation with wavelengths lying in the supersonic region (in which convective wavelengths λ_c and acoustic wavelengths λ_0 are related as $\lambda_0 < \lambda_c$) the numerical implementation of the method is fine; in the subsonic region, λ_c is still smaller than the acoustic one, hence the acoustic source array must be realise "ad hoc". In the next section, it is wanted to give more space to PEDE$_M$, a method which is able to emulate the TBL excitation through a numerical process which is lighter than a full stochastic simulation.

4.4 TBL expressed through PEDE$_M$

The mathematical background of PEDE$_M$ starts from the formulation of the Pseudo Excitation Method (PEM) [111]. By considering a linear system under a zero-mean stationary random excitation $f(t)$ with a given Cross-spectral density (CSD) $S_{FF}(\omega)$, it is wanted to obtain the time-response output $y(t)$ of the system subjected to this type of excitation. To acquire the system response, it is possible to use a pseudo-equivalent harmonic excitation $\hat{f}(t)$ defined as

$$\hat{f}(t) = \sqrt{S_{FF}(\omega)}e^{i\omega t} \tag{4.51}$$

As a consequence, the time-response output of the system would be formulated as follows

$$\hat{y}(t) = \sqrt{S_{FF}(\omega)}H_y(\omega)exp(i\omega t) \quad \rightarrow \quad \hat{y}^*\hat{y} = S_{yy}(\omega) \tag{4.52}$$

where $H_y(\omega)$ is the Frequency Response Function (FRF) and $S_{yy}(\omega)$ is the PSD of the response, obtained by multiplying the time-response $\hat{y}(t)$ with its complex conjugate.

The result of this formulation is that one can obtain the actual PSD response $S_{yy}(\omega)$ of a system to a random excitation by knowing the FRF — which is characteristic of the system — and by building a pseudo-equivalent harmonic excitation. PEM is valid also for vector responses so that the CSD matrix response is calculated as $[S_{yy}(\omega)] = \{\hat{y}\}^*\{\hat{y}\}^T$.

The realization of a pseudo-equivalent excitation vector is achievable through the modal decomposition and matrices properties. The original scheme used for PEM is the Cholesky formulation variant, also called as LDL decomposition, for which the CSD excitation matrix is decomposed in a lower unit triangular matrix $[L]$, having all 1 on the diagonal, and a diagonal matrix $[D]$, as it is formulated in the following expression

$$[S_{FF}(\omega)] = [L]^*[D][L]^T = \sum_{j=1}^{NR} d_j\{l_j\}^*\{l_j\}^T \quad NR \leq NG \tag{4.53}$$

The product between matrices can be expressed, in fact, as a summation of the product of the single columns of the matrix $[L]$, as it is reported in Equation 4.53. With NR, it is intended the rank of the matrix, which can indicate a lower number or at least an equal number of columns compared to the actual $[S_{FF}(\omega)]$ matrix size $[NG \times NG]$.

The Full Stochastic formulation of the CSD response of a system subjected to a random stationary excitation (Equations 4.27 and 4.28) is hence updated by considering PEM and the modal decomposition, so that the CSD matrix of the system displacement $[S_{WW}(\omega)]$ is expressed as

$$[S_{WW}(\omega)] = \sum_{i=1}^{NG} \{w^*(\omega, i)\}\{w^T(\omega, i)\} \tag{4.54}$$

where the single element of the displacement vector $\{w(\omega, i)\}$ is calculated as

$$w(\omega, i) = [\Phi][H(\omega)][\Phi^T]\{L^{(i)}\}\sqrt{d_i(\omega)} \tag{4.55}$$

By involving the modal decomposition of $[S_{FF}(\omega)]$, it is ensured the convergence of the structural response calculation to the exact solution, but only in the case when all the NR eigensolutions are used.

The Pseudo-Equivalent Deterministic Excitation method [107], or PEDE$_M$, wants to be a particular case of PEM, by applying it specifically to an aerodynamic excitation expression as the Corcos model and by analysing the two asymptotic behaviours that this excitation presents, introducing them inside the PEDE$_M$ methodology. The approximation of TBL is herein introduced in order to avoid the modal decomposition of $[S_{FF}(\omega)]$ matrix, since it requires anyway the full calculation of the load matrix and, moreover, the eigenvectors and eigenvalues extrapolation, which would take a copious computational time. By representing the TBL as CSD matrix, the modal decomposition is applied such that

$$[S_{FF}(\omega)] = \sum_{i=1}^{NR} d_i(\omega)\{\Theta_i(\omega)\}^*\{\Theta_i(\omega)\}^T \quad NR \leq NG \tag{4.56}$$

where $\{\Theta_i\}$ is the *i*-th column vector of eigenvectors matrix $[\Theta(\omega)]$ and $d_i(\omega)$ is the *i*-th eigenvalue of the eigenvalues diagonal matrix $[D]$. The TBL excitation matrix is defined as square and hermitian. Consequently, by the spectral theorem for Hermitian matrices, the right and left eigenvector matrix $[\Theta]$ are equal and are defined as unitary matrix, while the eigenvalues are all real.

In PEDE$_M$, these two aforementioned asymptotic behaviours are expressed in function of an adimensional frequency $\kappa = \omega\Delta/U_c$, which depends on the frequency ω, the convective flow speed U_c and the mesh size Δ; in particular:

- for $\kappa \to 0$, the spatial correlation is *totally correlated*, as it can be an Incident Diffuse Field [86]; a totally-correlation can be expressed with an all-1 matrix

  $$[\Theta] = \begin{bmatrix} 1 & 1 & \dots & 1 \\ 1 & 1 & \dots & 1 \\ \vdots & \vdots & \ddots & \vdots \\ 1 & 1 & \dots & 1 \end{bmatrix} \tag{4.57}$$

  Consequently, in order to approximate the TBL excitation in the LF region, it is considered that its eigenvectors would be equal to

  $$\chi^T = \gamma \begin{Bmatrix} 1 & 1 & \dots & 1 \end{Bmatrix} \tag{4.58}$$

  and that there will be only one non-null eigenvalue d_{LF}, which is the first element on the diagonal of $[D]$ matrix. The concept of totally correlated spatial field is, though, limited by the boundary layer thickness δ, as Bull well explained in his papers [132, 133].

- for $\kappa \to \infty$, the spatial correlation is *totally uncorrelated* which, as it has been stressed out more than once, is relative to a Rain-On-the-Roof excitation; a totally-uncorrelation is expressed in matrix form as

$$[\Theta] = \begin{bmatrix} 1 & 0 & 0 & \dots & 0 \\ 0 & 1 & 0 & \dots & 0 \\ 0 & 0 & \ddots & \dots & \vdots \\ \vdots & \vdots & \vdots & \ddots & 0 \\ 0 & 0 & \dots & 0 & 1 \end{bmatrix} \tag{4.59}$$

where the i-*th* column of $[\Theta]$ is representative of the i-*th* eigenvector of the load matrix. All elements of the eigenvalues matrix $[D]$ are equal to the same values d_{HF}.

The application of PEDE$_M$ on a 2D-system as a flat plate has been presented for just one convective speed and the eigenvalues expressions are not explicitly individuated [107]. It has been found that the first eigenvalue for the PEDE$_{M_{LF}}$ is equal to

$$d_{LF} = (\Delta x \Delta y)^2 \tag{4.60}$$

while all eigenvalues for the PEDE$_{M_{HF}}$ are equal to

$$d_{i,HF} = \frac{U_c^2}{\omega^2} \frac{4\alpha_x \Delta x \Delta y}{\alpha_y (1 + \alpha_x^2)} \tag{4.61}$$

Because of the strong analogy between the PEDE$_{M_{HF}}$ and the numerical formulations presented in Equations 4.49-4.50, it would be not a surprise if another expression for $d_{i,HF}$ could be

$$d_{i,HF} = \frac{\alpha_x (1 + \alpha_x^2) \pi \Delta x}{\omega / U_c} \frac{\alpha_y (1 + \alpha_y^2) \pi \Delta y}{\omega / U_c} \tag{4.62}$$

In Figures 4.6-4.7-4.8-4.9, both asymptotic solutions derived with PEDE$_M$ (with eigenvalues expressed with Equations 4.60-4.61) are compared with the analytical solution of the structural response of an aluminium panel subjected to a TBL Corcos-like excitation.

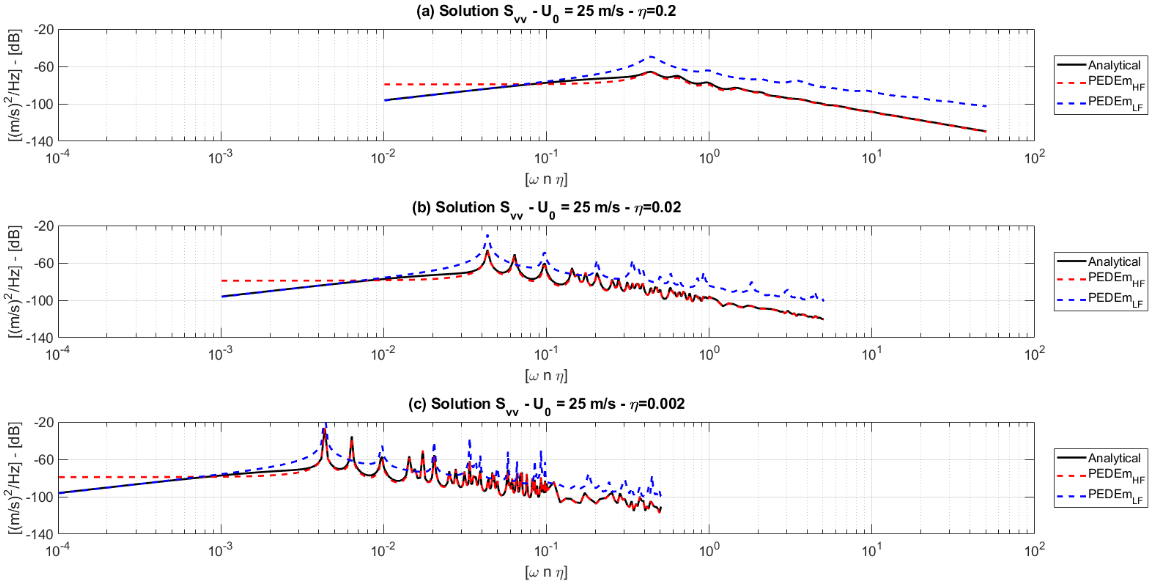

Figure 4.6: Velocity PSD of an aluminium plate subjected to a TBL excitation (U_0 = 25 m/s) calculated with the following methods: analytical (solid black line), PEDE$_{M,LF}$ (dashed blue line), PEDE$_{M,HF}$ (dashed red line). (a) $\eta = 0.2$; (b) $\eta = 0.02$; (c) $\eta = 0.002$.

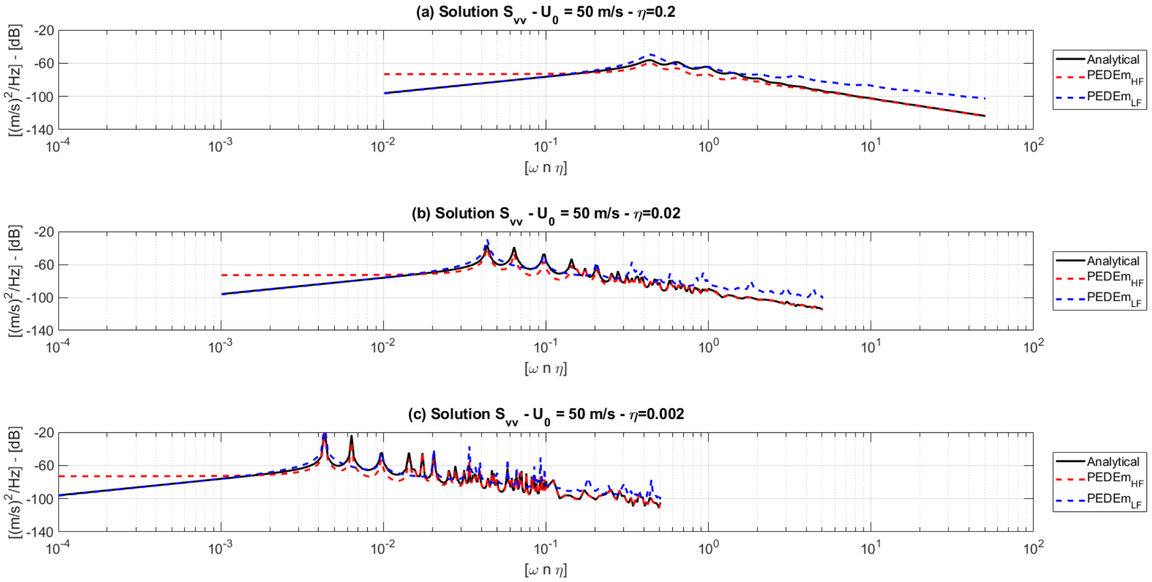

Figure 4.7: Velocity PSD of an aluminium plate subjected to a TBL excitation (U_0 = 50 m/s) calculated with the following methods: analytical (solid black line), PEDE$_{M,LF}$ (dashed blue line), PEDE$_{M,HF}$ (dashed red line). (a) $\eta = 0.2$; (b) $\eta = 0.02$; (c) $\eta = 0.002$.

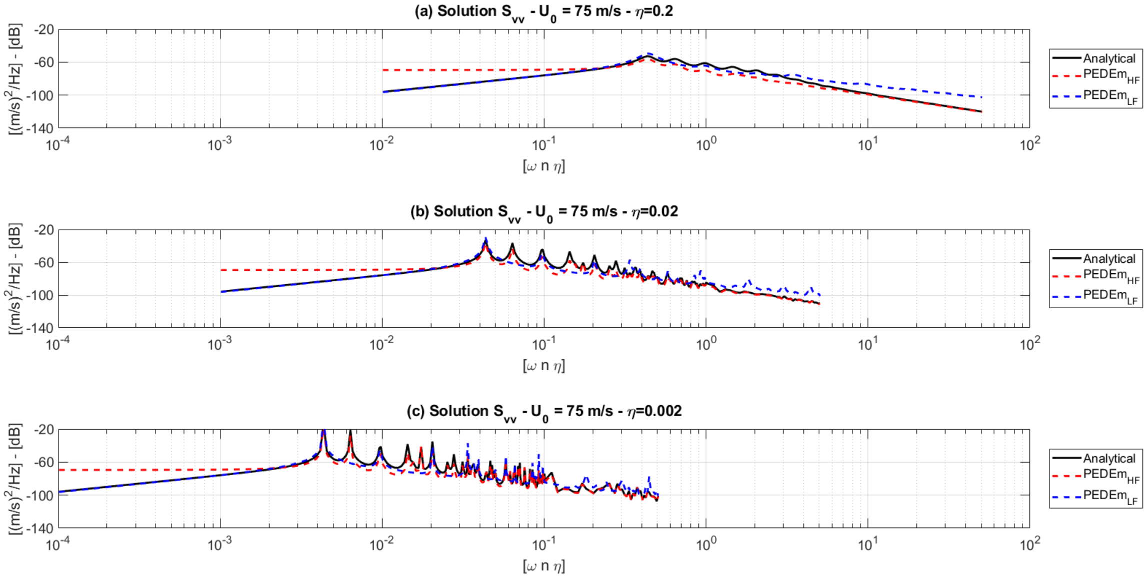

Figure 4.8: Velocity PSD of an aluminium plate subjected to a TBL excitation ($U_0 = 75$ m/s) calculated with the following methods: analytical (solid black line), PEDE$_{M,LF}$ (dashed blue line), PEDE$_{M,HF}$ (dashed red line). (a) $\eta = 0.2$; (b) $\eta = 0.02$; (c) $\eta = 0.002$.

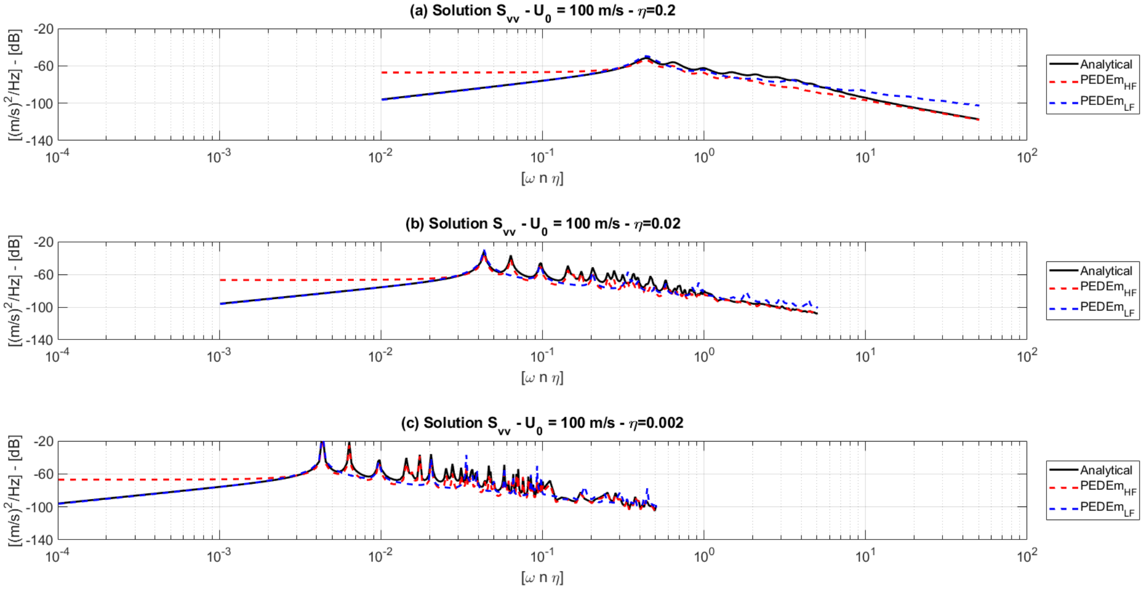

Figure 4.9: Velocity PSD of an aluminium plate subjected to a TBL excitation ($U_0 = 100$ m/s) calculated with the following methods: analytical (solid black line), PEDE$_{M,LF}$ (dashed blue line), PEDE$_{M,HF}$ (dashed red line). (a) $\eta = 0.2$; (b) $\eta = 0.02$; (c) $\eta = 0.002$.

Each figure is referred to a different asymptotic speed and presents three different cases depending on the damping value η. All curves have been plotted in function of the modal overlap factor (defined in Chapter 2, Equation 2.11), to see if both PEDE$_M$ solutions would suffer of some sort of dependence on modal density or damping. Lastly, it is wanted to precise that all curves have been calculated over a frequency range structured as follows

$$
\begin{aligned}
f &= [1;99]\text{Hz} \quad \text{with step} \quad \Delta f = 2\text{Hz} \\
f &= [100;999]\text{Hz} \quad \text{with step} \quad \Delta f = 6\text{Hz} \\
f &= [1000;5000]\text{Hz} \quad \text{with step} \quad \Delta f = 100\text{Hz}
\end{aligned}
$$

in order just to reduce the computational time required by the numerical simulation. Although it is quite evident that a possible frequency limit for the PEDE$_{M_{HF}}$ application might involve the convective coincidence frequency (Equation 4.34), on the other hand it is still not clear how determine the frequency limit for the PEDE$_{M_{LF}}$ application. Analyses over eigenvalues and eigenvectors behaviour have been carried on to individuate a coupling effect between the excitation and the structure. In particular, two matrices products have been recognised

$$[KN(\omega)] = [\Phi]^T[\Theta] \tag{4.63}$$

$$[IN(\omega)] = [H(\omega)][KN(\omega)][D^{1/2}(\omega)], \tag{4.64}$$

in order to study their determinants, but unfortunately all the study gave inconclusive results, therefore they are not here reported.

4.5 Conclusions

In this chapter, a theoretical background regarding the representation of the structural response to a TBL excitation has been explained, in order to provide to the reader all the tools required for the comprehension of the next chapter:

- The basic concepts of the Cross- and Power- Spectral Densities have been given, followed by the analytical representation of a stationary random excitation and the analytical formulation of the structural response.

- The equivalent numerical expressions have been provided too, focusing the attention on the difficulties encountered for the representation of a type of load as the TBL excitation.

- The main difficulty is the computational time; to recover it, different stages of approximations for the TBL have been shown, together with the approximations for the structural response formulation.

- The second difficulty is the TBL discretization over the structural mesh grid; the aliasing frequency has been explained in order to show the problem of the divergence of the numerical solution due to the TBL excitation.

- Equivalent expressions of the TBL are given; the approximation of the mentioned load as a ROR excitation has been explained from an analytical and numerical point of view.

- The PEDE$_M$ has been widely illustrated since it has been recognised that it is the only method able to summarised both the asymptotic behaviours of the TBL excitation and to give simplified formulations for its numerical calculation.

In the next chapter, it is wanted to apply PEDE$_M$ for experimental purposes, in order to obtain a structural response to a TBL excitation with the use of a deterministic force, which would simplify a lot the execution of the experiment. The experimental PEDE$_M$, or X-PEDE$_M$, will be introduced in details and then compared with two experimental data sets, which have been collected in two different wind tunnel facilities.

CHAPTER 5

OFF-LINE NUMERICAL-EXPERIMENTAL METHOD FOR THE PREDICTION OF THE STRUCTURAL RESPONSE TO A TBL EXCITATION

5.1 Introduction

In the previous chapters, it has been presented firstly the issues concerning the wind tunnel experiments, in particular regarding the unreliability of the collecting data due to the vibrational response contamination of the test structure through the contact with the structural support mounted inside the test section of the facility. Thus, it has been presented an easy methodology for a quick structural design — based on material and geometry choice — which would ensure a vibrational velocity level gap (in dB) between support and test structure. The guidelines have been developed with Statistical Energy Analysis, focusing on the minimization of one particular term: the transmitted power from the support to the test structure. The second main issue that it has been wanted to solve is the validation of the structural support, with another easy and quick methodology which would predict the vibrational response of the designed system subjected to a TBL excitation, without the actual use of a wind tunnel.

In Chapter 1 Section 1.4, different off-line methodologies have been discussed and evaluated based on their pros and cons, while in Chapter 4, the main theoretical background and the numerical method PEDE$_M$ have been introduced, in order to give to the reader all the instruments required for understanding the following chapter. Indeed, here it is wanted to present a development of PEDE$_M$, which has been called Experimental PEDE$_M$ (X-PEDE$_M$), which has as main objective the simulation of an experimental setup for the off-line measurement of the structural response of a system subjected to a TBL excitation. Therefore, in the following sections, it will be introduced firstly the methodology and, later, the numerical results calculated with the application of X-PEDE$_M$ over two different test panels, comparing them with the actual experimental results obtained with a wind tunnel.

5.2 PEDE$_M$ application for experimental purposes: X-PEDE$_M$

Most of the alternative methods presented in literature take advantage of the similarities encountered between the TBL excitation behaviour and an Uncorrelated Wall Plane Waves (UWPWs) field. As a consequence, by trying to reproduce a set of plane waves, the experiments are based on the use of loudspeakers. A disadvantage that might be point out is that it is necessary to know how to manage an acoustic source, in order to find the right conversion between diffuse field and TBL excitation representation.

On the contrary, the X-PEDE$_M$ does not depend on the type of excitation used, since it is mainly based on the calculation of the transfer functions characteristic of the structure. From a mathematical point of view, the X-PEDE$_M$ is developed in few steps, starting from the PEDE$_M$ definition of structural response in terms of displacement CSD

$$[S_{WW}(\omega)] = \sum_{i=1}^{NG} \{w^*(\omega, i)\}\{w^T(\omega, i)\} \tag{5.1}$$

$$\{w(\omega, i)\} = [\Phi][H(\omega)][\Phi^T]\{\Theta^{(i)}\}\sqrt{d_i(\omega)} \tag{5.2}$$

Equation 5.2 is a vector containing the displacements of all the grid points of the structure calculated when a deterministic excitation is applied on the i-*th* grid point. It can be said, then, that the vector $\{w(\omega, i)\}$ contains the structural responses of the structure acquired over all the grid points, and consequently, the CSD matrix is calculated for each different position of the deterministic excitation and then summed. The single element of the vector

$\{w(\omega, i)\}$ can be expressed as

$$w_j^{(i)}(\omega) = \sum_m \frac{\phi_m(P_j)\phi_m(P_i)F_m^{(i)}(\omega)}{h_m(\omega)} \tag{5.3}$$

where, again, $h_m(\omega)$ is the FRF characteristic of the system (see Chapter 4, Equation 4.23). The product $\phi_m(P_i)F_m^{(i)}(\omega)$ is the modal force applied on the excitation point P_i; by considering the specific case of a PEDE$_{M_{HF}}$ application, the term $F_m^{(i)}(\omega)$ is equal to

$$F_m^{(i)}(\omega) = \sqrt{d_i(\omega)} = \sqrt{S_{pp}^{ROR}\frac{U_c^2}{\omega^2}\frac{4\alpha_x \Delta x \Delta y}{\alpha_y(1+\alpha_x^2)}} \tag{5.4}$$

where S_{pp}^{ROR} is the pressure PSD of a ROR excitation, considered equal to unit value 1 Pa^2/Hz. As it can be easily noticed, the definition of the force amplitude is independent on the modal behaviour of the structure. From a mathematical point of view, this term can go outside the summation

$$w_j^{(i)}(\omega) = F^{(i)}(\omega) \sum_m \frac{\phi_m(P_j)\phi_m(P_i)}{h_m(\omega)} \tag{5.5}$$

while from a physical and experimental point of view, this means that it is just required to measure the structural response to a unit deterministic force and then post-process the collected data. For PEDE$_{M_{HF}}$, the response is registered in all points, for a number of excitation points less or equal to the total number of grid points NG.

With X-PEDE$_M$, it is wanted to demonstrate that with few acquisition points and few excitation points, it is still possible to obtain a prediction of the structural response to a TBL excitation. It is mainly based on two main phases: the experimental phase and the post-processing one, which are introduced in the following subsections.

5.2.1 X-PEDE$_M$ phase 1: data collection

It has been explained in the previous chapter that the convective coincidence frequency f_c might be taken as reference to individuate in which frequency region PEDE$_{M_{HF}}$ can be

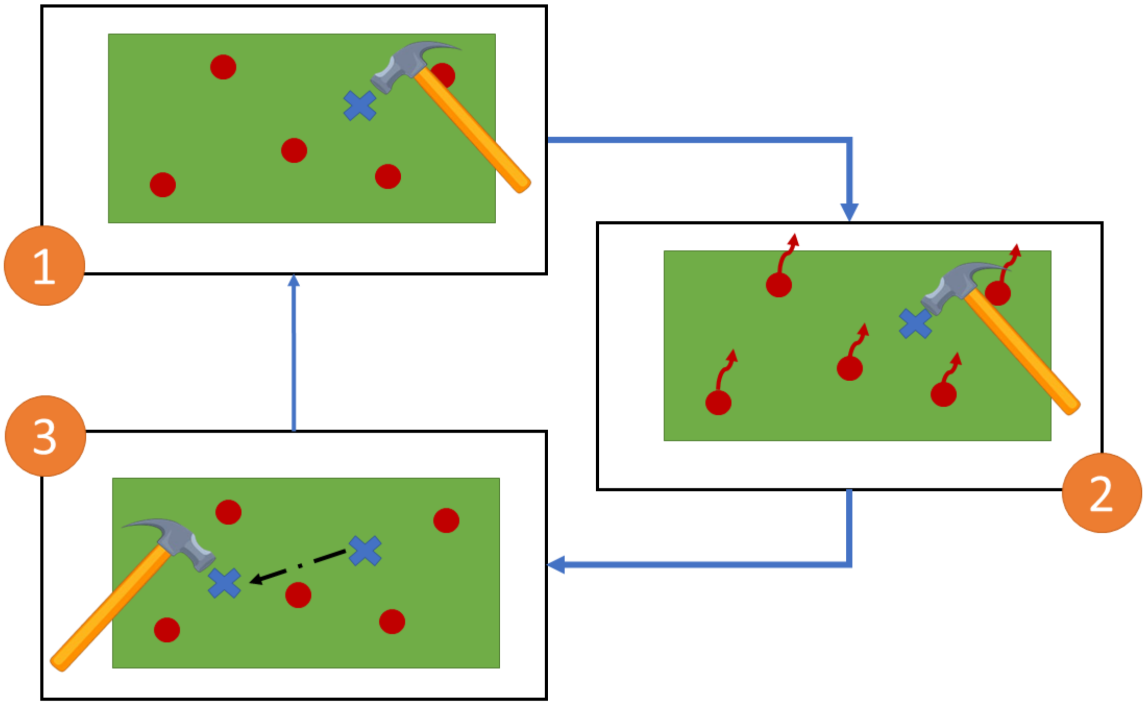

Figure 5.1: Experimental phase of X-PEDE$_M$ explained in three main steps: (1) fix the acquisition points and choose and excitation point; (2) acquire the structural response in terms of displacement in all the acquisition points; (3) change excitation point and repeat the process.

retained valid. As matter of fact, the TBL excitation is spatially uncorrelated and the load amplitude is equal on each point of the structure once the excitation frequency moves away from f_c towards the high frequency (HF) domain.

For these reasons, the first phase of X-PEDE$_M$ is mainly based on the data collection of the structural response in different points by exciting the structure in other different points with a unit force. Looking at Figure 5.1, the experimental process is easily explained; by taking as sample structure a flat plate, the experiment is organised as follows:

1. choose the accelerometers positions over the flat panel and fix them, then excite the structure in one point;
2. register the structural response in terms of displacement in all the acquisition points;
3. change the excitation point and then repeat the process.

The most important part of X-PEDE$_M$ is actually the post-processing phase, in which the collected data are re-elaborated in order to obtain the structural response to a TBL excitation.

5.2.2 X-PEDE$_M$ phase 2: post-processing data

At the moment of the data collection, each acquisition point would record a displacement vector $\{W^{(i)}(\omega)\}$, where each vector element $w_j^{(i)}$ is the displacement recorded in the i-*th* acquisition point at the j-*th* frequency. Consequently, to each excitation point is associated a set of displacement vectors. Hence the post-processing data phase is organised in these few steps:

1. for each excitation frequency ω, a vector $\{W\}$ is built, where each element W_i is the recorded displacement in a different acquisition point. If N_{ac} is the selected number of acquisition points, $\{W\}$ has dimensions [$N_{ac} \times 1$].
2. The displacements vector is multiplied by the value

$$F = \sqrt{d_i(\omega)} = \sqrt{S_{pp}^{ROR} \frac{U_c^2}{\omega^2} \frac{4\alpha_x A_{ex}}{\alpha_y(1+\alpha_x^2)}} \tag{5.6}$$

   With A_{ex}, it is indicated the area portion on which the deterministic force is applied. It is equal to the total surface of the flat plate divided by the number of chosen excitation points, $A_{ex} = A/N_{ex}$.

3. The CSD matrix is calculated; in this way, the cross correlations are registered too.
4. Steps (1) to (3) are repeated for each set of displacements vector collected for different excitation points. In this way, the superimposition of effect is completed and the reproduction of a pressure field over the system is realised.
5. The mean displacement PSD is finally obtained as

$$\bar{S}_{ww}(\omega) = \frac{1}{N_{ac}} \sum_{i=1}^{N_{ac}} [S_{WW}(\omega)]_{(i,i)} \tag{5.7}$$

Example panel information					
Geometry		Material		Mesh	
L_x	0.768 m	E	7.10e10 Pa	N_x	102
L_x	0.328 m	ρ	2700 kg/m^3	N_y	44
h	0.0016 m	ν	0.33	NG	4488
Boundary conditions:			simply-supported		

Table 5.1: Sample panel characteristics for the validation of X-PEDE$_M$.

By choosing $N_{ex} = NG$ and $N_{ac} = NG$, the formal application of PEDE$_{M_{HF}}$ is achieved. It is then a matter of understanding how many acquisition and excitation points are required. A numerical simulation has been effectuated in order to recreate the experimental condition. Then, two cases of experimental response to a TBL excitation measured in two different wind tunnels are compared with the numerical simulations of X-PEDE$_M$.

5.3 Numerical validation of X-PEDE$_M$

For the numerical validation of the method, a sample aluminium panel has been chosen; geometry, material, mesh size and boundary conditions are all reported in Table 5.1. By looking at the number of grid points selected for the mesh, it can be derived that the mesh element dimension is equal to $\Delta = 0.0076$ m.

The sample panel is studied for two different asymptotic flow speeds, $U_0 = 25$ m/s and $U_0 = 80$ m/s, so that the efficiency of the method can be compared depending on the convective coincidence frequency value, which determines the frequency domain in which X-PEDE$_M$ is valid. For $U_0 = 25$ m/s — for which it is expected a greater frequency domain of validity — different cases are studied in order to understand how the number of acquisition and excitation points can influence the results. On this matter, it is wanted here to report the work of Robert [134, 135], who studied already in the Eighties the reproduction of a vibrational response to a hydrodynamic load through the application of several random forces. In particular, he suggested an iterative method for which the number of forces increases until an optimal description of the vibrational response is reached.

X-PEDE$_M$ is compared with the analytical solution and with the PEDE$_{M_{HF}}$ solution as references, to check how far the two solutions deviate from each other; a unit PSD pressure is considered for the sake of the comparison. It is wanted also to underline that the numerical simulations are run over a frequency domain equal to $[1; 5000]$ Hz, with a frequency step $\Delta f = 6.25$ Hz, for a total of 801 excitation frequencies. While the full PEDE$_{M_{HF}}$ simulation took a computational time comparable to ≈ 2 hours and 30 minutes, the X-PEDE$_M$ simulation took a maximum of 12 seconds to run, over the same frequency domain for the same amount of excitation frequencies.

5.3.1 X-PEDE$_M$ for $U_0 = 25$ m/s - $N_{ex} = 9$ and $N_{acq} = 13$

As first validation of the method, 13 acquisition points and 9 excitation points have been chosen completely in a random way, avoiding only the grid points along the edges of the panel, since the boundary condition is simply-supported and the structural response registered in those points are always null (Figure 5.2a). It can be appreciated from Figure 5.2b that the choice $N_{ex} = 9$ and $N_{ac} = 13$ is good enough to obtain a satisfying reproduction of the structural response to a TBL excitation. The convective coincidence frequency f_c is indicated, to point out in which frequency region it can be seen the PEDE$_{M_{HF}}$ validity and, consequently, the X-PEDE$_M$ one too. It can be also noted that in the very low frequency (LF) domain, the X-PEDE$_M$ underestimates the PEDE$_{M_{HF}}$ solution, but then the two results start to overlap in the rest of the frequency domain.

5.3.2 X-PEDE$_M$ for $U_0 = 25$ m/s - $N_{ex} = 2$ and $N_{acq} = 5$

In the previous test, the amount of chosen acquisition points might have been too high, considering that, for an experimental setup, the number of accelerometers to be used is at least 3, but maximum 8 or 11, depending on the number of channels available on the hardware bench. As second validation, a reduced number of excitation and acquisition points

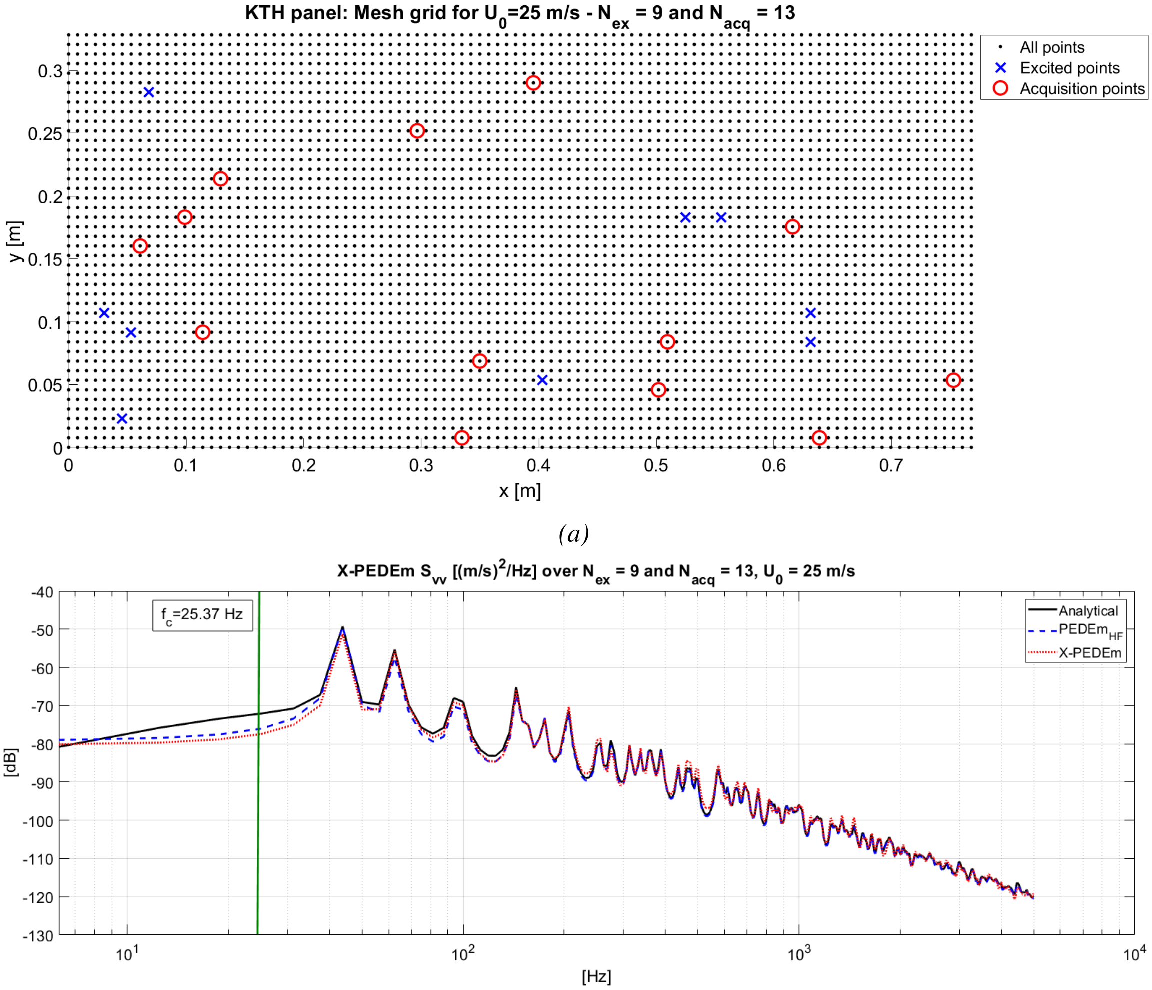

(a)

(b)

Figure 5.2: X-PEDE$_M$ validation over an aluminium panel for $N_{ex} = 9$ excitation points and $N_{acq} = 13$ acquisition points. (a) Grid point mesh with the selected points positions: (red circles) acquisition points; (blue crosses) excitation points; (black dots), all grid points. (b) Mean vibrational velocity PSD response to a TBL Corcos-like excitation with $U_0 = 25$ m/s: (black solid line) analytical solution; (blue dashed line) PEDE$_{M,HF}$ solution; (dotted red line) X-PEDE$_M$ solution.

is selected, always avoiding the points at the edges (Figure 5.3). The reduction of selected points has inevitably influenced the X-PEDE$_M$ results; the underestimation in the LF region is more accentuated and the overlap in HF domain is not accurate as in the previous case, but it still follows the behaviour of the reference result.

5.3.3 X-PEDE$_M$ for $U_0 = 25$ m/s - $N_{ex} = 7$ and $N_{acq} = 7$

As last validation case at low asymptotic flow speed, it is wanted to check if the choice of equal number of excitation and acquisition points would improve the results quality, hence 7 points for each category have been selected (Figure 5.4a). From Figure 5.4b, it is possible to notice that the underestimation in the LF region got a little improvement; in the remaining region of the frequency domain, the X-PEDE$_M$ solution follows very well the reference one, with a middle level of accuracy, if compared with the previous cases.

5.3.4 X-PEDE$_M$ for $U_0 = 80$ m/s - $N_{ex} = 9$ and $N_{acq} = 13$

Because the effect of the amount of acquisition and excitation points have been already discussed, with this last validation it is wanted to estimate the X-PEDE$_M$ efficacy for a higher flow speed equal to $U_0 = 80$ m/s. The frequency range of analysis is always the same, but the convective coincidence frequency is now higher, $f_c = 259.82$ Hz, defining the PEDE$_{M_{HF}}$ and the X-PEDE$_M$ validity in the highest frequency region. With this case, it is more evident how the experimental method follows perfectly the original method in the LF domain and not the analytical one, outlining that the convenience of X-PEDE$_M$ depends on a variable which involves surely the convective coincidence frequency.

In the next sections, the proposed methodology for the prediction of the structural response to a TBL excitation is tested for the prediction of an actual experimental result obtained in a wind tunnel facility. Two different experimental data sets are here used as references; they differ to each other for the different boundary conditions, wind tunnel

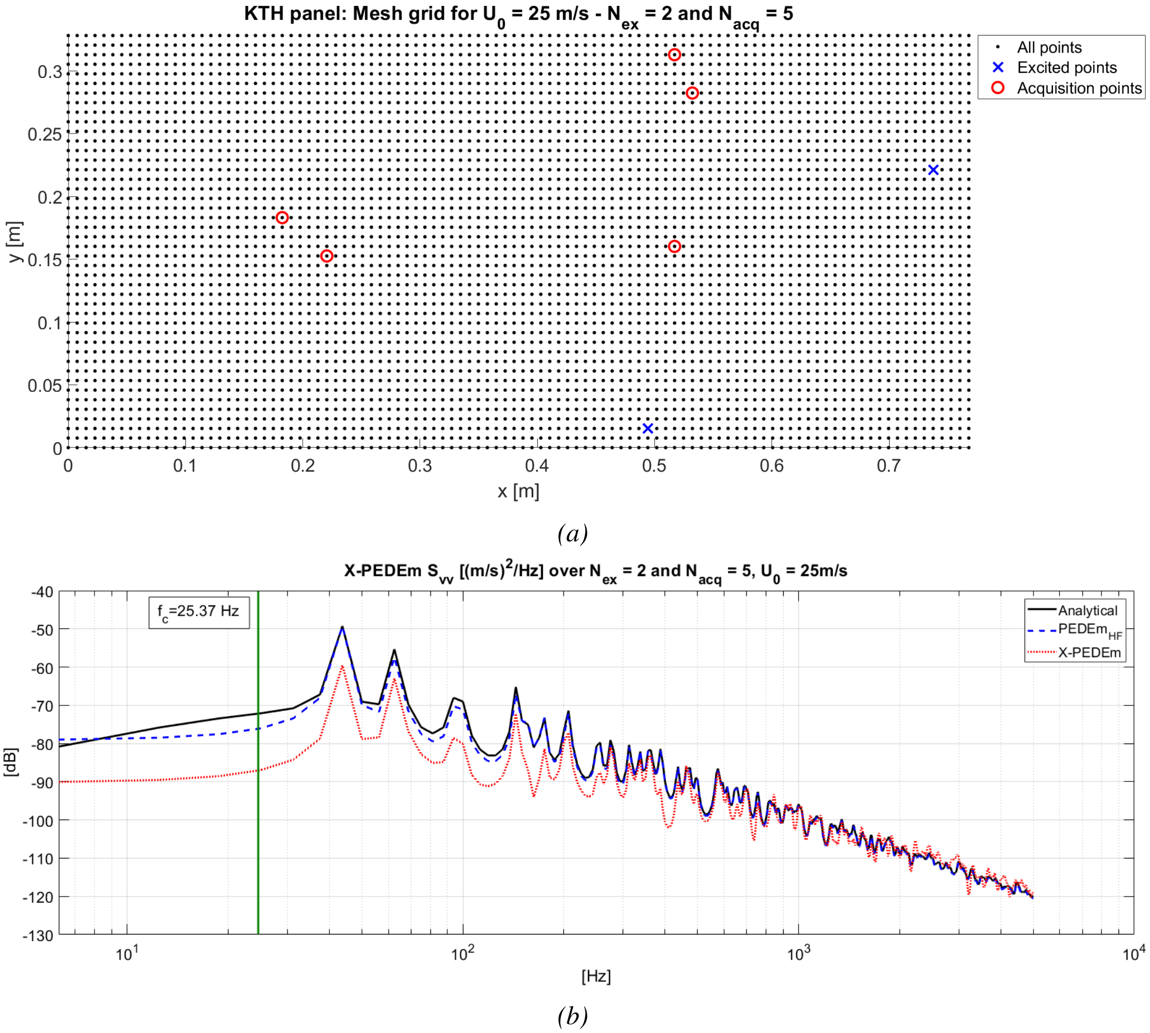

(a)

(b)

Figure 5.3: X-PEDE$_M$ validation over an aluminium panel for $N_{ex} = 2$ excitation points and $N_{acq} = 5$ acquisition points. (a) Grid point mesh with the selected points positions: (red circles) acquisition points; (blue crosses) excitation points; (black dots), all grid points. (b) Mean vibrational velocity PSD response to a TBL Corcos-like excitation with $U_0 = 25$ m/s: (black solid line) analytical solution; (blue dashed line) PEDE$_{M,HF}$ solution; (dotted red line) X-PEDE$_M$ solution.

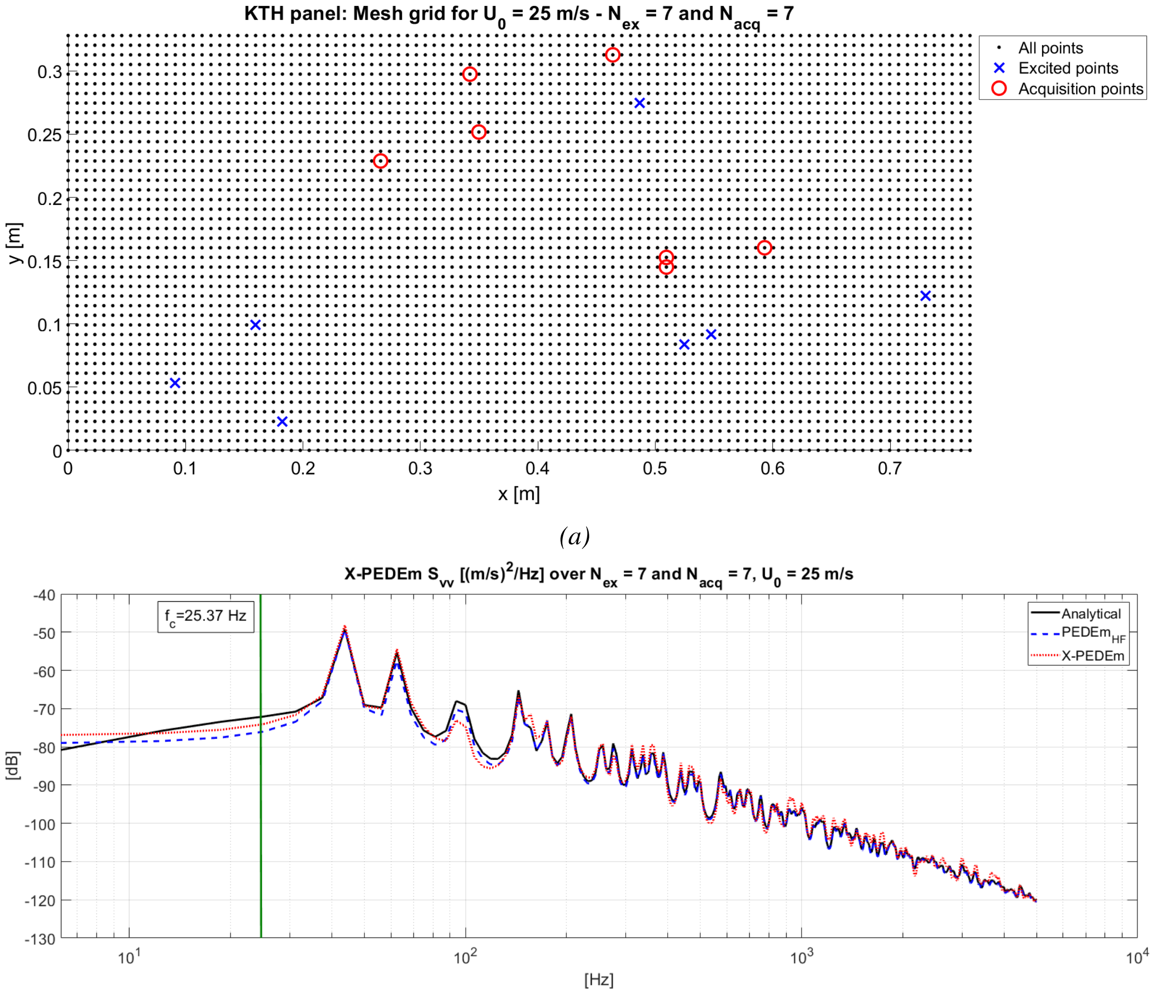

(a)

(b)

Figure 5.4: X-PEDE$_M$ validation over an aluminium panel for $N_{ex} = 7$ excitation points and $N_{acq} = 7$ acquisition points. (a) Grid point mesh with the selected points positions: (red circles) acquisition points; (blue crosses) excitation points; (black dots), all grid points. (b) Mean vibrational velocity PSD response to a TBL Corcos-like excitation with $U_0 = 25$ m/s: (black solid line) analytical solution; (blue dashed line) PEDE$_{M,HF}$ solution; (dotted red line) X-PEDE$_M$ solution.

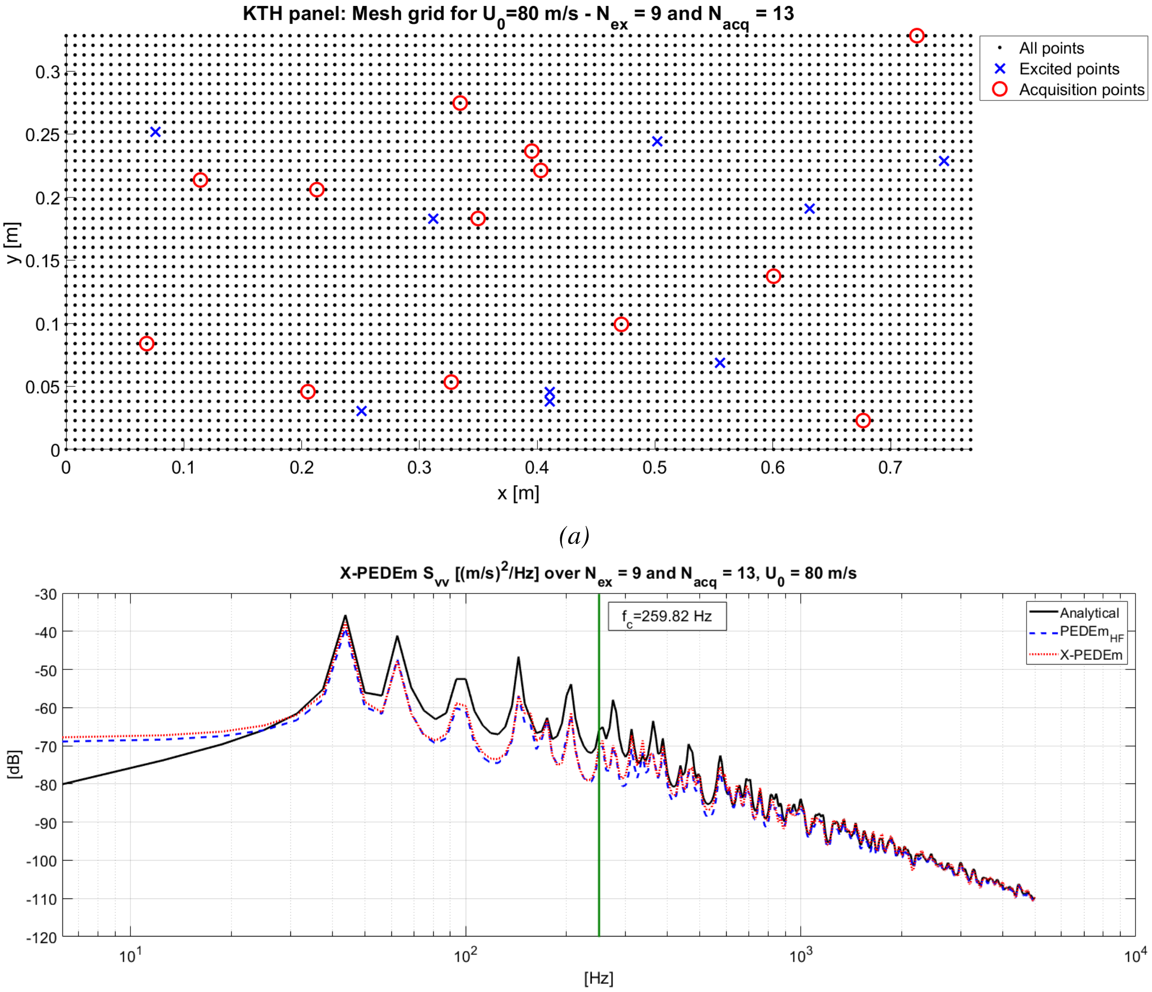

(a)

(b)

Figure 5.5: X-PEDE$_M$ validation over an aluminium panel for $N_{ex} = 9$ excitation points and $N_{acq} = 13$ acquisition points. (a) Grid point mesh with the selected points positions: (red circles) acquisition points; (blue crosses) excitation points; (black dots), all grid points. (b) Mean vibrational velocity PSD response to a TBL Corcos-like excitation with $U_0 = 80$ m/s: (black solid line) analytical solution; (blue dashed line) PEDE$_{M,HF}$ solution; (dotted red line) X-PEDE$_M$ solution calculated over 9 excitation points and 13 acquisition points.

Sherbrooke panel information					
Geometry		Material		Mesh	
L_x	0.480 m	E	6.89e10 Pa	N_x	81
L_x	0.420 m	ρ	2740 kg/m^3	N_y	71
h	0.00317 m	ν	0.3	NG	5751
Boundary conditions:					simply-supported

Table 5.2: Sherbrooke panel information for the X-PEDE$_M$ application

facility and flow speed.

5.4 Experimental results for a simply-supported panel: comparisons with different solutions

As first comparison with an experimental data set, the tests run in the Sherbrooke wind tunnel facility (see Figure 2.4) are taking as reference. All simulated and measured spectra are normalised to a unit pressure autospectrum; the autospectra used for the normalization have been measured by the *Groupe d'Acoustique de l'Université de Sherbrooke* (GAUS) of Sherbrooke University, in Canada. The details about the test panel are reported in Table 5.2, where also the mesh grid information are given.

5.4.1 Comparison with reference solutions: analytical and numerical results

As first stage to achieve before going with the validation of the proposed method, a comparison between the experimental data and the analytical and numerical solutions is made, in order to test how much different the experiment is from the theoretical solution. Both analytical and numerical are calculated for a simply supported plate, having natural frequencies and the mode shapes as

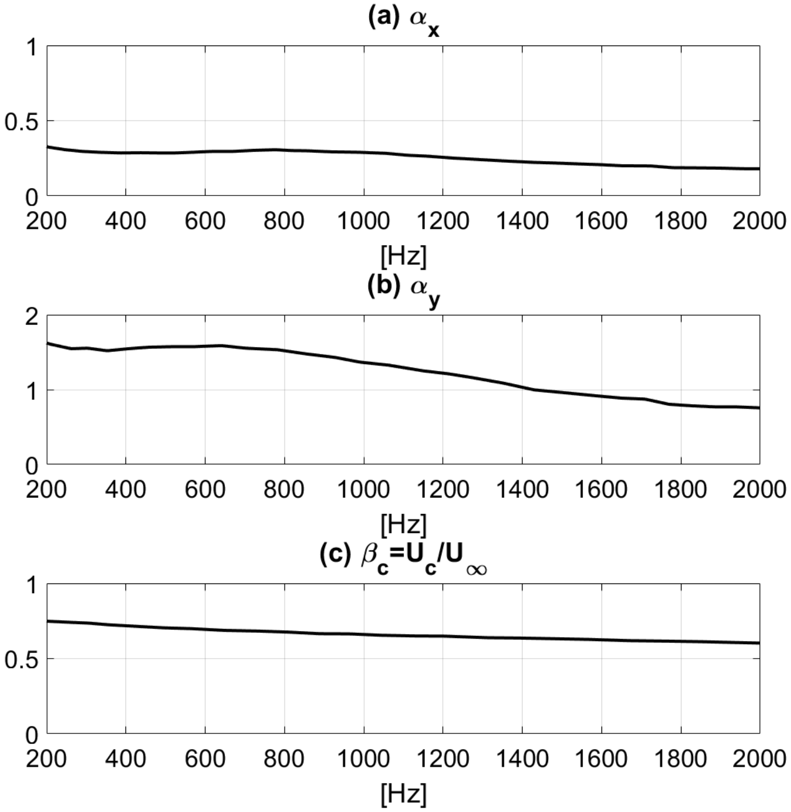

Figure 5.6: TBL properties measured during the experimental tests run in Sherbrooke wind tunnel facility. (a) Streamwise decay coefficient α_x; (b) crosswise decay coefficient α_y; (c) convective coefficient $\beta_c = U_c/U_0$.

$$\omega_m = \sqrt{\frac{Eh^2}{12\rho(1-\nu^2)}\left[\left(\frac{m_m\pi}{a}\right)^2 + \left(\frac{n_m\pi}{b}\right)^2\right]} \tag{5.8}$$

$$\Phi(x,y) = \sin\left(\frac{m_m\pi x_g}{a}\right)\sin\left(\frac{n_m\pi y_g}{b}\right) \tag{5.9}$$

while the TBL excitation has been calculated by solving the cross-acceptance function (Equation 4.25) using a Corcos model calculated with the experimental values, which have been found during the experiments run in the Sherbrooke wind tunnel [95]. The decay coefficients are thus reported in Figure 5.6, in the frequency range [200;2000] Hz.

It is important here to comment the measured coefficients. As it has been widely expressed by Hambric and Lysak [136], the decay and convective coefficients must be

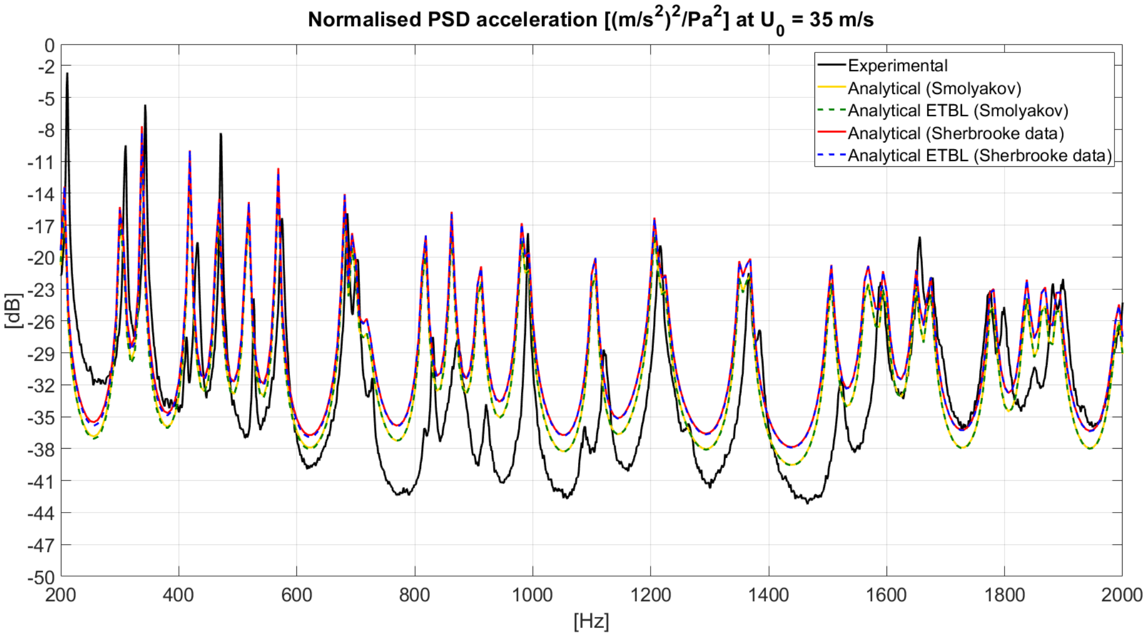

Figure 5.7: Normalised acceleration PSD response of the aluminium plate (Table 5.2) subjected to a TBL excitation. Comparison between: (solid black line) experimental solution measured in the Sherbrooke wind tunnel; (solid yellow line) analytical solution calculated with Corcos model using Smol'yakov formulations; (dashed green line) analytical solution calculated with the ETBL excitation using Smol'yakov formulations; (solid red line) analytical solution calculated with Corcos model using Sherbrooke measured data; (dashed blue line) analytical solution calculated with the ETBL excitation using Sherbrooke measured data.

physically reasonable, and the ones measured in the Sherbrooke wind tunnel facility are not, considering the high values that they present in the LF. Consequently, the structural response is obtained not only with this measured data, but also with the Smol'yakov formulations [137] — expressed in Equations 5.12 — which have demonstrated to have good robustness for different structural and flow conditions.

$$\beta_c = 0.60 + \frac{1.6(\omega\delta^*/U_0)}{1 + 16(\omega\delta^*/U_0)^2} \tag{5.10}$$

$$\alpha_x = 0.124\sqrt{1 - 0.25\left(\frac{U_c}{\omega\delta^*}\right) + \left(0.25\frac{U_c}{\omega\delta^*}\right)^2} \tag{5.11}$$

$$\alpha_y = 6.45\alpha_x \tag{5.12}$$

Figure 5.7 shows the comparison between experimental results with the analytical ones, calculated with both Smol'yakov formulations (boundary layer thickness $\delta^* = 0.0210$ m) and measured data, which they differ very little between them. The experimental natural frequencies of the panel well match the analytical ones, just presenting a slight shift moving on in the frequency domain; the peaks amplitudes are also coherent with the reference solution, especially in the LF and HF regions. A modest overestimation of around 6 dB is evident in the middle frequency region, between 600 Hz and 1600 Hz. The similarities between analytical and experimental data are good enough to validate the experiment; the mismatch in the middle frequency range might be due to a power loss of the drive system inside the wind tunnel, while the presence of some peaks which are not matched by the analytical solution might be due to the quasi-quadratic shape of the panel, meaning that there might be present some modes inside the experimental response which are not purely flexural.

It is then shown the comparison between experimental data, Full Stochastic (FS) numerical solution and the full PEDE$_{M_{HF}}$ one, both of them calculated using just the measured data. In Figure 5.8(a), the Corcos model has been used in order to calculate the FS numerical solution, while for the PEDE$_{M_{HF}}$ one, the ETBL approximation obtained with the spatial extent equivalence already mentioned in the previous chapter. In Figure 5.8(b), the FS solution has been performed using the Mellen model by keeping the same coefficients values presented in Figure 5.6; the PEDE$_{M_{HF}}$ solution, on the other hand, has been realised with the ETBL approximation presented by Bonness *et al.* [138] and reported in Equation 5.13, and an average approach of the Mellen correlation function in the wavenumber domain [139].

$$d_i(\omega) = \frac{U_c^2}{\omega^2} \frac{2\pi\alpha_x^2 \Delta x \Delta y}{\alpha_y (1 + \alpha_x^2)^{3/2}} \tag{5.13}$$

The averaged approach in the wavenumber domain consists in a direct equivalence between a correlation function expressed in the wavenumber domain $C(\kappa_x, \kappa_y; \omega)$ and an

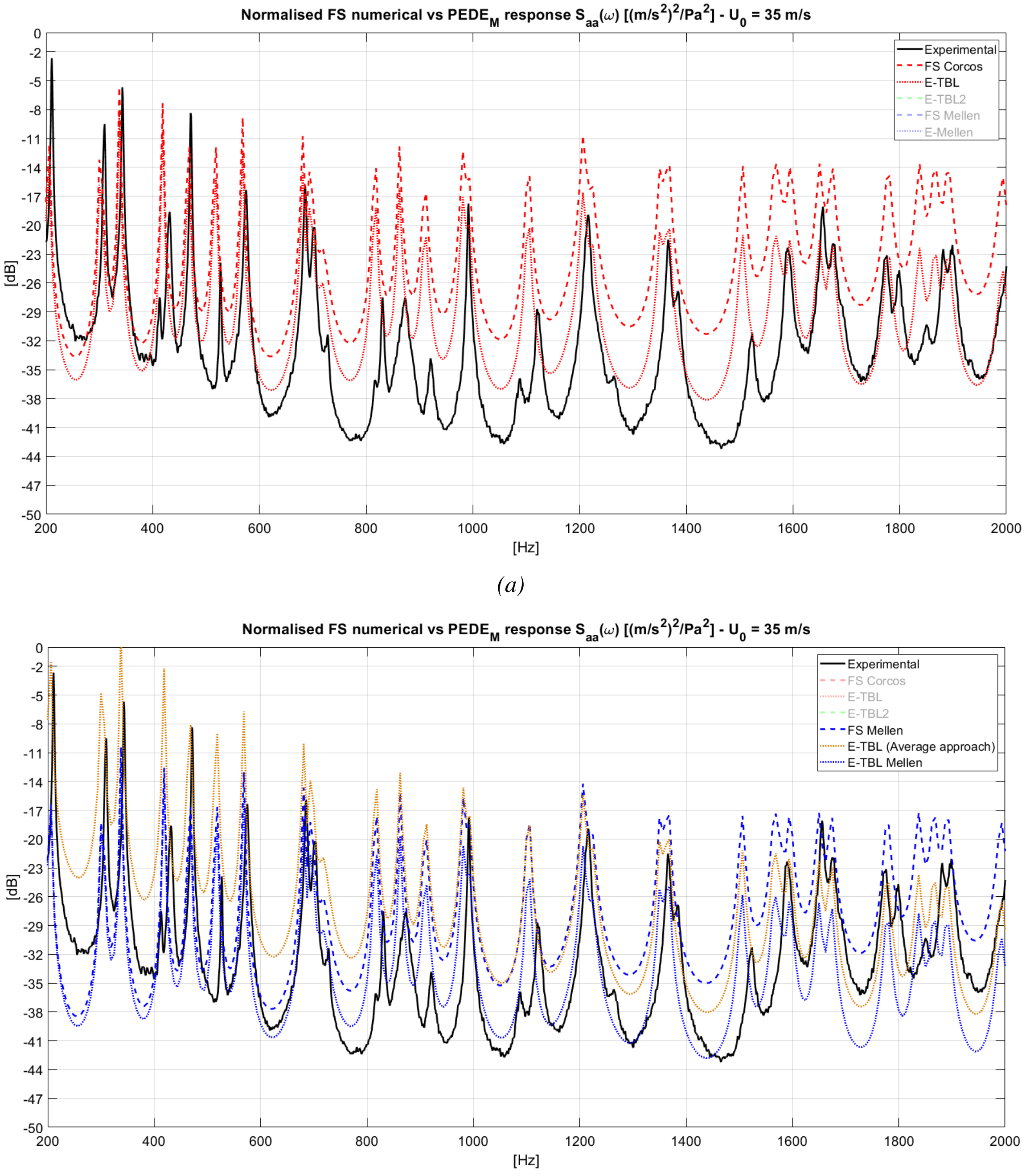

(a)

(b)

Figure 5.8: Experimental acceleration PSD collected in Sherbrooke wind tunnel ($U_0 = 35$ *m/s*) *in comparison with the Full Stochastic (FS) numerical solution and the* $PEDE_{M,HF}$ *solution. (a) (solid black line) experimental, (dashed red line) FS Numerical with Corcos model, (dotted red line)* $PEDE_{M,HF}$ *calculated with ETBL based on Corcos model (Equation 4.61). (b) (solid black line) experimental, (dashed blue line) FS Numerical with Mellen model, (dotted yellow line)* $PEDE_{M,HF}$ *calculated with the Average approach of the Mellen model (Equation 5.14), (dotted blue line)* $PEDE_{M,HF}$ *calculated with ETBL based on Mellen model (Equation 5.13).*

equivalent correlation function $C^{eq}(\omega)$ which presents a spatial distribution characteristic of a ROR excitation.

$$C(\kappa_x, \kappa_y; \omega) = \frac{C^{eq}(\omega)}{2\pi} \tag{5.14}$$

Equation 5.14 is valid in those certain frequency regions for which the wavenumber-frequency spectrum of excitation does not present evident variations. In other words, with the application of the averaged approach, it is assumed that the energetic content is equally distributed over the wavenumber domain.

As correlation function expressed in the wavenumber domain, it has been taken the $\kappa - \omega$ spectrum presented by Mellen [82]

$$C(\kappa_x, \kappa_y; \omega) = \frac{(\delta_x \delta_y)^2}{2\pi \left[(\delta_x \delta_y)^2 + (\delta_x \kappa_y)^2 + \delta_y^2(\kappa_x - \kappa_c)^2\right]^{3/2}} \tag{5.15}$$

where $\kappa_c = \omega / U_c$ is the convective wavenumber, $\delta_x = \alpha_x \kappa_c$ and $\delta_y = \alpha_y \kappa_c$ present two empirical coefficients, κ_x and κ_y are the flexural wavenumber components, characteristic of the structure under analysis.

It can be said, by looking at the comparison between the experimental data with the numerical solutions, that it is evident the problem of divergence. Because of the convective factor β_c variability over the frequency domain, it is not possible to determine an exact aliasing frequency. By taking an average value of $\bar{\beta}_c = 0.7$, the aliasing frequency is $f_{al} = 1021$ Hz. For the Corcos model, as well as for the Mellen model, the divergence seems to appear much before. For what concerning the convective coincidence frequency, it has been already said that it can be considered for a rapid, but approximate indication for the frequency limit from which the PEDE$_{M_{HF}}$ can be considered an accurate approximation; again, because β_c depends on frequency, it is not possible to individuate en effective frequency limit. As matter of fact, the use of f_{coinc} — as reference for the individuation of the frequency region in which PEDE$_{M_{HF}}$ is an adequate approximate formulation — has

Coordinates	P1	P2	P3	P4	P5	P6	P7
x (streamwise)	$0L_x$	$0.125L_x$	$0L_x$	$-0.17L_x$	$0.325L_x$	$0.21L_x$	$0.062L_x$
y (crosswise)	$0L_y$	$-0.13L_y$	$0.28L_y$	$-0.17L_y$	$-0.214L_y$	$0.333L_y$	$0L_y$

Table 5.3: Acquisition points coordinates over Sherbrooke panel.

its approximated validity if it is calculated with constant semi-empirical coefficients α_x, α_y and β_c. In this way, the determination of the correlation lengths are constant too, and consequently the TBL representation over the structural mesh grid is easily determined with Equation 4.34 and with a wavelength comparison (Figure 4.2). But having semi-empirical coefficients dependent on frequency makes the search of the most efficient mesh grid dimensions and of the frequency limit validity much more difficult. Moreover, the values of the experimental coefficient α_y used for this particular simulation (Figure 5.6b), are much higher than the one suggested in literature. These are the main reasons that have been found for the mismatch of the numerical models with the PEDE$_{M_{HF}}$ solutions.

5.4.2 Experimental vs X-PEDE$_M$: three different ETBL excitation applications

It has been laid out in the previous subsection the comparisons between the experimental data with the reference solutions, in particular with the analytical and numerical ones. It has been then shown the limits that a FS numerical solution can bring because of the choice of the mesh grid dimensions and the divergence effect that derived from it; it has been hence pointed out the advantage that approximate solutions as the PEDE$_{M_{HF}}$ can provide for a better representation of the structural response to a TBL excitation.

It is now wanted to validate, from a numerical point of view, the X-PEDE$_M$ solution, by comparing not only the acceleration PSD, but also the cross-correlations between the acquisition points. Taking as reference the work developed in [140], it has been selected the same acquisition points positions (Table 5.3), while the excitation points positions are taken randomly. In Figure 5.9, the positions of acquisition and excitation points are targeted.

The cross-correlations are considered between the point P1, at the centre of the plate, and

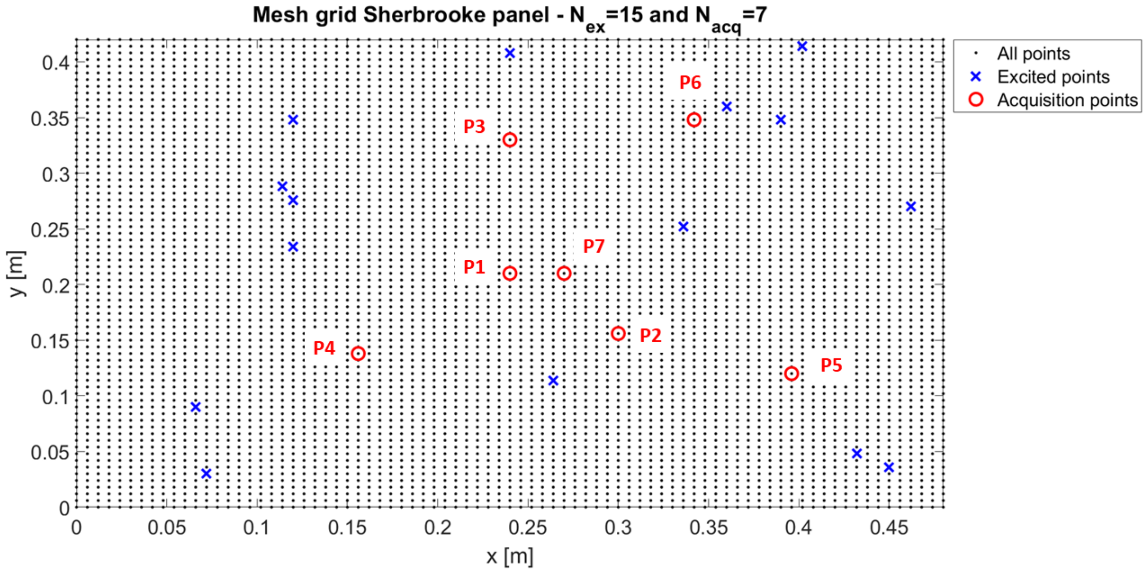

Figure 5.9: Sherbrooke panel mesh grid. (Black dots) total grid points $NG = 5751$. *(Red circles) Acquisition points* $N_{acq} = 7$. *(Blue crosses) Excitation points* $N_{ex} = 15$.

all the other points; in particular, the couples P1-P3 and P1-P7 analyse the cross-correlation respectively in the crosswise and streamwise directions. The couple P1-P4, on the other hand, analyses the cross-correlation along the diagonal direction. From Figure 5.10 to 5.15, all cross-correlations — expressed in module and phase — are plotted; it can be noticed that X-PEDE$_M$ calculated with 15 excitation random points can follow the PEDE$_{M_{HF}}$ solution for almost all the point couples CSD module. For what concerning the phase, some changes from 0 to $\pm\pi$ are reported; the phase oscillations between $-\pi$ and $+\pi$ must be retained as the same phase value is reported.

In Figure 5.16, the acceleration PSD averaged over all acquisition points is plotted; the X-PEDE$_M$ solution calculated for 15 random excitation points well describes the structural response of the Sherbrooke panel subjected to the TBL excitation.

To test also the other ETBL representations that have been introduced in this work (Equations 4.61-4.62-5.13-5.14), an X-PEDE$_M$ simulation has been run using the same set of acquisition and excitation points. Instead of using the experimental flow data (Figure 5.6), Smol'yakov formulations (Equation 5.12) have been applied for the description of the TBL approximations. In Figure 5.17, all four formulations are compared with the experimental

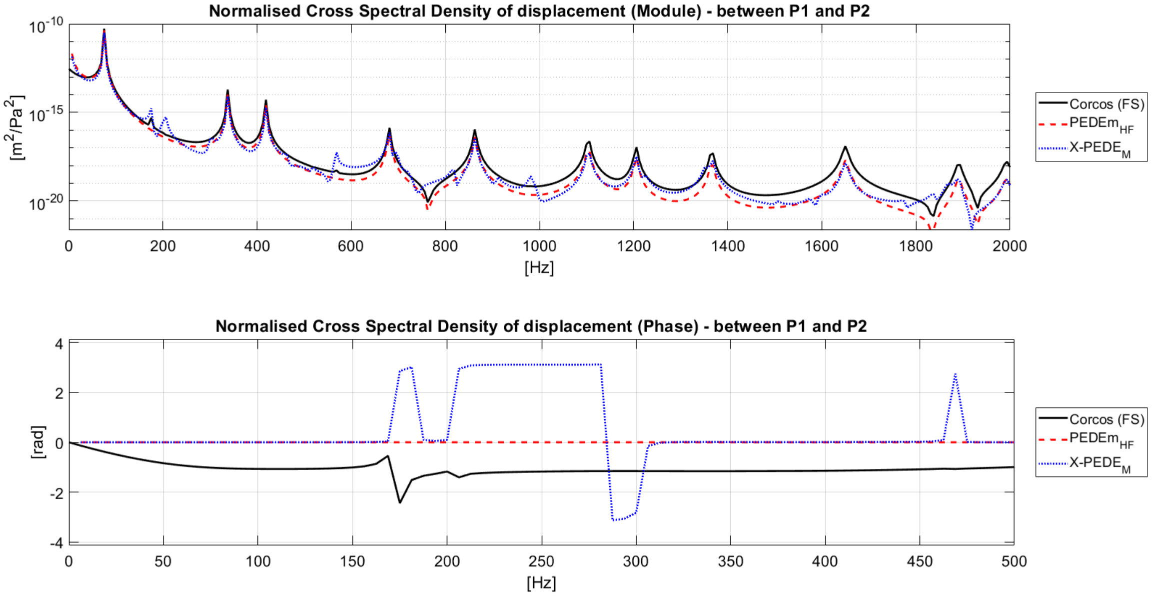

Figure 5.10: Displacement CSD module (top) and phase (bottom) between point P1 and P2. (Solid black line) FS Corcos model, (dashed red line) PEDE$_{M,HF}$, (dotted blue line) X-PEDE$_M$.

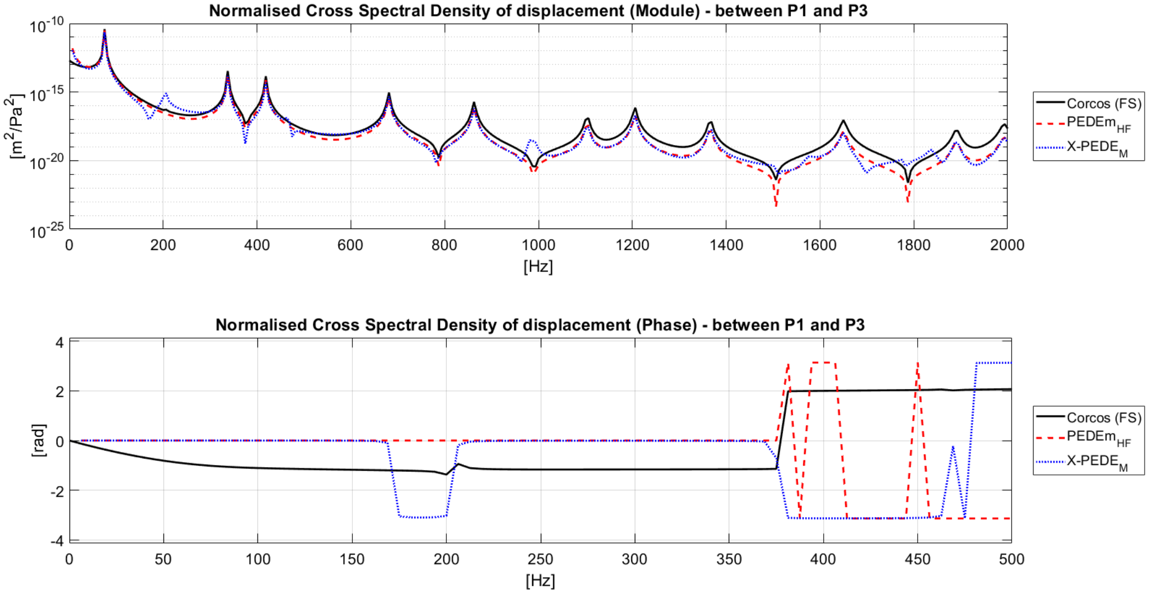

Figure 5.11: Displacement CSD module (top) and phase (bottom) between point P1 and P3. (Solid black line) FS Corcos model, (dashed red line) PEDE$_{M,HF}$, (dotted blue line) X-PEDE$_M$.

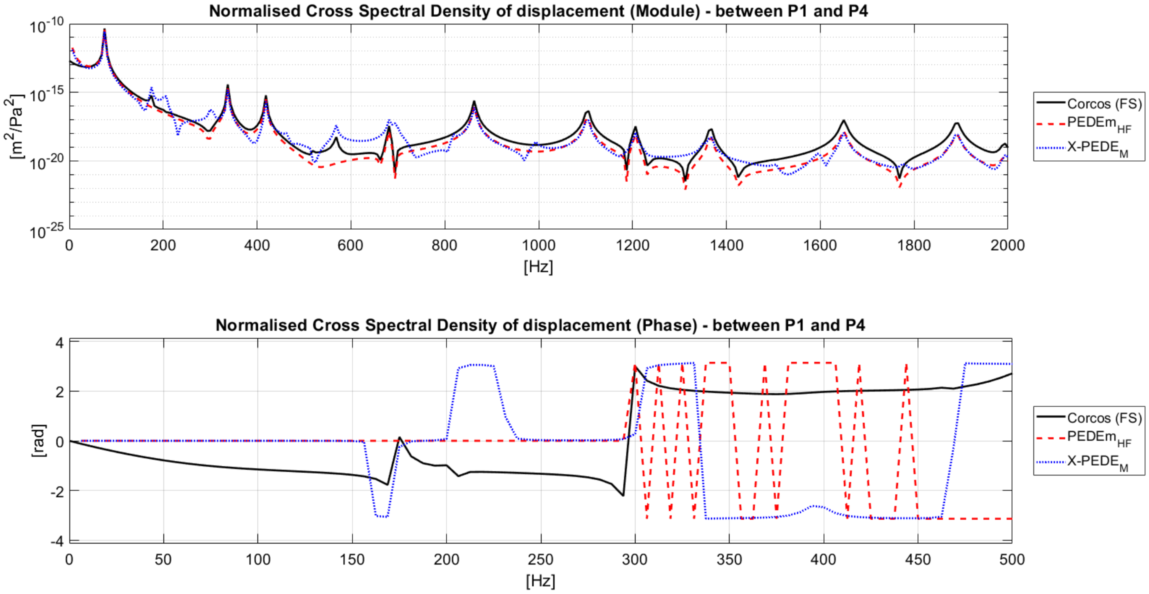

Figure 5.12: Displacement CSD module (top) and phase (bottom) between point P1 and P4. (Solid black line) FS Corcos model, (dashed red line) PEDE$_{M,HF}$, (dotted blue line) X-PEDE$_M$.

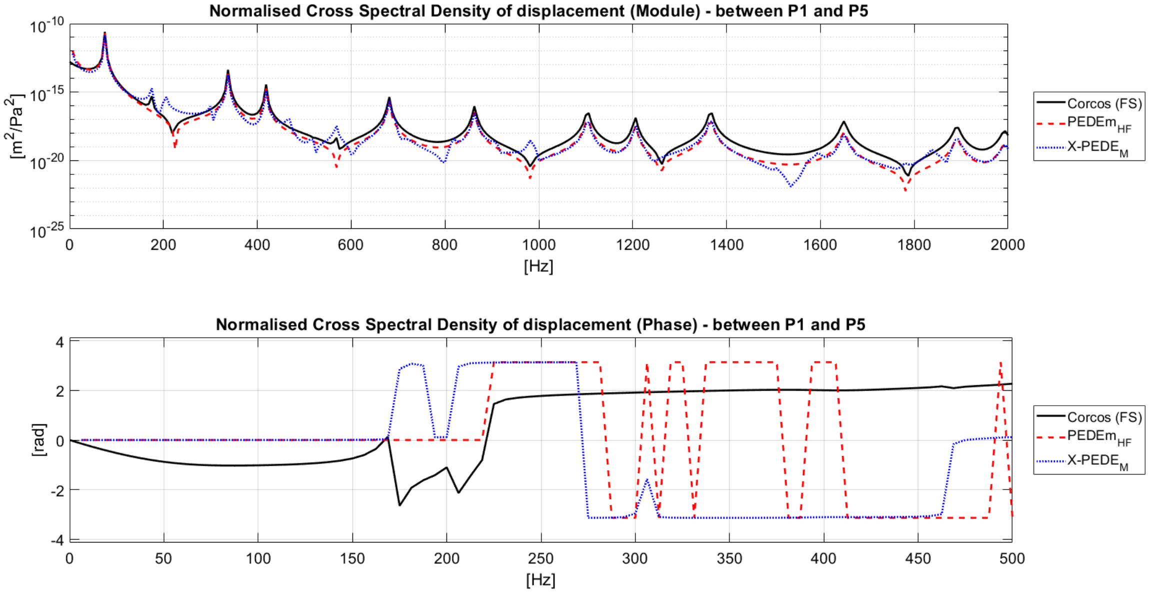

Figure 5.13: Displacement CSD module (top) and phase (bottom) between point P1 and P5. (Solid black line) FS Corcos model, (dashed red line) PEDE$_{M,HF}$, (dotted blue line) X-PEDE$_M$.

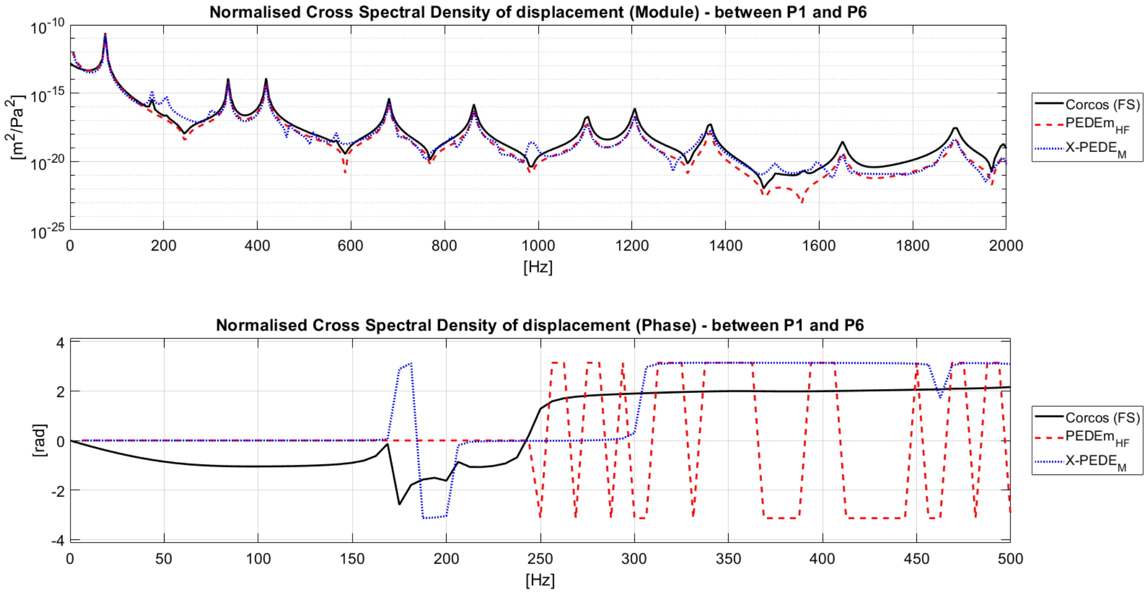

Figure 5.14: Displacement CSD module (top) and phase (bottom) between point P1 and P6. (Solid black line) FS Corcos model, (dashed red line) PEDE$_{M,HF}$, (dotted blue line) X-PEDE$_M$.

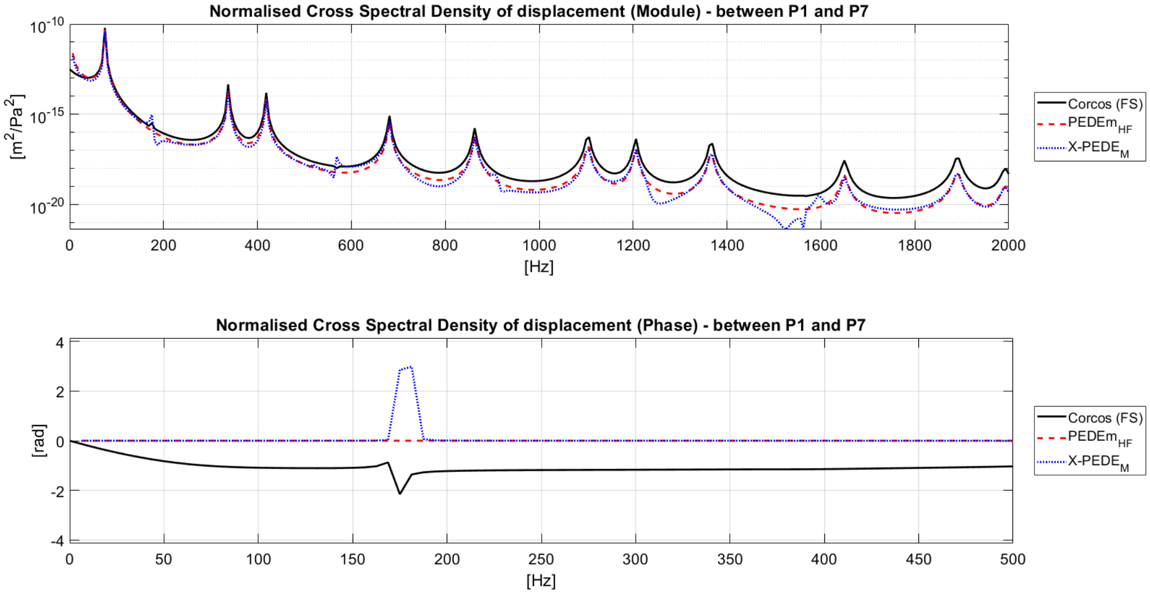

Figure 5.15: Displacement CSD module (top) and phase (bottom) between point P1 and P7. (Solid black line) FS Corcos model, (dashed red line) PEDE$_{M,HF}$, (dotted blue line) X-PEDE$_M$.

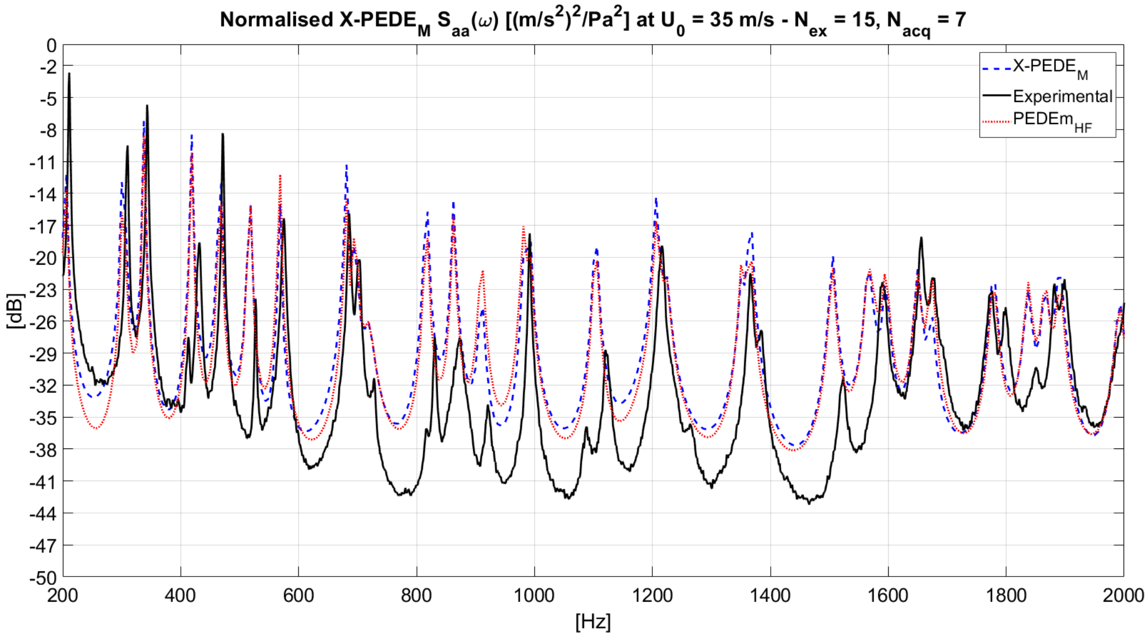

Figure 5.16: Acceleration PSD of Sherbrooke panel. (Slid black line) Experimental data, (dashed blue line) X-PEDE$_M$ with $N_{ex} = 15$ and $N_{acq} = 7$ and ETBL excitation, (dotted red line) PEDE$_{M,HF}$ calculated by using Corcos model.

results.

From the comparison of all four TBL approximations, it can be seen that the ETBL based on Corcos model is the one that describes better the experimental curve; the ETBL based on Mellen model, underestimates the solution; the ETBL obtained with the averaged approach of the Mellen model overestimates in the LF domain, but then follows the experimental curve in the HF domain; finally the ETBL2 model overestimates the experimental solution just in the middle range of frequency.

5.5 Experimental results for an all edges fixed panel: comparisons with different solutions

As second comparison between X-PEDE$_M$ and experimental solution obtained in wind tunnel, the aluminium panel analysed in the MWL/KTH facility is herein taken as sample. All simulated and measured spectra are normalised to a unit pressure autospectrum; the autospectra used for the normalization have been measured by the *Marcus Wallenberg*

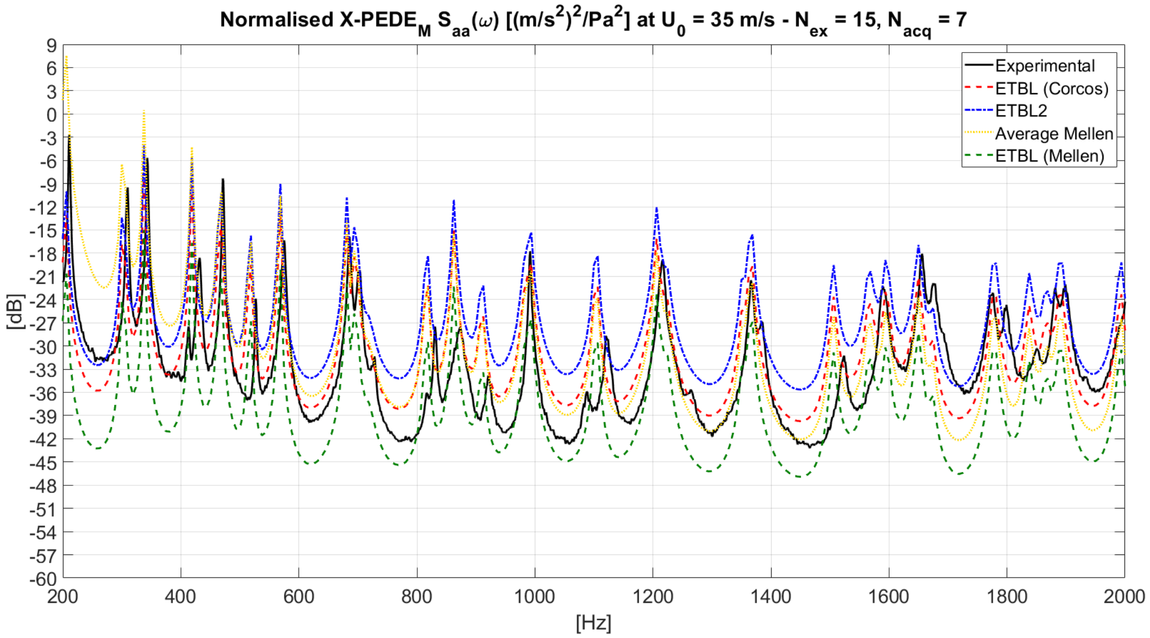

Figure 5.17: Acceleration PSD of Sherbrooke panel. (Solid black line) experimental data, (dashed red line) X-PEDE$_M$ with ETBL model based on Corcos model, (dot-dashed blue line) X-PEDE$_M$ with ETBL2 model, (dotted yellow line) X-PEDE$_M$ with Average approach of Mellen model, (dashed green line) X-PEDE$_M$ with ETBL model based on Mellen model.

Laboratory (MWL) of the KTH Royal Institute of Technology, in Stockholm, Sweden. All characteristics concerning the test model are reported in Table 5.4, together with the mesh grid dimensions chosen for the numerical simulation and the type of boundary condition.

The experimental flow data are taken from the original work [22], in which the convective flow speed is $U_c = 58$ m/s, referred to an asymptotic flow speed $U_0 = 80$ m/s; hence the convective factor is estimated constant and equal to $\beta_c = 0.725$. The streamwise and crosswise coefficients are, on the other hand, variable over the frequency range [100;5000]

KTH panel information					
Geometry		Material		Mesh	
L_x	0.768 m	E	7.10e10 Pa	N_x	102
L_x	0.328 m	ρ	2700 kg/m^3	N_y	44
h	0.0016 m	ν	0.33	NG	4488
Boundary conditions:			all edges clamped		

Table 5.4: KTH panel information for the X-PEDE$_M$ application

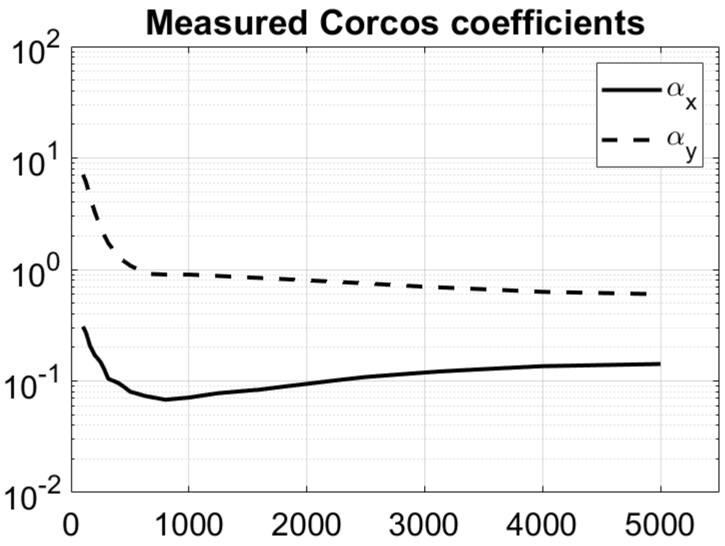

Figure 5.18: Corcos model coefficients measured in the MWL/KTH wind tunnel for an asymptotic speed $U_0 = 80$ m/s, $\beta_c = 0.725$.

Hz and plotted in Figure 5.18.

It is wanted to mention — as it is reported in the referenced paper — that several issues occurred during this experiment. One concerns a difference of pressure between inside and outside the test section of the wind tunnel; it resulted in a deflection of the clamped panel of about ≈ 0.004 m at its centre. For this reason, it has been used directly the experimental natural frequencies measured during the experiment; in Table 5.5, the comparison between experimental and analytical natural frequencies for the KTH panel is shown. The analytical frequencies have been calculated following the Blevins formulation [141] for a panel with all clamped edges. Moreover, different Corcos coefficients values are herein provided in order to describe better the experimental solution through a numerical simulation. For the sake of a physical consistency, Smol'yakov's formulation (Equations 5.12, for a boundary layer thickness $\delta^* = 0.0051$m) is again used to calculate the decay coefficients for the aerodynamic load representation during the X-PEDE$_M$ simulation.

	Natural frequencies [Hz]						
Analytical	87.9	105.9	138.6	186.6	233.1	249.4	251.3
Experimental	133.5	168.8	217.7	267.1	277.7	303.1	350.3

Table 5.5: Natural frequencies of KTH panel: analytical (Blevins formula) and experimental values.

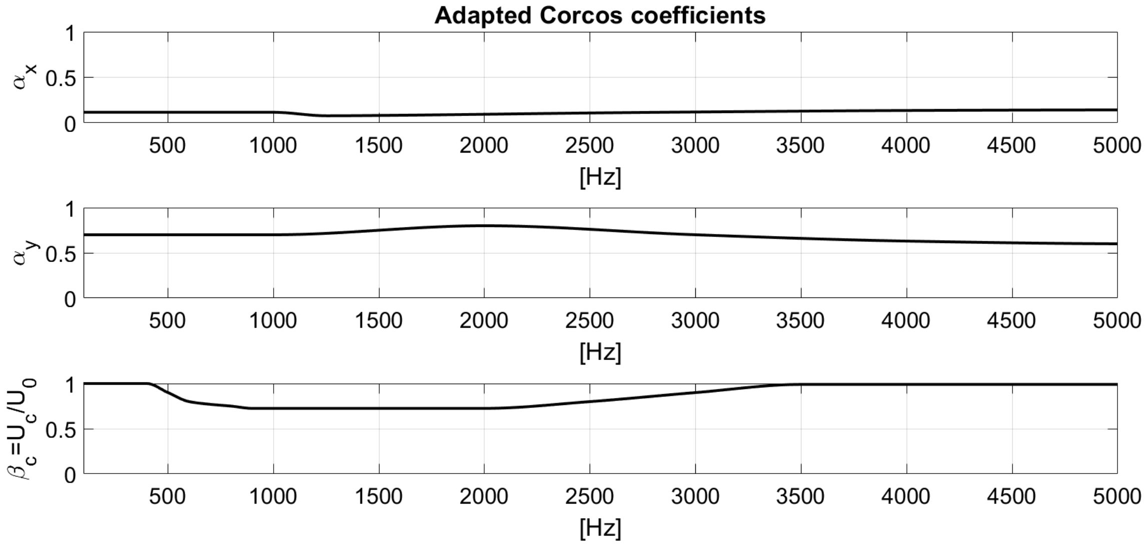

Figure 5.19: Adapted flow data coefficients for the different TBL excitation representations.

5.5.1 Comparison with reference solutions: numerical results

For the validation of the experimental data set, only the numerical solution has been calculated as reference. It is shown firstly the Full Stochastic (FS) numerical solutions calculated with the experimental flow data; then, the same solutions, compared with the PEDE$_{M_{HF}}$ ones, calculated with the adapted flow data, which are reported in Figure 5.19.

By following the indications given in [22], the convective speed is $U_c = 58$ m/s over all the frequency region; this implies that $f_{al} = 1907$ Hz and $f_{coinc} = 144.06$ Hz. This means that the FS numerical solution should cover the LF domain and starts to diverge right after f_{al}; at the same time, the PEDE$_{M_{HF}}$ should give an adequate description of the structural response to a TBL excitation in the HF domain, starting at around 200 Hz. What it can be seen in Figure 5.20, firstly, is that both FS numerical solutions underestimate the experimental result in the very LF region. The divergence around 1900 Hz is not evident for the Corcos model solution, which it appears to diverge even before the aliasing frequency; on the other hand, the Mellen model solution seems to never diverge and follow the experimental result until the end of the frequency domain of interest. Indeed, if the PEDE$_{M_{HF}}$ solutions are now taken in consideration, it can be noticed that both models underestimate the experimental solution in the HF domain. Considering the issues involved during the experiment and mentioned before, it is thus not clear if the experimental response has been perfectly measured, or there are some discrepancies in the experimental flow coefficients data. With the adapted flow coefficients data (Figure 5.19), the FS numerical solutions perfectly follow the experimental one in the LF domain, as it can be appreciated in Figure 5.21.

The PEDE$_{M_{HF}}$ solution calculated with the ETBL approximation well matches the experimental data over the frequency range. Unfortunately, the adaptation of the flow coefficients data did not work at the best for the E-Mellen approximation, which once again underestimates the structural response.

A last comparison is herein shown in Figure 5.22, for which the PEDE$_{M_{HF}}$ has been calculated by using the second version of ETBL approximation (Equation 4.62), previously presented in Chapter 4. The numerical solution well follows the experimental one in the HF domain and presents a difference of ≈ 6 dB in the middle frequency range.

As result of this first analysis, only ETBL and ETBL2 models are chosen for the X-PEDE$_M$ application.

5.5.2 Experimental vs X-PEDE$_M$: three different ETBL excitation applications

On the mesh grid composed by $NG = 4488$ grid points, 15 excitation points and 7 acquisition points have been selected in a random way, avoiding just the grid points on the boundaries, since they are clamped. In Figure 5.23, their positions are individuated.

As foreseen and shown in Figure 5.24, X-PEDE$_M$ follows perfectly the PEDE$_{M_{HF}}$ solution for most of all the frequency range, until at the high frequencies it can be noticed

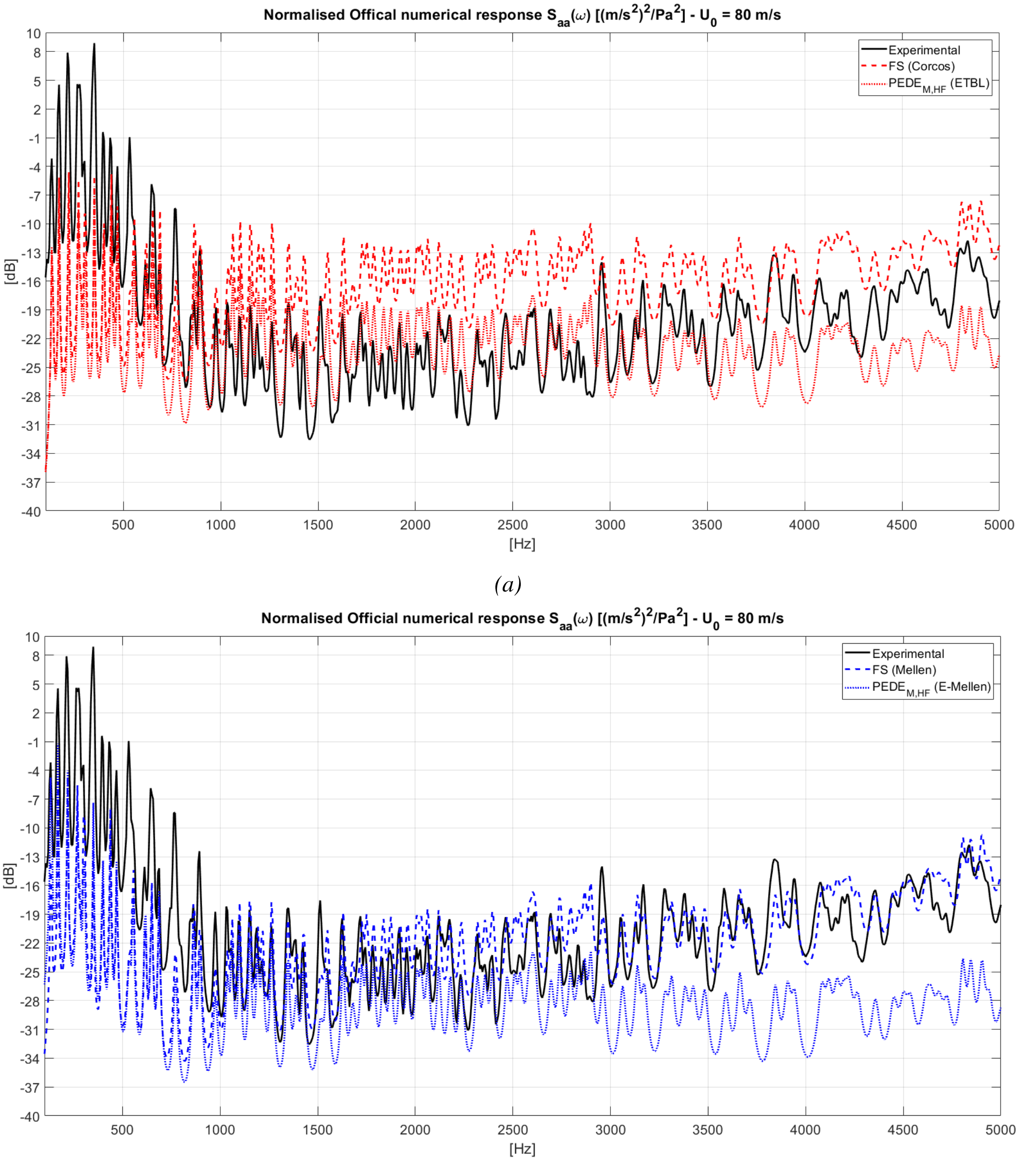

(a)

(b)

Figure 5.20: Experimental acceleration PSD measured in MWL/KTH wind tunnel ($U_0 = 80$ m/s) in comparison with the Full Stochastic (FS) numerical solution and $PEDE_{M,HF}$, calculated with experimental flow data (Figure 5.18). (a) (solid black line) experimental, (dashed red line) FS Numerical with Corcos model, (dotted red line) $PEDE_{M,HF}$ calculated with ETBL (Equation 4.61). (b) (solid black line) experimental, (dashed blue line) FS Numerical with Mellen model, (dotted blue line) $PEDE_{M,HF}$ calculated with an Equivalent Mellen model (Equation 5.14).

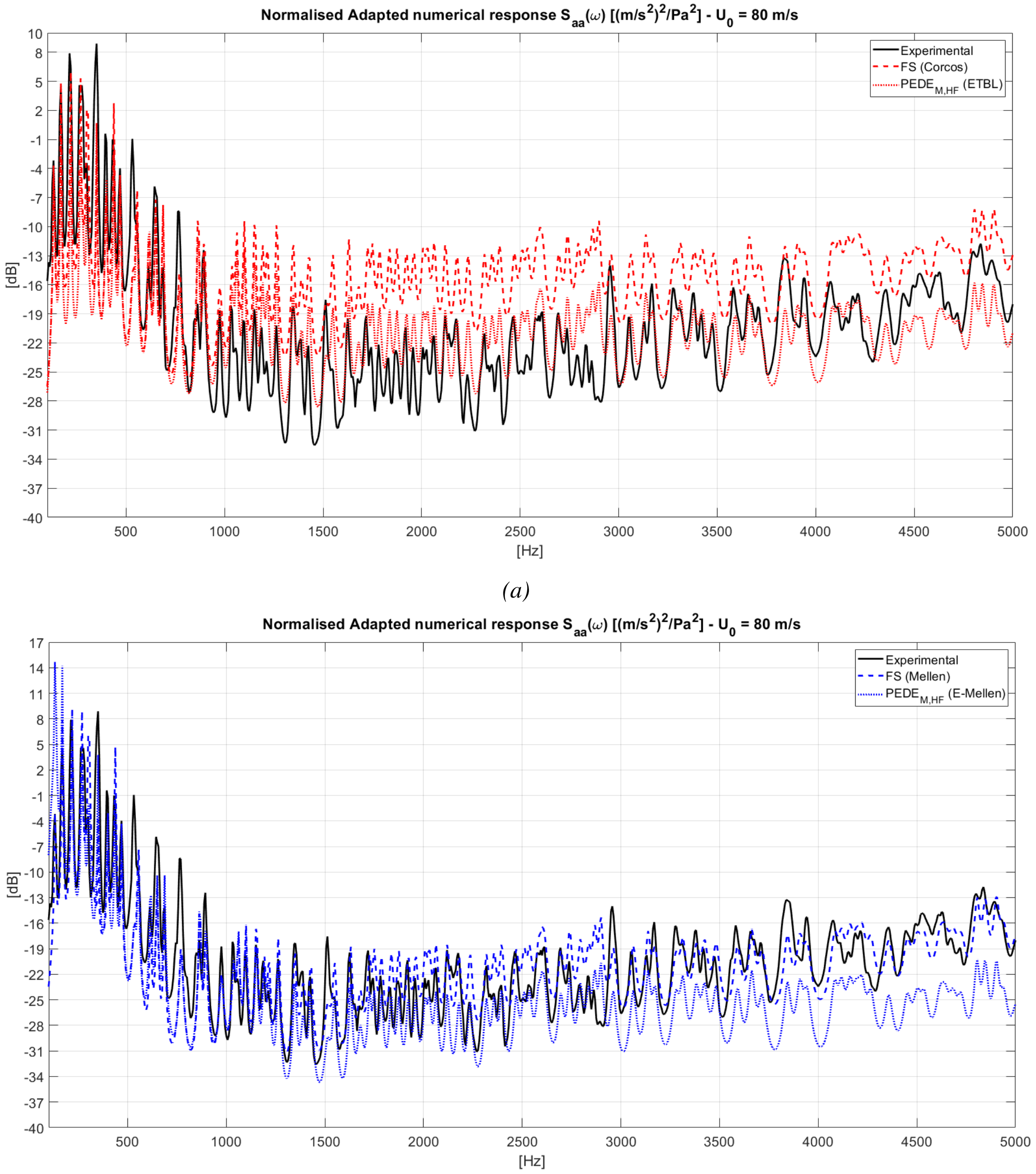

(a)

(b)

Figure 5.21: Experimental acceleration PSD collected in MWL/KTH wind tunnel ($U_0 = 80$ m/s) in comparison with the Full Stochastic (FS) numerical solution and PEDE$_{M,HF}$, calculated with adapted flow data (Figure 5.19). (a) (solid black line) experimental, (dashed red line) FS Numerical with Corcos model, (dotted red line) PEDE$_{M,HF}$ calculated with ETBL (Equation 4.61). (b) (solid black line) experimental, (dashed blue line) FS Numerical with Mellen model, (dotted blue line) PEDE$_{M,HF}$ calculated with an Equivalent Mellen model (Equation 5.14).

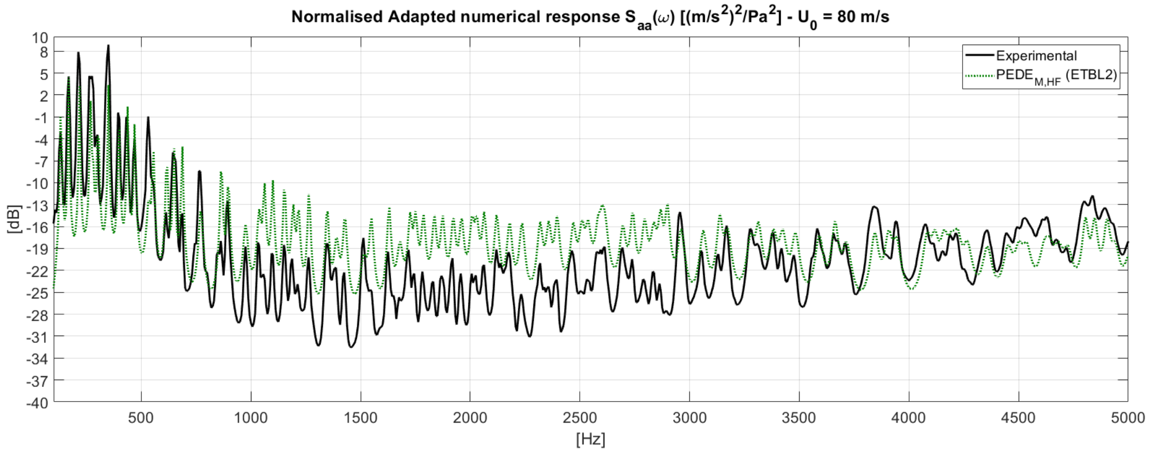

Figure 5.22: Experimental acceleration PSD collected in MWL/KTH wind tunnel ($U_0 = 80$ m/s) in comparison with $PEDE_{M,HF}$, calculated with adapted flow data (Figure 5.19). (solid black line) experimental, (dotted green line) $PEDE_{M,HF}$ calculated with ETBL2 (Equation 4.62).

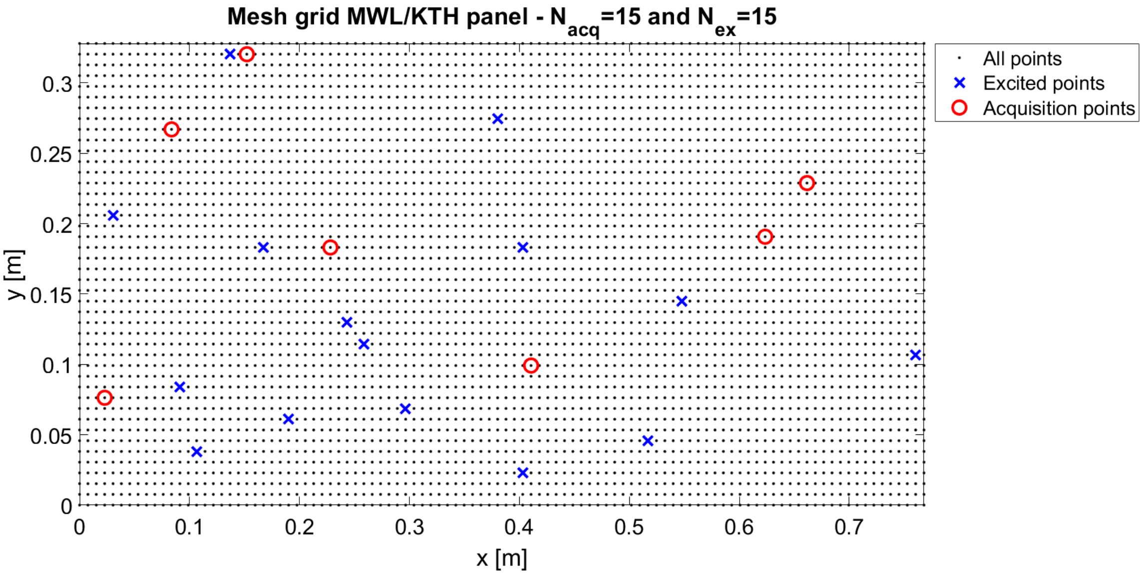

Figure 5.23: MWL/KTH panel mesh grid. (Black dots) total grid points $NG = 4488$, (red circles) acquisition points $N_{acq} = 7$, (blue crosses), excitation points $N_{ex} = 15$.

a very slight difference in the amplitudes peaks, even though the curve behaviours are respected. It can be said, then, X-PEDE$_M$ is able to give an approximate estimation of the structural response of a panel subjected to an aerodynamic load as the TBL.

Always for sake of physical consistency, X-PEDE$_M$ has been applied by using Smol'yakov coefficients too (Figure 5.25).

Even with this description of the TBL decay coefficients, it is possible to notice that the overlap with the experimental data is reached only with the ETBL2 approximation. As before, the ETBL based on Mellen model is not able to describe the vibrational response of the sample under study; the ETBL based on the Corcos model, on the other hand, seems to underestimates the solution in the LF and just slightly in the HF domain.

5.6 Conclusions

In this fifth chapter, a method adapted for experimental simulations has been introduced. X-PEDE$_M$ is indeed a variation of the original method PEDE$_M$, which is able to reproduce the structural response to a TBL excitation by reproducing the two asymptotic behaviours: a fully correlated excitation, as an Incident Diffuse Field at low frequencies, and a totally uncorrelated excitation as the Rain-On-the-Roof. X-PEDE$_M$ takes this last approximation and implements it for experimental purposes: by choosing a discrete number of acquisition and excitation points, it is possible to obtain a reproduction of a structural response to a TBL excitation.

The numerical formulation have been introduced and the procedure for an experimental application of the method has been explained. A numerical validation, then, has been given, for different sets of acquisition and excitation points, which vary for positions and quantity of selected points.

Finally, X-PEDE$_M$ is put to the test with two experimental data sets, referred to two different panels studied in two different wind tunnel facilities. The first one has been analysed at the Sherbrooke wind tunnel for an asymptotic speed of $U_0 = 35$ m/s; X-PEDE$_M$

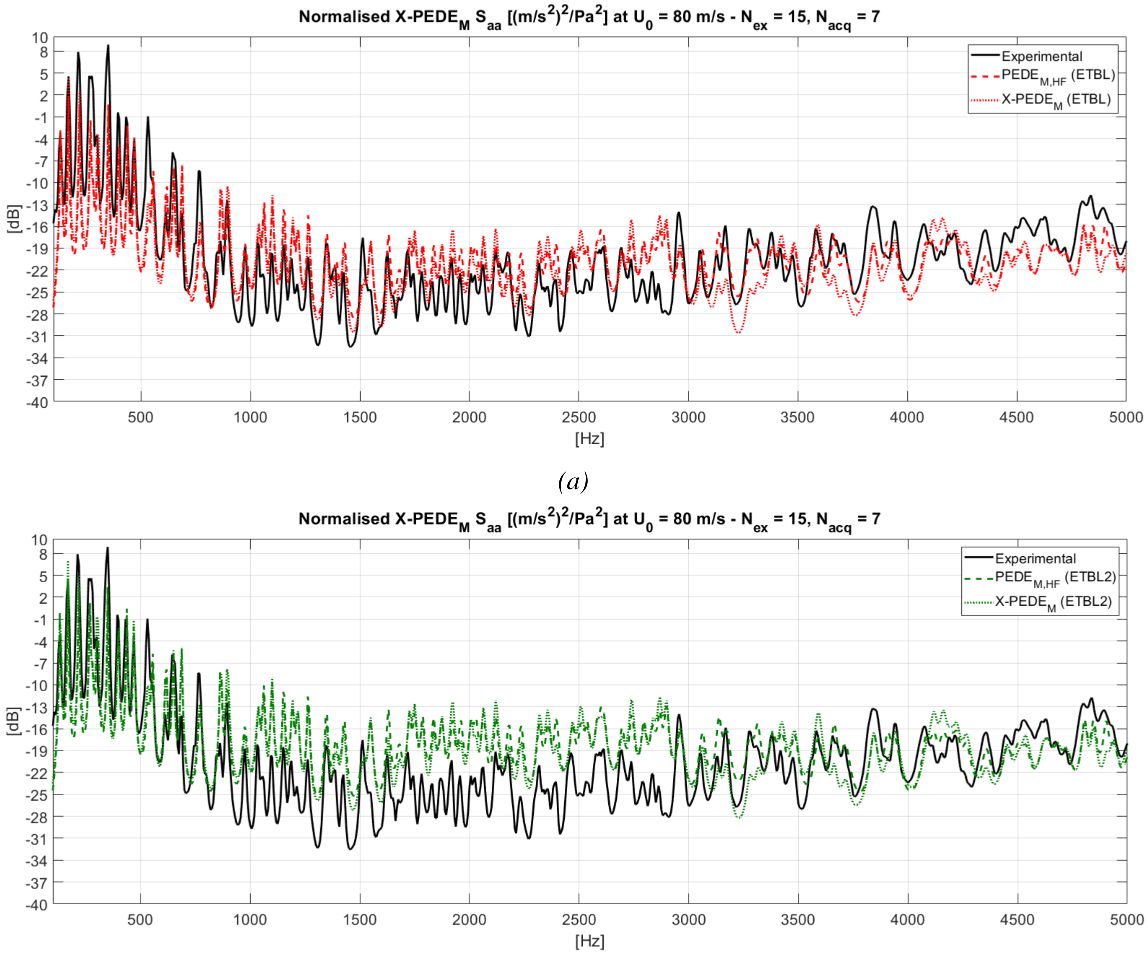

(a)

(b)

Figure 5.24: Experimental acceleration PSD collected in MWL/KTH wind tunnel ($U_0 = 80$ m/s) in comparison with PEDE$_{M,HF}$, calculated with adapted flow data (Figure 5.19) and X-PEDE$_M$ over $N_{acq} = 7$ and $N_{ex} = 15$. (a) (solid black line) experimental, (dashed red line) PEDE$_{M,HF}$ calculated with ETBL (Equation 4.61), (dotted red line) X-PEDE$_M$ calculated with ETBL (Equation 4.61). (b) (solid black line) experimental, (dashed green line) PEDE$_{M,HF}$ calculated with ETBL2 (Equation 4.62), (dotted green line) X-PEDE$_M$ calculated with ETBL2 (Equation 4.62).

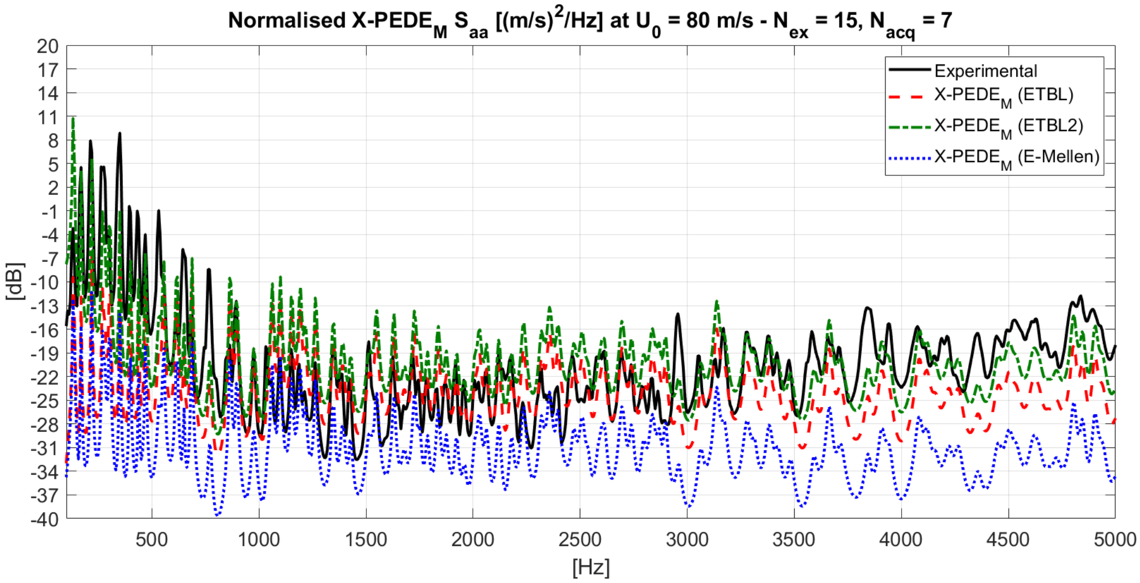

Figure 5.25: Experimental acceleration PSD collected in MWL/KTH wind tunnel ($U_0 = 80$ m/s) in comparison with X-PEDE$_M$, calculated with Smol'yakov formulation (Equations 5.12) over $N_{acq} = 7$ and $N_{ex} = 15$. (solid black line) experimental, (dashed red line) X-PEDE$_M$ calculated with ETBL (Equation 4.61), (dotted red line) X-PEDE$_M$ calculated with ETBL (Equation 4.61), (dashed-dotted green line) X-PEDE$_M$ calculated with ETBL2 (Equation 4.62), (dotted blue line) X-PEDE$_M$ calculated with ETBL based on Mellen model (Equation 5.13).

has been applied for 7 specific acquisition points and 15 random excitation points. The acceleration PSD has been compared with four different formulations of X-PEDE$_M$: the ETBL obtained from the Corcos model, the Equivalent-Mellen obtained from the average approach over the wavenumber-frequency domain of the Mellen correlation function, the ETBL2 obtained in [86] as extension to the 2D case of Hong and Shin [87] and ETBL approximation based on Mellen model obtained through spatial extent equivalence as it has been done with Corcos model. Moreover, the cross-correlations among acquisition points have been checked and compared with the cross-correlations calculated with a full stochastic numerical solution and the original PEDE$_{M_{HF}}$ one.

The second panel has been analysed at the MWL/KTH wind tunnel facility for an asymptotic speed of $U_0 = 80$ m/s. Only the acceleration PSD has been compared with X-PEDE$_M$, achieving a good result just with the ETBL2 approximation model, both with the experimental data collected during the wind tunnel test and with the Smol'yakov coefficients.

Conclusions

The presented research has had as objective the development of a structural device for vibroacoustic measurements over flat panels performed inside a wind tunnel facility. To address the problem, a literature survey has been conducted about three main topics: the wind tunnel architectures, with a focus on design techniques of support systems for test models; energy transmission decoupling between two systems, in order to avoid any influence of the support system on the test models; methods for the reproduction of a structural response to a TBL excitation, with the purpose of validate the structural device.

From the first literature research, it has been verified that among the design techniques for wind tunnels facilities, there are no generic design guidelines that can ensure an energy decoupling between support and test model.

From the second survey, the Statistical Energy Analysis has been selected as benchmark method for the development of the design guidelines for the support. In Chapter 2, the process of development of the design guidelines is exposed. These guidelines are based on the main intention of reducing at the minimum the transmitted power from one SEA-subsystem to another, ensuring in a difference between the two vibrational velocities of 20 dB. By knowing the asymptotic mobilities of both subsystems, it is possible to choose *a priori* type of material and geometry (in terms of thickness and area) for the support that can ensure the energy decoupling. Moreover, because the asymptotic mobility formulation is valid for any kind of system, these guidelines are versatile. The design rules have been first applied on a simple system consisting in a test panel allocated in a frame, and then in Chapter 3, they are applied for the development of a 3D structure which would sustain flat panels and that would be suspended inside a large-scale wind tunnel. The final design resulted in a oval shaped structure, named *ogive*, made with sandwich shells, having the skins in aluminium and core in honeycomb, that can allocate sample panels with dimensions 0.5×0.4 m^2 and that can ensure also acoustic measurements in its inner acoustic volume.

This support has been analysed at high frequencies with the commercial software VA-One and at low frequencies with the commercial software COMSOL Multiphysics. At high frequencies, the vibrational velocity of the test panel resulted 20 dB higher than the mean vibrational velocity of the ogive, and a higher level of radiated sound power of the test panel inside the central acoustic cavity. At low frequencies, mode shapes and natural frequencies of the test model and ogive were easily distinguishable, even though the test panel shows other deformations when the ogive mode shapes occur.

With the structural design of the support system, an "off-line" validation method has been proposed through the third literature survey. Indeed the Pseudo-Equivalent Deterministic Excitation method (PEDE_M) has been adapted for experimental purposes in order to simulate a TBL excitation over a structure by using deterministic forces. The experimental version of PEDE_M (X-PEDE_M) has been validated numerically over two different aluminium plates whose structural responses have been compared with their experimental data collected in two different wind tunnel facilities.

Future works

The design guidelines developed with SEA are valid in the high frequency regime, but it is not sure that their application would guarantee an energy decoupling also at low frequencies. An extension of the frequency range of applicability of the design rules is required in order to ensure the measurements purity in a broadband frequency range. A numerical application of X-PEDE_M over the ogive model developed in Chapter 3 is necessary in order to extent the method validation to complex structures; as second step, the actual experimental application of X-PEDE_M over the two aforementioned sample panels is required, so that a comparison between the two different experimental solutions can be analysed. Moreover, because X-PEDE_M is based on the choice of a restricted number of excitation and acquisition points, a study about which is the adequate number of points to take and which are the best positions to assign, is highly suggested for the optimization of the "off-line" experimental method.

REFERENCES

[1] J Green and J Quest. “A short history of the European Transonic Wind Tunnel ETW”. In: *Progress in Aerospace Sciences* 47.5 (2011), pp. 319–368.

[2] PBS Lissaman. “Low-Reynolds-number airfoils”. In: *Annual review of fluid mechanics* 15.1 (1983), pp. 223–239.

[3] LA Meyn and KD James. “Full-scale wind-tunnel studies of F/A-18 tail buffet”. In: *Journal of Aircraft* 33.3 (1996), pp. 589–595.

[4] CJ Baker and NJ Brockie. “Wind tunnel tests to obtain train aerodynamic drag coefficients: Reynolds number and ground simulation effects”. In: *Journal of Wind Engineering and Industrial Aerodynamics* 38.1 (1991), pp. 23–28.

[5] A Cogotti. “Evolution of performance of an automotive wind tunnel”. In: *Journal of Wind Engineering and Industrial Aerodynamics* 96.6-7 (2008), pp. 667–700.

[6] JE Cermak. “Wind-tunnel development and trends in applications to civil engineering”. In: *Journal of wind engineering and industrial aerodynamics* 91.3 (2003), pp. 355–370.

[7] Y Li et al. “Wind characteristics at bridge site in a deep-cutting gorge by wind tunnel test”. In: *Journal of Wind Engineering and Industrial Aerodynamics* 160 (2017), pp. 30–46.

[8] G Cousin. “Sound from TBL-induced vibrations”. In: *4th AIAA/CEAS Aeroacoustics Conference*. 1998, p. 2216.

[9] JM Pallis and RD Mehta. “Aerodynamics and hydrodynamics in sports”. In: *The Engineering of Sport* 4 (2002), pp. 31–39.

[10] MG Dodson and DS Miklosovic. “An historical and applied aerodynamic study of the Wright Brothers’ wind tunnel test program and application to successful manned flight”. In: *Fluids Engineering Division Summer Meeting*. Vol. 41987. 2005, pp. 269–278.

[11] M-S Kim et al. *Hyundai full scale aero-acoustic wind tunnel*. Tech. rep. SAE Technical Paper, 2001.

[12] G Ocokoljić, B Rašuo, and M Kozić. “Supporting system interference on aerodynamic characteristics of an aircraft model in a low-speed wind tunnel”. In: *Aerospace Science and Technology* 64 (2017), pp. 133–146.

[13] P Bradshaw and RC Pankhurst. “The design of low-speed wind tunnels”. In: *Progress in Aerospace Sciences* 5 (1964), pp. 1–69.

[14] RD Mehta and P Bradshaw. “Design rules for small low speed wind tunnels”. In: *Aeronautical Journal* 83.827 (1979), pp. 443–449.

[15] A Pope and KL Goin. *High Speed Wind Tunnel Testing*. John Wiley & Sons, 1965.

[16] JB Barlow, WH Rae, and A Pope. *Low-speed wind tunnel testing*. John wiley & sons, 1999.

[17] L Cattafesta, C Bahr, and J Mathew. “Fundamentals of wind-tunnel design”. In: *Encyclopedia of Aerospace Engineering* (2010).

[18] P Liu et al. “Design and performance of a small-scale aeroacoustic wind tunnel”. In: *Applied Acoustics* 116 (2017), pp. 65–69.

[19] J Mathew et al. “Design, fabrication, and characterization of an anechoic wind tunnel facility”. In: *11th AIAA/CEAS Aeroacoustics Conference*. 2005, p. 3052.

[20] F Giardino and J Rocha. “Design and Characterization of a High-Speed Subsonic Aeroacoustic Wind Tunnel”. In: *Journal of Aircraft* 56.1 (2019), pp. 108–120.

[21] M Remillieux et al. “Calibration and demonstration of the new Virginia Tech anechoic wind tunnel”. In: *14th AIAA/CEAS Aeroacoustics Conference (29th AIAA Aeroacoustics Conference)*. 2008, p. 2911.

[22] S Finnveden et al. “A model of wall pressure correlation for prediction of turbulence-induced vibration”. In: *Journal of Fluids and Structures* 20.8 (2005), pp. 1127–1143.

[23] E Ciappi et al. “On the dynamic behavior of composite panels under turbulent boundary layer excitations”. In: *Journal of Sound and Vibration* 364 (2016), pp. 77–109.

[24] C Marchetto et al. “Measurement techniques of the sensitivity functions to characterize the vibration response of panels under turbulent boundary layer excitation”. In: *International Conference on Flow Induced Noise and Vibration Issues and Aspects*. Springer. 2017, pp. 339–355.

[25] M Smith et al. “Validation tests for flow induced excitation and noise radiation from a car window”. In: *18th AIAA/CEAS Aeroacoustics Conference (33rd AIAA Aeroacoustics Conference)*. 2012, p. 2201.

[26] J Park, T Siegmund, and L Mongeau. “Analysis of the flow-induced vibrations of viscoelastically supported rectangular plates”. In: *Journal of Sound and Vibration* 261.2 (2003), pp. 225–245.

[27] J Park, L Mongeau, and T Siegmund. “Influence of support properties on the sound radiated from the vibrations of rectangular plates”. In: *Journal of sound and vibration* 264.4 (2003), pp. 775–794.

[28] J Park, L Mongeau, and T Siegmund. “An investigation of the flow-induced sound and vibration of viscoelastically supported rectangular plates: experiments and model verification”. In: *Journal of sound and vibration* 275.1-2 (2004), pp. 249–265.

[29] RH Lyon and G Maidanik. “Power flow between linearly coupled oscillators”. In: *The journal of the Acoustical Society of America* 34.5 (1962), pp. 623–639.

[30] RH Lyon and E Eichler. “Random vibration of connected structures”. In: *The Journal of the Acoustical Society of America* 36.7 (1964), pp. 1344–1354.

[31] RH Lyon and TD Scharton. “Vibrational-Energy Transmission in a Three-Element Structure”. In: *The Journal of the Acoustical Society of America* 38.2 (1965), pp. 253–261.

[32] DE Newland. “Calculation of power flow between coupled oscillators”. In: *Journal of sound and vibration* 3.3 (1966), pp. 262–276.

[33] RH Lyon. “Statistical energy analysis of dynamical systems”. In: *Theory and Applications* (1975).

[34] RH Lyon and RG DeJong. *Theory and application of Statistical Energy Analysis*. Butterworth-Heinemann, 2nd Edition, 1995.

[35] S De Rosa, F Franco, and F Ricci. *Introduzione alla tecnica statistico-energetica (SEA) per la dinamica strutturale e l’acustica interna*. Liguori, 1999.

[36] A Le Bot. *Foundation of statistical energy analysis in vibroacoustics*. OUP Oxford, 2015.

[37] SH Crandall and R Lotz. “On the coupling loss factor in statistical energy analysis”. In: *The Journal of the Acoustical Society of America* 49.1B (1971), pp. 352–356.

[38] FJ Fahy. “Statistical energy analysis: a critical overview”. In: *Philosophical Transactions of the Royal Society of London. Series A: Physical and Engineering Sciences* 346.1681 (1994), pp. 431–447.

[39] T Lafont, N Totaro, and A Le Bot. “Review of statistical energy analysis hypotheses in vibroacoustics”. In: *Proceedings of the Royal Society A: Mathematical, Physical and Engineering Sciences* 470.2162 (2014), p. 20130515.

[40] DJ Nefske. “Power flow finite element analysis of dynamic systems: Basic theory and applicaton to beams, Trans”. In: *ASME, J. Vib., Acoust., Stress & Reliability* 115 (1989), pp. 94–100.

[41] JC Wohlever and RJ Bernhard. “Mechanical energy flow models of rods and beams”. In: *Journal of sound and vibration* 153.1 (1992), pp. 1–19.

[42] OM Bouthier and RJ Bernhard. “Simple models of energy flow in vibrating membranes”. In: *Journal of Sound and Vibration* 182.1 (1995), pp. 129–147.

[43] OM Bouthier and RJ Bernhard. “Simple models of the energetics of transversely vibrating plates”. In: *Journal of Sound and Vibration* 182.1 (1995), pp. 149–164.

[44] OM Bouthier. “Energetics of vibrating systems”. PhD thesis. Purdue University, 1992.

[45] F Han, RJ Bernhard, and LG Mongeau. “Energy flow analysis of vibrating beams and plates for discrete random excitations”. In: *Journal of sound and vibration* 208.5 (1997), pp. 841–859.

[46] D-H Park et al. “Power flow models and analysis of in-plane waves in finite coupled thin plates”. In: *Journal of Sound and Vibration* 244.4 (2001), pp. 651–668.

[47] Y-H Park. “Energy flow analysis of out-of-plane vibration in coplanar coupled finite Mindlin plates”. In: *International Journal of Naval Architecture and Ocean Engineering* 7.1 (2015), pp. 174–194.

[48] J-B Han, S-Y Hong, and J-H Song. “Energy flow model for thin plate considering fluid loading with mean flow”. In: *Journal of sound and vibration* 331.24 (2012), pp. 5326–5346.

[49] RS Langley. “On the vibrational conductivity approach to high frequency dynamics for two-dimensional structural components”. In: *Journal of sound and vibration* 182.4 (1995), pp. 637–657.

[50] MN Ichchou, A Le Bot, and L Jezequel. “Energy models of one-dimensional, multi-propagative systems”. In: *Journal of Sound and Vibration* 201.5 (1997), pp. 535–554.

[51] A Le Bot, MN Ichchou, and L Jezequel. “Energy flow analysis for curved beams”. In: *The Journal of the Acoustical Society of America* 102.2 (1997), pp. 943–954.

[52] A Le Bot. “Geometric diffusion of vibrational energy and comparison with the vibrational conductivity approach”. In: *Journal of Sound and Vibration* 212.4 (1998), pp. 637–647.

[53] MN Ichchou, A Le Bot, and L Jezequel. “A transient local energy approach as an alternative to transient sea: wave and telegraph equations”. In: *Journal of Sound and Vibration* 246.5 (2001), pp. 829–840.

[54] V Cotoni, A Le Bot, and L Jezequel. “Sound transmission through a plate by an energy flow approach”. In: *Acta Acustica united with Acustica* 88.6 (2002), pp. 827–836.

[55] BR Mace. “The statistics of power flow between two continuous one-dimensional subsystems”. In: *Journal of Sound and Vibration* 154.2 (1992), pp. 321–341.

[56] BR Mace. “The statistical energy analysis of two continuous one-dimensional subsystems”. In: *Journal of Sound and Vibration* 166.3 (1993), pp. 429–461.

[57] BR Mace. “On the statistical energy analysis hypothesis of coupling power proportionality and some implications of its failure”. In: *Journal of Sound and Vibration* 178.1 (1994), pp. 95–112.

[58] ECN Wester and BR Mace. “Statistical energy analysis of two edge-coupled rectangular plates: ensemble averages”. In: *Journal of Sound and Vibration* 193.4 (1996), pp. 793–822.

[59] BR Mace and J Rosenberg. “The SEA of two coupled plates: an investigation into the effects of subsystem irregularity”. In: *Journal of Sound and Vibration* 212.3 (1998), pp. 395–415.

[60] BR Mace and PJ Shorter. “Energy flow models from finite element analysis”. In: *Journal of sound and vibration* 233.3 (2000), pp. 369–389.

[61] BR Mace. “Statistical energy analysis, energy distribution models and system modes”. In: *Journal of sound and vibration* 264.2 (2003), pp. 391–409.

[62] BR Mace. “Statistical energy analysis: coupling loss factors, indirect coupling and system modes”. In: *Journal of Sound and Vibration* 279.1-2 (2005), pp. 141–170.

[63] L Maxit and J-L Guyader. “Estimation of SEA coupling loss factors using a dual formulation and FEM modal information, part I: theory”. In: *Journal of sound and vibration* 239.5 (2001), pp. 907–930.

[64] L Maxit and J-L Guyader. “Estimation of SEA coupling loss factors using a dual formulation and FEM modal information, part II: numerical applications”. In: *Journal of sound and vibration* 239.5 (2001), pp. 931–948.

[65] R Stelzer et al. “Non resonant contribution and energy distributions using Statistical modal Energy distribution Analysis (SmEdA)”. In: *Proceedings of International Conference on Noise and Vibration Engineering*. 2010.

[66] N Totaro and J-L Guyader. “Extension of the statistical modal energy distribution analysis for estimating energy density in coupled subsystems”. In: *Journal of Sound and Vibration* 331.13 (2012), pp. 3114–3129.

[67] N Totaro and J-L Guyader. “Modal energy analysis”. In: *Journal of Sound and Vibration* 332.16 (2013), pp. 3735–3749.

[68] PW Smith Jr. “Statistical models of coupled dynamical systems and the transition from weak to strong coupling”. In: *The Journal of the Acoustical Society of America* 65.3 (1979), pp. 695–698.

[69] S Finnveden. “A quantitative criterion validating coupling power proportionality in statistical energy analysis”. In: *Journal of Sound and Vibration* 330.1 (2011), pp. 87–109.

[70] F Bessac, L Gagliardini, and J-L Guyader. “Coupling eigenvalues and eigenvectors: a tool for investigating the vibroacoustic behaviour of coupled vibrating systems”. In: *Journal of Sound and Vibration* 191.5 (1996), pp. 881–899.

[71] T Lafont, N Totaro, and A Le Bot. “Coupling strength assumption in statistical energy analysis”. In: *Proceedings of the Royal Society A: Mathematical, Physical and Engineering Sciences* 473.2200 (2017), p. 20160927.

[72] JL Guyader, C Boisson, and C Lesueur. “Energy transmission in finite coupled plates, part I: Theory”. In: *Journal of Sound and Vibration* 81.1 (1982), pp. 81–92.

[73] EK Dimitriadis and AD Pierce. “Analytical solution for the power exchange between strongly coupled plates under random excitation: a test of statistical energy analysis concepts”. In: *Journal of Sound and Vibration* 123.3 (1988), pp. 397–412.

[74] J Pan and DA Bies. “The effect of fluid–structural coupling on sound waves in an enclosure—theoretical part”. In: *The Journal of the Acoustical Society of America* 87.2 (1990), pp. 691–707.

[75] I Elishakoff. *Probabilistic theory of structures*. Courier Corporation, 1999.

[76] WK Blake. “Turbulent boundary-layer wall-pressure fluctuations on smooth and rough walls”. In: *Journal of Fluid Mechanics* 44.4 (1970), pp. 637–660.

[77] D Juvé, M Berton, and E Salze. “Spectral properties of wall-pressure fluctuations and their estimation from computational fluid dynamics”. In: *Flinovia-Flow Induced Noise and Vibration Issues and Aspects*. Springer, 2015, pp. 27–46.

[78] M Goody. “Empirical spectral model of surface pressure fluctuations”. In: *AIAA journal* 42.9 (2004), pp. 1788–1794.

[79] MS Howe and MS Howe. *Acoustics of fluid-structure interactions*. Cambridge university press, 1998.

[80] GM Corcos. “The structure of the turbulent pressure field in boundary-layer flows”. In: *Journal of Fluid Mechanics* 18.3 (1964), pp. 353–378.

[81] GM Corcos. “The resolution of turbulent pressures at the wall of a boundary layer”. In: *Journal of Sound and Vibration* 6.1 (1967), pp. 59–70.

[82] RH Mellen. “On modeling convective turbulence”. In: *The journal of the Acoustical Society of America* 88.6 (1990), pp. 2891–2893.

[83] DM Chase. “Modeling the wavevector-frequency spectrum of turbulent boundary layer wall pressure”. In: *Journal of sound and Vibration* 70.1 (1980), pp. 29–67.

[84] G Maidanik. “Use of delta function for the correlations of pressure fields”. In: *The Journal of the Acoustical Society of America* 33.11 (1961), pp. 1598–1606.

[85] MN Ichchou, B Hiverniau, and B Troclet. “Equivalent ‘rain on the roof’loads for random spatially correlated excitations in the mid–high frequency range”. In: *Journal of Sound and Vibration* 322.4-5 (2009), pp. 926–940.

[86] F Franco, S De Rosa, and E Ciappi. “Numerical approximations on the predictive responses of plates under stochastic and convective loads”. In: *Journal of Fluids and Structures* 42 (2013), pp. 296–312.

[87] C Hong and K-K Shin. “Modeling of wall pressure fluctuations for finite element structural analysis”. In: *Journal of Sound and Vibration* 329.10 (2010), pp. 1673–1685.

[88] FJ Fahy. “On simulating the transmission through structures of noise from turbulent boundary layer pressure fluctuations”. In: *Journal of Sound and Vibration* 3.1 (1966), pp. 57–81.

[89] SJ Elliott, C Maury, and P Gardonio. “The synthesis of spatially correlated random pressure fields”. In: *The Journal of the Acoustical Society of America* 117.3 (2005), pp. 1186–1201.

[90] C Maury and T Bravo. “The experimental synthesis of random pressure fields: Practical feasibility”. In: *The Journal of the Acoustical Society of America* 120.5 (2006), pp. 2712–2723.

[91] T Bravo and C Maury. “The experimental synthesis of random pressure fields: Methodology”. In: *The Journal of the Acoustical Society of America* 120.5 (2006), pp. 2702–2711.

[92] M Aucejo, L Maxit, and J-L Guyader. “Experimental simulation of turbulent boundary layer induced vibrations by using a synthetic array”. In: *Journal of sound and vibration* 331.16 (2012), pp. 3824–3843.

[93] L Maxit. “Simulation of the pressure field beneath a turbulent boundary layer using realizations of uncorrelated wall plane waves”. In: *The Journal of the Acoustical Society of America* 140.2 (2016), pp. 1268–1285.

[94] C Marchetto et al. “Vibroacoustic response of panels under diffuse acoustic field excitation from sensitivity functions and reciprocity principles”. In: *The Journal of the Acoustical Society of America* 141.6 (2017), pp. 4508–4521.

[95] C Marchetto et al. “Experimental prediction of the vibration response of panels under a turbulent boundary layer excitation from sensitivity functions”. In: *The Journal of the Acoustical Society of America* 143.5 (2018), pp. 2954–2964.

[96] C Marchetto et al. “Measurement Techniques of the Sensitivity Functions to Characterize the Vibration Response of Panels Under Turbulent Boundary Layer Excitation”. In: *Flinovia—Flow Induced Noise and Vibration Issues and Aspects-II* (2019), p. 339.

[97] M Karimi et al. “Analytical and numerical prediction of acoustic radiation from a panel under turbulent boundary layer excitation”. In: *Journal of Sound and Vibration* 479 (2020), p. 115372.

[98] M Karimi et al. “A hybrid numerical approach to predict the vibrational responses of panels excited by a turbulent boundary layer”. In: *Journal of Fluids and Structures* 92 (2020), p. 102814.

[99] M Karimi et al. “Simulation of airfoil surface pressure due to incident turbulence using realizations of uncorrelated wall plane waves”. In: *The Journal of the Acoustical Society of America* 149.2 (2021), pp. 1085–1096.

[100] C Maury, SJ Elliott, and P Gardonio. “Turbulent boundary-layer simulation with an array of loudspeakers”. In: *AIAA journal* 42.4 (2004), pp. 706–713.

[101] T Bravo and C Maury. “A synthesis approach for reproducing the response of aircraft panels to a turbulent boundary layer excitation”. In: *The Journal of the Acoustical Society of America* 129.1 (2011), pp. 143–153.

[102] A Berry, R Dia, and O Robin. “A wave field synthesis approach to reproduction of spatially correlated sound fields”. In: *The Journal of the Acoustical Society of America* 131.2 (2012), pp. 1226–1239.

[103] AJ Berkhout, D de Vries, and P Vogel. “Acoustic control by wave field synthesis”. In: *The Journal of the Acoustical Society of America* 93.5 (1993), pp. 2764–2778.

[104] O Robin, A Berry, and S Moreau. “Reproduction of random pressure fields based on planar nearfield acoustic holography”. In: *The Journal of the Acoustical Society of America* 133.6 (2013), pp. 3885–3899.

[105] O Robin, A Berry, and S Moreau. “Experimental vibroacoustic testing of plane panels using synthesized random pressure fields”. In: *The Journal of the Acoustical Society of America* 135.6 (2014), pp. 3434–3445.

[106] O Robin, A Berry, and S Moreau. “Experimental Synthesis of Spatially-Correlated Pressure Fields for the Vibroacoustic Testing of Panels”. In: *Flinovia-Flow Induced Noise and Vibration Issues and Aspects*. Springer, 2015, pp. 151–185.

[107] S De Rosa, F Franco, and E Ciappi. “A simplified method for the analysis of the stochastic response in discrete coordinates”. In: *Journal of Sound and Vibration* 339 (2015), pp. 359–375.

[108] A Der Kiureghian. *A response spectrum method for random vibrations*. University of California, Earthquake Engineering Research Center Berkeley . . ., 1980.

[109] EL Wilson, A Der Kiureghian, and EP Bayo. “A replacement for the SRSS method in seismic analysis”. In: *Earthquake Engineering & Structural Dynamics* 9.2 (1981), pp. 187–192.

[110] L Jiahao. “A fast CQC algorithm of PSD matrices for random seismic responses”. In: *Computers & Structures* 44.3 (1992), pp. 683–687.

[111] J Lin, W Zhang, and FW Williams. “Pseudo-excitation algorithm for nonstationary random seismic responses”. In: *Engineering Structures* 16.4 (1994), pp. 270–276.

[112] YL Xu et al. “Pseudo-excitation method for vibration analysis of wind-excited structures”. In: *Journal of Wind Engineering and Industrial Aerodynamics* 83.1-3 (1999), pp. 443–454.

[113] X-L Guo and D-S Li. “Experiment study of structural random loading identification by the inverse pseudo excitation method”. In: *Structural Engineering and Mechanics* 18.6 (2004), pp. 791–806.

[114] JH Lin, YH Zhang, and Y Zhao. “Pseudo excitation method and some recent developments”. In: *Procedia Engineering* 14 (2011), pp. 2453–2458.

[115] PMC Morse and KU Ingard. *Theoretical acoustics*. Princeton university press, 1986.

[116] A Seçgin. “Numerical determination of statistical energy analysis parameters of directly coupled composite plates using a modal-based approach”. In: *Journal of sound and vibration* 332.2 (2013), pp. 361–377.

[117] S Ghinet and N Atalla. “Vibro-acoustic behaviors of flat sandwich composite panels”. In: *Transactions of the Canadian Society for Mechanical Engineering* 30.4 (2006), pp. 473–493.

[118] L Guillaumie. “Vibroacoustic flexural properties of symmetric honeycomb sandwich panels with composite faces”. In: *Journal of Sound and Vibration* 343 (2015), pp. 71–103.

[119] L Cremer and M Heckl. *Structure-borne sound: structural vibrations and sound radiation at audio frequencies*. Springer Science & Business Media, 2013.

[120] W Wöhle, Th Beckmann, and H Schreckenbach. “Coupling loss factors for statistical energy analysis of sound transmission at rectangular structural slab joints, part I”. In: *Journal of Sound and Vibration* 77.3 (1981), pp. 323–334.

[121] I Bosmans, P Mees, and G Vermeir. “Structure-borne sound transmission between thin orthotropic plates: analytical solutions”. In: *Journal of sound and vibration* 191.1 (1996), pp. 75–90.

[122] I Bosmans, G Vermeir, and P Mees. “Coupling loss factors for coupled anisotropic plates”. In: *Journal of sound and vibration* 250.2 (2002), pp. 351–355.

[123] C Droz, O Bareille, and MN Ichchou. “A new procedure for the determination of structural characteristics of sandwich plates in medium frequencies”. In: *Composites Part B: Engineering* 112 (2017), pp. 103–111.

[124] AD Nashif, DIG Jones, and JP Henderson. *Vibration damping*. John Wiley & Sons, 1985.

[125] RD Adams and MR Maheri. “The dynamic shear properties of structural honeycomb materials”. In: *Composites science and technology* 47.1 (1993), pp. 15–23.

[126] JA Cockburn and JE Robertson. “Vibration response of spacecraft shrouds toin-flight fluctuating pressures”. In: *Journal of Sound and Vibration* 33.4 (1974), pp. 399–425.

[127] E Szechenyi. “Modal densities and radiation efficiencies of unstiffened cylinders using statistical methods”. In: *Journal of Sound and Vibration* 19.1 (1971), pp. 65–81.

[128] RS Langley. “The modal density and mode count of thin cylinders and curved panels”. In: *Journal of Sound and Vibration* 169.1 (1994), pp. 43–53.

[129] Paul R Donavan and Wlliam K Blake. “Measurement, Prediction, and Reduction of High-Frequency Aerodynamic Noise Generated and Radiated from Surfaces of Various Textures”. In: *International Conference on Flow Induced Noise and Vibration Issues and Aspects*. Springer. 2017, pp. 147–154.

[130] JS Bendat and AG Piersol. *Engineering applications of correlation and spectral analysis*. Wiley-Interscience publication, 1980.

[131] S De Rosa et al. “Structural acoustic calculations in the low-frequency range”. In: *Journal of aircraft* 31.6 (1994), pp. 1387–1394.

[132] MK Bull. “Wall-pressure fluctuations associated with subsonic turbulent boundary layer flow”. In: *Journal of Fluid Mechanics* 28.4 (1967), pp. 719–754.

[133] MK Bull. “Wall-pressure fluctuations beneath turbulent boundary layers: some reflections on forty years of research”. In: *Journal of Sound and vibration* 190.3 (1996), pp. 299–315.

[134] G Robert. “Modélisation et simulation du champ excitateur induit sur une structure par une couche limite turbulente”. PhD thesis. Ecole Centrale de Lyon, 1984.

[135] G Robert and J Sabot. “Use of random forces to simulate the vibroacoustic response of a plate excited by a hydrodynamic turbulent boundary layer”. In: *Proceedings of the ASME Winter Meeting: Symposium on Flow-Induced Vibrations*. Vol. 5. 1984, pp. 53–61.

[136] Stephen Hambric and Peter Lysak. “Validation of a Simple Empirical Model for Calculating the Vibration of Flat Plates Excited by Incompressible Homogeneous Turbulent Boundary Layer Flow”. In: *International Conference on Flow Induced Noise and Vibration Issues and Aspects*. Springer. 2019, pp. 61–85.

[137] AV Smol'yakov. "A new model for the cross spectrum and wavenumber-frequency spectrum of turbulent pressure fluctuations in a boundary layer". In: *Acoustical Physics* 52.3 (2006), pp. 331–337.

[138] William K Bonness et al. "Modal forcing functions for structural vibration from turbulent boundary layer flow". In: *Journal of Sound and Vibration* 395 (2017), pp. 224–239.

[139] B Hiverniau. "Transmissions solidiennes: methodologie de prevision vibroacoustique moyennes et hautes frequences sous excitations aeroacoustiques". PhD thesis. Ecole Centrale de Lyon, 2007.

[140] F Franco et al. "Similitude laws for the structural response of flat plates under a turbulent boundary layer excitation". In: *Mechanical Systems and Signal Processing* 129 (2019), pp. 590–613.

[141] Robert D Blevins. *Formulas for dynamics, acoustics and vibration*. John Wiley & Sons, 2015.

ACKNOWLEDGEMENTS

These acknowledgements are written on the 3rd of December 2021, almost three months after the *soutenance de thèse* happened the 20th of September. I am actually very happy of having taken so much time to revise the thesis, since the point of view about these three years radically changed from before to after the soutenance. The PhD is supposed to form a student and specialise it in a particular topic. It is an occasion for the student to enrich the academic research with his/her contribution and expand (even just a little) the knowledge that the humankind has about... well, basically everything. For me, the PhD was an opportunity not only to expand my knowledge, but also to develop THE METHOD. The method with which you approach the different, the unknown. The method with which you overcome the fear of being inadequate, with which you learn to erase the negative connotation of the phrase "I don't understand sh*t". The method by which you learn to ask questions and not to be afraid of looking stupid when you ask them. The method with which you learn to weigh your doubts, to give them value or to minimise them. The method by which you enjoy life through curiosity. The method by which you nourish your curiosity, day after day, because you know that by doing so, every day will be a surprise. The method by which in front the unexpected, you do not see problems, but only other opportunities. And here is the 'icing on the cake': the method cannot be taught, nor researched in books. It has to be created from scratch, by you, through experience, your own experience, which can never be the same as another's. The method cannot be copied, cannot be stolen, it has to be created by oneself, for oneself. Each of us has our own way of approaching the unknown. Choosing to do a PhD, to devote yourself to research, means embracing the unknown and making it your travelling companion. To arrive at this point of state of mind is hard, or at least I felt it in this way. And as I said before, the unexpected can happen and during my PhD I encountered many unexpected things; for each one, I met someone that helped me to embrace the unexpected.

I thank Sonia, the first Italian I met in Lyon, who hosted me until I could find a place where to live. A sincere gesture of help towards an unknown person found by chance on social networks.

I thank Emanuele, the first Napolitan I met in Lyon, who became one of the most trusted friends, a reference, an anchor in the storm when I felt down and not able to continue my research.

I thank the Italian group: Andrea, Silvia, Veronica, Betta, Lucia, Manuel, even Giorgio that arrived in the last period. A safe haven to share laughter, games, advice, adventures, but above all the culture of good food, of knowing how to be together, regardless of which dialect you speak.

I would like to thank the office colleagues with whom I spent the first year: Nassardin, Liu, Zhu, Wu and Bo. We may not have spoken much, but we always exchanged a smile, a laugh, a kindness, sometimes a clementine.

I would like to thank Christophe who, when he saw me in a complete panic, did not judge or mock me, he simply picked me up and put me back on track.

I thank Rita for introducing me to yoga and for having trusted me during a difficult time for her. In her too I found a great friend and a point of reference and I hope I have become one for her too.

I thank Fabia and the countless coffee breaks spent walking around the ECL camp, going to the "forest" to be able to vent all our frustrations, exchange the most ridiculous gossip and to confide in our vulnerability. A toast to our falls, peeled knees and dislocated ankles.

I thank the improvised group of the evenings in residence: Barbara, Firas, Daniel, Dongze, Lun, Xiaoyan, Ali. You gave me moments of pure happiness, fun and a sense of belonging. Special thanks go to Xuefeng who not only participated in these evenings, but also made life in the office fun and light. I hope I deserve the trust you place in me every day when you seek advice from me.

I would like to thank my colleagues from E6: Felix, Zakaria, Pradeep, Pascal, Kevin, Jonathan, Adrien, Mouhamed, Alexys. With you I have shared lunches, raclettes, barbecues, coffee breaks, cigarettes and, of course, endless discussions on politics.

I thank the Italians of the LMFA: Cristina, Livia, Fabio, Andrea, Sofia, Jheyson. Another safe haven when I was homesick. A second thank you to Cristina, because she has been a lifeline, a breath of femininity in a world of men.

I would like to thank my colleagues of the DII of "Federico II": Alessandro, Dario, Leandro, Vittorio, Giordana. Returning to Naples to experience research "alla Napoletana" opened my mind during a time of despair, and taught me that living in another country does not mean losing one's identity, but rather emphasising it because it certainly has strengths that other cultures do not have.

Thanks to my distant friends who have been able to be close to me: Giorgia, Marta, Marco, Andrea, and the guys from D&D who have been able to nourish my fantastic side in my most analytical and scientific period ever faced.

And now the warmest thanks: I thank my French supervisors, prof. Ichchou and prof Bareille, for welcoming me to their team at Ecole Centrale de Lyon. I thank my Italian supervisors, prof De Rosa, prof Franco and Giuseppe, who offered me this great opportunity to be able to do a doctorate abroad, maintaining a co-tutorship with "Federico II", the University that trained me and that it will always be home base for me. In a time as devastating as the COVID-19 lockdown, I had lost all faith in my abilities, and there is nothing more painful than having your ruthless judgment reverberate within the four walls of your own bedroom. You have been able to see beyond and take care of my sensitivity. If I finished this PhD it's because the credits are all yours.

I thank my family: mom, dad and my brother Andrea. It has been three years of evolution for both me and you. A further thanks to my brother Andrea, who will always be a guide and the greatest source of reflection and self-awareness that I can ever have.

And finally, thank you Jimmy. Out of respect for your great shyness, I just say: you already know why I thank you.